Syntheses of Enantiomerically Pure Chiral Hosts using Amino Acid Derived Ligands with Fe(III), Ni(II) and Cu(II) ions

A
Thesis Submitted
In Partial Fulfillment of the Requirements
for the Degree of
DOCTOR OF PHILOSOPHY

By
Md. Akhtarul Alam

Department of Chemistry
Indian Institute of Technology Guwahati
Guwahati-781039
March, 2004

Dedicated to my parents

INDIAN INSTITUTE OF TECHNOLOGY GUWAHATI

Department of Chemistry

STATEMENT

I hereby declare that the matter embodied in this thesis is the result of investigations carried out by me in the Department of Chemistry, Indian Institute of Technology Guwahati, India under the supervision of Dr. Manabendra Ray Assistant Professor in Chemistry.

In keeping with the general practice of reporting observations, due acknowledgements have been made wherever the work described is based on the findings of other investigators.

I.I.T. Guwahati — Md. Akhtarul Alam

March, 2004

Dr. Manabendra Ray
Assistant Professor
INDIAN INSTITUTE OF TECHNOLOGY GUWAHATI
Department of Chemistry
Tel. 91 361 2582310
E-mail: manabray@iitg.ernet.in Fax. 91 361 2690762

CERTIFICATE

This is to certify that Mr. Md. Akhtarul Alam has been working under my supervision since August 2, 1999. I am forwarding his thesis entitled "**Syntheses of Enantiomerically Pure Chiral Hosts using Amino Acid Derived Ligands with Fe(III), Ni(II) and Cu(II) ions**" being submitted for the Ph.D. degree of this Institute. I certify that he has fulfilled all the requirements according to the rules of this Institute and regarding the investigations embodied in his thesis and work has not been submitted elsewhere for a degree.

I.I.T. Guwahati Dr. Manabendra Ray
March, 2004 Supervisor

INDIAN INSTITUTE OF TECHNOLOGY GUWAHATI

Department of Chemistry

COURSE CERTIFICATE

This is to certify that Mr. Md. Akhtarul Alam has satisfactorily completed all the courses required for the Ph.D. degree programme. These courses include:

CH 611 Bioinorganic Chemistry

CH 631 Experimental Spectroscopy

CH 620 Art in Organic Synthesis

CH 630 A Fundamental Approach to Physical Chemistry

Mr. Md. Akhtarul Alam has successfully completed his Ph. D. qualifying examination in February 2001.

Dr. Jubaraj B. Baruah
Head
Department of Chemistry
I.I.T. Guwahati

Dr. Anil Kumar Saikia
Secretary
Departmental Post Graduate Committee
Department of chemistry
I.I.T. Guwahati

INDIAN INSTITUTE OF TECHNOLOGY GUWAHATI

Department of Chemistry

Ph.D. GRADE CARD

Name: Md. Akhtarul Alam Department: Chemistry

Roll No: 994501 Semester: July-November, 1999

Course	Course Name	Credit	Grade
CH 611	Bioinorganic Chemistry	6	AB
CH 631	Experimental Spectroscopy	6	BB
CH 620	Art in Organic Synthesis	6	AA
CH 630	A Fundamental Approach to Physical Chemistry	6	BC

Semester Performance Index (S.P.I): 8.50

Cumulative Performance Index (C.P.I): 8.50

I.I.T. Guwahati Assistant Registrar

March, 2004 Academic

Acknowledgements

I convey my sincere sense of gratitude to my supervisor Dr. Manabendra Ray who has initiated me to the artistic science of inorganic chemistry and crystal engineering. His active leadership, priceless suggestions and invaluable support, revitalized my curiosity in the subject. His continuous imaginative initiatives and decisive insights assisted me to become skilled, both in the theoretical and practical aspects of my subject. As his first student, working with him was a great opportunity and delight for me.

I express my sincere appreciation to Dr. M. Nethaji at Indian Institute of Science Bangalore, for his enormous help and tremendous patience in recording the data and solving the X-ray structure of all my crystals, without his help it would be impossible to proceed any further during my research work. I also thank to Prof. T. N. Guru Row, who first took the initiative for solving the crystal structure of my compounds.

I would like to thank Prof. R. N. Mukherjee, who allowed me to perform the variable temperature magnetic susceptibility measurements and EPR studies reported in this thesis at his laboratory. His Ph. D. student V. Balamurugan was instrumental in recording the variable temperature magnetic susceptibility measurements at I.I.T. Kanpur.

I wish to show my gratitude to Dr. P. K. Madhusudanan (CDRI, Lucknow) for ^{1}H NMR, elemental analysis and optical rotation facilities made available to me.

I am always indebted to Prof. Mihir K. Chaudhury for his tremendous input and encouragement throughout this tenure as the Head of my Doctoral Committee. My honest regards are due to all the faculty members of the department and fellow friends for their motivation and encouragement that guided me to this end. I convey my regards to Dr. Nikhil Gucchait for his encouragement.

My parents and other family members were always behind me with their constant encouragement, inspiration and support. I specially thank to Rupa Sultana for her love, inspiration and support. I also thank my friend Tridib and Deepa di.

The financial support from Council of Scientific and Industrial Research (CSIR), New Delhi [No. 9/731(28)/2003] is duly acknowledged. I thank Indian Institute of Technology, Guwahati for all the facilities that were made available to me and for the initial financial support.

Md. Akhtarul Alam

Abstract

This thesis represents our attempt to synthesize enantiopure chiral cavities, with our exploration of the coordination chemistry of the amino acid derived chiral tetradentate ligands and three first row transition metal ions namely Fe(III), Ni(II) and Cu(II). In the process we have been successful in the synthesis and characterization of three chiral cavities of different size and shape, one porous 1D helical network and two structural models for metalloenzyme active sites.

The thesis has been divided into seven chapters. Chapter wise summary of the work is presented below.

Chapter I

Introduction

In this chapter we present the importance of research works and recent developments related to the technologically potent area involving the synthesis of enantiomerically pure chiral host and their applications. Recognition of chiral molecule by a host is an important area of research having applications in chiral separation, enantiopure drug synthesis, stereospecific synthesis of organic molecules and in the domain of chiral sensors. A diverse set of approaches in the design and functioning of hosts have been reported in the recent literature ranging from rigid and bulky organic molecules changing color with one enantiomer having preferred binding of the enantiomer inside chiral nanoporous channels to chirally modified polymers changing frequency of a coated crystal with one enantiomer.

Recognition of a molecule, chiral or achiral, inside a molecular cavity working as a host has been pursued intensely in the last three decades. Within the last few years witnessed synthesis of several synthetically challenging, architecturally beautiful molecular cup, bowl, and capsule shaped guest molecules. Literature survey showed that a majority of these have been synthesized in multi-step processes and most of them are achiral and thus a major requirement for chiral recognition is missing.

The objective of this thesis has been set to synthesize multinuclear enantiopure transition metal complexes with available binding sites inside a cavity. The advantage of using a metal complex stems from the fact that the metal ion gives the conformational rigidity to the otherwise flexible organic ligand.

Chapter II

Ligand Synthesis

In this chapter we present the experimental conditions for the synthesis of polydentate ligands with potential to form enantiomerically pure chiral complexes. We have chosen the relatively less explored amino acid derived reduced Schiff base ligands. The reason is that the natural amino acids are available in pure enantiomeric form rather cheaply. In addition, the ligand was designed to have several possible H-bond formation sites to assist in assembling multinuclear assembly through H-bonding.

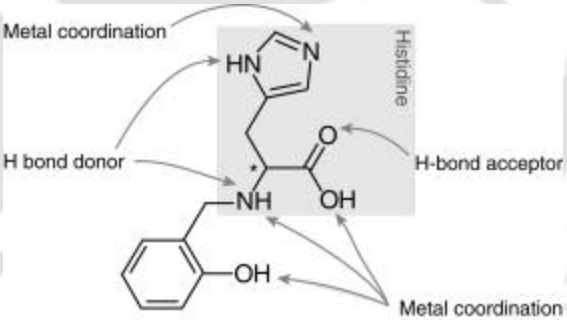

Figure 1. The histidine-derived ligand (*S*-H_2Salhis)

Chapter III

Synthesis and solution properties of a self-assembled molecular capsule with copper (II) complex

This chapter contains the synthesis and characterization of an octameric Cu(II) complex with the formula $[Cu_8(S\text{-Salhis})_8Py_{10}].Py.3MeOH.(C_2H_5)_2O$. The crystal structure showed that eight CuL units form a capsular cavity that traps four pyridine molecules. In this capsular cavity top to bottom distance was about 13.6 Å and across the

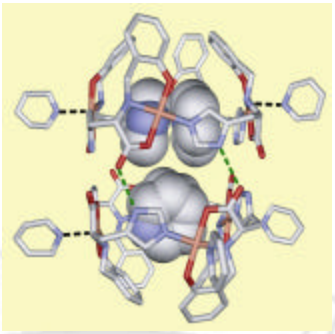

Figure 2. Capsular structure of the octameric Cu(II) complex

cavity was about 10.0 Å. To understand the stability of the capsule in different chemical environments, we further studied the characteristics of the complex using a combination of spectroscopic methods and recrystallization techniques in various solvents. We observed the assembly and disassembly of the capsule in different solvent medium and using external ligands. These experimental results suggest that the capsular complex synthesized has potential for use as storage (holding a guest inside the capsule) and delivery agent (either solvent or imidazole mediated) for trapped guest molecules.

Chapter IV

Synthesis and characterization of a 1D chiral microporous channels with a Fe(III) complex and insertion of iodine inside the channels

This chapter contains the synthesis and characterization of a dinuclear iron(III) complex $[Fe_2(\hat{i}–OH)(\hat{i}–OAc)(S\text{-Salhis})_2].4H_2O$. Crystal structure of the complex showed the formation of one-dimensional (1D) helical channels with diameter of 7-9 Å in the crystal lattice. The channels are filled with water molecules. These water molecules are H-bonded with the bridging hydroxo group and the ligand carboxylate oxygen. The usability of the channels as hosts has been ascertained by removing water from the channel thermally and filled the evacuated channels with iodine. Structural characterization of the empty crystals and the iodine filled channels showed that the iodine molecules inside the channels were organized in a helical array similar to those of water molecules inside the channels.

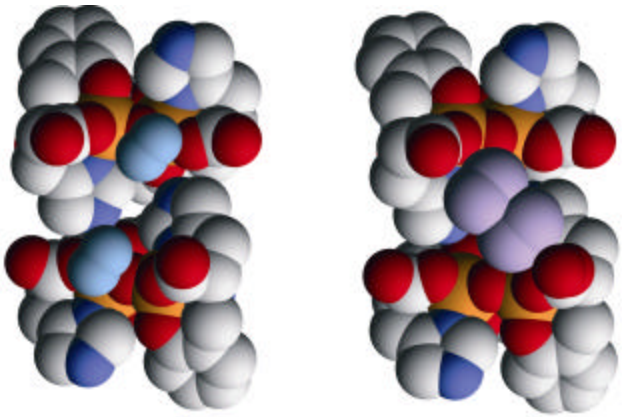

Figure 3. Water (left) and iodine (right) inside the channel, atoms appearing in pairs indicate positional disorder

Importantly the removal and refilling of the molecules did not destroy the lattice structure. The complex is also important as $[Fe^{III}(\mu\text{-}OH)(\mu\text{-carboxylato})Fe^{III}]^{4+}$ core has been proposed to be present in the active site of protein mammalian purple acid phosphatases. To the best of our knowledge this is the first structurally characterized complex containing the core bound with the imidazole, phenolate and carboxylate donors closely resembling the histidine, tyrosine and aspartate donors present in the protein.

Chapter V

Synthesis and characterization of a binuclear Ni(II) complex

In this chapter we present the synthesis and characterization of a binuclear Ni(II) complex which has a C_2 symmetric cavity around the polar carboxylate groups. One Na^+ is bound inside the cavity in the solid state, as evidenced from the X-ray crystallography. The Fe(III) complex discussed in chapter IV had a C_2 symmetric cavity formed around the acetate ion. On the other side of the molecule, where hydrophilic pocket holds the water and iodine, the cavity is open. In order to form a chiral cavity around the hydrophilic carboxylate groups that might favor binding of chiral amines we decided to use a different metal center Ni (II).

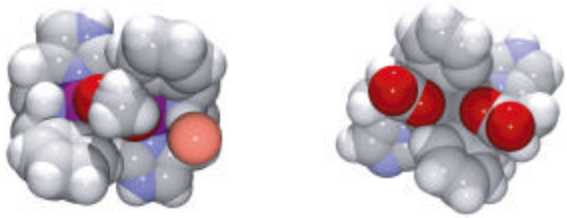

Figure 4. Space filling model of $[Fe_2(\mu\text{-}OH)(\mu\text{-}OAc)(S\text{-}Salhis)_2]$ (left) and $Na[Ni_2(\mu\text{-}OAc)(S\text{-}Salhis)_2]$ (right) showed the C_2 symmetric chiral cavity

Chapter VI

Nitrate bridged Iron(III) complexes for colorimetric and conductometric detection of amines in solution and vapor phase

Described in this chapter are the synthesis and characterization of three high-spin binuclear iron(III) complexes with the general formula, $[Fe_2(L)_2(NO_3)_2]$. Each of the complexes displays a strong phenolate to Fe(III) charge-transfer transition in the range of 520-585 nm with a moderately high extinction coefficient. These binuclear Fe(III) complexes change color in presence of amines. Also, the molar conductance of the complexes in methanol, showed values characteristic of 1:1 electrolytes, however, addition of amines to the methanolic solution containing the complex increase the molar conductivity to that of a 1:2 electrolyte. This chapter contains the results of both conductometric and colorimetric titration of these complexes with various amines and some other bases enabling us to look for the possible reasons for the color changes.

Figure 5. Fe(III) complex coated on a filter paper before (left) and after (right) exposing to amine vapor

Chapter VII

Syntheses and characterization of mononuclear Iron(III) catecholate complexes

In this chapter we present the synthesis and characterization of two mononuclear Iron(III) complexes of general formula [Fe^{III}(L)(catecholate)] (L = histidine or methionine derived ligand) where two *cis* sites in octahedral the complexes were blocked by the catecholate forming mononuclear complexes. Our choice of catecholate as a bidentate ligand was influenced by the idea that the resulting complex (with histidine derived ligand) might serve as a structural model for the active site of catechol dioxygenase, a catechol-cleaving enzyme. Various spectroscopic techniques were utilized to characterize the complexes formed.

Contents

Chapter I

Introduction

1.1 Purpose of the present investigation

Chiral molecules are non-superimposable mirror image isomers with opposite light rotating property and each of the isomers is called enantiomer. Enantiomerically pure chemicals are important in bioinorganic, inorganic and pharmaceutical chemistry. One such example is the drug methylphenidate, most commonly prescribed psychotropic medication for children with attention deficiency disorder, which is marketed as a racemate even though the D-*threo* isomer is 13 times more active than its mirror image isomer.[1] There are several methods for obtaining enantiomerically pure chemicals through either enantioselective synthesis or separation from racemic mixture using chromatography, biotransformation or diastereoisomeric crystallization.[2] Despite the availability of such methods, obtaining one enantiomer in pure form remains a synthetically and commercially challenging task owing to the chemical similarities of the enantiomers.

Recognition of enantiomers or chiral molecules inside a cavity working as host is an important area of research with applications in chiral separation, chiral sensor, enantiopure drug synthesis, stereo specific synthesis etc. A diverse set of approaches in the design and functioning of hosts have been reported in the recent literature ranges from rigid and bulky organic molecule changing color with one enantiomer,[3] preferred binding of an enantiomer inside chiral nanoporous channels[4] to chirally modified polymers[5] changing frequency of a quoted crystals with one enantiomer.

Since the discovery of crown ethers, numerous studies were done on cyclic and cage compounds those are capable of binding atoms, ions or molecules in their cavities leading to the development of host-guest chemistry,[6,7] molecular recognition[8] and supramolecular chemistry.[9] Last few years witnessed synthesis of several synthetically challenging, architecturally beautiful molecular cages,[10] squares[11] and capsule[12] shaped host molecules.

The purpose of this thesis work is to develop enantiopure host molecules based on metal complex association from simple enantiomerically pure ligands to make low molecular weight chiral metal complexes assembled by metal ligand coordination and/or by intermolecular H-bonding. In the following paragraphs we have summarized the literature on different type of mostly achiral and few chiral host molecules reported and finally our approach to synthesize enantiopure metal complex based chiral host.

1.2 Metal-ligand macrocycles

In the literature, several metal-ligand macrocycles with open cage from both sides have been described. The first self-assembled macrocyclic host synthesized shown in **1** (Figure 1.1) containing two Cu(II) ions was reported by Maverick and Klavetter.[13] This both sides open inorganic macrocycle showed a strong binding affinity towards 1,4-diazabicyclo[2.2.2.]octane as evidenced by X-ray crystallography. Schwabacher[14] and co-workers have developed the self-assembled receptor **2** (Figure 1.1) acting as a host for bicyclic aromatics in water. Metal binding by the bis(amino acid) receptors forms a macrocycle with an appropriate size for guest binding. The hydrophobic binding site was shown to be effective for pyrene transport through a liquid membrane. The rate of the transport depended on the metal ion employed, for example, Ni(II) and Co(II) showed the highest efficiency for binding the aromatic guests. Macrocyclic dinuclear Pd(II) complex **3** (Figure 1.1) characterized by FAB-MS, has a hydrophobic cavity.[15] The dimerization of the zinc-porphyrin with pyridine terminus resulted in the formation of macrocyclic complex **4** (Figure 1.1) with inwardly directed hydrogen bonding sites.[16] This macrocycle showed a binding affinity towards a terephthalic acid derivative through efficient hydrogen bond formation.

Recently, Lehn and co-workers reported the self-assembly of circular helices whose frameworks are templated by their counter anion.[17] The self-assembly of trisbipyridine ligand **5** (Figure 1.1) with $FeCl_2$ salts yields pentanuclear complex **6** (Figure 1.1) which incorporates a chloride ion in the cavity as evidenced by X-ray analysis, whereas the same ligand forms hexanuclear complex when treated with $Fe(BF_4)_2$, $FeSO_4$, or $FeSiF_6$. The most probable reasoning for the formation of the complex stems from the fact that the macrocyle carries one counter ion in the void at the center.

The host molecules described in this section utilizes metal coordination as the driving force in the formation of the assemblies and thus they retain their identity in solution. On the other hand relatively open nature of the cage framework allows the guest molecules to be in and out from the host quite easily. Thus except for **1** and **2**, (Figure 1.1) where coordination site is available inside the cage, binding of the guest is weak in nature in case of the other macrocycles.

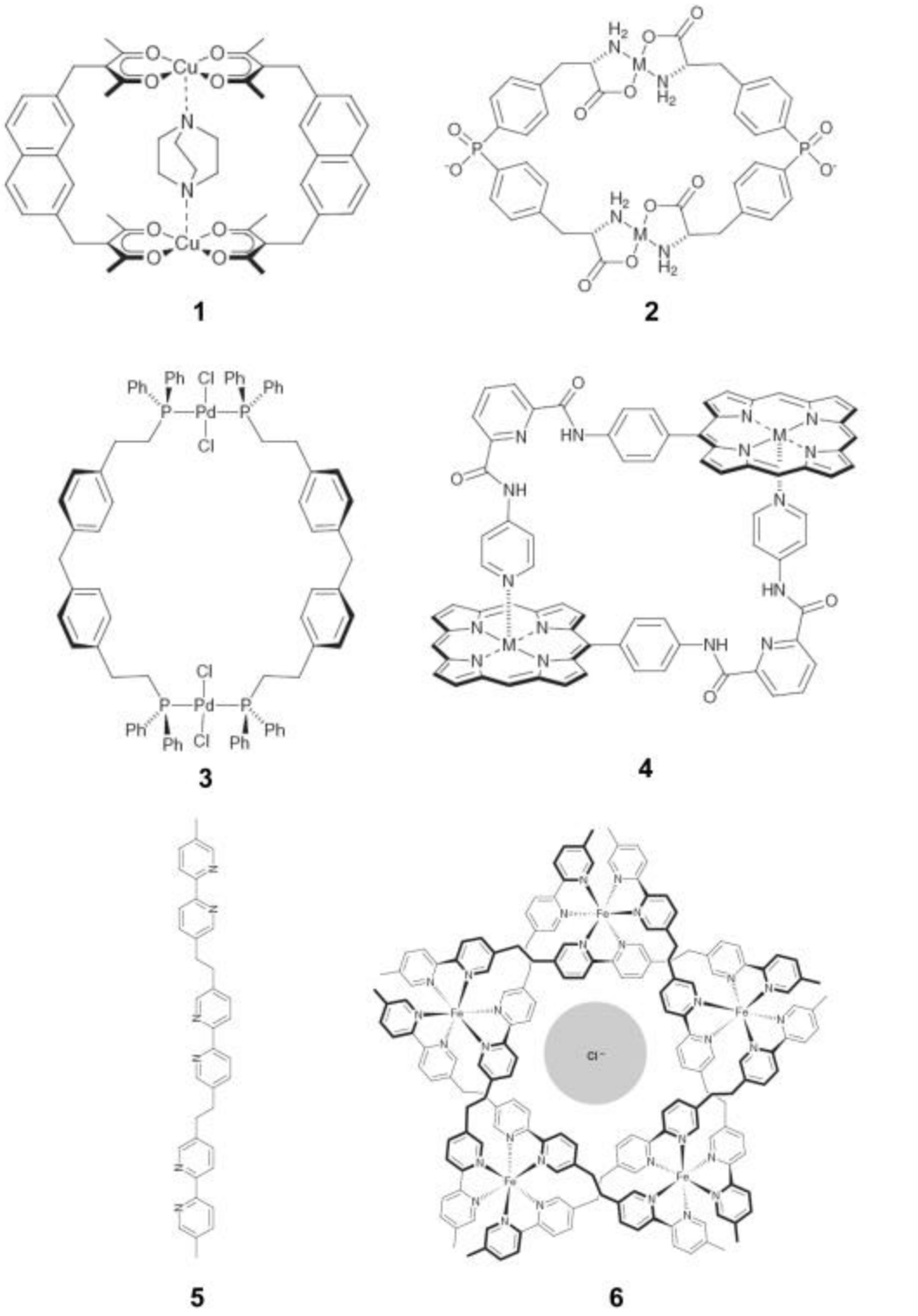

Figure 1.1 Metal-ligand macrocycles

1.3 Self-assembled molecular square

The basic concept in the designing of the molecular square is to facilitate the incorporation of spacers into the *cis*-protected square-planar metal complexes. In a novel approach, an ethylenediamine protected M(II) complex (where M = Pd or Pt) was successfully incorporated into a tetranuclear square framework [18a] by complexation with simple bridging ligand 4, 4'-bipyridine as reported by Fujita *et al.* and shown in **7** (Figure 1.2). Long *et al.* used the 4, 4'-bipyridine *N, N'*-dioxide as a bridging hydrogen bond acceptor to prepared molecular square, helices etc.[18b] On the other hand Yaghi *et al.* found that multidentate linkers such as carboxylates allow for the formation of more rigid frameworks over the 4, 4'-bipyridine linker due to their ability to aggregate metal ions into M-O-C clusters. However, the resulting hosts are not chiral.[18c]

On the other hand Stang *et al.* synthesized phosphine derivative **8** (Figure 1.2)[19] soluble in organic solvents. Using the phosphine protective starting materials, his group has been extending the chemistry of square compounds. For example, chiral squares, metal-hypervalent iodine hybrid squares, nano-sized squares, functional squares with ferrocene, crown ether or porphyrin units have been developed.[11] A similar self-assembly strategy was employed by Hupp and co-workers for the preparation of Pd(II)-Re(I) or Pt(II)-Re(I) bimetallic square complex **9** (Figure 1.2) that shows a luminescent property.[20] Porphyrin square **10** (Figure 1.2) was also reported by Drain and Lehn,[21] though its structure was deduced by inference. An inorganic calix[4]arene analogous **11** was also prepared by Lippard and co-workers.[22]

1.3.1 Self-assembly chiral molecular square

Stang *et al.* prepared optically active molecular squares of type **12** (Figure 1.2) using [4-(4-pyridyl)phenyl]iodonium triflate and [Pd(*R*-(+)-binap)(H_2O)][OTf]$_2$ or [Pt(*R*-(+)-binap)(H_2O)][OTf]$_2$.[23] In this case the diaza ligands of the iodonium species possess rotation symmetries about their linkages; therefore, molecular squares **12** is optically active exclusively due to the chiral transition metal auxiliary (binap) in the assembly. On the other hand molecular squares of the type **13** were prepared via reaction of bis(3-pyridyl)iodonium triflate and chiral Pd(II) or Pt(II) complexes.

Lin *et al.* prepared a chiral molecular square using the enantiopure atropisomeric 6,6'-dichloro-2,2'-diethoxy-1,1'-binaphthyl-4,4'-bipyridine ligand and $ClRe(CO)_5$ salt. The molecular square exhibits interesting enantioselective luminescence quenching by chiral amino alcohols.[24]

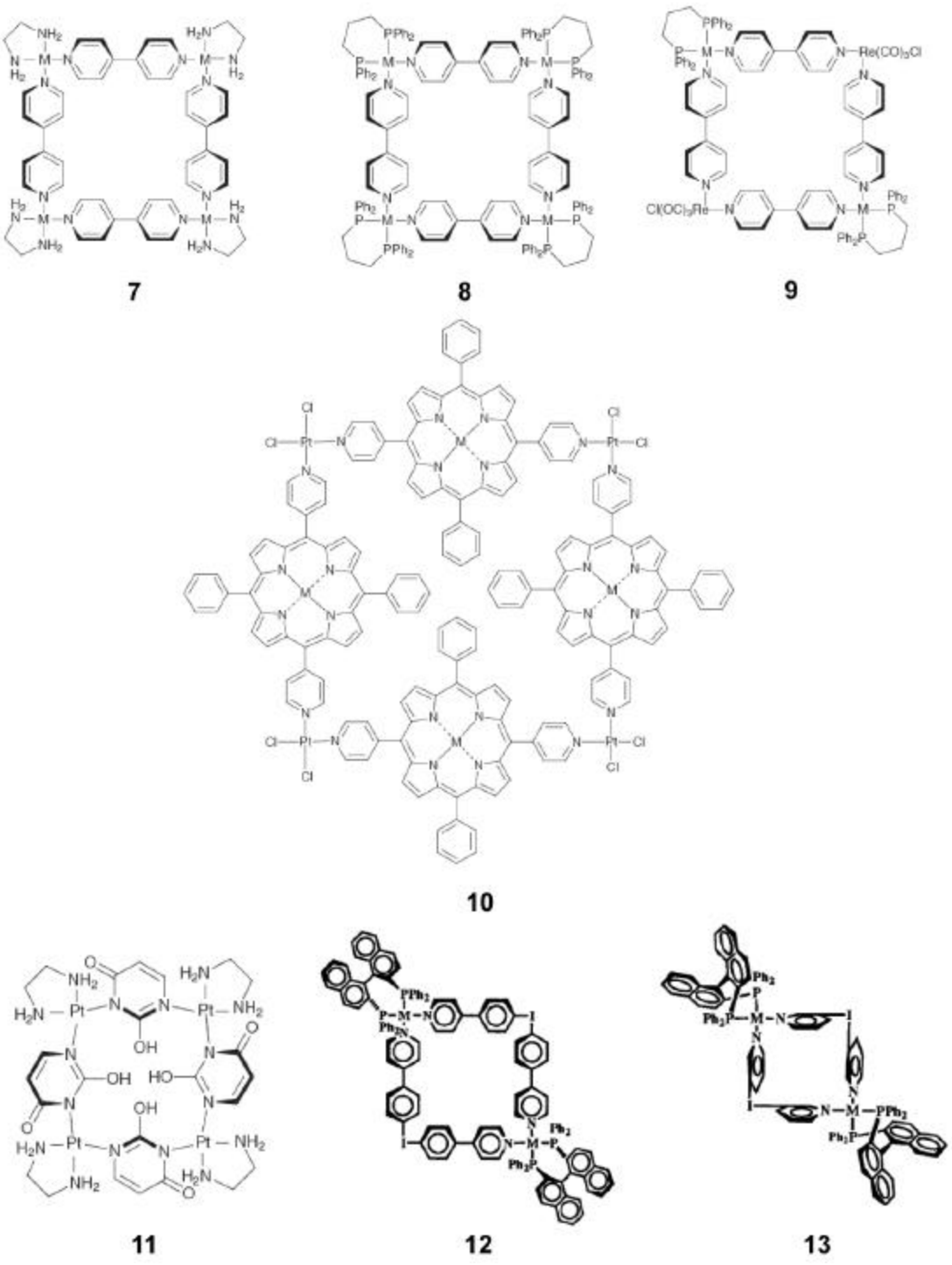

Figure 1.2 Self-assembled chiral and achiral molecular square

One advantage of molecular squares is that by stacking on top of each other in the solid state they can form porous solid with channels of different size and shape where guest molecules can bind selectively and even reaction between different guest molecules can occur. The reaction in such a confined environment can be very different than occurring in a solution, giving rise to unusual reaction product. Depending on the choice of spacer molecules, for example, 4,4'-bipyridine in **7** the channel diameter can also be tuned. The majority of the molecules described in this section uses square planar metal complexes in the corner of the square and 4,4'-bipyridyl as the spacer and as a result active group for binding guest inside the square is absent. On the other hand, utilizing different spacer molecules in **9** and **10** binding site inside the square has been incorporated.

1.4 Molecular capsules

Over the last few years there has been a breakthrough in the design and synthesis of nanoscale moleculer containers- cavitands, hemicarcerands and capsules.[25] These nanocavities are designed for selective binding, molecular separation, sensing of smaller molecules or ions,[26] molecular transport and delivery, stabilization of reactive intermediates[27] and catalysis through encapsulation.[28] They also mimic the hydrophobic pockets of enzymes. The field has grown since the first report of hollow calixarenes developed by Collet,[29] Cram[6] and Gutsche,[30] which were able to trap a single solvent or gas molecule. In the early 1980s, their investigations confirmed that the capsules contained giant cavities of 15-20 Å inner dimensions and 1500 $Å^3$ internal volume.

1.4.1 Metal directed self-assembly of cage compounds

The first three dimensional cage complex was synthesized by Saalfrank.[31] Metallation of the ligand **14** (Figure 1.3) in the presence of MgI_2 followed by addition of oxalyl chloride resulted in the formation of the complex. The structure **15** (Figure 1.3) was evidenced by X-ray crystallography. The metal center could be replaced by transition metals such as Mn, Co, Ni or Fe. The three dimensional cavity could be expanded by inserting a phenylene spacer into the ligand framework **14** (bottom). Analogous M_4L_6 cage structures have been also reported by Raymond and co-workers.[32]

1.4.2 Tetrahedral metal-ligand cage

The host-guest chemistry of tetrahedral metal ligand clusters has been developed by Raymond *et al*. In their system, six bis(catechol) ligands span the edges between four metal atoms that define the corner at a tetrahedron. Bis(catechol) **16** (Figure 1.3) self-assemble to form M_4L_6 tetrahedron capsule **17** (Figure 1.3) upon coordination with Ti^{IV}, Ga^{III} or Fe^{III} ions,[33] which encapsulate positively charged guest molecules. On the other hand, the anthracene-briged ligand shows more interesting behavior. In absence of guests, the anthracene-briged ligand combines with Ti^{IV} or Ga^{III} subunit resulted in the formation of the M_2L_3 helicates as the most stable structure. On addition of tetramethyl ammonium ion to the mixture it formed M_4L_6 tetrahedral molecular capsule.

1.4.3 Glycoluril-derived molecular capsules

Kim *et al*. reported a novel molecular container cucurbituril **18**, this macrocyclic cavitand has a hollow core of about 5.5 Å diameter.[34] This cucurbituril is normally insoluble in water but soluble in alkali metal salts (0.2M). The X-ray analysis of crystals grown from aqueous sodium sulfate showed that sodium ions provide a "lid" on both the top and bottom of the macrocycle. Two sodium ions and five water molecules form a network of hydrogen bonds and electrostatic interactions between the six carbonyl groups. This cucurbituril can encapsulate small organic molecules such as THF and benzene. Most interesting observation was the inclusion and release of the guest molecule in cesium- cucurbituril complex as studied by change in pH of the system.[35]

The monomer **19** (Figure 1.3) consists of two glycoluril subunits provide curvature and self-complementary hydrogen-bonding motif **20** which is called "soft-tennis ball" **21** according to Rebek.[36] The tennis ball includes small molecule such as methane, ethane and ethylene. However, larger guests such as propane, allene and isobutylene are excluded. By variation of the spacer in the glycoluril units Rebek *et al*. controlled the volume of the soft-tennis ball and encapsulated larger guest molecules. They showed that the rate of reactivity of the Diels-Alder reaction accelerated nearly 200-fold inside the cavity.[28] They also used the soft-tennis ball for chiral separation and recognition.[37]

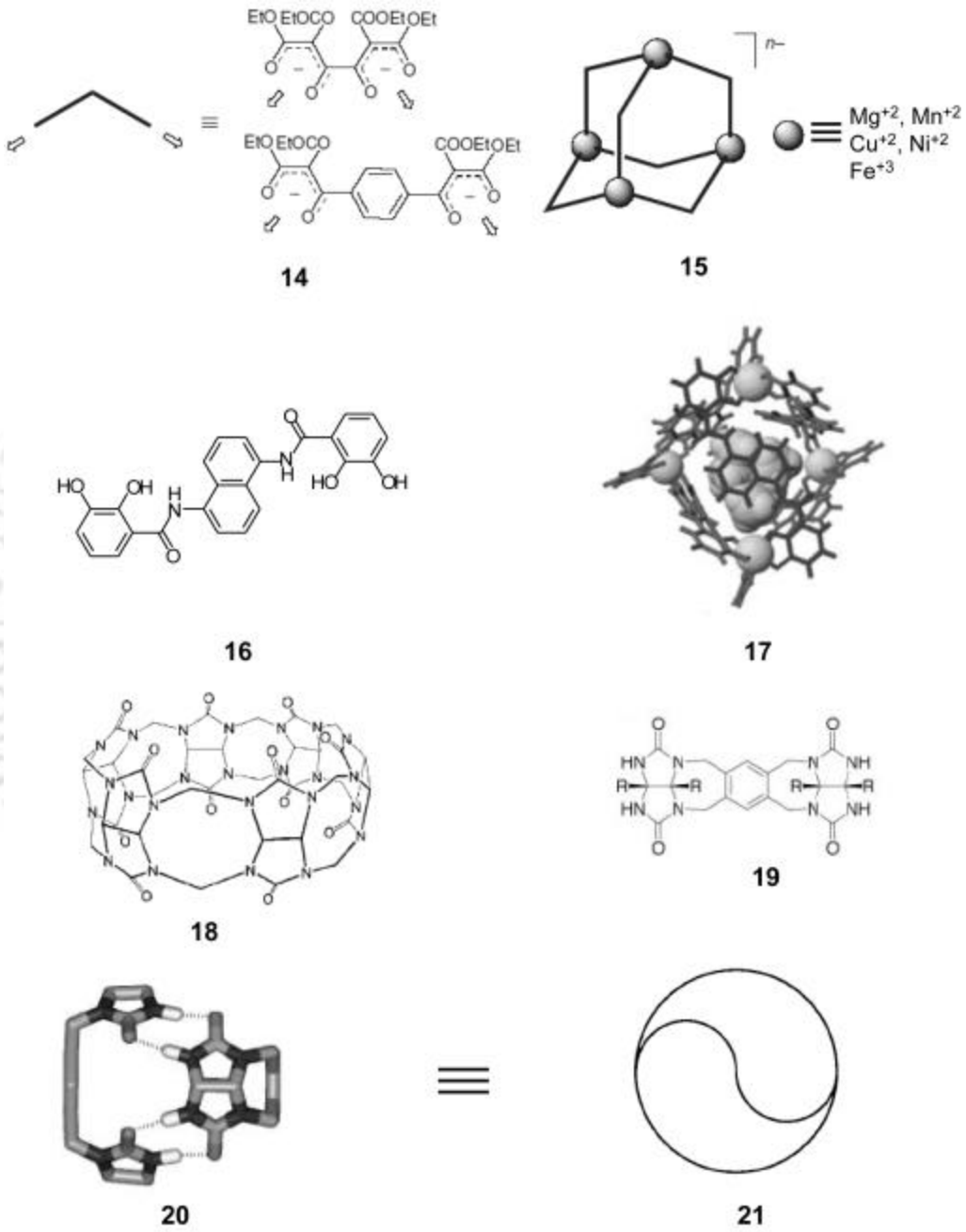

Figure 1.3 Metal cages or molecular capsules

1.4.4 Cyclophane-derived molecular capsules

Calix[4]arene and resorcin[4]arene are standard subunits for synthesizing self-assembled molecular capsules.[25] Both molecules exhibit variable conformations. Through appropriate derivatization, they can be fixed into a single bowl-shaped conformation. For example, secondary ureas were installed on the lower wider rim in calix[4]arene. In the presence of an appropriate aromatic, aliphatic or cationic guest molecule, these two units dimerised through hydrogen bonding. Larger calix[6]arene capsules have also recently been reported.[38]

Atwood *et al*. reported different varieties bowl shape of calixarenes[39] and resorcinarene[40] by changing the upper or lower rime of the corresponding unites. They also reported a chiral hexameric capsule[41] in the solid state **22**. The structure shows a chiral arrangement of six resorcinarene subunits enclosing an enormous cavity of about 1375 $Å^3$ (Figure 1.4). The hexameric capsule features a total of 60 hydrogen bonds, in which 8 ordered water molecules are recruited to integrate the architecture.

1.4.5 Resorcin[4]arene-derived metal-based molecular capsules

Shinkai and co-workers have demonstrated that the substitution of pyridines into the calix[4]arenas also resulted in the self-assembly of supramolecular capsules **23** (Figure 1.4). A rigidified calixarene monomer displaying four pyridine ligands undergoes metal-directed self-assembly to produce capsule[42] **24** (Figure 1.4) in a manner analogous to that of **23**. Just by bridging glycol substituents at the lower rim of the calixarene produce a supramolecular capsule, which even can encapsulate fullerene (C_{60}).[43]

The list of metal ions useful for directing encapsulation continues to grow. Harrison and co-workers introduced tridentate chelating ligands as structural elements. A resorcinarene functionalized with four iminodiacetate groups **25** (Figure 1.4) showed an affinity for binding with Co^{II}, Cu^{II} and Fe^{II} salts.[44-47] The result is the complexation of each metal center in a chelated pseudooctahedral environment and the generation of supramolecular capsules **26**. They are stable in aqueous medium and can encapsulate a wide variety of organic compounds, such as cyclic and acyclic aliphatic alcohols, ethers, ketones, esters and halides, within a cavity of approximate volume 215$Å^3$.

Dalcanale and co-workers have created a variety of bridged resorcinarenes functionalized with four nitrile groups for the generation of metal-ligand directed self-assembly of a new cavitands –based coordination cages in which two tetracyano cavitands **27** are connected through four Pd^{II} or Pt^{II} square-planar complexes **28**.[48]

So far, cage molecules have been constructed mainly by formation of covalent bonds as well as self-assembly through noncovalent interactions such as hydrogen bonding and metal-induced self-assembly. In most of the cases redox inactive metal has been used. The exception was the effort by Harrison *et al.* who used the redox active metal such as Co^{II}, Cu^{II} and Fe^{II} **26** (Figure 1.4). Generally metal-assembled molecules are ionic in nature and suitable to attract charged guest molecules. Moreover, cage stability and binding of the guest molecules could be varied by simply changing the metal oxidation state.

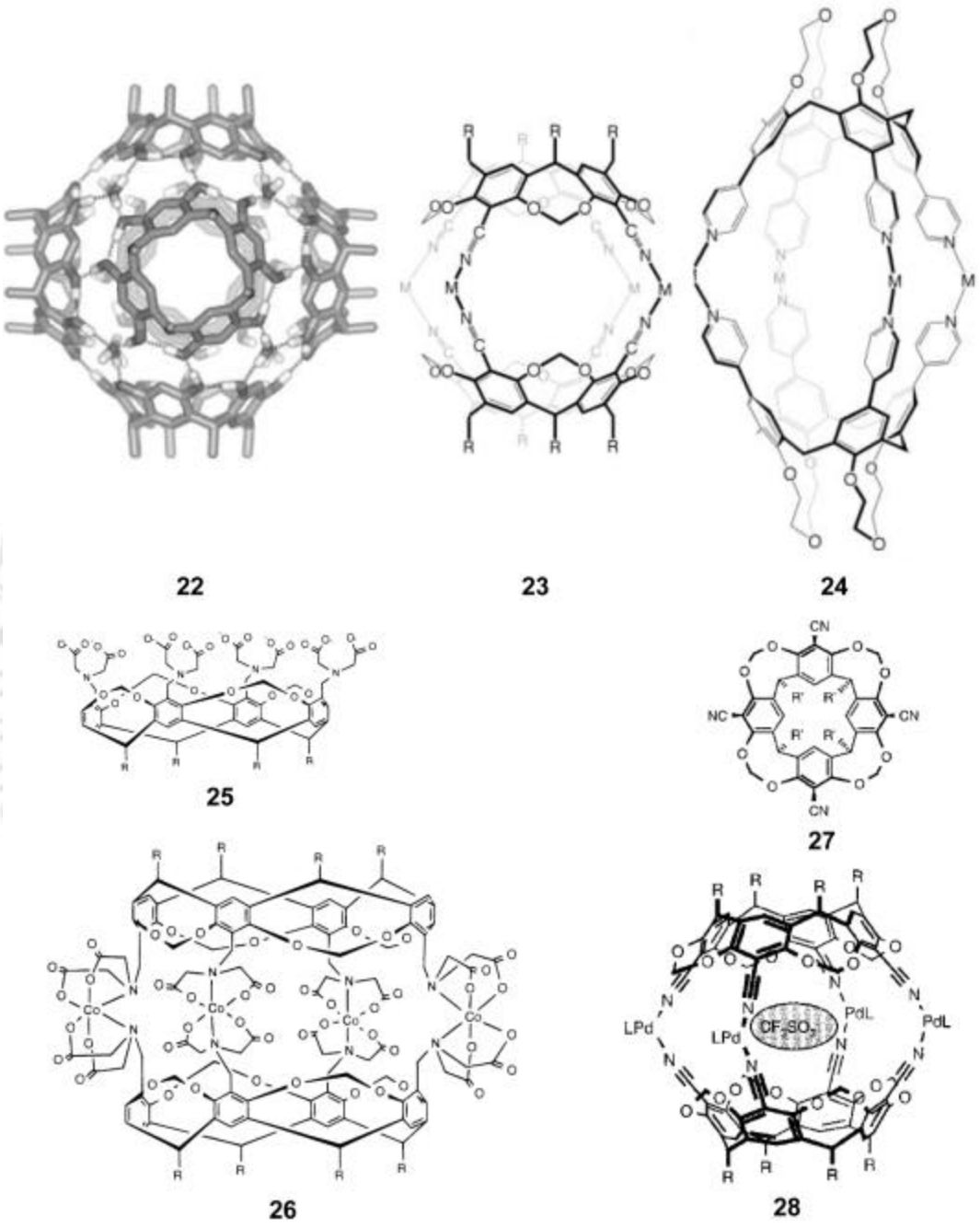

Figure 1.4 Resorcin[4]arene-derived metal based molecular capsules

1.5 Complexes based on tris(pyridine) and tris(primidine) ligands

Fujita *et al*. have used triangular heterocyclic ligands in combination with *cis*-enforced square-planar Pd and Pt complexes for the construction of highly symmetric supramolecular capsules. The positively charged metal centers impart water solubility on the complexes, and their relatively hydrophobic cavities bind a variety of organic guest molecules.[49] Tris(pyridylmethyl)ligand **29** (Figure 1.5) was combined with ethylenediamine-protected Pd(II) complex in presence of a suitable organic guest. Two ligands of **29** bind a total of three metal centers to produce a C_{3v}-symmetric supramolecular capsule **32**. The palladium-pyridine bonds are stable in protic solvents and the high overall charge (+6) of the complex imparts water solubility. The hydrophobic interior of the capsule is aptly filled by organic anions such as adamantanecarboxylate. The subunits aggregate into an uncharacterized oligomeric state in the absence of a suitable guest. Ligand **30** with three 4-pyridyl subunit around a central triazine core, forms square-planar Pd or Pt subunit. The metal atoms reside at each corner of an octahedron with the longest metal-metal separation being 1.9 nm and volume enclosed by the capsule about 500$Å^3$. The platinum-based capsule **33** is remarkably stable and encapsulates several guests of the size of adamantine.[50] The 3-pyridyl substituted ligand **31** is unable to form a closed shell topology with organometallic corner subunits. Four units of ligand **31** and six units of ethylenediamine-protected Pd(II) complex self-assemble into an open bowl-shaped structure **34**.[51] These hemispherical superstructure **34** assemble in aqueous medium to form discrete dimeric supramolecular capsules **35** in presence of large aromatic guests. X-ray crystallographic studies reveal that four units of *m*-terphenyl or six units of *cis*-stilbene form compact hydrophobic clusters that are encapsulated by the discrete dimeric superstructure. Only dispersive forces and hydrophobic effect act to hold the capsule together. There is no direct metal-ligand bonding between the supramolecular bowls that comprise the capsule halves. In absence of direct contacts between the molecules that make up the bowls, it is the guests bound within both bowls that provide the bridging interactions that drive dimerization.

The focus of this section is the construction of three dimensional molecular cages of different shapes and sizes by simply linking two dimensional planar organic components with different coordination position of the ligand nitrogen and *cis* protected ethylenediamine Pd(II) or Pt(II) metal complexes.

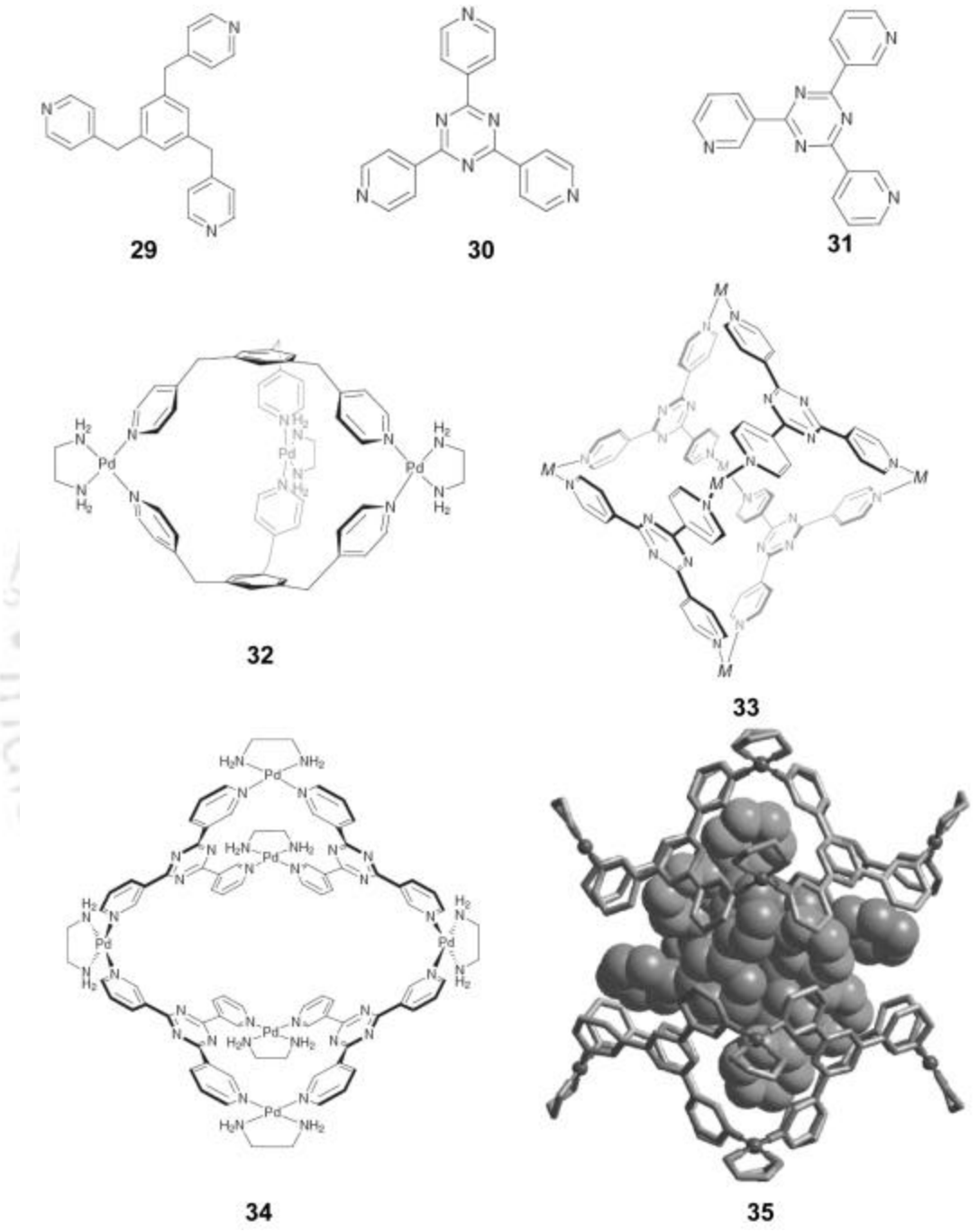

Figure 1.5 Complexes based on tris(pyridine) and tris(primidine) ligands

1.6 Enantiomeric separation using chiral metal center

Kim *et al*. prepared a homochiral metal-organic porous material **38** (Figure 1.6),[4] that allows the enantioselective inclusion of metal complexes in its pores and catalyses a transesterification reaction in an enantioselective manner. To prepare the large homochiral metal-organic porous material, they have used chiral trinuclear clusters **37** as building blocks. The metal-organic clusters are obtained from the enantiopure chiral organic building block **36**, which could easily be synthesized from D-tartaric acid, followed by reaction with Zn^{2+} ions to produce the homochiral open-framework solid **37**.

Chin and co-worker designed a Co(III) based metal complex **40** (Figure 1.6) with the tetradentate ligand **39**. The complex binds more tightly with the D-forms of amino acids. With alanine the complex showed both regiospecific and stereospecific behavior. The regiospecificity is controlled by electrostatic effects while the stereospecificity is controlled by steric effects **41**.[52]

Vagg *et al*. prepared a *L*-α-[Co(*S*,*S*-picchxnMe$_2$)Cl$_2$]$^+$ (*S*,*S*-picchxnMe$_2$ is *N*,*N*'-dimethyl-*N*,*N*'-di(2-picolyl)-1*S*,2*S*-diaminocyclohaxane) complex, which reacts with the α-amino acids prioline, alanine or 2-amino-2-methylpropandioic acid (AMMAH$_2$), the two chloride ions are replaced by the O, N-bidentates with retention of configuration at the metal center. The steric environment generated by the metal complex is shown to enantiospecifically discriminate in favour of *S*-proline from a racemic mixture due to the steric requirements of this amino acid. With the less bulky alanine and AMMAH$_2$ ligands there is no enantiomeric preference observed upon their coordination. When the mixed diastereoisomeric *L*-α-[Co(*S*,*S*-picchxnMe$_2$)(AMMAH)]$^{2+}$ precursors were decarboxylated under warm acidic conditions, no isomer of alanine was found to predominate in the product.[53]

Comba *et al.* introduced the separation of racemic mixtures based on stereoselective ligand exchange reactions specifically involving coordination of chiral substrate molecules to a chiral matrix host. For this purpose he prepared the ligand **42**, **43** and **44** and used two metal centers Co(III) and Ni(II).[54,55]

Kubo *et al*. synthesized a chiral calix[4]crown **45**, which contains an optically active 1,1'-binaphthyl subunit and two indophenol chromophores. Chromophores were introduced to serve as a visually detectable sensor for certain stereogenic guests.

Compound **45** gives red color solution at 515.5 nm in ethanol, when (*R*)-phenylglycinol **46** was added color changed to blue-violet, with the appearance of two new bands at 538 nm and 652.5 nm. Similar experiment was performed with the (*S*) isomer and the color of the solution did not change. [56]

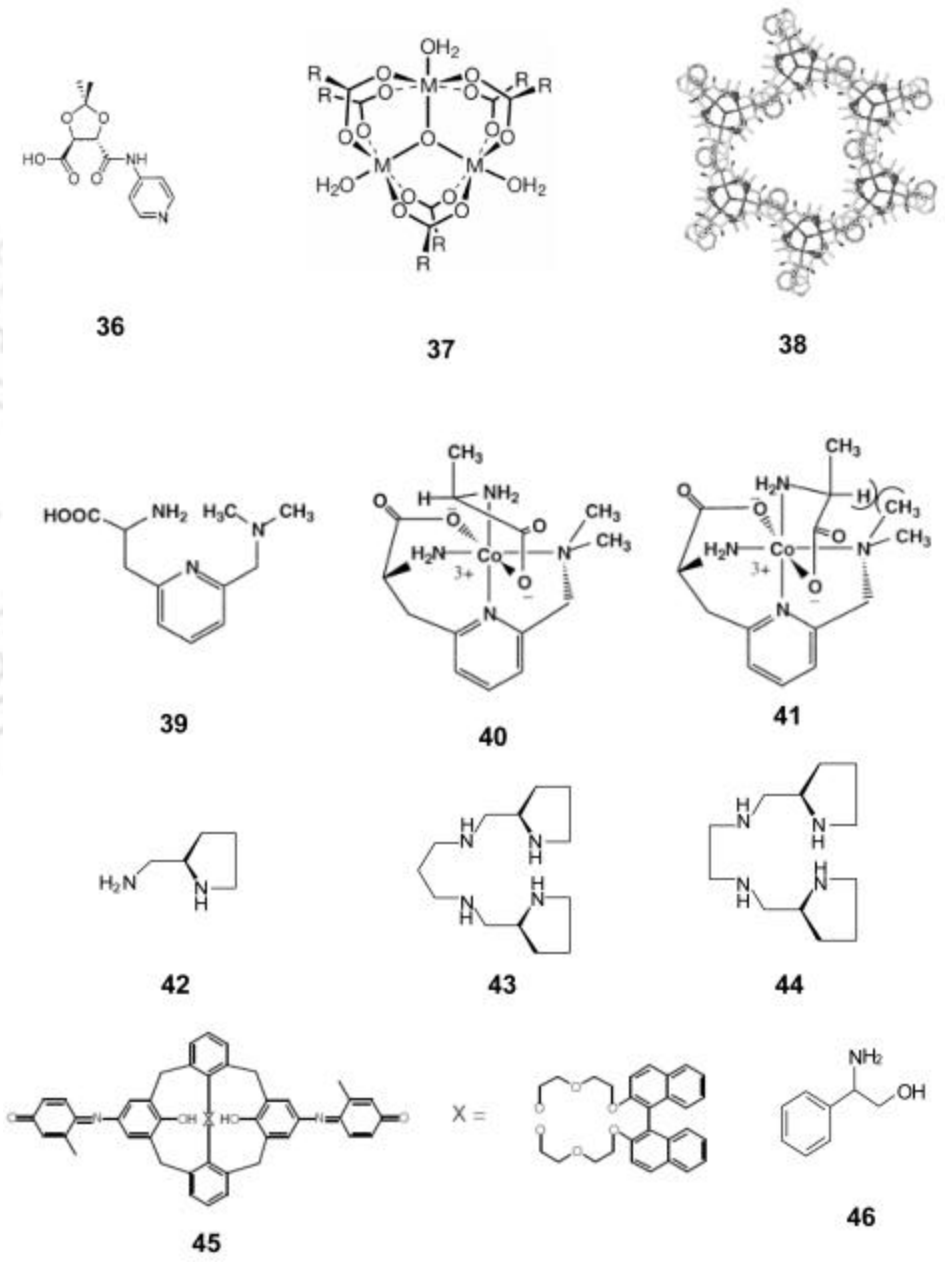

Figure 1.6 Chiral metal complexes

Separation or recognition of racemic mixtures based on stereoselective ligand exchange reactions specifically involves coordination of chiral substrate molecules to a chiral matrix host. The relative stabilities of the diastereomeric adducts at equilibrium determines the degree of selectivity. So it is possible to separate the enantiomer by the chiral host complexes.

1.7 Cavity with Schiff bases

Matsumoto and co-worker used multidentate Schiff base ligands, containing imidazole groups with potential donor and accepter character in the formation of coordination bond as well as hydrogen bond with the Cu(II) metal ion.[57] They can function as a ligand-complex or as a self-complementary building block for the construction of the assembly structure with the formation of a coordination bond or hydrogen bond. In such self-complementary complexes, the monomers **47** and **49** (Figure 1.7) was stabilized as a protonated species under acidic conditions. Under appropriate basic conditions the generated imidazolate nitrogen atom coordinates to the Cu(II) ion of the adjacent unit or hydrogen-bonded to the imidazole group of the adjacent unit to give assembled structures in the crystals, depending on the ligand framework and the preferred coordination number of the Cu(II) ion **48** and **50** (Figure 1.7). The inter conversion between the monomer and the self-assembled oligomer is reversible with pH adjustment.

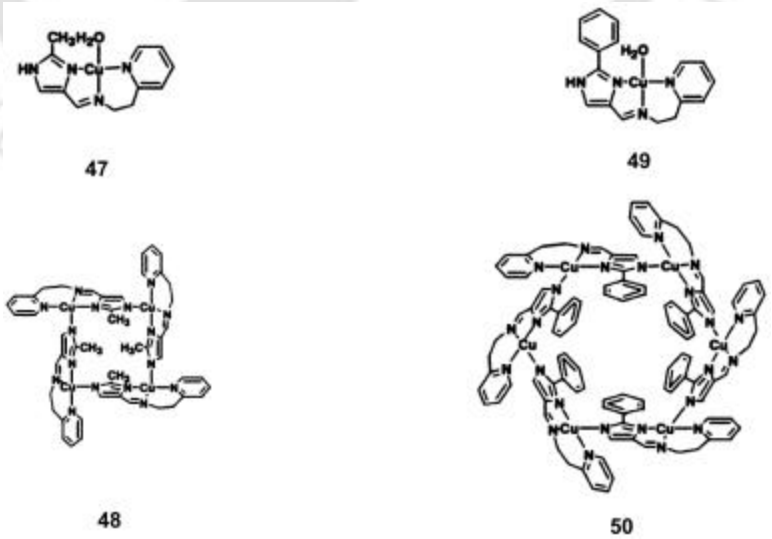

Figure 1.7 Schiff-base metal complexes with cavity

1.8 Definition of the problem

Discussions in the previous sections revealed that (a) metal complexes form a variety of cage structures with different shapes and cavity sizes,[18] (b) large molecular cage structures can be successfully synthesized from low molecular weight metal complexes using self-assembly process,[48] (c) H-bonding can be utilized effectively in the cage formation[36] specially in case of organic superstructure.

Discussion in the previous section identified lack of literature on

1) Molecular cages with redox active metal with available binding site inside the cavity
2) Easily synthesizable enantiomerically pure molecular cages.

1.9 Objectives of the thesis

Our objectives in this thesis are:

1) To synthesize chiral metal complexes in the enantiomerically pure form
2) To form large chiral molecular assembly with available binding site for guest molecules, from the low molecular weight metal complexes
3) To understand the assembly process and stability of the cages in solution

In this thesis we have presented the design and synthesis of four enantiomerically pure ligands derived from chiral amino acids and explored the coordination property of the ligands with transition metal complexes. In the course of study we have synthesized and structurally characterized a nano-sized capsular cavity, a microporous crystal with empty helical channels and binuclear Ni(II) complexes with chiral cavity.

Chapter II

Ligand Synthesis

In this chapter we have discussed the rational behind our choice of ligand and present the synthesis and characterization of the ligands. Conformational preference of the ligands in solution was identified analyzing the ^{1}H NMR spectra of the ligands.

2.1 Choice of ligand

In our approach to make chiral metal complex assembly capable of recognizing one enantiomer over other we needed ligands satisfying the following criteria

- Ligand should be enantiomerically pure to avoid difficult separation of racemic metal complex.
- Ligand should have less than five donor atoms to avoid filling all the coordination sites in the metal ion (usually six donor for octahedral or five for square pyramidal needed to complete the coordination). Filling all the coordination sites will prevent guest binding and large assembly formation.
- Ligands should be designed such that in octahedral metal complex involving the ligand, two vacant coordination sites should be *cis* to each other, as vacant sites in trans position will allow linear polymer formation.
- Ligand should preferably have H-bond donor and acceptor sites so that self-assembling into larger molecular assembly can be achieved.
- Based on these criteria we have chosen two amino acids (histidine and methionine) derived ligands. The histidine-derived ligand is shown below.

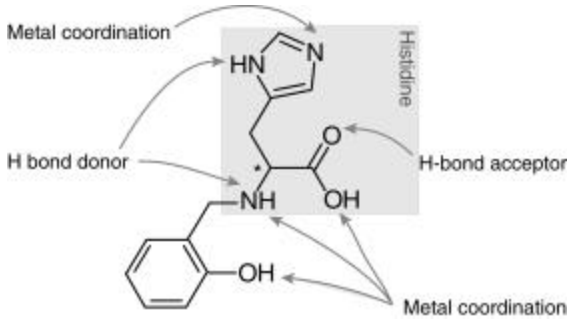

Figure 2.1 Histidine-derived ligand

The advantages of the present ligands are

- The natural amino acids are available in pure enantiomeric form and rather cheap
- The ligands have four coordination sites
- Non-planarity of the ligand indicates that in an octahedral coordination with a metal ion, two coordination sites in the *cis* position will remain vacant
- The ligands have several possible H-bond donor/acceptor sites
- The synthetic procedures for the ligands (Scheme 2.I) are easy and could be synthesized in a bulk amount.

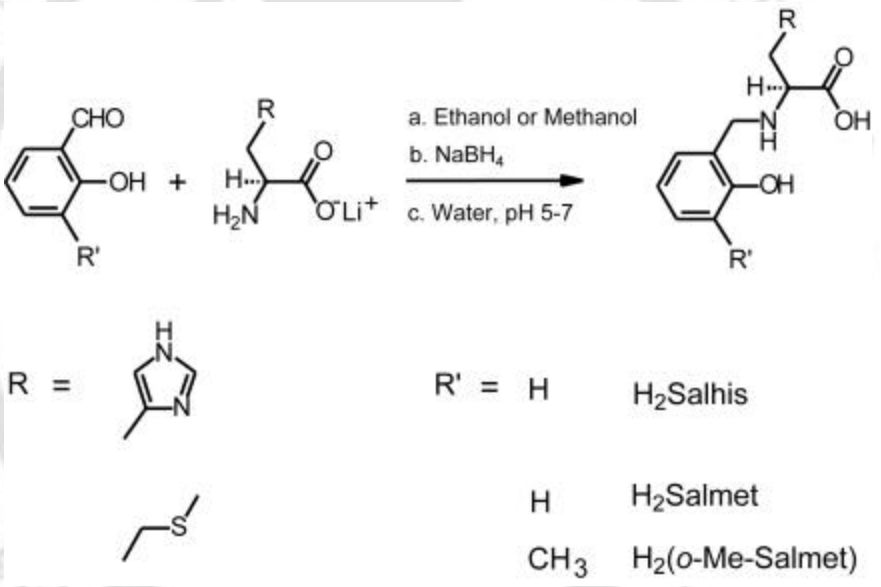

Scheme 2.I Syntheses of ligands

2.2 Literature on the metal complexes of the ligands chosen in this work

Transition metal complexes of Schiff base ligands synthesized from chiral or racemic amino acids and salicylaldehyde have been well explored.[58,59] However, the reduced Schiff bases ligands derived from amino acids are few.[60,61] Two ligands used in this thesis were mentioned as part of a series of skin care product formulation patent.[62] Structural aspects of two complexes based on the amino acid derived reduced Schiff base

ligands have been reported till date, one is a Co(III) complex with *N*-(2-Hydroxybenzyl)-L-histidine[63] ($Salhis^{2-}$) and the other one is a Cu(II) complex with [*N*-(2-pyridylmethyl)-L-histidine][64] .

Although the synthesis of the ligand *N*-(2-Hydroxybenzyl)-L-histidine and its pharmaceutical activities have been explored long back, very little studies have been made on the complexation of these reduced Schiff bases with different metal centers. That has led to our anxiety to explore the under anticipated *N*-(2-Hydroxybenzyl)-L-histidine and *N*-(2-Hydroxybenzyl)-L-methionine ligands complexation capability with various metal centers and their self-assembly behavior in different environments.

2.3 Experimental Section

2.3.1 Solvents and Reagents

Solvents and reagents were obtained from commercial sources and used without further purification unless otherwise stated. Methanol (MeOH) was distilled over magnesium methoxide [$Mg(OCH_3)_2$]. Ethanol (EtOH) was distilled over magnesium ethoxide [$Mg(OCH_2CH_3)_2$]. Diethyl ether (Et_2O) was dried first with anhydrous calcium chloride ($CaCl_2$) and then refluxed with metal sodium wire and finally distilled and kept over sodium wire. $CHCl_3$ was purified by washing with saturated sodium bicarbonate solution, followed by washing five to six times with water and finally kept over anhydrous $CaCl_2$ for 24 hour and distilled. Hexane and ethyl acetate were distilled before use. *o*-Cresol was purified by distillation under reduced pressure. All amino acids were brought from Sisco Research Laboratories Pvt. Ltd. (SRL), India, and were used without further purification.

2.3.2 Measurements

The IR spectra were recorded on a Nicolet Impact 410 FT-IR spectrophotometer with KBr discs in the range 4000-400 cm^{-1} and electronic spectra on a Shimadju U-2001 spectrophotometer. The electrospray ionization mass spectra (ESI-MS) and ^1H NMR spectra were recorded on a Micromass Quattro II triple Quadrupole Mass Spectrometer and a Bruker 300 MHz instrument respectively at Central Drug Research Institute, Lucknow, India. For ESI-MS the methanolic solution of the sample were introduced into

the ESI source through a syringe pump at the rate of 5 mL per min. The ESI capillary was set at 3.5 kV and the cone voltage was 40 V unless stated otherwise. The mass spectra were collected in 6 s scans and were averaged over 6-8 scans. The optical rotations of the methanolic solutions were measured either on Perkin-Elmer 343 or Rudolf Autopol III polarimeter.

2.4 Syntheses of ligands

2.4.1 *S*-2-(2-Hydroxy-benzylamino)-3-(1H-imidazole-4-yl)-propionic acid [(*S*)-H_2Salhis] (1)

A mixture of L-histidine monohydrochloride monohydrate (0.800 g, 3.81 mmol) and LiOH· H_2O (0.323 g, 7.70 mmol) in 15 mL dry ethanol was warmed to dissolve most of the histidine. To this solution, ethanolic solution of 2-hydroxy-benzaldehyde (Salicylaldehyde) (0.47 gm, 3.84 mmol) was added drop wise with constant stirring. Small quantity of white precipitate formed initially which was dissolved to give a clear bright yellow solution after 15 min. Spectroscopic investigations of the imine formed resulted in the following observations: IR (KBr, cm^{-1}) ν(C=N) 1634(s), ν $(COO)_{assym}$ 1609(sh), ν $(COO)_{sym}$ 1416; UV-visible (EtOH, nm) 255, 280(sh), 317, 404. The yellow solution was treated with sodium borohydride (0.072 g, 1.91 mmol) with constant stirring upon which the solution became colorless. The solvent was evaporated under reduced pressure and the sticky solid was dissolved in 20 mL of warm water. A clear solution was obtained. The solution was acidified with dil. HCl (pH~5-7). The ligand was precipitated as a white solid. The solution was filtered and the residue was washed thoroughly with water. The solid was dried in the oven at ~90°C for 3-4 hour (yield 0.790 gm, 80%). IR (KBr, cm^{-1}): $\nu(COO)_{assym}$ 1604(s); $\nu(COO)_{sym}$ 1388(s). $[a]_{589}^{25}$ = –75° in MeOH, c = 0.77, (c in gm/100 ml) in presence of 2 equivalent LiOH· H_2O.

2.4.2 *R*-2-(2-Hydroxy-benzylamino)-3-(1H-imidazole-4-yl)-propionic acid [(*R*)-H_2Salhis] (2)

Ligand [*R*-2-(2-Hydroxy-benzylamino)-3-(1H-imidazol-4-yl)-propionic acid] was synthesized by the same procedure (Section 2.4.1) as mentioned above. D-histidine monohydrochloride monohydrate was taken instead of L-histidine monohydrochloride

monohydrate. Ligand yield was 70%. IR (KBr, cm^{-1}): $\nu(COO)_{assym}$ 1604(s); $\nu(COO)_{sym}$ 1388(s). $[\alpha]_{589}^{25}$ = + 74° in MeOH, c = 0.77, in presence of 2 equivalent LiOH· H_2O.

2.4.3 *S*-2- (2-Hydroxy-benzylamino)-4-methylsulfanyl-butyric acid [(*S*)-H_2Salmet)] (3)

A mixture of L-methionine (1.00 gm, 6.71 mmol) and LiOH· H_2O (0.284 gm, 6.77 mmol) in methanol (dry, 30 mL) was stirred for 30 min. Salicylaldehyde (0.820 gm, 6.72 mmol) in methanol was added slowly drop by drop. After stirring for 20 min. clear yellow color solution was obtained. UV-Visible spectra in methanol showed characteristic peaks at 258 nm, 317 nm, 405 nm, whereas IR of the imine showed characteristic bands as follows, (KBr, cm^{-1}): ν(C=N) 1645(s) $\nu(COO)_{assym}$ 1604(s), $\nu(COO)_{sym}$ 1430. The yellow color solution was treated with sodium borohydride (0.248 gm, 6.71 mmol) with constant stirring upon which the solution became colorless (UV-visible in MeOH, 276 nm). The solvent was evaporated by rotary evaporation. The sticky material was dissolved in water. Clear solution was obtained, which was acidified with dilute HCl (pH 5-7). White solid ligand was precipitated, solution was filtered off and residue was thoroughly washed with water. The solid was dried under reduced pressure (yield 1.45 gm, 80%). IR (KBr, cm^{-1}) $\nu(COO)_{asym}$ 1615(s); $\nu(COO)_{sym}$ 1430(m). $[\alpha]_{589}^{25}$ = – 42° in MeOH, c = 0.77, in presence of 2 equivalent LiOH· H_2O.

2.4.4 2-Hydroxy-3-methylbenzaldehyde

2-Hydroxy-3-methylbenzaldehyde was synthesized from *o*-cresol following the literature procedure.[65] The *o*- product being steam volatile was distilled along with the water from the mixture whereas the *p*- product remained in the original mixture. The distillate was extracted with diethyl ether and dried using anhydrous sodium sulfate. 2-Hydroxy-3-methylbenzaldehyde was isolated as a liquid along with unreacted *o*-cresol. Pure product was obtained after passing through the silica gel column with 5% ethylacetate / hexane (yield 20%). ^{1}H NMR ($CDCl_3$, 300 MHz, ppm), 2.33 (-C**H**$_3$, s, 3H), 6.3 (*m*-benzaldehyde, t, *J*=7.2 and 7.5 1H), 6.82 (*p*-benzaldehyde, d, *J*=7.2, 1H), 6.89 (*o*-benzaldehyde, d, *J*= 7.5 1H), 9.86 (phenolic -O**H**, s, 1H), 11.26(-C**H**O, s, 1H).

2.4.5 *S*-2-(2-Hydroxy-3-methyl-benzylamino)-4-methylsulfanyl-butyric acid [*o*-Me-(*S*)H_2Salmet] (4)

A mixture of L-methionine (0.553 gm, 3.71 mmol) and LiOH· H_2O (0.156 gm, 3.72 mmol) in 15 mL dry methanol was stirred for 30 min. 2-hyrdoxy-3-methylbenzaldehyde (0.505 gm, 3.71 mmol) was added slowly drop by drop with constant stirring. After 30 min. clear yellow color solution was obtained (UV-visible in MeOH, 258 nm, 317 nm, 405 nm; IR of the imine (KBr, cm^{-1}): ν(C=N) 1645(s) $\nu(COO)_{assym}$ 1604(sh), $\nu(COO)_{sym}$ 1430). The yellow color solution was treated with sodium borohydride (0.137 gm, 3.69 mmol) with constant stirring, immediately the solution became colorless (UV-visible in MeOH, 276 nm). Solvent was evaporated on a rotary evaporator. The sticky material obtained was dissolved in water. Clear solution was obtained, which was neutralized with dilute HCl (pH 5-7). The ligand was precipitated as white solid, solution was filtered off and residue was thoroughly washed with water. The white solid product was dried under reduced pressure (yield 0.750 gm, 75%). IR (KBr, cm^{-1}) $\nu(COO)_{asym}$ 1615; $\nu(COO)_{sym}$ 1398. $[a]_{589}^{25} = -40°$ in MeOH, c = 0.77, in presence of 2 equivalent LiOH· H_2O.

2.5 Syntheses and Selected Properties

All the ligands were synthesized by reducing the Schiff base formed in the solution by condensation of salicylaldehyde or ring substituted derivative of salicylaldehyde with the appropriate deprotonated amino acids. The reducing agent used is $NaBH_4$. The formation and reduction of Schiff bases were monitored using the appearance of a characteristic ν(C=N) stretches between 1645-1634 cm^{-1} in the infrared (IR) spectra as well as the yellow color of the solution after the addition of aldehyde followed by the disappearance of the ν(C=N) stretches and the yellow color after the

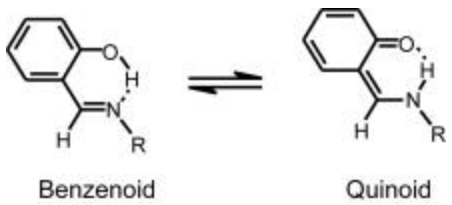

Scheme 2.II Tautomeric equilibrium of keto-enol form

reduction. The strong yellow color of the Schiff bases are due to the intense absorption at ~ 400 nm (Figure 2.2) attributed to the tautomeric equilibrium of the kind shown in Scheme 2.II. Upon substitution of the reaction medium from MeOH to EtOH, the Shiff base precipitates as yellow solid.

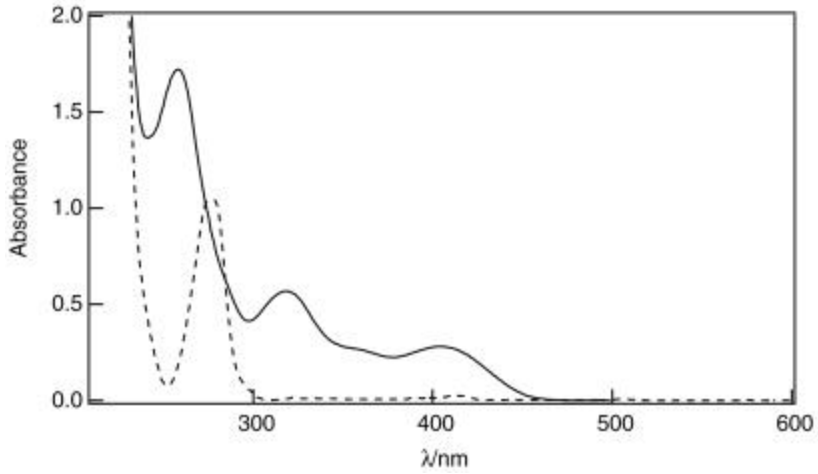

Figure 2.2 UV-visible spectra of ligand (*S*)-H_2Salhis, before reduction (——), after reduction (· · · · · · · · ·)

All the ligands precipitated almost quantitatively at neutral pH (5-7) and are insoluble in water and almost all the common organic solvents. The IR spectra of the ligands showed the asymmetric carboxylate stretching between 1604-1595 cm^{-1}, symmetric carboxylate stretching between 1408-1397 cm^{-1} and a peak at 3119 cm^{-1} for secondary amine ν(N-H) (Experimental Section). The elemental analyses of the ligands (Table 2.A), mass spectra (Table 2.B) and ^{1}H NMR data (next section) of the lithium salt of the ligands support the purity and the identity of the ligands.

Table 2.A Microanalytical Data[a] of ligands

Ligands	Empirical Formula	% C	% H	% N
1	$C_{13}H_{15}N_3O_3$	60.19 (59.76)	5.95 (5.79)	16.19 (16.08)
3	$C_{12}H_{17}NO_3S$	55.92 (56.44)	6.74 (6.71)	5.37 (5.48)
4	$C_{13}H_{19}NO_3S$	57.71 (57.96)	7.23 (7.11)	5.15 (5.20)

[a] Value in parentheses are calculated ones

Table 2.B ESI-MS (–) of the ligands

	1	**2**	**3**	**4**
$(L\text{-}H)^-$	260	260	254	268
$(L)^{2-}Li^+$		266		274

Purity of the ligands were checked by ^1H NMR spectral measurements (Section 2. 3. 2) A representative ^1H NMR spectrum of the ligands Li_2[(*S*)-(Salhis)]and Li_2[(*S*)-(Salmet)]are shown in Figure 2.4 and Figure 2.5 respectively.

2.6 ^1H NMR Spectra

As none of the ligands were soluble in common deuterated solvents in the neutral form, the ^1H NMR spectra were recorded for dilithium salt prepared from neutral ligand and two equimolar $LiOH\cdot H_2O$. The dilithium salts were highly soluble in CD_3OD. All the deprotonated ligands showed sharp, well resolved resonances. All the assignments were based on the peak positions, splitting patterns and integrations (Table 2.C). The coupling constants and chemical shifts of the protons showing multiplets were calculated through computer simulation[66] with manually calculated values as a starting point. The final simulated peak positions are within 0.002 ppm of the recorded spectra.

Aromatic protons (H^a- H^d): Aromatic protons were identified from their position (6-7 ppm) and splitting pattern. The aromatic protons in the ligands showed overall increase in shielding effect with resonances in the range of 6.3 – 7 ppm compared to the values of 2-methyl phenol[67] in $CDCl_3$ (6.7-7.1 ppm). 2-Methyl phenol is similar to the aromatic fragment present in the ligands. The increase in shielding effect is most pronounced in *p*-proton (6.69 ppm in 2-methyl phenol). This is possibly due to the negative charge on the deprotonated ligands compared to the 2-methyl phenol.

Benzyl methylene protons (H^e and $H^{e'}$): Benzyl methylene protons in all the ligands show strong geminal coupling with coupling constants of 11.4-12 Hz due to the presence of chiral center. The $\Delta\nu/J$ value, which indicates the difference of environment of the diastereotopic protons, are 10 to 11.8 in case of the present ligands. This is much higher compared to the $\Delta\nu/J$ values of 2-6 reported for a group of reduced Schiff base ligands derived from salicylaldehyde and alanine, leucine and isoleucine.[60] The higher $\Delta\nu/J$

value in the present case indicates the greater diastereotopic environment in the present set of ligands.

Table 2.C ^{1}H NMR of the ligands

	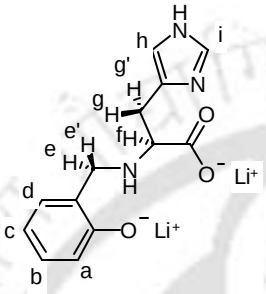	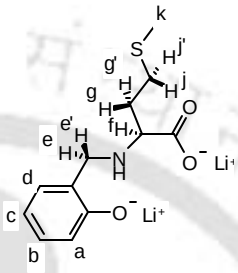	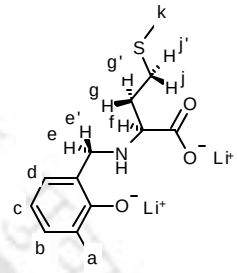
	$Li_2[(S)$-(Salhis)$]^{-2}$	$Li_2[(R)$-(Salhis)$]^{-2}$	$Li_2[(S)$-(Salmet)$]^{-2}$	$Li_2[o$-Me-(S)-(Salmet)$]^{-2}$
H^a	6.59	6.63	6.65	(ar-Me) 2.15
H^b	6.92	6.95	6.97	6.89
H^c	6.35	6.37	6.44	6.36
H^d	6.82	6.86	6.97	6.81
H^e	3.31	3.35	3.44	3.45
$H^{e'}$	3.77	3.80	3.83	3.87
H^f	3.28	3.31	3.19	3.18
H^g	2.71	2.75	1.86	1.88
$H^{g'}$	3.04	3.07	1.97	1.99
H^h	6.81	6.85	-	-
H^i	7.54	7.57	-	-
H^j	-	-	2.57	2.57
$H^{j'}$	-	-	2.57	2.57
H^k	-	-	2.06	2.06
$J_{a,b}$	8.1	8.1	8.7	-
$J_{a,c}$	0.9	n.o	-	-
$J_{b,d}$	1.8	1.5	-	n.o
$J_{b,c}$	7.2	7.2	7.2	7.5
$J_{c,d}$	7.5	7.5	7.2	7.2
$J_{e,e'}$	11.7	11.4	11.7	12
$J_{f,g}$	3.6	3.9	7.9	6
$J_{f,g'}$	9.9	9.6	7.6	5.7
$J_{g,g'}$	14.7	14.7	14.3	14.1
$J_{g,j}$	-	-	7.3	7.8
$J_{g',j'}$	-	-	5.5	7.8

[a]n.o = not observed

Amino acid fragments: Due to the presence of chiral center in the carbon atom bonded to the H^f, the diastereotopic methylene protons next to it (H^g, $H^{g'}$) shows strong geminal coupling (Jgg' ~ -14Hz). Effect of the chiral proton diminishes with the intervening carbon atom and geminal coupling was not observed in the second methylene protons (H^j and $H^{j'}$) in case of methionine-derived protons. The proton NMR spectrum of histidine at various pH was analyzed thoroughly in the past[68,69]. It was concluded that the difference in coupling constant of the methylene protons with that of the chiral proton ($J_{f,g}$ = 4.5 Hz and $J_{f,g'}$ = 8.7 Hz) in histidine indicates a gauche-trans conformation as the preferred conformation of histidine in alkaline solution [Figure 2.3 (b)]. The difference in coupling constants ($J_{f,g}$ =3.6 Hz, $J_{f,g'}$ = 9.9 Hz) in histidine derived ligand H_2Salhis are very similar to that reported for histidine. Thus the histidine fragment of the ligand retains their preferred *gauche-trans* conformation in methanolic solution. We have not come across any such analysis on methionine in literature but almost identical coupling constants ($J_{f,g}$ =7.9 Hz, $J_{f,g'}$ = 7.6 Hz) in methionine derived ligand suggest either a symmetrical conformation [Figure 3.1(b)] or existence of several interconverting conformer which negates the observable difference.

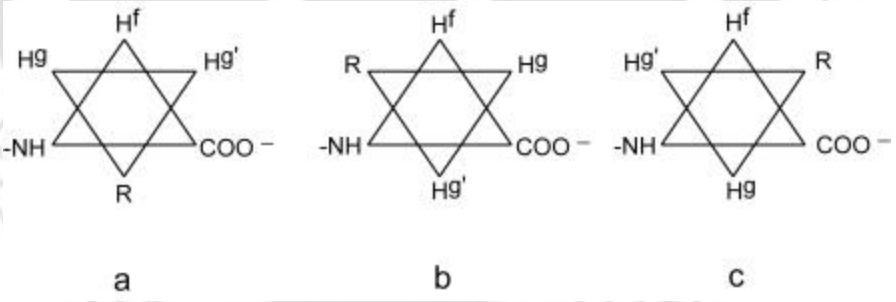

Figure 2.3 (a) Gauche-φ (COO^-/R =60°) (b) Gauche – trans φ (COO^-/R =180°) (c) Gauche-φ (COO^-/R =300°)

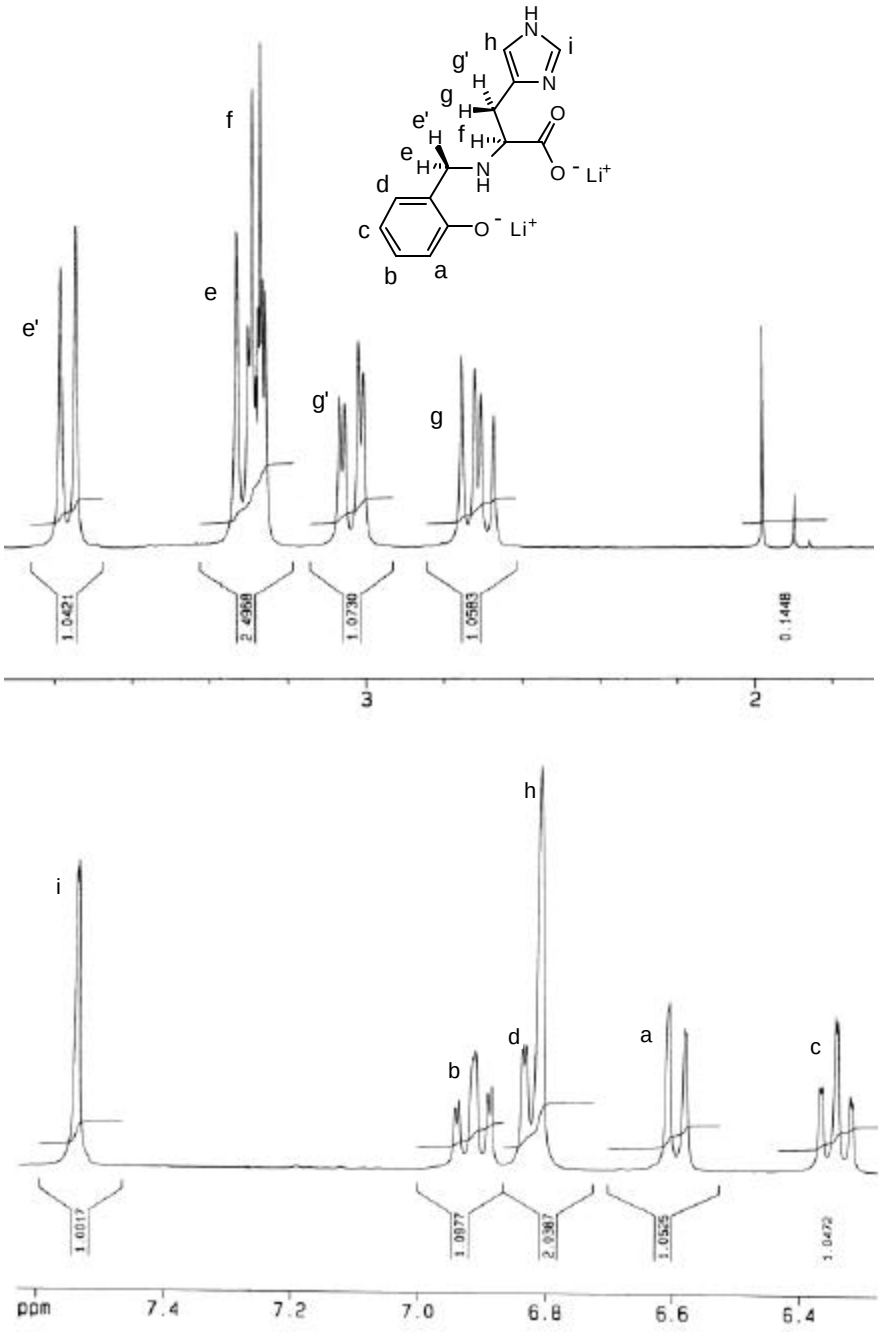

Figure 2.4 ^{1}H NMR of the ligand $Li_2[(S)\text{-(Salhis)}]^{-2}$ in CD_3OD

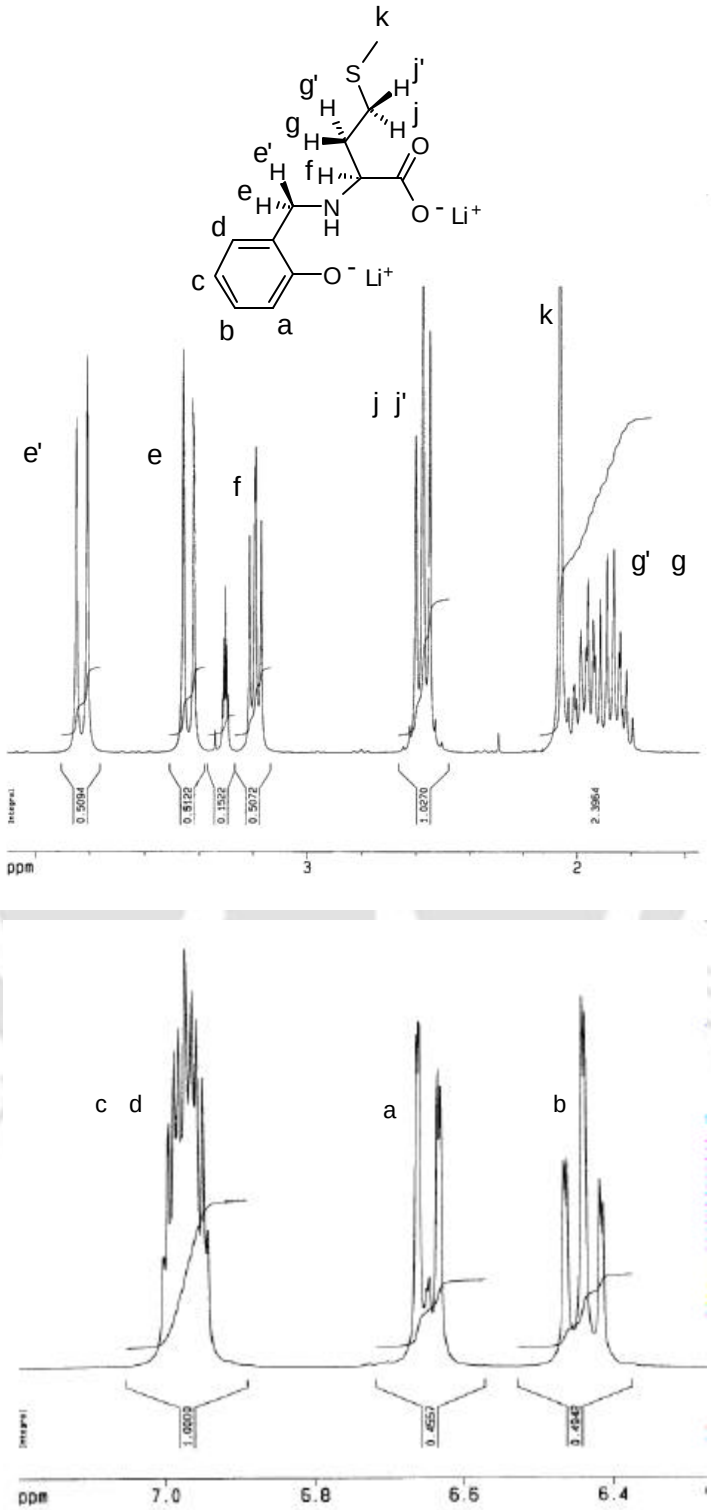

Figure 2.5 ^{1}H NMR of the ligand $Li_2[(S)\text{-(Salmet)}]^{-2}$ in CD_3OD

Conclusions

(1) These ligands are enantiomerically pure, as we have started with the enantiomerically chiral amino acid histidine and methionine.

(2) Ligands has the donor analogous to the most commonly protein residue His, Tyr and Asp.

(3) Ligands have four coordination site, leave two *cis* site vacant in octahedral complex.

(4) Ligands have both soft and hard donor site present.

(5) Most interesting point ligands have both H-bond donor and acceptor groups. So, inter-molecular H-bonding may be played an important role in the formation of molecular crystal.

(6) Ligands donor side is easily replaceable by changing the amino acid groups.

Chapter III

Synthesis and solution properties of a self-assembled molecular capsule with copper (II) complex

Synthesis of molecules and molecular assemblies with cavities of different size and shape to encapsulate guest molecules have been a subject of active research in view of their potential use as selective host for anion sensing, catalysis, selective recognition and separation of guest molecules.[10,18,70] Rebek, Jr. and coworkers recently demonstrated that reagent binding inside a capsular cavity boosts Diels-Alder reaction rate.[28] Self-assembly of relatively small molecules through hydrogen bonding and metal-ligand interaction are proved to be very useful in forming large capsular cavity.[10,18,70] On the other hand Fujita *et al.* explored the intermolecular [2+2] photochemical reaction and control the stereo-and regiochemistry of olefins with self-assembled coordination cages.[71] While several capsular cavities have been synthesized using organic framework (e.g. resorcinarene, calixarene),[10,18,70] as well as coordination complexes with redox stable metal center[11] and a few with redox active metal center, [44-47] there is no report of a capsular cavity with the redox active metal center having available binding site inside the capsule. Synthesis of capsular cavity with available coordination site at redox active metal centers inside the pocket can, in principle, facilitate study of reactivity of the bound guest inside a cavity. In our effort to synthesize capsular cavity with redox center, we have synthesized a self-assembled capsule of octameric Cu(II) coordination complex using the ligand [(*S*)-H_2Salhis].

3.1 Experimental Section

3.1.1 Solvents and Reagents

Diethyl ether (Et_2O) was dried first with anhydrous calcium chloride ($CaCl_2$) and then refluxed with sodium metal using benzophenone (as a indicator) and distilled over sodium metal wire. Pyridine (Py) was refluxed over KOH and then distilled with careful exclusion of moisture. *N, N*-Dimethylformamide (DMF) was purified first by azeotropic distillation with benzene followed by shaking with alumina (neutral) and finally by vacuum distillation. Tetra-n-butylammonium perchlorate (TBAP) was prepared from tetra-n-butylammonium bromide and 70% aqueous perchloric acid. Details of solvent purification and starting materials other than that stated above are already discussed in Chapter 2 (Section 2.3.1). The ligand [(*S*)-H_2Salhis] preparation was described in previous chapter 2 (Section 2. 4. 1).

3.1.2 Measurements

The thermogravimetric analysis of the compounds were performed by using an SDTA 851^e TGA thermal analyzer (Mettler Toledo) with a heating rate of 5° C per min. in a N_2 atmosphere using a sample size of 5-10 mg per run.

Solid-state magnetic susceptibility of the complexes at room temperature was recorded using Sherwood Scientific balance MSB–1. Variable-temperature (80 to 300 K) solid-state magnetic susceptibility measurements were recorded by the Faraday technique using a locally built magnetometer at IIT Kanpur, India. The magnetometer consists of an electromagnet with constant gradient pole caps (polytronic Corporation, Mumbai, India), Sartorius M25-D/S balance (Germany), a closed cycle refrigerator and a Lake Shore temperature controller (Cryo Industries, USA). All measurements were made at fixed main field strength of 10 kG.

X-Band EPR spectra were recorded with a Varian E-109 C spectrometer fitted with a quartz dewar for measurements at liquid nitrogen temperature. The spectra were calibrated with DPPH (g = 2.0037)

Cyclic voltammetric measurements were performed on Electrochemical workstation CH660 manufactured by CH Instruments, USA using either glassy carbon or platinum working electrode, platinum wire auxiliary electrode and Ag^+/Ag reference electrode. Calibrated with ferrocene.

Solution electrical conductivity measurements were made with a Systronics Conductivity Meter 306 by using 0.01N KCl solution as calibrate.

Caution! Perchlorate salts are potentially dangerous as explosives and should only be handled in small quantities, although we worked with these ClO_4^- salts without any incident.

3.1.3 X-ray Data Collection, Structure Solution and Refinement

The crystal structures of ($[Cu_8L_8(Py)_{10}]\cdot Py\cdot 3MeOH\cdot (C_2H_5)_2O$) (**1**) and $[Cu(S\text{-}Salhis)]_8\cdot 15H_2O$ (**2**) were obtained by single crystal X-ray diffraction technique. Single crystal of **1** was obtained by slow diffusion of diethyl ether into the pyridine solution of the complex. Single crystal of **2** was grown by slow evaporation of the methanolic solution of the complex. The complex **1** was mounted with mother solvent inside the capillary and **2** on a glass fiber.

All geometric and intensity data for **1** and **2** were collected at room temperature using an automated Enraf-Nonius CAD 4 diffractometer equipped with Mo-Kα radiation (λ = 0.71073 Å). Intensity data, collected using ω–2θ scan mode were corrected for Lorentz – polarization effects and for absorption.[72] Structures were solved by the combination of Direct-method and Fourier techniques and refined by full-matrix least-square method using SHELX system of programs.[73] The intensity data for **1** was collected using a Bruker SMART APEX CCD diffractometer, equipped with a fine focus 1.75 kW sealed tube Mo-Kα X-ray source, with increasing ω (width of 0.3° per frame) at a scan speed of 3 s/frame. The SMART software was used for data acquisition and the SAINT software for data extraction. Absorption corrections were done using SDABS.[74] All non-hydrogen atoms were refined anisotropically. The hydrogen atoms were located from the difference Fourier maps and were refined isotropically. Selected crystallographic data are summarized in Table 3.A. Perspective view of the complex was obtained by ORTEP.[75]

Table 3.A Selected crystallographic data for the complexes

Complexes	**1**	**2**
Empirical formula	$C_{166}H_{181}Cu_8N_{35}O_{28}$	$C_{16}H_{20}CuN_5O_{4.5}$
Formula weight	3622.8	417.91
Temperature	293(2) K	293(2) K
Wavelength	0.71073 Å	0.71073 Å
Crystal system, space group	Triclinic, *P*1	Monoclinic, *P*2(1)
Unit cell dimensions	a = 16.845(4) Å	a = 19.625(12) Å
	b = 18.268(4) Å	b = 9.617(6) Å
	c = 20.167(4) Å	c = 41.56(3) Å
	α = 92.507(4)°	α = 90.00°
	β = 112.207(4)°	β = 92.260(11)°
	γ = 105.636(4)°	γ = 90.00°
Volume	5459(2) $Å^3$	7837(9) $Å^3$
Z, Calculated density	1, 1.102 Mg/m^3	16, 1.417 Mg/m^3
Absorption coefficient	0.8254 mm^{-1}	1.147 mm^{-1}
F(000)	1878	3456
Crystal size	0.3 × 0.3 × 0.2 mm	0.35 × 0.3 × 0.25 mm
Theta range for data collection	1.11 to 27.81°	0.98 to 25.06°

Reflections collected / unique	60205 / 44425 [*R* (int) = 0.0963]	36028 / 26886 [*R* (int) = 0.0794]
Completeness to theta	90.2%	98.3%
Absorption correction	None	None
Refinement method	Full-matrix-block least-squares on F^2	Full-matrix-block least-squares on F^2
Data / restraints / parameters	44425 / 3 / 2046	26886 / 1 / 1904
Goodness-of-fit on F^2	0.730	0.955
Final R indices [*I*>2sigma(*I*)]	*R*1 = 0.0868, *wR*2 = 0.2164	*R*1 = 0.1044, *wR*2 = 0.2324
R indices (all data)	*R*1 = 0.2725, *wR*2 = 0.2890	*R*1 = 0.2080, *wR*2 = 0.2932
Absolute structure parameter	0.021(16)	0.06(2)
Largest diff. peak and hole	0.784 and -0.526 e. A^{-3}	0.847 and -0.664 e. A^{-3}

3.2 Syntheses of Cu(II) complexes

Detailed synthetic methodologies are given below. Analytical data as well as spectroscopic data are in Table 3.B, 3.C and 3.H.

3.2.1 $[Cu_8(S\text{-Salhis})_8 \cdot (pyridine)_4 \cdot 8H_2O]$ (1)

A methanolic solution of $Cu(ClO_4)_2 \cdot 6H_2O$ (0.436 gm, 1.176 mmol) was added drop wise to a clear solution of *S*-H_2Salhis (0.2967 gm, 1.135 mmol) and KOH (0.1344 gm, 2 .4 mmol) in 25 mL of dry methanol . The resulting dark green color solution along with some undissolved white particles was stirred for 30 min. The solution was filtered through a medium-porosity frit, after which the volume of the filtrate was reduced by rotary evaporation and the complex was precipitated by the addition of diethyl ether. The resulting light green powder was filtered off and washed with diethyl ether prior to drying under vacuum in a desiccator (yield: 0.380 gm, 103 %, yield is very high because $KClO_4$ present as a impurity). IR (KBr, cm^{-1}) $\nu(COO)_{asym}$ 1598; $\nu(COO)_{sym}$ 1403, $\nu(ClO_4)$ 1100.

Purification and Recrystallization: Diffusion of diethyl ether into the solution of the complex in pyridine, afforded dark green crystals free from ClO_4^- suitable for X-ray analysis. The single crystal X-ray analysis revealed that the crystal contains eleven pyridine molecules per octanuclear complex but the crystal easily efflorescenced and the elemental analysis agreed with the chemical formula $[Cu_8(C_{13}H_{13}N_3O_3)_8 \cdot (C_5H_5N)_4 \cdot 8H_2O]$, yield: 65 %. IR (KBr, cm^{-1}) í(COO)$_{assym}$ 1615(sh), 1598, í(COO)$_{sym}$ 1388(s).

3.2.2 [Cu(*S*-Salhis)· (Imidazole)]· $2H_2O$ (2)

Complex **1** (0.200 gm, 0.526 mmol) was taken in 20 mL of dry methanol followed by addition of imidazole (0.100 gm, 1.47 mmol) to the methanolic solution. The reaction mixture was refluxed with stirring for 1 hour. Color of the solution was changed light green to deep green. Rotary Evaporation was used to reduce the volume of the solution to ~ 5 mL, the solution was kept for slow evaporation at room temperature. After 48 hours green crystals were formed. The crystals were filtered and washed with methanol and dried in vacuum, in a desiccator. Yield: 0.120gm, (60 %). IR (KBr, cm^{-1}) $\acute{\nu}(COO)_{assym}$ 1601, $\acute{\nu}(COO)_{sym}$ 1396.

3.3 Results and Discussion

3.3.1 Syntheses and Selected Properties

Complex **1** was synthesized using the corresponding ligand with two equivalents of KOH and $Cu(ClO_4)_2\cdot 6H_2O$ in MeOH. The complex **1** retained some amount of $KClO_4$ as impurity. Dissolving impure **1** in pyridine followed by filtration removed the insoluble $KClO_4$ present in the sample.

For the complexes **1** and **2** the IR absorption band around 3420 cm^{-1} confirmed the presence of water molecules in the complexes. For both the complexes, the sharp band in the region 3157-3240 cm^{-1} has been assigned to N-H stretching mode. The IR spectra of the complex **1** $\nu(COO)_{asym}$ band was shifted to higher frequency from $\acute{\nu}(COO)_{assym}$ 1604 cm^{-1} in the ligand to $\acute{\nu}(COO)_{assym}$ 1615 cm^{-1}. We observed that the separation (Δ value) between $\nu(COO)_{asym} - \nu(COO)_{sym}$ (1388 cm^{-1}) are 227 cm^{-1} for complex **1** and 205 cm^{-1} for the complex **2**, which are much greater than the ionic complexes (~ 150 to 200 cm^{-1}). This indicate that the carboxylate groups of the amino acid are bound in a unidentate fashion.[76] The band around 1266-1296 cm^{-1} might be assigned to ν(C-O) of phenolic group.[76]

Elemental analyses of the desiccated sample matched with the formula Cu_8(*S*-Salhis)$_8\cdot$ (pyridine)$_4\cdot$ $8H_2O$ for **1**, and Cu(*S*-Salhis)(Imidazole)$\cdot$ $2H_2O$ for **2** (Table 3.B).

Table 3.B Microanalytical Data[a] of the Cu(II) complexes

Complexes	Empirical formula	% C	% H	% N
1	Cu_8(*S*-Salhis)$_8$· (Py)$_4$· 8H_2O	48.68 (48.94)	4.51 (4.64)	12.92 (12.88)
2	Cu(*S*-Salhis)(Imz)· 2H_2O	45.21 (45.01)	5.20 (4.96)	15.93 (16.40)

Py = Pyridine, Imz = Imidazole, [a] Values in parentheses are calculated ones

The very low molar conductance of the complexes in methanol confirmed the non-electrolytic nature of the complexes[77] (Table 3.C). The room temperature magnetic moment (experimental section) is less than expected for a S=1/2 system 1.73 B.M.[78,79] (Table 3.C) indicating the presence of antiferromagnetic coupling between the Cu(II) centers.

Table 3.C Magnetic moments and Conductance values of the Cu(II) complexes

Complexes	**1**	**2**
μ_{eff}(solid, 298 K); μ_B/Cu	1.63	1.61
Λ_M (MeOH) S cm^{-2} mol^{-1}	2	4

3.3.2 X-ray Structure of crystal 1

The crystallization of the complex **1** from pyridine and diethyl ether afforded deep green crystals of ([Cu_8(*S*-Salhis)$_8$(Py)$_{10}$]· Py· 3MeOH· (C_2H_5)$_2$O). The complex was crystallized in the chiral space group of *P*1(#1) with two slightly different cup shaped tetrameric units (**1a** and **1b**) in the unit cell. The lattice diagram shows that **1a** and **1b** are on the top of each other forming a capsule bound through eight hydrogen bonding interaction between imidazole NH of one tetramer with non bonded carboxylate oxygen of the other tetramer[80,81] (Figure 3.1). The capsule trapped four pyridine molecules inside the cavities. Selected bond distances and angles are listed in Table 3.D

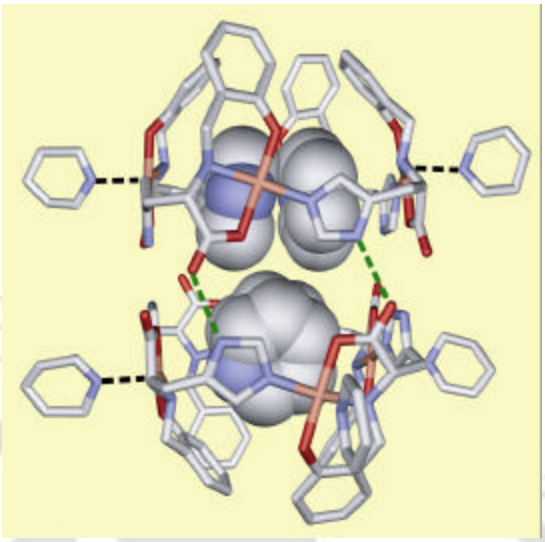

Figure 3.1 Molecular structure of **1**. solvent molecules are omitted for clarity

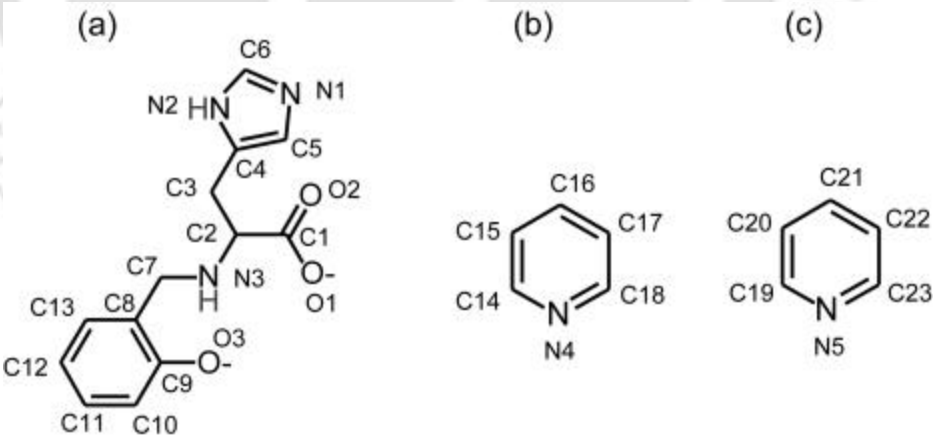

Figure 3.2 Numbering scheme (a) ligand, (b) pyridine out side the cavity, (c) pyridine inside the cavity

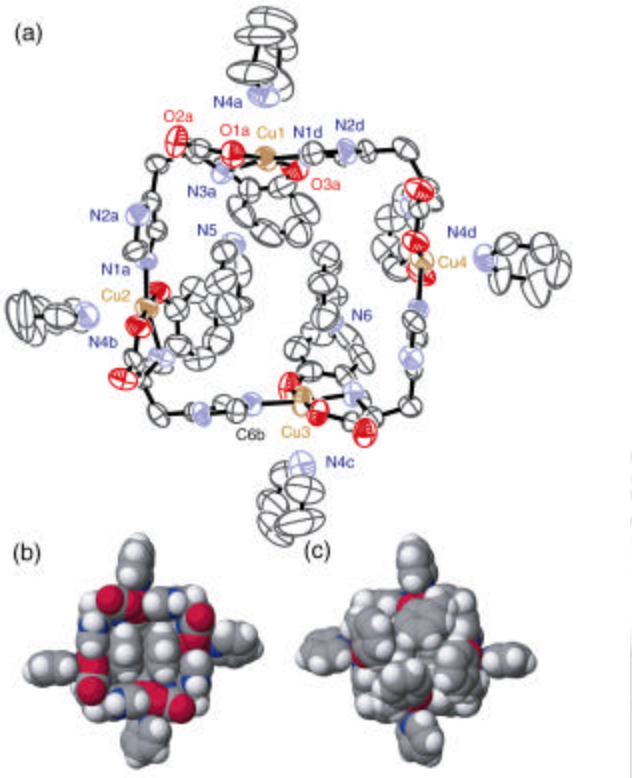

Figure 3.3 (a) One tetrameric copper unit **1a** [$Cu_4L_4Py_6$] ORTEP diagram, thermal ellipsoids set to 50% probability), (b) Space-filling model of **1a** top view and (c) bottom view

The **1a** (Figure 3.3) is a cyclic tetramer with imidazole arm from one monomeric unit coordinated to the next monomeric unit forming the cycle. The coordination geometry around the each Cu(II) center is N_3O_2 donor environment [amine, histidine imidazole, pyridine, phenolate and carboxylate]. Each Cu(II) center is best described as square pyramidal with a trigonal-bipyramidal component τ (Table 3.D) [$\tau = (\beta-\alpha)/60$, with α and β being the two largest coordination angles]. In a perfect square-pyramidal geometry τ equal to 0, while it is 1 in a perfect trigonal-bipyramidal geometry.[82] The four phenolate rings are organized in such a manner to effectively close one side of the square and thus making a cup shaped tetramer (Figure 3.3. c). Two pyridine molecules were trapped inside **1a** side by side, with each N atom of the pyridine facing the amine nitrogen of the ligand. The N (trapped pyridine)-N (amine) distances (N5-N3a 2.990 Å, N6-N3c 3.025 Å) are within the range of 2.68-3.09 Å observed for N…N hydrogen bond

distances.[83,84] The space-filling model clearly demonstrates that the two side-by-side pyridine filled the cavity perfectly [Figure 3.3.(a)].

In **1b** the cyclic tetramer was formed in the same manner (Figure 3.4). However, two sides of the cup bend inwardly. Unlike in **1a**, the trapped pyridines here are coordinated to the Cu(II) center instead of being H-bonded to amines (Figure 3.5). This coordination of pyridine from inside the box to the Cu(II) resulted in the deviation of Cu8 & Cu6 atom from the plane of O1, N3, O3, N1 towards the trapped pyridine (shift of 0.194 and 0.203 Å for Cu8 and Cu6 respectively) and consequently non-coordination of the external pyridines for Cu8 and Cu6 occurs as square pyramidal geometry is preferred for Cu(II) over octahedral geometry due to Jahn-Teller distortion. Thus the coordination sites at the copper centers are accessible from inside.

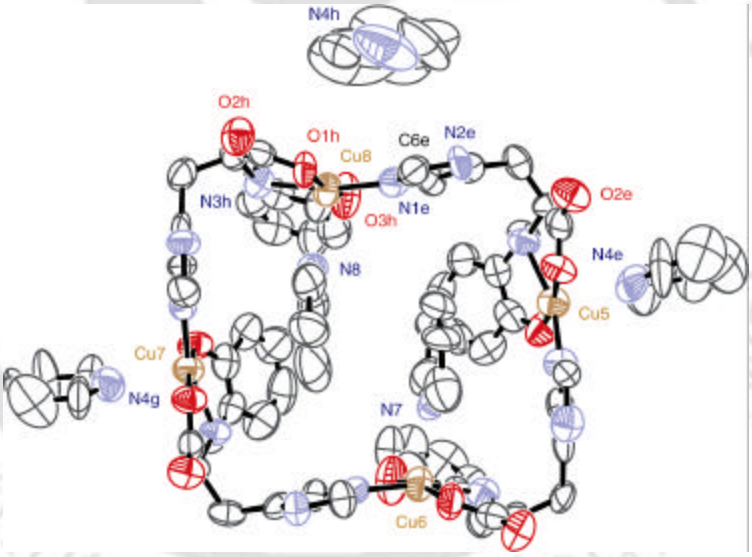

Figure 3.4 Tetrameric copper unit **1b** $[Cu_4L_4Py_4]Py$, ORTEP diagram, thermal ellipsoids set to 50% probability)

Guest binding occurred in the two halves of the capsule differently. In **1a**, Cu1 is coordinated to the external pyridine but not to the trapped pyridine (same for Cu3). On the other hand, in **1b** the pyridine nitrogen (N8) is coordinated to Cu8 (same for Cu6). The N8-N3h (amine) distance of 3.104 Å in **1b** is closer to N…N hydrogen bonding distance range of 2.68 - 3.09 Å (Figure 3.5). Thus the presence of a N-H close to the Cu(II) allow trapped pyridines in **1b** to bind using both metal–ligand interaction and hydrogen bonding simultaneously. This possibly makes the trapped pyridines less labile

compared to the external pyridines as observed in the solution studies (see below). We are not aware of this type of binding in any other reported capsular cavity.

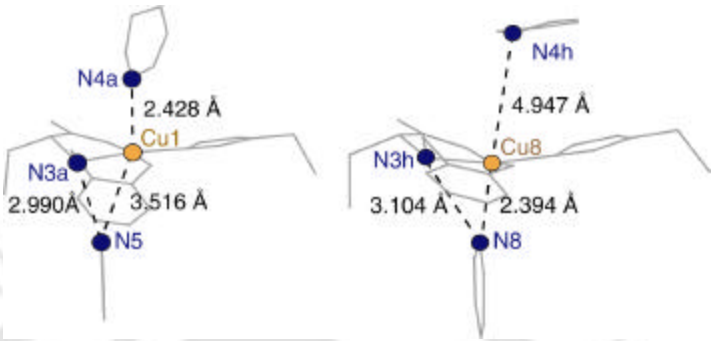

Figure 3.5 Part of the Cu_4L_4 unit of **1a** and **1b** showing the change in bonding interactions between trapped pyridine molecules, amine N atoms, Cu(II) centers, and external pyridine molecules

The Cu-N (external pyridine) distances in molecules **1a** and **1b** (2.4 – 2.5 Å), are considerably longer than Cu-N (apical pyridine) distance of 2.17 Å in [Cu(Cyclops)py] ClO_4[85] and 2.12, 2.13 Å in $Cu_2(acetate)_4(py)_2$,[86] but within the range of 2.6-2.8 Å for apical Cu-N bond distances.[87] This makes the externally bound pyridines particularly labile.

Thermogravimetric analysis: The Thermogravimetric analysis of the sample was performed in order to prove the presence of the solvent as indicated by elemental analysis. TGA of complex **1** (Figure 3.6) shows the loss of 15.1 % of total weight in the 30-110 °C temperature range and 180 - 230 °C temperature range, corresponding to the loss of eight water molecules and four pyridine molecules (expected 16.7 % weight loss). After the temperature of 230 °C the compound starts to decompose.

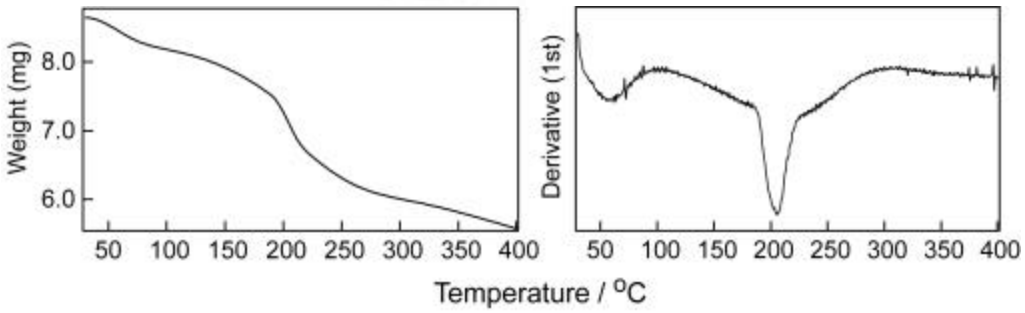

Figure 3.6 TGA and DTA plot of the complex **1**

Table 3.D Selected bond distances (Å) and angles (°) of complex **1**

	Cu1	Cu2	Cu3	Cu4	Cu5	Cu6	Cu7	Cu8
$Cu\text{-}O1_{acetate}$[1]	2.029(7)	1.985(6)	1.989(6)	1.946(6)	2.007(7)	1.989(7)	1.987(6)	1.958(7)
$Cu\text{-}O3_{phenolate}$	1.926(7)	1.910(7)	1.865(7)	1.941(7)	1.897(8)	1.867(8)	1.923(6)	1.918(8)
$Cu\text{-}N3_{amine}$	2.000(8)	2.030(7)	1.980(8)	1.999(7)	2.034(8)	2.018(7)	2.034(7)	2.017(7)
$Cu\text{-}N1_{imidazole}$	2.009(8)	1.967(7)	2.005(8)	1.993(7)	1.928(9)	2.015(7)	1.966(8)	1.976(7)
$Cu\text{-}N4_{pyridine}$	2.430(9)	2.425(11)	2.548[5]	2.407(10)				
$N3_{amine}\text{-}Cu\text{-}O1_{acetate}$	82.2(3)	83.1(3)	83.7(3)	83.3(3)	80.5(3)	83.9(3)	82.3(3)	83.5(3)
$O1_{acetate}\text{-}Cu\text{-}N1_{imidazole}$	92.5(3)	89.7(3)	92.8(3)	91.2(3)	93.9(3)	91.4(3)	92.7(3)	92.4(3)
$N1_{imidazole}\text{-}Cu\text{-}O3_{phenolate}$	90.2(3)	92.9(3)	89.6(2)	90.9(3)	91.1(3)	89.3(3)	91.0(3)	89.1(3)
$O3_{phenolate}\text{-}Cu\text{-}N3_{amine}$	94.2(3)	93.5(3)	93.4(3)	92.9(3)	93.3(3)	93.2(3)	92.3(3)	92.8(3)
$N3_{amine}\text{-}Cu\text{-}N1_{imidazole}$	165.5(3)	161.4(3)	172.8(3)	165.7(3)	159.8(3)	167.4(3)	161.4(3)	168.6(3)
$O1_{acetate}\text{-}Cu\text{-}O3_{phenolate}$	175.0(3)	175.9(3)	175.5(3)	172.1(3)	173.3(3)	169.4(4)	172.7(3)	168.7(4)
$N4_{pyridine}\text{-}Cu\text{-}N3_{amine}$	100.5(3)	97.1(2)	96.513	99.3(2)	99.0(3)		100.4(3)	111.129
$N4_{pyridine}\text{-}Cu\text{-}N1_{imidazole}$	92.9(3)	100.3(2)	89.775[5]	94.3(2)	100.2(3)		97.6(3)	58.139[5]
$Cu\text{-}N_{pyridine}$[2]	3.511[5]		3.260[5]			2.409(11)		2.393(9)
$N_{amine}\text{-}N_{pyridine}$[2]	2.990[5]		3.025[5]			2.407[5]		2.394[5]
τ	0.158	0.242	0.045	0.107	0.225	0.033	0.188	0.002

[1]Atoms of the ligands coordinated to Cu1 have a suffix a, Cu2 have a suffix b and so on in the ORTEP diagram.
[2] Trapped pyridines. Atom numbers does not have a suffix.
[3] N1 is the imidazole N from the L^{2-} coordinated to neighboring Cu.
[4] negative sign indicates the deviation of Cu from the plane towards trapped pyridine.
[5] Calculated using CACHE molecular modeling program by Fujitsu Limited.

3.3.3 Assembly and disassembly of the molecular capsule

One of the possible uses of supramolecular assembly in the form of molecular cages or dendrimer is its use as carrier of molecules such as drug or reagent. For an efficient carrier, the selective disassembly of the carrier through a chemical event releasing the guest and reassembly of the host later would be important. Disassembly process could be triggered by chemical events such as pH change, light or redox induced processes or may be through a simple chemical selectivity for the particular carrier. It is relevant to mention that nature utilizes recyclable carrier in certain microbes. For example extraction of iron from the surrounding by a carrier is done by releasing chemicals (siderophores) which after carrying encapsulated iron into cell releases the iron due to the pH difference in the cell and the carrier is re-released to continue the cycle.[88] While a great deal of effort being put into assembling molecular cages or dendrimers, the literature on the disassembling and reassembling those potential carriers are few. Few notable work utilizes photoinduced[89] cleavage, pH dependent[57] disassembly/reassembly process and recently a fascinating "cascade-release dendrimers" have been reported where the dendrimer gets completely disassembled by a single chemical trigger.[90]

Thus to test the stability of the capsular Cu(II) assembly **1** and suitability of the capsule as a reusable carrier we have studied the assembled and disassembled behavior of the complex in different environments. The summary of the results is presented in Scheme 3.I. The elemental analysis of the dried crystals matched with the formula $[Cu_8(S\text{-Salhis})_8(py)_4]\cdot 8H_2O$ reproducibly, rather than $[[Cu_8(S\text{-Salhis})_8(py)_{10}]\cdot py\cdot 3MeOH\cdot$ (diethyl ether) found in crystal structure analysis carried out on crystals with mother liquor (pyridine and diethylether) in sealed tube. This might be due to the fact that crystals of **1** lost the weakly coordinated external pyridines (external Cu-N_{py} 2.4-2.5 Å) rapidly under vacuum while drying. The ESI-MS (+ve) of the crystals in MeOH shows prominent $\{[Cu_4(S\text{-Salhis})_4]H\}^+$ and $\{[Cu_3(S\text{-Salhis})_3]H\}^+$ molecular ion peaks but did not show any fragments with pyridine or molecular ion peak of $\{[Cu_8(S\text{-Salhis})_8]H\}^+$. The IR spectra of the crystals from pyridine and powder precipitated from methanolic solution of the crystals are almost identical suggesting very little structural change on dissolving the crystals in MeOH. These results and the fact that two halves of the capsule is joined at the corners through H-bond only (Figure 3.1) suggested that the separation of the two halves into two tetranuclear cups in polar solvent such as MeOH

and thereby releasing the trapped pyridines into the solution. The releasing of pyridines from the cage was confirmed by doing a TLC of the concentrated methanolic solution on silica gel (referenced with pyridine).

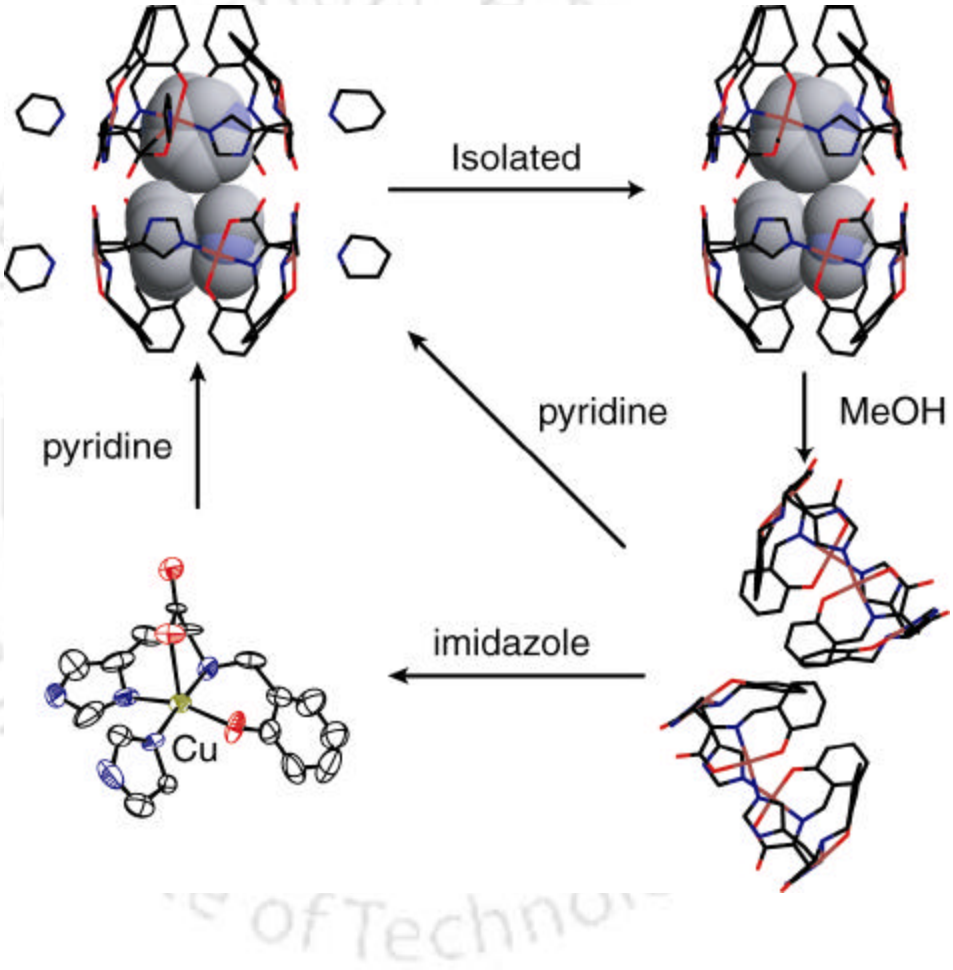

Scheme 3.I Assembly and disassembly of the molecular capsule

The cage could be reassembled from pyridine again as crystals of **1**. While trying to bind some N based heterocycles inside the cage e.g. pyrazine (pKa 0.78) and imidazole, (pKa 6.92) we found no sign of pyrazine binding (isolation followed by analysis), but crystals of mononuclear complex [Cu(*S*-Salhis)(Imidazole)]· $2H_2O$ **2** was isolated with the addition of imidazole (3 equivalent/Cu) almost quantitatively. The complex **2** was characterized using X-ray diffraction (next section) and other standard characterization techniques. The ESI-MS of complex **2** shows molecular ion peak {[Cu(*S*-Salhis)(imidazole)]H}$^+$ as the major peak. However, the {[Cu_4(*S*-Salhis)$_4$]H}$^+$ and {Cu_3(*S*-Salhis)$_3$]H}$^+$ peaks are also present, suggesting an equilibrium between the monomeric and tertrameric species in methanolic solution of **2**. This explains the requirements of excess imidazole (3eq/Cu) in disassembling the capsule to shift the equilibrium in favor of monomeric species.

3.3.4 X-Ray Structure of [Cu(*S*-Salhis)(Imidazole)]· $2H_2O$ (2)

The complex [Cu(*S*-Salhis)(Imz)]· $2H_2O$ **2** (Imz = imidazole) was crystallized in space group *P*2(1) containing eight unique mononuclear units of Cu(*S*-Salhis) and fifteen water molecules held together with array of H-bonds. The ORTEP diagram of one unit along with numbering scheme is given in Figure 3.7. The other mononuclear units were numbered similarly but with different subscript (Cu1 with subscript a, Cu2 with subscript b and so on). Selected bond distances and angles are listed in Table 3.E.

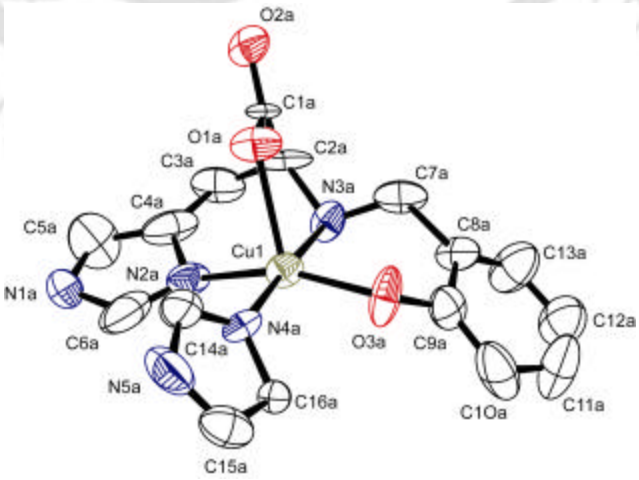

Figure 3.7 ORTEP diagram of one unit [Cu(*S*-Salhis)(Imidazole)], thermal ellipsoids set to 50% probability, solvent molecules are omitted for clarity

Table 3.E Selected bond distances (Å) and bond angles (°) of complex **2**

	Cu1	Cu2	Cu3	Cu4	Cu5	Cu6	Cu7	Cu8
Cu-$O1_{acetate}$	2.262(13)	2.219(10)	2.305(12)	2.344(13)	2.332(12)	2.299(11)	2.277(12)	2.349(13)
Cu-$O3_{phenolate}$	1.930(9)	1.978(11)	1.936911)	1.938(11)	1.888(12)	1.891(12)	1.934(10)	1.922(12)
Cu-$N3_{amine}$	2.051(11)	2.014(11)	2.049(11)	1.998(12)	1.960(14)	2.002(12)	2.002(13)	2.036(11)
Cu-$N2_{imidazole}$[1]	2.042(12)	2.008(12)	1.999(13)	2.014(11)	2.039(12)	2.008(15)	2.026(15)	2.004(12)
Cu-$N4_{imidazole}$[2]	1.989(13)	1.891(13)	1.985(14)	1.986(12)	1.989(14)	2.000(17)	1.976(15)	1.960(13)
$N3_{amine}$-Cu-$O1_{acetate}$	77.6(4)	79.2(5)	77.2(4)	76.8(5)	77.2(5)	76.1(4)	77.0(5)	78.3(5)
$O1_{acetate}$-Cu-$N2_{imidazole}$[1]	87.2(5)	95.4(5)	90.0(5)	97.6(5)	97.2(5)	87.7(5)	88.5(5)	95.0(5)
$N2_{imidazole}$[1]-Cu-$O3_{phenolate}$	164.7(5)	168.9(5)	149.2(5)	143.2(5)	144.8(6)	152.7(6)	160.4(6)	158.6(6)
$O3_{phenolate}$-Cu-$N3_{amine}$	92.0(4)	93.5(5)	92.9(4)	93.7(5)	93.3(6)	94.7(5)	92.3(5)	95.7(5)
$N3_{amine}$-Cu-$N2_{imidazole}$[1]	90.8(5)	86.5(5)	92.4(5)	89.0(5)	90.7(5)	91.4(6)	89.7(6)	87.7(5)
$O1_{acetate}$-Cu-$O3_{phenolate}$	108.1(5)	95.5(5)	120.8(5)	118.7(5)	117.8(6)	119.5(5)	110.9(6)	106.4(6)
$N4_{imidazole}$[2]	175.4(5)	175.3(6)	162.6(6)	165.1(5)	164.9(5)	170.3(6)	177.0(6)	168.8(6)
Cu-$N3_{amine}$ $N4_{imidazole}$[2]	93.7(5)	92.1(5)	95.3(6)	96.3(5)	96.1(5)	92.1(7)	93.2(6)	91.0(5)
Cu-$N2_{imidazole}$[1] $N4_{imidazole}$[2]	102.0(5)	105.5(5)	87.1(6)	88.7(5)	88.6(5)	94.9(6)	103.9(5)	90.7(6)
Cu-$O1_{acetate}$ $N4_{imidazole}$[2]	83.8(5)	86.9(5)	88.5(5)	90.5(5)	88.8(5)	86.4(6)	84.7(5)	89.6(5)
Cu-$O3_{phenolate}$ Cu1-O1-C1	110.1(11)	106.7(12)	108.8(10)	103.7(10)	99.7(12)	108.1(10)	110.8(10)	103.9(12)
τ	0.12	0.11	0.22	0.37	0.34	.029	0.28	0.17

[1]Imidazole is from ligand (*S*-Salhis) $^{-2}$

[2]Imidazole external ligand.

All the Cu(II) centers are five coordinated with four donors from $Salhis^{2-}$ and one from imidazole making a N_3O_2 type environment around Cu(II) center. The coordination geometry at the Cu(II) is best described as square-pyramidal with a trigonal mono pyramidal (TBP) component τ which can be calculated from structural data[82]. The value of τ is 0 for perfect square-pyramidal geometry and 1 for perfect TBP structure. In **2**, the τ values for eight unique [Cu(*S*-Salhis)(Imz)] units vary from 0.11 at Cu2 to 0.37 at Cu4 (Table 3.E) indicating significant TBP component in the geometry. The in-plane Cu-N and Cu-O bond lengths are similar to that found for **1** (Table 3.D) and is typical for Cu(II) complexes.[60] The axial Cu-O(carboxylate) bond in **2** is long and varies from 2.217 to 2.352 Å (Table 3.E). The axial bond in square-pyramidal Cu(II) is usually long (2.12 to 2.6 Å) due to Jahn-Teller distortion. The long axial Cu-carboxylate bond observed in the complexes [Cu(Sbal)(phen)][91] (2.185 Å: H_2Sbal" is *N*-(2-hydroxybenzyl)-β-alanine and "phen" is 1, 10-phenanthroline), [Cu(bpg)]$(NO_3)\cdot H_2O$[92] (2.195 Å: bpg^{1-} = *N*,*N*-di-(2-pyridylmethyl)glycine) and [Cu(bpa)]$(SO_3CF_3)\cdot H_2O$[92] (2.279 Å: bpa^{1-} = *N*,*N*-di-(2-pyridylmethyl)alanine) are similar to the present complex. The range of axial Cu–O1 bond length observed in **2** seems to depend on the Cu–O1–C1, the longer the axial bond lower is the angle. This is possibly due to the strain on the carboxylate arm imposed by the geometry of the complex. The conformation at the chiral carbon for all the eight units are *S* as the ligand used was synthesized from *S*-isomer of the histidine. In addition to the asymmetric carbon in the ligand, the coordination of the amine nitrogen (N3a to N3h for Cu1 to Cu8) to the metal center gives rise to an asymmetric secondary nitrogen atom, which has the *R* absolute conformation.

All the potential H-bond donors (amine, imidazole, imidazole in histidine fragment) and acceptors (phenolate oxygen, two carboxylate oxygen) in each of the ligand and the 15 water molecules in the unit cell take part in inter-molecular H-bond formation forming a giant interwoven H-bonded network in the crystal. The eight monomeric units are connected by two type of H-bond; (1) imidazole N-H of the ligand from one monomer H-bonded with coordinated phenolate O from another monomeric unit, (2) non-coordinated carboxylate O from one monomer to secondary amine N-H from another unit (Table 3.F, Figure 3.8). Water molecules are within H-bonding distances (Table 3.G) of the monomeric Cu(II) units.

Several interesting arrangements of H-bonded water molecules have been observed in the lattice. The two sets of water molecules labeled O1, O6, O5 and O3, O7, O4 form two different helical water chains (Figure 3.9) from one end of the crystal to the other end. The only deviation from perfect helix is that O6 –O1 distance in the first set is 3.27 Å, larger than hydrogen bond and O2-O6 in the first set is <3 Å, thus making the helices discontinuous and slightly irregular. The water labeled O13, O8 and O15 forms a triangle, however, the triangles are not connected (minimum separation O8-O13 is 5.789 Å). It should be noted that stabilization of water clusters and one-dimensional chains in crystals[93,94] have attracted lot of interest due to their importance in probing anomalous properties of water[95] and functioning of chains as "proton wires"[96].

Table 3.F Inter-molecular H-bonding which hold the eight monomeric unites together

Atoms	Distances (Å)	Atoms	Distances (Å)
O2a-N3c	2.831	O3a-N1d	2.808
O2b-N3e	2.989	O3b-N1c	2.837
O2f-N3g	2.865	O3f-N1b	2.718
O2h-N3d	2.832		

Table 3.G Water H-bonded with ligand bonded carboxylated oxygen, non bonded carboxylated oxygen, bonded phenolate oxygen and ligand imidazole N-H

Atoms	Distances (Å)	Atoms	Distances (Å)
O1 $_{water}$-O5 $_{water}$	2.850	O6 $_{water}$-O1a $_{carboxylate}$	3.223
O1 $_{water}$-O6 $_{water}$	3.272	O7 $_{water}$-O9 $_{water}$	2.730
O2 $_{water}$-O3d $_{phenolate}$	2.752	O8 $_{water}$-N1f $_{ligand\ imidazole}$	2.910
O2 $_{water}$-O6 $_{water}$	2.710	O8 $_{water}$-O15 $_{water}$	2.775
O3 $_{water}$-O1g $_{carboxylate}$	2.824	O9 $_{water}$-O2e $_{carboxylate}$	2.783
O3 $_{water}$-O7 $_{water}$	3.294	O10 $_{water}$-O1c $_{carboxylate}$	2.817
O4 $_{water}$-O1e $_{carboxylate}$	3.278	O11 $_{water}$-O2e $_{carboxylate}$	2.831
O4 $_{water}$-O2e $_{carboxylate}$	3.020	O11 $_{water}$-O12 $_{water}$	2.816
O4 $_{water}$-O7 $_{water}$	2.968	O13 $_{water}$-O3h $_{phenolate}$	3.083
O5 $_{water}$-O2d $_{carboxylate}$	2.992	O14 $_{water}$-O1b $_{carboxylate}$	2.999
O5 $_{water}$-O6 $_{water}$	2.900	O15 $_{water}$-O13 $_{water}$	2.911

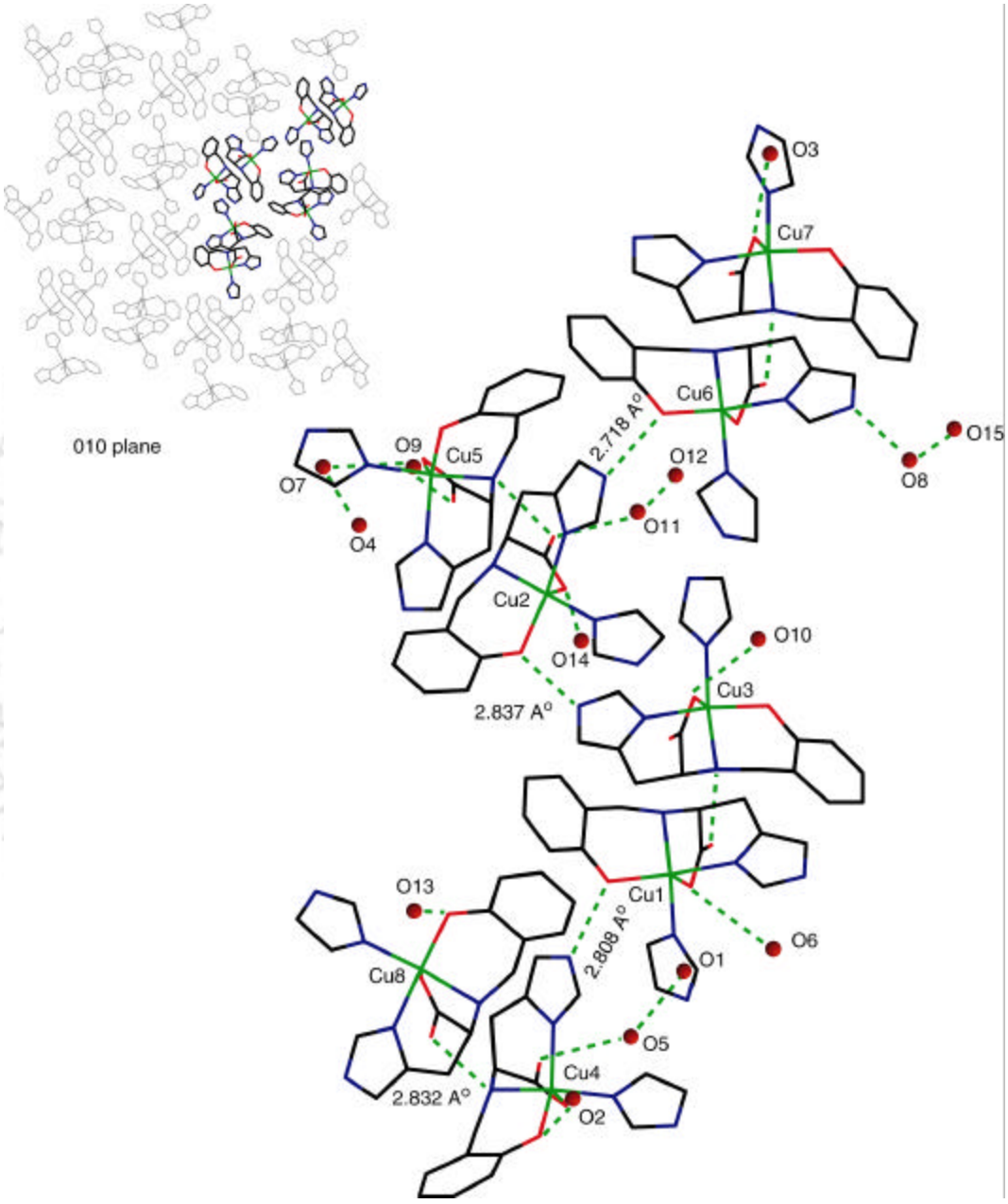

Figure 3.8 Three different types of inter-molecular H-bonding in the crystal

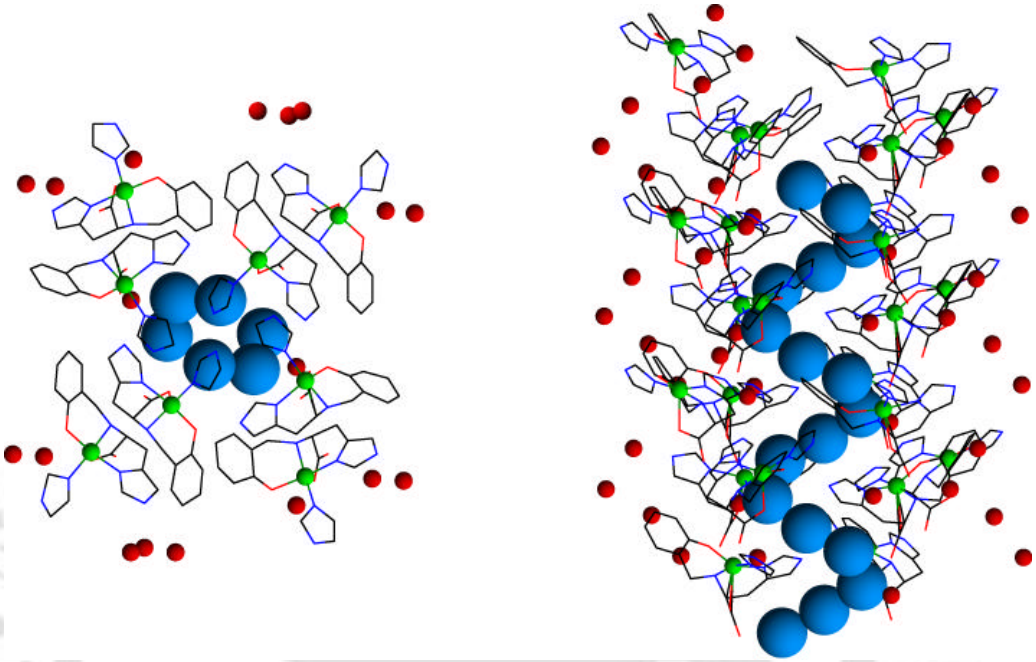

Figure 3.9 In the crystal lattice H-bonded water molecules form helical water chains right handed helix top view (left) and side view (right) of one water chain. The helical water oxygen atoms are shown with blue sphere.

Thermogravimetric analysis: The thermogravimetric analysis of the complex 2 was performed in order to prove the presence of the solvent as indicated by elemental analysis. TGA of complex **2** showed the loss of 8.43 % of total weight in the 30-150 °C temperature ranges, corresponding to the loss of two water molecules (expected 9.04 % weight loss). After the temperature of 200 °C the compound starts to decompose.

3.3.5 Absorption Spectra

The UV-visible spectral characteristic of both the complexes are shown in Figure 3.10-3.11 and the data are shown in Table 3.H. The absorption maxima at ~ 275 nm is due to intra-ligand charge transfer and was observed at 275 nm in methanolic solution of the Salhis^{2-}. The absorption maxima ~ 400 nm is likely to be of LMCT origin evident from high ε value (≥ 500 dm^3 mol^{-1} cm^{-1}/Cu). The absorption maxima between 600 – 700 nm with ε value ~150 dm^3 mol^{-1} cm^{-1} are of ligand field origin. Several other square-pyramidal Cu(II) complexes with N_3O_2 donor environment have similar spectral characteristics.[91, 97] Comparison of spectra of **1** and **2** in MeOH shows very little change (Figure 3.11) between capsule and the monomer due to almost identical coordination environment. It is to be noted that ligand field transition (620 nm) in DMF is greatly shifted compared to that of in other solvents (668 nm to 686 nm) and it is not due to solvent polarity as dielectric constant (DEC) of DMF (DEC 38.3) and MeOH (DEC 32.6) are closer than pyridine (DEC 12.5). The identity of the complex in DMF might be different.

Table 3.H UV-visible data of the complexes [λ_{max} /nm (ε /dm^3 mol^{-1} cm^{-1})/Cu]

	1	**2**
Pyridine	416 (520), 668 (170)	
DMF	288 (4300) 412 (450), 620 (150)	
MeOH	273 (5700), 382 (920), 686 (150)	277 (4800) 395 (500) 671 (120)

3.3.6 Redox stability of the cage

One important aspect of the present capsule/cage over the other cages in the literature is the presence of potentially redox active Cu(II). The complex is soluble in MeOH, pyridine and DMF but not in acetonitrile, dichloromethane or other non-polar solvents with large redox window required for cyclic voltammetric study. As we were not sure about the identity of the complex in DMF (section UV-visible) we had decided to do the cyclic voltammetric study in MeOH. The redox window available in MeOH is rather limited (+1 V to −0.6 V vs. SCE). Within that range the complex showed a poorly resolved irreversible reduction close to the limits of the solvent (-0.5V). This prompted us

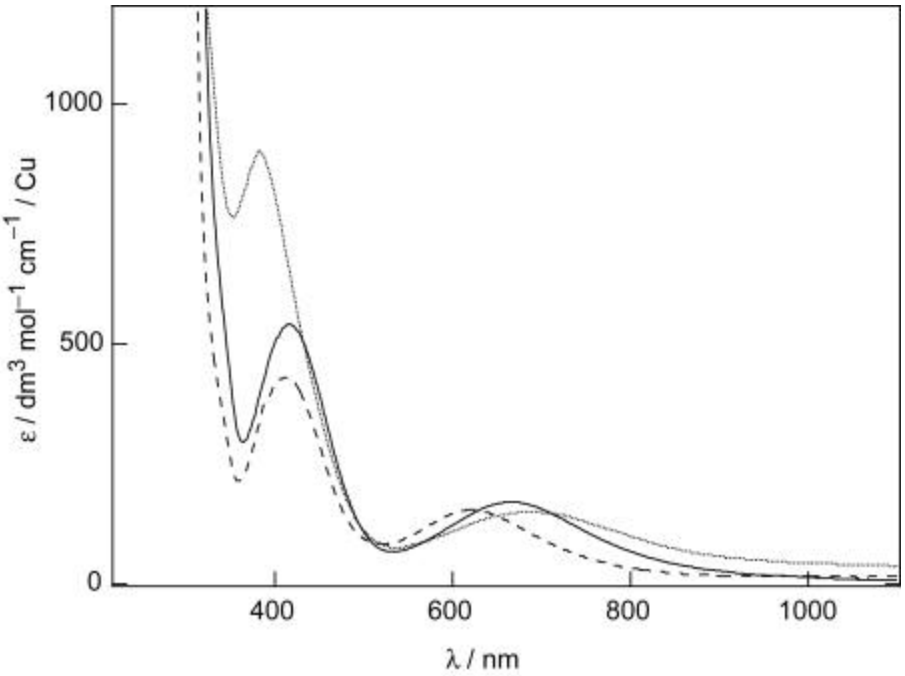

Figure 3.10 UV-visible spectrum of complex **1** in MeOH (·····), in pyridine (—) and in DMF (- - -)

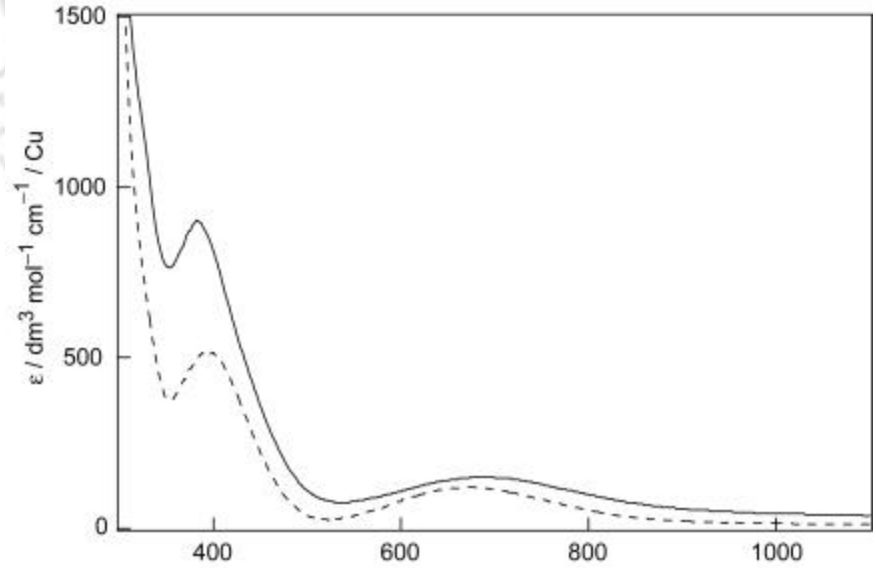

Figure 3.11 UV-visible spectrum of complex **1** (—) and complex **2** (----) in MeOH

to resort the chemical reduction. Addition of $NaBH_4$ in different ratio (1eq, 2eq, 5eq /Cu) immediately decolorizes the solution, which if kept open, changed back to the original green color again. Increasing amount of $NaBH_4$ increases the time required to get back the color. In absence of air, metallic copper deposition took place after a day in a similar experiment. In order to understand the process of reduction and redevelopment of green color we monitored the reduction and aerobic reoxidation using UV-visible and EPR spectroscopy. The ligand field transition of **1** disappears after addition of $NaBH_4$ (1 eq /Cu) and after ~10 min ligand field transition reappears at 651 nm with a 35 nm blue shift compared to **1**. To check whether the ligand has been reduced or not, we decomposed the complex with dilute acid and isolated the ligand. The ligand was unchanged (checked with IR). We had crystallized the green complex from the reaction mixture and it was identical with **1**. Similar experiments were performed with **1** in an EPR tube. The complex **1** in MeOH at 77K shows a typical square pyramidal EPR spectra[98] ($g_{\parallel}$ = 2.253, $g_{\perp}$= 2.060 and A = 175 G, Figure 3.12), which disappears completely after addition of 1 eq. (per Cu) of $NaBH_4$ (addition at room temperature, EPR at 77K). On thawing the solution and periodically checking the EPR at 77 K, EPR signal reappears gradually ($g_{\parallel}$ = 2.252, $g_{\perp}$= 2.056 and A = 170). These experiments suggest that the Cu(II) in **1** could be reduced reversibly in presence of oxygen. However, these results do not confirm the quantitative recovery of **1**. Future efforts will be to quantify the recovery process and the identity of the cage after reduction.

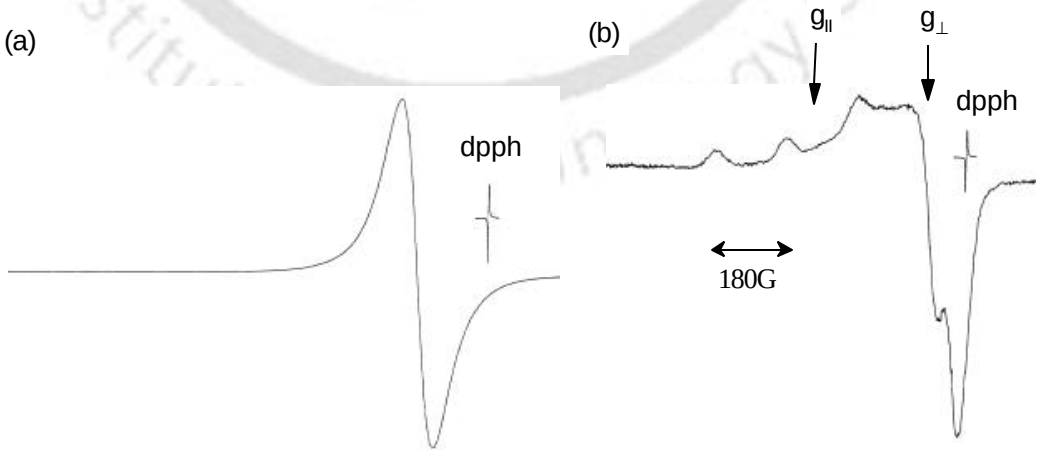

Figure 3.12 EPR spectra of Complex **1** (a) powder at 77 K, (b) in MeOH at 77 K

3.3.7 Magnetism

The solid-state room temperature magnetic moments of **1** and **2** are 1.63 and 1.61 B.M. respectively. In the absence of magnetic exchange between Cu(II) the expected value is ~ 1.9 B.M.[78,79] The lower value indicates magnetic interaction between two Cu(II) centers. In order to determine the magnetic exchange coupling constant (*J*), we have measured the temperature dependent susceptibility for **1** between 81-300K (Table 3.I). The plot of $1/X_M$ vs *T* is shown Figure 3.13. Using Curie-Weiss equation[78,79] *q* was determined as −85.17. The negative sign indicates the presence of antiferromagnetic coupling. Fitting the data with Bleaney-Bowers equation[99] using a program gave a *J* value ~ -29 cm^{-1} (Fitting parameter, *J* = -29 cm^{-1}, TIP $4.38x10^{-4}$ cm^3 mol^{-1}, g = 1.705, error = 7.633). However, the fitting was not acceptable (Figure 3.13). The reason might be that in the capsule four Cu(II) are interconnected by symmetry and the equation used is for dimer. Due to the lack of expertise in forming Hamiltonian and lack of literature on magnetic analysis of cyclic tetrameric Cu(II) complexes we were unable to determine the correct *J* value (s). We have not attempted temperature dependent magnetic measurements of monomeric **2**.

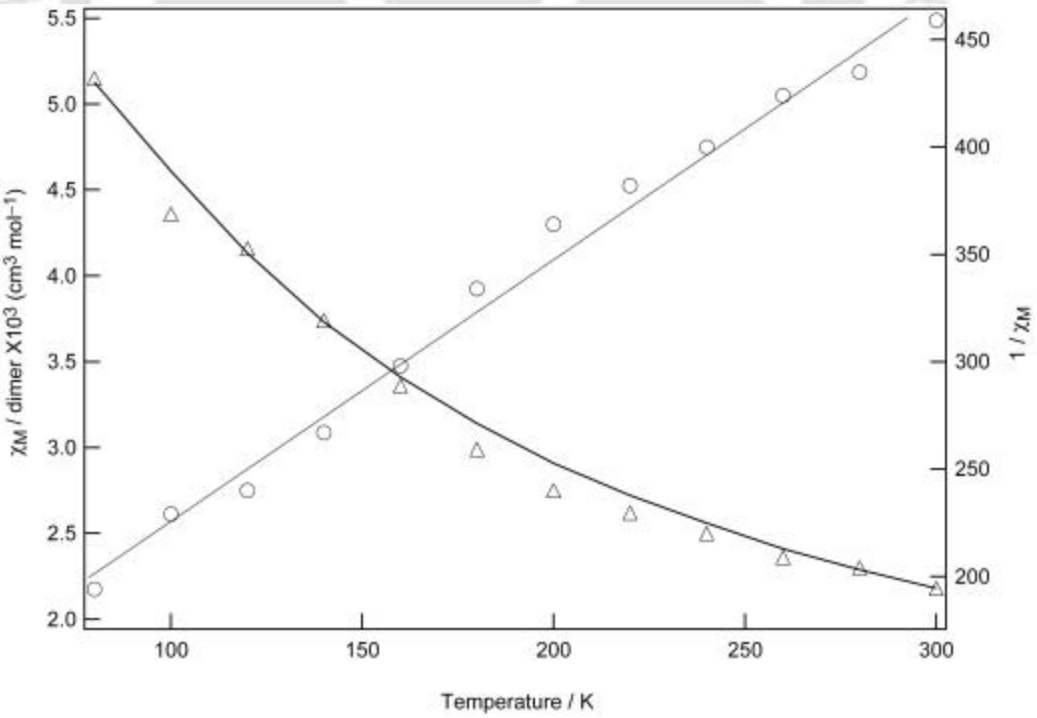

Figure 3.13 Plot of χ_M and $1/\chi_M$ *vs. T* per dinuclear complex of **1**

Table 3.I Variable Temperature Magnetic Susceptibility data for the complex **1**

Temperature / K	χ_M / dimer × 10^3 (cm^3 mol^{-1})	Temperature / K	χ_M / dimer × 10^3 (cm^3 mol^{-1})
300	2.18	180	2.99
280	2.30	160	3.36
260	2.36	140	3.74
240	2.50	120	4.16
220	2.62	100	4.36
200	2.75	81	5.15

Conclusions

In this chapter we have reported synthesis, characterization and structural analysis of a multinuclear Cu(II) based capsular cavity trapping four pyridine molecules. Further studies showed that (a) the tetrameric cavity is stable in MeOH (b) the tetrameric unit can be disassembled into monomeric units **2** using a specific chemical agent (imidazole) (c) capsule could be reassembled from pyridine again. Additionally, pyridines inside **1** and lattice of monomeric **2** shows interesting H-bonding scheme because of the presence of H-bond capable donor/acceptors in the ligand.

Chapter IV

Synthesis and characterization of a 1D chiral microporous channels with a Fe(III) complex and insertion of iodine inside the channels

Helical organization and channel are two important structural motifs present in nature. The channels in the membrane bound potassium channels[100] or water permeation protein aquaporins[101-103] are formed out of several peptide helices in an approximately C_4 symmetric fashion to form narrow channels (2.8-20 Å dia.) as gateway for K^+ ion or water molecules selectively. The narrow channels in amyloid fibres (11.8 Å dia.) from extracellular amyloid plaques found in Alzheimer patients,[104] aquaporin (18 to 2.8 Å dia.) and C_5 symmetric mechanosensitive channels from mycobacterium tuberculosis (18-2 Å dia.)[105,106] contain chain of water molecules important for their biochemical functions. Apart from the channels present in nature, materials with channels of different pore diameter have been synthesized because of their anticipated use as molecular sieves, sensors, ion exchangers and catalysts.[107-111] Recently porous channels have been used as template to synthesize nano fibres[112] and one dimensional array of oxygen molecules.[113] Thus, several reports appeared on synthesis of materials with channels, helical structures with chiral or achiral ligand metal complex recently.[114-128] Despite this, literatures regarding the formation of microporous helical channels with water molecules inside are few[114,116,118-120] and to our knowledge only one group reported the removal of water from non helical hydrophobic channels[114] and small molecules were inserted.

In this chapter we discuss the synthesis and structure of binuclear iron (III) complexes, with (*S*)-H_2Salhis and (*R*)-H_2Salhis ligands. The crystals of the complexes have one dimensional microporous helical channels filled with easily removable water molecules. [129] Using of two enantiomers of the ligand, [(*R*)-H_2Salhis] and [(*S*)-H_2Salhis], helicity of the channels were found to be reverse as well. Further, we could remove water from the channels and iodine was inserted into the channels as confirmed by the X-ray structure.

4.1 Experimental Section

Details of solvent purification, analytical measurements and starting materials have already been discussed in Chapter 2. The ligands [(*S*)-H_2Salhis] and [(*R*)-H_2Salhis)] preparation were described in previous chapter 2 (Section 2.4.1 and Section 2.4.2 respectively).

4.1.1 X-ray Data Collection, Structure Solution and Refinement

Data were collected on a Bruker Smart CCD Area Detector system with graphite monochromator. The structures were solved by direct methods and refined on F^2 by full-matrix-block least squares (program SHELXL-97, G. M. Sheldrick, University of Göttingen). Refinements of F^2 were done against all reflections. The weighted R-factor wR and goodness of fit S are based on F^2, conventional R-factors are based on F, with F set to zero for negative F^2. The threshold expression of $F^2 > 2$ sigma(F^2) is used only for calculating R-factors(gt) etc. and is not relevant to the choice of reflections for refinement. R-factors based on F^2 are statistically about twice as large as those based on F and R-factors based on all data will be even larger. Selected crystallographic data and refinement details are displayed in Table 4.A.

Table 4.A Crystal data and structure refinement details

Complexes	**1**	**2**	**3**	**4**
Formula	$C_{28}H_{37}Fe_2N_6O_{13}$	$C_{28}H_{32}Fe_2N_6O_{10}$	$C_{28}H_{32}Fe_2I_2N_6O_{10}$	$C_{28}H_{32}Fe_2N_6O_{11}$
M	777.33	724.30	978.10	740.30
T/K	293(2)	293(2)	293(2)	293(2)
Wavelength (Å)	0.71073	0.71073	0.71073	0.71073
Crystal size/mm	0.40×0.35×0.30	0.40×0.40×0.35	0.50× 0.50 × 0.45	0.40×0.40×0.35
Lattice type	hexagonal	hexagonal	hexagonal	hexagonal
Space group	*P*6(1)	*P*6(1)	*P*6(1)	*P*6(5)
a/Å	13.164(3)	13.161(7)	13.252(4)	13.151(4)
b/ Å	13.164(3)	13.161(7)	13.252(4)	13.151(4)
c/ Å	36.305(11)	36.559(4)	36.253(2)	36.558(2)
g /º	120	120	120	120
V/ Å^3	5449(2)	5484(7)	5514(4)	5476(4)
Z	6	6	6	6
D_c/mg m^{-3}	1.421	1.316	1.767	1.347
Absorption coefficient/ mm^{-1}	0.866	0.850	2.527	0.854
F(000)	2418	2244	2880	2292
q range/º	1.79–26.04	1.79-27.21	1.77-27.75	1.79-27.24
Completeness to θ	99.9%	97.0%	95.6%	97.7
Reflections collected	42827	41609	44120	56517

Independent reflections	7101[R(int)= 0.0453]	7704[R(int)= 0.0490	8063[R(int)= 0.0443	7816[R(int)= 0.0245
Absorption correction	None	Semi-empirical from equivalents	Semi-empirical from equivalents	None
Refinement method	Full-matrix least-squares on F^2	Full-matrix least-squares on F^2	Full-matrix least-squares on F^2	Full-matrix least-squares on F^2
Data/ restraints/ parameters	7101 / 1 / 535	7704 / 3 / 472	8063 / 1 / 440	7816/ 1/ 470
Goodness-of-fit of F_2	0.995	1.133	1.273	1.199
Final R indices [I>2σ(I)]	R1 = 0.0387, wR2 = 0.0842	R1=0.0574, wR2=0.1423	R1=0.1097, wR2=0.2868	R1=0.0416, wR2=0.1190
R indices (all data)	R1 = 0.0488, wR2 = 0.0879	R1=0.0747, wR2=0.1525	R1=0.1295,wR2= 0.3066	R1=0.0461, wR2=0.1235
Absolute structure Parameter	0.028(12)	0.005(19)	0.05(4)	0.014(13)
Largest diff. Peak and hole/ e $Å^{-3}$	0.370 and -0 .181	0.993 and –0.355	1.901 and –1.863	0.677 and –0.265

4.2 Syntheses of Fe(III) complexes

4.2.1 [Fe_2(OAc)(OH)(*S*-Salhis)$_2$]· 4H_2O (1)

The complex **1** was synthesized by adding a methanolic (10 mL) solution of $Fe(NO_3)_3$· $9H_2O$ (0.592 g, 1.46 mmol) to a stirred methanolic (20 mL) solution of [*S*-H_2Salhis] (0.383 g, 1.46 mmol) and NaOH (0.117 g, 2.93 mmol), followed by addition of NaOAc· $3H_2O$ (0.598 g, 4.39 mmol) in 5 mL MeOH and the mixture was stirred for 15 min. The final color of the solution was reddish purple. The volume of the solution was reduced to ~10 mL and diethyl ether was added. Cooling the solution in a refrigerator for three days yielded dark colored diamond shaped crystals of **1**. The crystals were washed with ether and dried in a vacuum desiccator (yield, 65%). Further studies including X-ray structural studies were performed on these crystals. Recrystallization from MeOH could be done in presence of an acid ($HClO_4$ or CH_3COOH) to prevent deprotonation of bridging hydroxyl group.

$Fe_2C_{28}H_{38}N_6O_{13}$: IR (KBr, cm^{-1}) ν (OH) 3405 (broad); ν $(Carboxylate)_{asym}$ 1644; ν $(Carboxylate)_{sym}$ 1384; for bridge ν $(OAc)_{asym}$ 1542; ν $(OAc)_{sym}$ 1457; ν (NH)

3110; ν (phenolic, CO) 1270. Λ_M: (MeOH), 12 S cm^{-2} mol^{-1} (much lower than expected for 1:1 electrolyte in MeOH ~80-115 S cm^{-2} mol^{-1}). UV-visible: λ_{max} /nm (ε /dm^3 mol^{-1} cm^{-1}) (MeOH), 273 (11300), 302(sh), 481 (2900). μ_{eff} (powder, 298 K) 6.46 B.M. / dimer.

4.2.2 Single crystals of [Fe_2 (μ-OH)(μ-OAc)(*S*-L)$_2$]· H_2O (2)

Crystals of **1** were dried at 95 -100º C under reduced pressure for 2h. The loss of water (3 H_2O) compared to **1** was confirmed by TGA, which showed the weight loss of 1.7 % (calculated for 1 H_2O, 2.48 %) between 95 - 140ºC but negligible weight loss (0.1%) between 30-95º. X-ray diffraction studies were done on these crystals sealed in a capillary to avoid moisture. IR and UV-visible of these crystals were compared with that of **1** and found identical.

4.2.3 Single crystals of [Fe_2 (μ-OH)(μ-OAc)(*S*-L)$_2$]· H_2O· I_2 (3)

Crystals of **1** were dried at 95-100º C under reduced pressure for 2h (**2**). 50mg of **2** in a vial along with solid I_2 in a separate vial were kept inside a round bottom flask (50 mL) containing dry silica gel to minimize moisture content. This setup was evacuated first and then warmed to 40-50º C for few minutes. This was done to remove air (moisture) as much as possible and heating ensured production of enough I_2 vapor to fill the void. The setup was kept in this way for five days to saturate the crystals with iodine and the resultant crystals were sealed in a glass capillary for X-ray diffraction studies. The I_2 content of the crystals were measured using titration (described below) and tallied with weight loss in TGA. We arrived at the above procedure after repeating the I_2 doping followed by titration experiments under various conditions. We found that if the silica gel was not used (presence of moisture) the amount of I_2 incorporated is only 7-9 % after three days and resulting crystals do not diffract well. After application of vacuum followed by warming to produce I_2 we could get the crystals that diffract and I_2 content of the crystals were found to be 12 % (repeatedly) using the same procedure. While 12 % I_2 content is lower than calculated 25 % for [Fe_2 (μ-OH)(μ-OAc)(*S*-L)$_2$]· H_2O· I_2, discrepancy might be (at least one factor) due to the loss of I_2 during washing before the estimation. For X-ray diffraction studied we did not wash the crystals to ensure that crystals stay saturated with I_2 and loss during X-ray experiment is minimized.

Estimation of I_2 in (3) Single crystals or coarsely grinded crystals of **1** (~10-20 mg exactly weighted) were heated in water bath at 100 °C under reduced pressure for 2 hr. and then were stored in a closed chamber containing I_2 crystals for 5 days. In this arrangement only iodine vapor can be absorbed in the crystal at room temperature. After 5 days, the samples were washed thoroughly with CCl_4 (three times) at room temperature to remove any I_2 absorbed on the surface of the crystals. The washed crystals were then put into the freshly distilled CCl_4 (~ 6 mL measured) and 6 mL of water was added into the mixture and shaken vigorously. The CCl_4 layer became strongly purple colored due to the released I_2. The I_2 concentration in CCl_4 layer was measured spectrophotometrically. I_2 estimated was found to be 12 % (calculated 25 % for one I_2 /dimer).

Note: *It is difficult to wash the surface only without loosing some iodine from the channels as crystal binds iodine loosely. The structure was done in a sealed tube without washing the crystals.*

4.2.4 $[Fe_2(\mu\text{-OH})(\mu\text{-OAc})(R\text{-Salhis})_2]\cdot 2H_2O$ (4)

The complex **4**, $[Fe_2(\mu\text{-OH})(\mu\text{-OAc})L_2]\cdot 2H_2O$, as crystals (60% yield) was synthesized following the procedure described for **1** using the D-histidine derived ligand (*R*-H_2L).

$Fe_2C_{28}H_{34}N_6O_{11}$: IR (KBr, cm^{-1}) ν (OH) 3405 (broad); ν $(Carboxylate)_{asym}$ 1644, 1598 ν $(Carboxylate)_{sym}$ 1384; for bridge ν $(OAc)_{asym}$ 1542; ν $(OAc)_{sym}$ 1461; ν (NH) 3110; ν (phenolic,CO) 1270. Λ_M: (MeOH), 15 S cm^{-2} mol^{-1} (much lower than expected for 1:1 electrolyte in MeOH ~80-115 S cm^{-2} mol^{-1}). UV-visible: λ_{max} /nm (ε /dm^3 mol^{-1} cm^{-1}) (MeOH), 275 (12500), 302(sh), 479 (2700). μ_{eff} (powder, 298 K) 6.00 B.M. / dimer.

4.3 Results and Discussion

4.3.1 Synthesis and Selected Properties

By mixing $Fe^{III}(NO_3)_3\cdot 9H_2O$, H_2S-L, NaOH and NaOAc in MeOH at 1:1:2:3 ratio, the solution turned red-purple. Addition of diethyl ether afforded complex **1** or **4** (with H_2R-L) as diamond shaped crystals in ~60-65 % yield. Comparing the IR spectra of **1** and **4** with that of deprotonated ligand and the Cu(II) complexes which has

been characterized in the previous chapter, the peaks at 1640 and 1365 cm^{-1} were identified as asymmetric and symmetric carboxylate stretches respectively originated from the ligand. Both the complexes also show broad stretches at 3410 cm^{-1} and two sharp stretches at 3185, 3111 cm^{-1} due to OH (water or H-bonded OH) stretch and N-H stretches (from ligand) respectively. Further the complexes show the appearance of two bands at 1544 and 1452 cm^{-1} with $\Delta\nu$ 92 cm^{-1}, attributed to the ν_{asym} and ν_{sym} stretching modes of the acetate anion coordinated to the Fe^{III} centers in the bridging form.[76] The IR does not show any stretches for NO_3^-. The elemental analysis (Table 4.B) support the formulation of the complexes as $[Fe_2(OAc)(OH)(S\text{-Salhis})_2]\cdot 4H_2O$ and $[Fe_2(OAc)(OH)(R\text{-Salhis})_2]\cdot 2H_2O$ for **1** and **4** respectively. The thermogravimetric analysis (TGA) between 30- 140°C shows weight loss of 7.76 % for **1** and 3.7 % for **4** as against the calculated values of 9.24 % ($4H_2O$) and 4.8 % ($2H_2O$) respectively. The room temperature magnetic moment for **1** and **4** at 4.57 and 4.38 B.M. /per iron respectively are less than expected for an uncoupled S=5/2 system but higher than low-spin S=1/2 system (expected 5.93 B.M. for S= 5/2 and 1.73 to 2.5 B.M. for S=1/2 uncoupled system)[78,79] indicating the possible presence of antiferromagnetic coupling between two high-spin Fe(III) centers. Structural characterization of the complexes confirmed their formulation. The antiferromagnetic coupling constant *J* for **1**, determined from structural parameters using Gorun and Lippard equation was found to be -11.9 cm^{-1} and is consistent with a hydroxo bridge formulation.[130]

The molar conductance of **1** and **4** were found to be 12 and 20 S cm^2 mol^{-1} respectively in methanol (expected for 1:1 electrolyte in methanol is in the range of 85-115 S cm^2 mol^{-1}).[77] Conductance of both the complexes are very much lower than 1:1 electrolyte in methanol. The low conductance of both the complexes are possibly due to the bridge hydroxo proton getting deprotonated in presence of solvent.

Table 4.B Microanalytical Data[a] of Fe(III) complexes

Complexes	Empirical Formula	% C	% H	% N
1	$C_{28}H_{38}N_6O_{13}Fe_2$	43.39 (43.18)	4.56 (4.92)	10.81 (10.79)
2	$C_{28}H_{32}N_6O_{10}Fe_2$	46.98 (46.43)	4.74 (4.45)	12.08 (11.60)
3	$C_{28}H_{32}N_6O_{10}Fe_20.6I_2$	36.10 (38.36)	3.38 (3.67)	8.08 (9.58)
4	$C_{28}H_{34}N_6O_{11}Fe_2$	45.38 (45.30)	5.24 (4.62)	11.37 (11.32)

[a] Values in parentheses are calculated ones

4.3.2 Structures of 1 and 4

The single crystals of complexes **1** and **4** were isolated from reaction mixture itself upon addition of diethyl ether. The complex **1** was crystallized in the chiral space group $P6_1$ (No. 169) and **4** in opposite chiral space group $P6_5$ (No. 170). Structures of **1** and **4** are enantiomer to each other. Thus discussions below were done with **1** applicable to **4** as well. The molecular structure of **1** and **4** are shown in Figure 4.1. Selected bond distances and angles are listed in Table 4.C

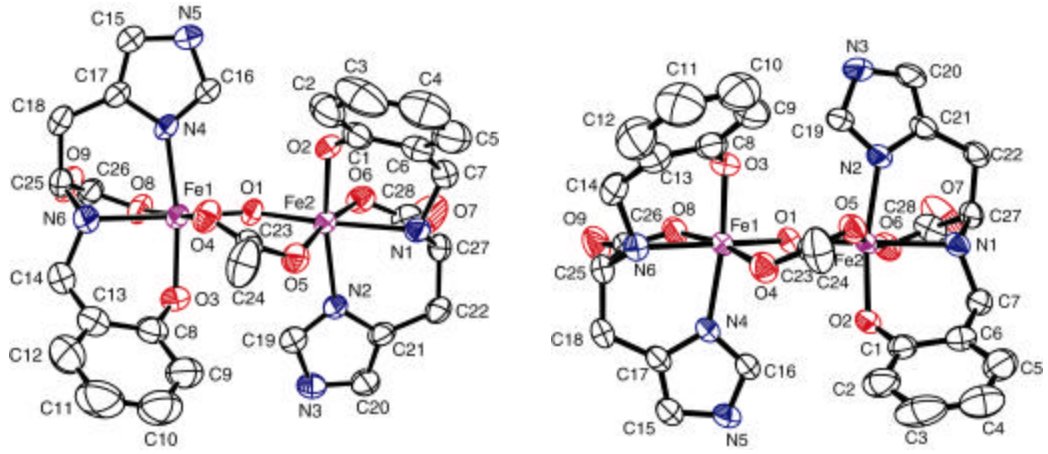

Figure 4.1 ORTEP diagram for complex **1** (left) and complex **4** (right), thermal ellipsoids set to 50% probability, solvent molecules are omitted for clarity

In **1**, each of the two hexadentate irons are ligated with a tetradentate [*S*-(Salhis)$^{2-}$] and is bridged through one hydroxo and one bidentate acetate ligand. The Fe-O1 distances (~1.97 Å, Table 4.3) are characteristic of Fe(III)-OH bridge and are significantly higher from those of Fe(III)-Oxo bridge distances (<1.8 Å).[131-134] This confirms the bridge as a hydroxo bridge and not an oxo bridge. The Fe…Fe distance [3.517 Å] is higher among the few structurally characterized iron(III) dimers containing two bridges where at least one is OH bridge. It should be noted that [Fe^{III}(μ-OH)(μ-carboxylato)Fe^{III}]$^{4+}$ core have been proposed in the active site of protein mammalian purple acid phosphatase[135] and to date this is the first structurally characterized complex containing the core as well as with the imidazole, phenolate, carboxylate donors closely resembling the histidine, tyrosine and aspartate donor present in the protein.

Table 4.C Selected bond lengths (Å) and angles (°) of the complexes

Complexes	**1**	**2**	**3**	**4**
Fe1…Fe2	3.5175(7)	3.522	3.527	3.522
Fe1-O1	1.9722(18)	1.969(3)	1.983(6)	1.971(2)
Fe1-O4	1.9875(26)	1.995(3)	1.992(6)	1.997(2)
Fe1-N4	2.1314(23)	2.142(4)	2.119(6)	2.136(3)
Fe1-N6	2.2030(22)	2.211(4)	2.213(7)	2.220(3)
Fe1-O3	1.9463(19)	1.957(3)	1.961(5)	1.961(2)
Fe1-O8	1.9988(26)	2.000(3)	2.016(5)	2.001(2)
Fe2-O1	1.9695(21)	1.972(3)	1.966(5)	1.968(2)
Fe2-O5	2.0309(24)	2.031(3)	2.034(6)	2.034(2)
Fe2- N2	2.1400(22)	2.151(4)	2.144(6)	2.141(3)
Fe2-N1	2.2006(22)	2.206(3)	2.216(6)	2.211(3)
Fe2-O2	1.9314(19)	1.94693)	1.931(6)	1.943(2)
Fe2-O6	2.0179(24)	2.016(3)	2.024(6)	2.024(2)
Fe1-O1-Fe2	126.35(11)	126.69(16)	126.6(3)	126.83(12)
N4-Fe1-O3	169.24(0.09)	169.22(15)	169.0(3)	168.88(11)
O4-Fe1-N6	93.99(0.09)	94.13(14)	93.9(3)	94.17(11)
N6-Fe1-O8	77.90(0.10)	77.51(14)	78.4(2)	78.01(11)
O8-Fe1-O1	94.37(0.09)	94.60(13)	94.3(2)	94.10(10)
O1-Fe1-O4	93.62(0.09)	93.69(12)	93.3(2)	93.59(10)
N2-Fe2-O2	168.62(0.09)	168.76(13)	169.8(3)	168.36(11)
O5-Fe2-N1	97.14(0.08)	97.08(12)	96.5(2)	97.56(9)
N1-Fe2-O6	76.49(8)	76.45(12)	76.6(2)	76.07(10)
O6-Fe2-O1	90.56(0.09)	90.84(13)	90.9(2)	90.53(10)
O1-Fe2-O5	95.63(0.09)	95.43(12)	95.8(2)	95.66(9)

The conformation at the chiral carbon of the ligand is *S* in **1** and *R* in **4**. In addition to the asymmetric carbon centre in the ligand, the coordination of amine N to the iron gives rise to an asymmetric secondary nitrogen atom, N1 and N6, which has the *R* configuration in **1** and *S* configuration in **4**. The lower dihedral angles between Fe-N amine and the methylene arm of the phenolate rings results in a folding of the phenolate ring forming a bowl shaped C_2 symmetric chiral and essentially hydrophobic cavity around the bridging acetate (Figure 4.2a). Similar bending was responsible for closing the capsular cavity ends in our copper complex with this ligand (Chapter III).

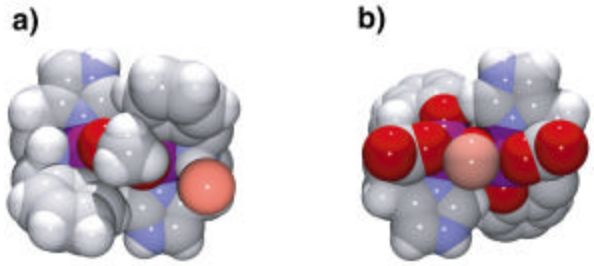

Figure 4.2 Space filling model of one dimer **1** (a) viewed from acetate and (b) hydroxo bridge side.

For complex **1** the lattice diagram viewed normal to 001 plane shows hexagonal channels filled with water from one end to the other end of the crystals (Figure 4.3). Close observation reveals that the molecules of **1** with hydroxo bridge facing the channel and a water molecule within H-bonding distance of the hydroxo bridge (O1-O11 2.6961Å) form right-handed helices (Figure 4.3b, thick lines). On the other hand, the crystals of **4** have left-handed helices (Figure 4.3c).

A notable feature of the molecule which helps guest molecules to orient in a helical fashion is the formation of a crescent moon shaped hydrophilic binding site (Figure 4.2b and 4.4, left) formed by lining up hydroxo bridge (H-bond donor) and all four oxygen atom of the carboxylate oxygen (H-bond acceptor). This creates a situation

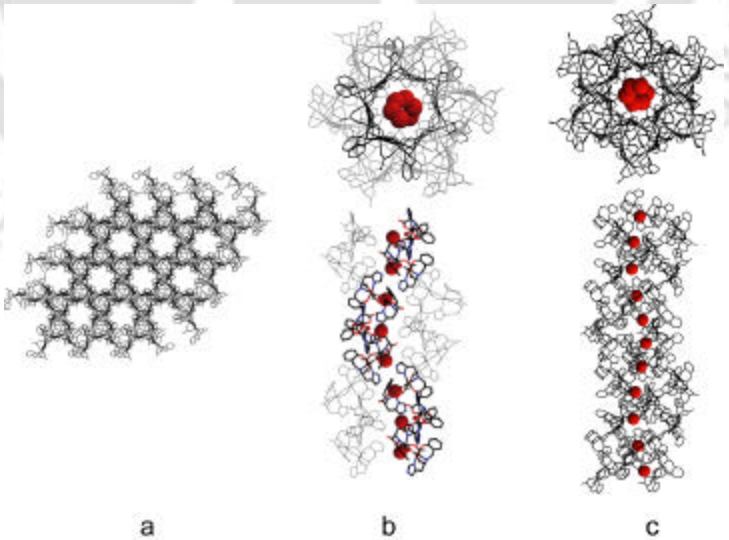

Figure 4.3 (a) View of the crystal lattice normal to the 001 plane. (b) Right handed helix and side view of one channel showing the water oxygen atoms (red sphere) H-bonded to the hydroxo bridge of complex **1** (c) Left handed helix and side view of the channel in **4**

where three water molecules per dimer (three water molecule disordered over six position) form a H-bonded column of water (Figure. 4.4, right) similar to the biological[102] and a few synthetic[129,118] chain of water reported before. Each of the water sites in the channel **1** form a helix from one end of the crystal to the other end. In case of **4**, the structure shows only one water molecule inside the channel present within H-bonding distance of bridging hydroxo group. This might be due to the fact that two water molecules in **1**, other than the one H-bonded to bridging hydroxide, are only H-bonded to each other and to the one H-bonded to the bridging hydroxide, thus more susceptible to be removed easily. So their presence depends on the storage condition, moisture content, and temperature during X-ray etc. and was not present in this particular set of crystals of **4**.

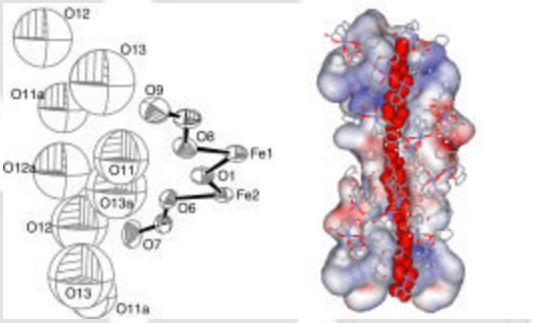

Figure 4.4 ORTEP diagram of the disordered water molecules in the channel (left), thermal ellipsoids set to 50% probability and surface representation of the channel (right)

Table 4.D H- bond distances (Å) of the complexes

Complexes	**1**	**4**
O1-O11	2.696()	2.790
O1-O13a	2.794	-
O11-O12	3.081()	-
O12-O13a	2.293	-
O13-O13a	3.000	-
O13a-O12a	2.777	-
O12-O13	2.489	-
N3-O2	2.918	2.890
N5-O3	2.945	2.937
O7-O10	2.781	2.843
N1-O9	2.901	2.916
N6-O10	2.993	3.034

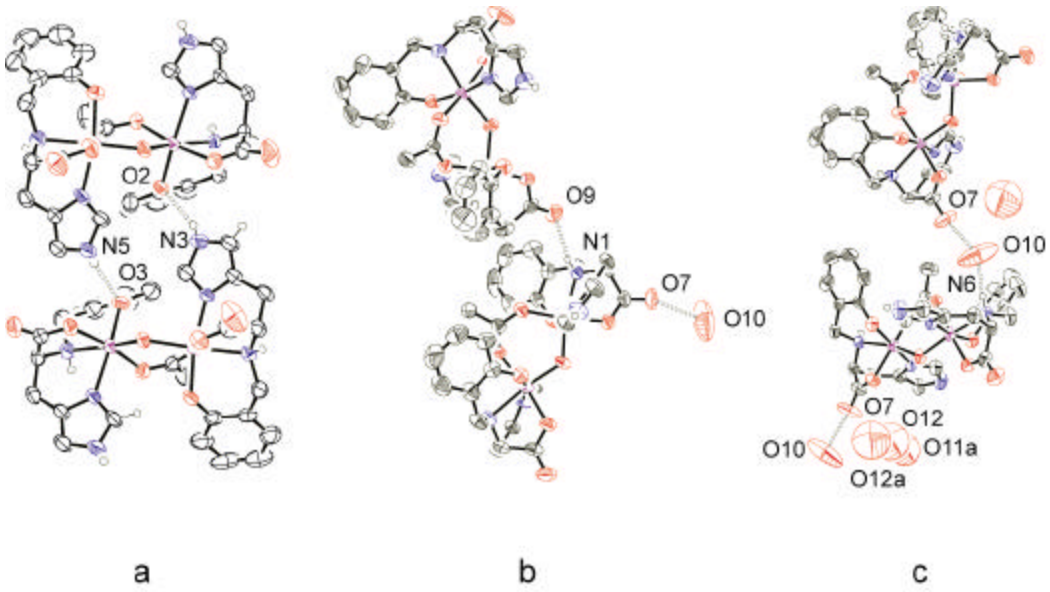

Figure 4.5 Inter-molecular hydrogen-bonding networks in the crystal

The helical arrangement of the hydrophilic sites (Figure 4.3) like a spiral is formed by the inter-molecular H-bonding between imidazole hydrogen of one molecule and oxygen atom of the coordinated phenol from the next molecule (Figure 4.5a). To accommodate these pair of H-bond one molecule gets rotated by 60º compared to the previous one and this continues with the next one resulting in a right-handed helix of hydrophilic binding sites. The neighbouring molecules in the channel have the hydrophobic methyl group of bridging acetate facing the cavity. All the H-bond distances showed here are within literature limits[136,137] (Table 4.D). The channel diameter as calculated from bridging oxygen (O1) to facing phenolate carbon (C11) distance is 7.35 Å and methyl carbon of acetate bridge (C24) to facing carboxylate oxygen (O8) is 9.81 Å. This is intermediate between the other two reported helical channels (~11 Å[121] and 5.5 Å[124]).

4.3.3 Types of water in 1 and 4 from TGA

Out of the four water molecules present in **1**, one (O13a) is within hydrogen bonded distance with bridging hydroxo group (Table 4.D, Figure 4.4) and another (O10) forms hydrogen bonded bridge between carboxylate of one molecule and neighbouring amine of the other molecule (O7…O10 2.7808 and O10…N6 2.993 Å).[136,129]

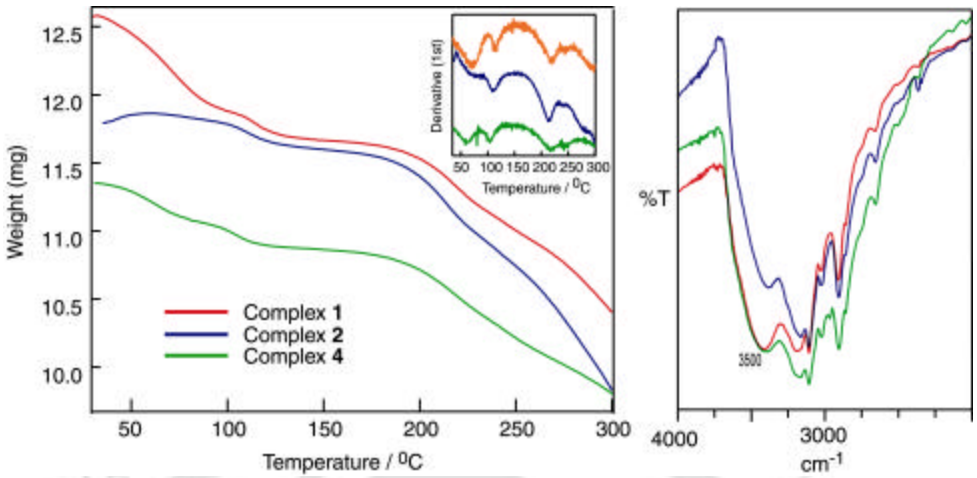

Figure 4.7 TGA plot and partial IR spectra of **1, 2** and **4** with derivative (DTA) plot of TGA as inset

This feature is retained in **4**. Two more water molecules present in **1** are disordered in the channel. All the disordered positions are within hydrogen bonding distances with each other. Thus in **1**, there are three relatively labile water molecules in the channel and one water molecules formed bridge (O10) between two neighbouring units of **1**. This was reflected in the TGA of **1** (Figure 4.7), the crystals lost 3 H_2O per dimer between 30-95°C and one water between 110-130°C. On the other hand, **4** have one water molecule in the channel and one water as a H-bonded bridge. In **4** (Figure 4.7) weight loss between 30-95°C is 2.34 % (calculated for H_2O loss 2.42 %) and loss between 95 - 140° C is 1.38 % (calculated for $1H_2O$ loss 2.42 %). These clearly shows that the loss of channel water molecules take place between 30-95° C and the bridging H_2O (O10) between 100-140° C.

Taking cue from this observation, the crystals of **1** were heated at 90-100°C under reduced pressure for 2h. The TGA of the dried crystals **2** shows weight loss of 1.7 % (calculated for 1 H_2O, 2.48 %) between 95 - 140°C but negligible weight loss (0.1 %) between 30-95°C indicating the loss of channel waters (Figure 4.7). The crystals **2** dried this way, were structurally characterized. As expected, three waters from inside the channel of **1** are missing but water (O10) in the lattice remains. This also shows that the crystals are thermally stable at least up to 100°C. After 150°C weight loss is rapid possibly due to decomposition. Heating up to 250°C results in a yet uncharacterised brown material, which does not give characteristic purple colour of **1**.

4.3.4 Insertion of I_2 in 2

To check if small molecules can be inserted in the channel, we exposed the crystals of **2** to I_2 vapours in a closed container for 5 days and structurally characterized **3**. The structural parameters of **3** are almost identical with that of **1** and **2** (Table 4.A). The comparison of the structures of **1,** dehydrated crystals **2** and iodine doped crystals **3** are shown in Figure 4.8. The structure of **3** shows that one molecule of I_2 (slightly disordered) per binuclear complex has been incorporated in the channel. The iodine to ligand carboxylate oxygen distances (I1-O7 3.07Å and I2-O8 3.01 Å) shows that one end of the I_2 is within weak interaction distances of non-coordinated carboxylate oxygen (O7) of one molecule and the other end is closer to metal coordinated carboxylate oxygen (O8) from another molecule (Figure 4.8c). Weak polar interaction of one end of I_2 with oxygen

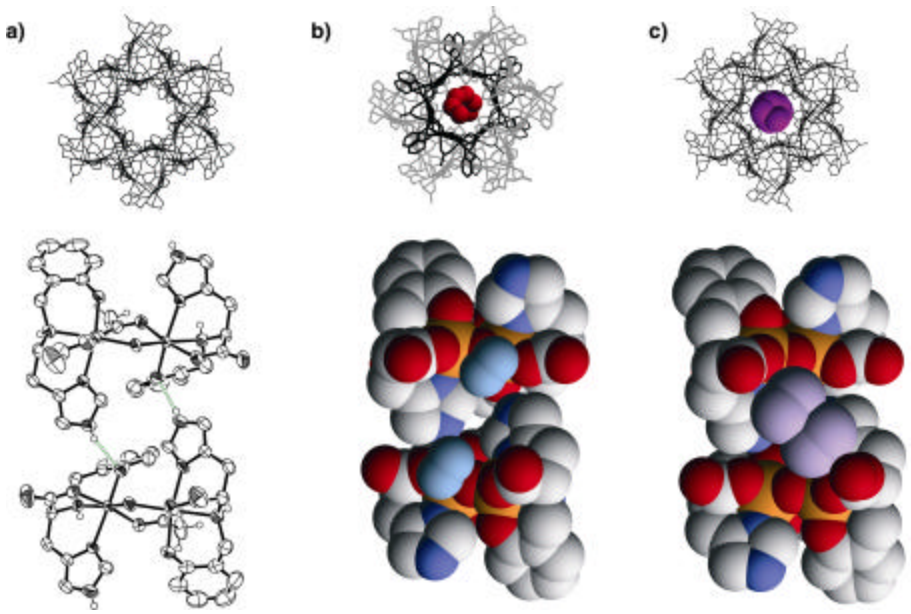

Figure 4.8 A part of the lattice structure viewed through the 001 plane (top) and H-bonding interaction between two binuclear complexes inside the channel (bottom) in the (a) dehydrated crystal **2**, (b) water (light blue, disordered) inside the channel of **1** and (c) iodine (purple, disordered) doped crystal **3**

atom inside a crystal have been observed previously[138,139] but we have not come across of any example of I_2 with both side interactions. Like the water molecules H-bonded to bridging hydroxide in **1**, I_2 molecules inside a channel orients in a helical fashion. The water (O11) in **1** utilizes the bridge proton to form H-bond but in **3**, the iodine uses the

oxygen atom to get oriented. Thus the helical arrangement of the polar cavity organizes host molecules helically using different weak interactions.

The intactness of I_2 and **1** in crystals of **3** were confirmed from their visible spectra in CCl_4 and water respectively.[140] The I_2 content of **3** estimated to be (Experimental section) 16% as opposed to calculated value of 26% for $[Fe_2(OAc)(OH)(S\text{-}Salhis)_2]\cdot H_2O\cdot I_2$. As crystals might adhere some I_2 on the surface we analyzed the crystals for I_2 also after repeated washing with CCl_4 and I_2 was found to be 12 %. Considering the fact that I_2 molecules are weakly bound and repeated washings might wash away some of the I_2 molecules from the channel, we assume that the channels have around half of the iodine sites filled with I_2. These experiments also confirm that the I_2 incorporated in the channel retains its chemical identity. Estimation of iodine under different condition showed that (a) iodine molecules are loosely bound inside the channels and tend to loose in solution, (b) surface adsorption of iodine is possible and (c) iodine is disordered inside the channel (X-ray studies) while, the resulting uncertainty on the quantity of iodine per gram of the crystal does not effect our conclusion on the incorporation of iodine inside the channel (from X-ray, TGA, analysis after washing to remove surface iodine), it affects the elemental analysis.

4.3.5 Determination of pKa of bridging hydroxide from UV-visible spectra

Complex **1** (as well as **4**) have high-spin Fe(III) center which is not expected to show any ligand field transitions (both Laporte and Spin forbidden). The Fe(III) coordinated to phenolate on the other hand are known to show strong phenolate → Fe(III)

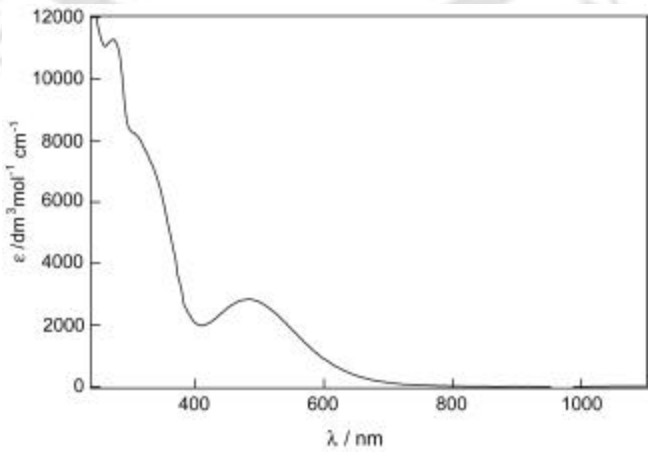

Figure 4.9 Electronic spectra of the complex **1** in MeOH.

Table 4.E UV-visible data of the complexes

Complexes	λ_{max} /nm (ε /dm^3 mol^{-1} cm^{-1})	Ref.
1	MeOH, 273 (11300), 302(sh), 481 (2900)	This work
4	MeOH, 275 (12500), 302(sh), 479 (2700)	This work
$Fe_2L_2O(OBz)^+$	CH_2Cl_2 336(8900), 400(sh), 522(3300),	133
$[Fe_2(OH)_2(NE)_2](NO_3)_2$	250(10500), 350(10380), 400(5400), 490(2060),	142

L=*N*-(*o*-hydroxybenzyl)-*N*,*N*-bis(2-pyridyl methyl)amine; HNE = *N*-(4-nitro-2-hydroxy -phenylmethyl-*N*-(2-pyridylmethyl)-amine.

charge transfer (CT) transitions.[141] The representative spectrum and experimental values for the absorption maxima of the complexes are depicted in Figure 4.9 and Table 4.E respectively. The absorption maxima at ~ 500 nm is assigned as the phenolate→ Fe(III) CT transitions comparing with other known complexes.[141] The absorption maxima at 273 nm is of original ligand as seen in the Cu(II) complex (Chapter III) and the deprotonated ligand (Chapter II). The shoulder at ~ 400 nm probably arises due to both phenolate- and oxo to Fe(III) CT transitions as observed in other hydroxo and oxo bridged complexes with phenolate containing ligand.[133]

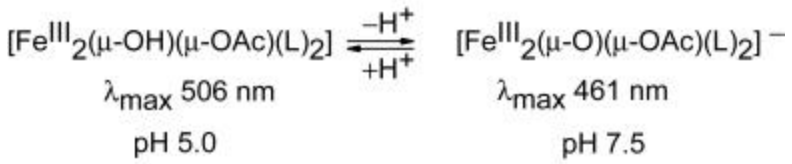

Scheme 4.I Protonation deprotonation equilibrium of **1** in water

Complex **1** in water gives violet color, which on treatment with alkali (NaOH solution) turned to brown. On addition of acid (perchloric acid) the brown color changed back to deep violet again. Figure 4.10 shows the spectrophotometric titration of **1** with varying amount of $HClO_4$. For this titration first we dissolved the complex in water at pH 7. Then NaOH was added slowly to get the pH 8.5, at this stage solution color was brown. To this solution dilute $HClO_4$ was added. The spectral changes demonstrated that the

addition of $HClO_4$ to this brown color solution leads to a progressive shift of the phenolate to iron(III) charge transfer transition (LMCT) from 460 nm to higher wavelengths. Finally, when pH was lower than 4.5, the maximum absorption shifted to 530 nm, and thereafter no further change took place. Excess amount of acid destroys the color completely possibly due to decomposition of the complex. These color changes can be explained by formation of oxo and hydroxo species in basic and acidic pH respectively (Scheme 4.I). Such equilibrium is not unusual. Occurance of phenolate → Fe(III) CT transition at higher energy (lower wavelength) in case of oxo bridged iron(III) dimer compared to corresponding hydroxo bridged dimer have been observed before.[133] This is probably due to protonation of the oxo-bridge leading to an increase of Lewis acidity of the iron(III), which facilitates charge transfer at lower energies. Considering the existence of **1** as only μ-OH species at pH 4.25 and as only μ-O species at pH 7.5, the pKa of the bridging proton was determined to be ~ 5.5 (Figure 4.10) as the concentration of both species at this point are 1:1. This is higher than the pKa of 3.5 determined for the other hydroxo bridged diiron(III) complex. Table 4.F shows few hydroxo bridged complexes where pKa was determined.

Table 4.F pKa value of bridging OH complexes

Complexes	Distance (Å),Angles(°)	pKa values	Ref.
$[Fe_2(OH)(O_2CCH_3)(SalHis)_2]$	Fe...Fe 3.517, Fe-O-Fe 126.35°, Fe1-O1 1.972, Fe2-O1 1.969	5.5	This work
$[Fe_2(OH)(O_2CCH_3)_2(HBpz_3)_2]^+$	Fe...Fe 3.439, Fe-O-Fe 123.1°, Fe1-O1 1.960, Fe2-O1 1.952	~3.5	134
Mammalian PAP	Fe...Fe 3.31Å, Fe-O-Fe 105. 7°, Fe1-O1 2.08Å, Fe2-O1 2.08 Å		143

$HBpz_3$ = hydrotris(1-pyrazolyl)borate;

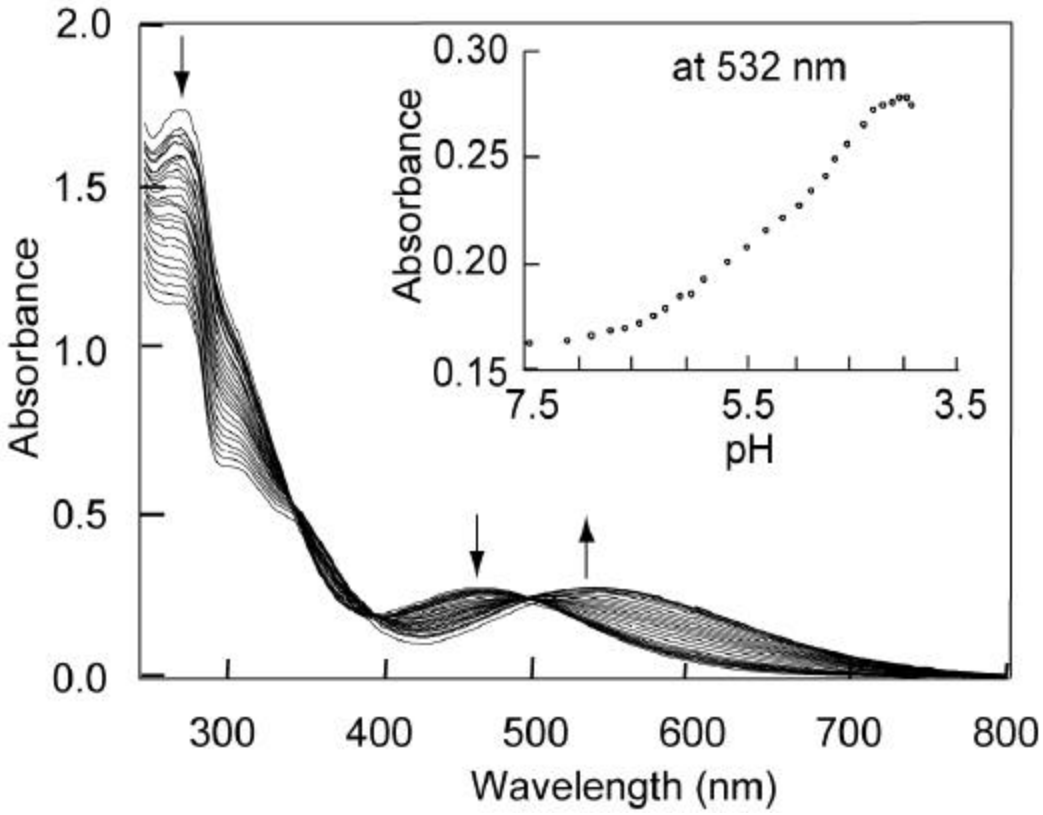

Figure 4.10 UV-visible spectra of **1** at various pH, arrow heads depict the increase or decrease of absorbance at a particular wavelength (inset) change in absorbance with respect to pH at 532 nm

Complex 1 as active site model of purple acid phosphatases (PAPs): Altogether complex **1** compares quite well as a structural model for oxidized inactive form of mammalian PAP active site. The imidazole, phenolate, carboxylate donors of the ligand closely resemble the histidine, tyrosine and aspartate donor present in the protein. The phenolate→ Fe(III) charge-transfer of aqueous solution **1** occur at 530nm (hydroxo form, pH 4-6) compared to PAPs 550nm. Crystallization of pig PAP at pH 5 results isolation of the protein with hydroxide bridge. This suggest that pKa of the hydroxo bridge of the protein might be higher than 3.5 because bridging hydroxo with pKa of 3.5 will have oxo: hydroxo ratio of ~32:1 at pH 5 (using Henderson's equation). Thus **1** has a hydroxo bridge with pKa value closer to that of pig PAPs.

Conclusion

In conclusion, we have synthesized a reusable enantiopure solid with one-dimensional helical channels (7-9 Å diameter). The presence of complementary H-bond donor (imidazole, amine) and acceptor (phenolate, carboxylate) in the same ligand contributed to the robustness of the crystal. Also helical arrangement of weak interaction capable group (hydroxo, carboxylato) inside a channel strongly influences the guest organization, a concept behind the use of channels for chiral separation[4] or template[4] which has not been shown before. Further, the molecules of **1** and **4** have a hydrophilic chiral cavity (Figure 4.2b) which might hold guest molecules through weak interaction. Unfortunately the cavity is not deep enough and is unlikely to distinguish between enantiomeric guests. On the other hand the cavity formed around the acetate group (Figure 4.2a) has a deeper cavity but the acetate has to be replaced first. In chapter 5 we have found a way to circumvent this problem by apparently flipping the phenolate rings forming a deeper cavity around the hydrophilic site.

Chapter V

Synthesis and characterization of a binuclear Ni(II) complex

In the previous chapter we have discussed about the synthesis of a binuclear Fe(III) complex with a C_2 symmetric cavity formed around the acetate ion. In the same Fe(III) complex a relatively open hydrophilic cavity capable of holding either water or iodine molecules in the solid state was present. The hydrophilic cavity in the iron complex had four carboxylate oxygen (H-bond acceptor) and one hydroxo bridge (H-bond donor), which in principle can interact with a chiral amine or any chiral guest through H-bond interaction. However, the shallowness of the cavity was disadvantageous. We explored the possibility of performing same reaction with a different metal center such as nickel(II). The idea was that Ni(II) will form a similar complex with chiral helix or phenoxo bridged dimer relatively common in Ni(II) or Cu(II) chemistry and by virtue of different bridging situation the cavity might be of different shape. This chapter presents the synthesis and characterization of a binuclear Ni(II) complex with a C_2 symmetric cavity around the polar carboxylate groups. One Na^+ is bound inside the cavity in the solid state, as evidenced from the X-ray crystallography.

5.1 Experimental Section

5.1.1 Solvents and Reagents

Details of the solvent purification, analytical measurements and starting materials have already discussed in Chapter 2 and Chapter 3. The details of ligand synthesis are given in Chapter 2 (Section 2.4.1).

5.1.2 X-ray Data Collection, Structure Solution and Refinement

Blue rod shaped crystals were grown by cooling concentrated methanolic solution of the Ni(II) complex. The crystals tend to loose solvent molecules easily, hence were sealed in a capillary tube for X-ray data collection. The reflection data were collected on a Bruker Smart CCD Area Detector diffractometer at 293(2) K using graphite monochromated MoKα radiation (λ = 0.71073 Å). Crystallographic data, together with details of data collection and structure refinement, are listed in Table 5.A. The absorption corrections were applied on the basis of ψ scans. The structure were solved by use of program SHELXL-97, G. M. Sheldrick, University of Göttingen.[73] and the refinement of *F* was carried out full-matrix block least-squares. All hydrogen atoms were placed at calculated positions (C-H = 0.96Å) and their parameters were fixed. The function minimized was $\Sigma w(F_0 - F_c)^2$, where $w = 1/\sigma^2(F_0)$ was used.

Table 5.A Selected crystallographic data for $Na[Ni_2(S\text{-Salhis})_2(OAc)]\cdot 6MeOH$

Empirical formula	$C_{34}\,H_{53}\,N_6\,Na\,Ni_2\,O_{14}$
Formula weight	910.23
Temperature	293(2) K
Wavelength	0.71073 Å
Crystal system, space group	Orthorhombic, $P2_12_12_1$
Unit cell dimensions	a = 11.106(3)Å alpha = 90 deg.
	b = 13.721(3) Å beta = 90 deg.
	c = 27.411(6) Å gamma = 90 deg.
Volume	4177.1(16) $Å^3$
Z, Calculated density	4, 1.447 Mg/m^3
Absorption coefficient	0.982 mm^{-1}
F(000)	1912
Crystal size	0.3 x 0.25 x 0.25 mm
Theta range for data collection	1.49 to 28.02 deg.
Limiting indices	-14<=h<=14, -18<=k<=16, -36<=l<=36
Reflections collected / unique	36977 / 9781 [R(int) = 0.0284]
Completeness to theta	28.02 98.1 %
Absorption correction	None
Refinement method	Full-matrix-block least-squares on F^2
Data / restraints / parameters	9781 / 0 / 593
Goodness-of-fit on F^2	1.025
Final R indices [I>2sigma(I)]	R1 = 0.0514, wR2 = 0.1370
R indices (all data)	R1 = 0.0657, wR2 = 0.1475
Absolute structure parameter	0.00
Largest diff. peak and hole	0.526 and -0.602 $e.A^{-3}$

5.2 Synthesis of $Na[Ni_2(S\text{-Salhis})_2(OAc)]\cdot 4H_2O$ (1)

A methanolic solution of $Ni(NO_3)_2\cdot 6H_2O$ (0.291 gm, 1.00 mmol) was added drop wise to a clear solution of *S*-H_2Salhis (0.269 gm, 1.00 mmol) and KOH (0.112 gm, 2 mmol) in 25 mL dry methanol. Color of the solution was changed from light blue to

greenish-blue with gelatinous precipitate. Excess sodium acetate (0.280 gm, 2 mmol) in methanol was added to this reaction mixture. The precipitate was dissolved and the color was changed to blue. The reaction mixture was stirred for 30 min. Volume of the reaction mixture was reduced by rotary evaporation to ~ 10 mL and kept in the refrigerator. After a day, blue rod shaped crystals were formed which was filtered and washed with cold methanol. The crystals were dried under vacuum, yield 80 %. The crystals lost crystallinity after drying. Crystal structure showed six MeOH molecules present but the CHN analysis matched with the formula $Na[Ni_2(S\text{-Salhis})_2(OAc)]\cdot 4H_2O$. Cal: C, 42.57; H, 4.72; N, 10.64; Ni, 14.7 % Found: C, 42.57; H, 5.19; N, 10.92; Ni, 13.2 %.

Ni(II) Estimation: In complex **1** nickel was estimated gravimetrically,[144] using ethanolic solution of dimethylgyloxime (DMG). In a typical experiment, exact amount (0.0735 gm) of the complex **1** was dissolved in aqueous HCl (10 ml 0.5 N). The solution was warmed in hot water and ethanolic solution of DMG was added (5 ml 1 % DMG). The reaction mixture was made alkaline using NH_4OH and was allowed to stand on the steam bath for 20-30 minutes whereupon red precipitates were settled out. Precipitate was filtered through a Gooch crucible and dried at 110-120º C and weighted. Ni(II) in the complex **1** was found to be 13.2 % (expected 14.7 %).

5.3 Results and Discussion

5.3.1 Synthesis and Selected Properties

Stirring $Ni(NO_3)_2\cdot 6H_2O$, H_2S-L, NaOH and NaOAc together in MeOH at 1:1:2:2 ratio, the solution turned light blue color. Upon concentrating the solution followed by overnight cooling yielded the needle shaped crystals in ~70-75 % yield. Comparing the IR spectra of **1** with that of deprotonated ligand and the Fe(III) complexes characterized in the previous chapter, two closely spaced peaks at 1610, 1593 and a peak at 1348 cm^{-1} were identified as asymmetric and symmetric carboxylate stretches originated from the ligand respectively. The complex **1** showed broad stretches at 3469 cm^{-1} due to OH (water or H-bonded OH) stretch. Due to broadness of the OH peak NH stretch could not be identified clearly. Further the complex has two peaks at 1560 and 1452 cm^{-1}, with $\Delta\nu$ 108 cm^{-1}, attributed to the ν_{asym} and ν_{sym} stretching modes of the acetate anion

coordinated to the Ni(II) centers in the bridging form.[76, 145] The stretches for NO_3^- from starting material was absent.

The elemental analysis support the formulation of the complex as $Na[Ni_2(OAc)(S\text{-}Salhis)_2]\cdot 4H_2O$. The thermogravimetric analysis (TGA) between 30- 190ºC shows weight loss of 8.3 % for **1** against the calculated values of 9.11 % ($4H_2O$) Figure 5.1. Complex **1** heated at 190ºC temperature, was dissolved in MeOH and the UV-visible spectrum was checked. The spectrum was identical with **1**, confirming that only solvent was lost during heating. After the temperature of 250º C complex **1** decomposes and the complex turned black insoluble powder. TGA also support the above formulation of the complex.

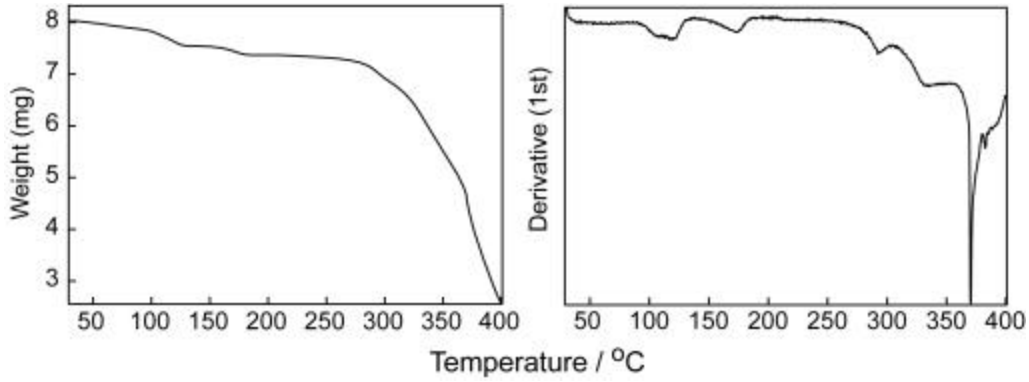

Figure 5.1 TGA and DTA plot of complex **1**

The molar conductance of **1** is 70 S cm^2 mol^{-1} in methanol (expected for 1:1 electrolyte in methanol is in the range of 85-115 S cm^2 mol^{-1}).[77] Conductance of the complex is slightly lower than 1:1 electrolyte in methanol but very much higher that of the non-electrolyte.

The room temperature magnetic moment of the complex **1** was found to be 3.07 per Ni atom. Similar values were reported for other bridged dinuclear Ni(II) complexes (Table 5.B).

Table 5.B Magnetic moment of dinuclear Ni(II) complexes

Complexes	μ_{eff} (BM) /Ni	Ref.
$[Ni_2(S\text{-Salhis})_2(OAc)]Na$	3.07	This work
$[Ni_2(Phsal)_4(OAc)]^-$	3.18	146
$[Ni_2(L^2)(OAc)]^{2+}$	2.94	147
$[Ni_2(L^3)(Opr)]^{2+}$	3.15	148
$[Ni_2(L^1)(OAc)]^{2+}$	3.14	148

HL^1 = *N,N,N',N'*-tetrakis[(1-methyl-2-benzimidazolyl)methyl]-2-hydroxy-1,3-diaminopropane; HL^2 = 2-(2-Hydroxyphenyl)-1,10-phenanthroline; HL^3 = *N,N,N',N'*-tetrakis[(1-ethyl-2-benzimidazolyl)-methyl]-2-hydroxy-1,3-diaminopropane; Phsal = phenylsalicylaldimine.

5.3.2 Crystal structure of complex $Na[Ni_2(S\text{-Salhis})_2(OAc)]\cdot 6MeOH$ (1)

The complex **1** was crystallized in the chiral space group $P2_12_12_1$ in the orthorhombic crystal system. An ORTEP[75] view of the complex **1** is shown in Figure 5.2 together with the numbering scheme. Selected bond distances and angles are given in Table 5.C.

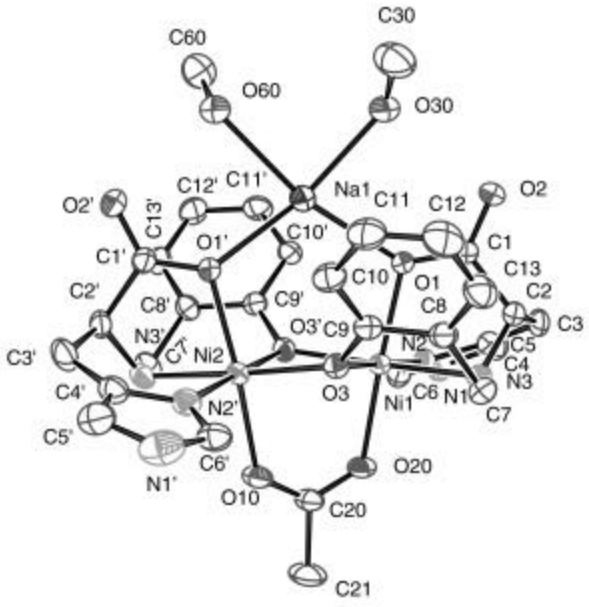

Figure 5.2 An ORTEP drawing of $Na[Ni_2(OAc)(S\text{-Salhis})_2]$ with the atom numbering scheme. Thermal ellipsoids are drawn at the 50% probability level, solvent molecules are omitted for clarity

Table 5.C Selected bond distances (Å) and angles (°) of the complex **1**

	Atoms	Distances /Angles	Atoms	Distances /Angles
	Ni1…Ni2	3.004		
Ni-imidazole	Ni1-N2	2.070 (3)	Ni2-N2'	2.032 (4)
Ni-amine	Ni1-N3	2.088 (4)	Ni2-N3'	2.073 (4)
Ni-phenolate	Ni1-O3	2.060 (3)	Ni2-O3'	2.057 (3)
Ni-phenolate2	Ni1-O3'	2.037 (3)	Ni2-O3	2.028 (2)
Ni-acetate	Ni1-O20	2.077 (3)	Ni2-O10	2.089 (3)
Ni-carboxylate	Ni1-O1	2.064 (3)	Ni2-O1'	2.081 (3)
Na-carboxylate	Na1-O1	2.386 (3)	Na1-O1'	2.334 (3)
Na-methanol	Na1-O30	2.3459 (18)	Na1-O60	2.410 (2)
Ni-bridge-Ni	Ni1-O3-Ni2	94.57 (11)	Ni1-O3'-Ni2	94.42 (11)
	N2-Ni1-N3	86.50 (14)	N2'-Ni2-N3'	86.48 (15)
	N3-Ni1-O3	90.86 (12)	N3'-Ni2-O3'	92.40 (12)
	O3-Ni1-O3'	83.98 (11)	O3'-Ni2-O3	84.30 (11)
	O3'-Ni1-N2	98.60 (12)	O3-Ni2-N2'	96.86 (14)
	O3-Ni1-O1	88.55 (11)	O3-Ni2-O1'	97.28 (11)
	O1-Ni1-N3	81.46 (12)	O1'-Ni2-N3'	80.59 (13)
	O1-Ni-O20	175.05 (12)	O1'-Ni2-O10	173.12 (12)
	O1'-Na1-O1	112.16 (11)	O60-Na1-O30	86.82 (6)
	O1'-Na1-O60	81.88 (9)	O1-Na1-O30	80.92 (9)

The complex **1** has two octahedral Ni(II) bridged by two phenolate oxygen and one acetate group. The Ni1…Ni2 separation is 3.004 Å which is substantially shorter than the other acetate bridged Ni(II) complexes but comparable to the other known bis phenolato, acetate tribridged Ni(II) dimers (Table 5.D). Each nickel atom comprises an N_2O_4 donor set from a bridging acetate, two bridging phenolate from two ligands, a carboxylate oxygen and two nitrogen atoms one from imidazole group and another from secondary amine. The phenolate to Ni(II) distances are 2.060 (Ni1-O3) and 2.028 (Ni2-O3)(Table 5.C). Similar triply bridged Ni(II) dimers have been reported with similar higher asymmetry.[146,147] The acetato group bridges symmetrically with the two

nickel(II) atoms at a distance of Ni1-O20 and Ni2-O10 is 2.077(3) and 2.089(3)Å respectively.

Table 5.D Tri-bridged Ni(II) dimers (bis-phenolato and mono acetato)

Complexes	Ni…Ni distances	No. of OAc bridge	Ref.
$[Ni_2(S\text{-Salhis})_2(OAc)]^-$	3.004	1	This work
$[Ni_2(Phsal)_4(OAc)]^-$	3.101(2)	1	146
$[Ni_2(L^2)(OAc)]^{2+}$		1	147

Phsal = phenylsalicylaldimine; HL^2 = 2-(2-Hydroxyphenyl)-1,10-phenanthroline.

The conformation at the chiral carbon of the ligand in **1** is *S*. In addition to the asymmetric carbon centre in the ligand, the coordination of amine N to the Ni(II) gives rise to an asymmetric secondary nitrogen atom, N3 which has the *R* configuration. The lower dihedral angles between Ni-N_{amine} and the methylene arm of the phenolate rings results in a folding of the phenolate ring forming a bowl shaped C_2 symmetric and essentially hydrophilic cavity around carboxylate groups (Figure 5.3 left).

The sodium atom situated at the cavity, is weakly coordinated to two carboxylate oxygen O1 and O1' at a distance of 2.386(3) and 2.334(3) Å respectively (Figure 5.3) and two solvent methanol molecules O30 and O60 at a distance of 2.3459(18) and 2.410(2) respectively. The coordination around the sodium ion is almost square planer.

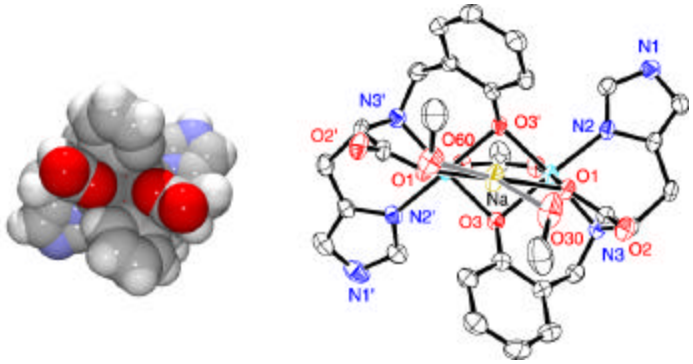

Figure 5.3 A C_2 symmetric cavity around the polar carboxylate groups, Na^+ is inside the cavity in the solid state, as evidenced from the X-ray crystallography (for clarity we have removed the Na^+ ion from the space filling model left)

Several type of hydrogen bonding was observed in the crystal lattice. H-bonding schemes are presented in Figure 5.4 and H-bond distances are in Table 5.E. The two dimeric units are held together by the solvent molecule methanol O80 (Figure 5.4b). The methanol O80 is hydrogen bonded with N3'(amine nitrogen) and O10 (acetate oxygen) at a distance of 3.1871Å and 2.7230 Å of one dimeric unit and (imidazole nitrogen) N1 of another dimeric unit at a distance of 2.9303 Å (Figure 5.4b). The solvent methanol molecule O30 and O60 not only coordinated with the sodium atom but also hydrogen bonded with the two carboxylate oxygen atoms (bonded and non bonded oxygen). The solvent methanol molecule O30 is H-bonded with carboxylate atoms O1 and O2 at a distance of 3.0709 Å and 2.6877 Å. The methanol molecule O60 is H-bonded with O1'and O2' at a distance of 3.1100Å and 2.6824 Å (Figure 5.4a). Apart from this the carboxylate oxygen O2 is hydrogen bonded with another methanol molecule O70 at a distance 2.7033 Å. The imidazole N1' is hydrogen bonded with two solvent molecule O60 and O70 at a distance of 3.3284 Å and 2.8585 Å respectively. Another molecule of imidazole N1 is hydrogen bonded with two solvent molecules O80 and O50 at a distance of 2.9303 Å and 2.9749 Å respectively. The solvent molecule O50 a lso H-bonded with another solvent molecule O40 at a distance 2.6803Å.

Out of the six H-bonded methanol present in the lattice, O80 is within H-bonded distances of three H-bond donor/acceptor (Table 5.E). Although the CH_3OH molecules in the crystal get readily replaced by H_2O, the one water molecule which is lost during heating at relatively higher temperature (150-190º C) might be the one which replaces O80. However, it could not be confirmed at this stage.

Table 5.E Hydrogen-bond distances

Atoms	Distances (Å)	Atoms	Distances (Å)
Na1-O30	2.3459	Na1-O60	2.4102
N1-O50	3.1665	N1-O80	2.9289
N1'-O70	2.8585	N1'-O60	3.2670
O10-N3'	3.0161	O20-N3	3.0602
O20-O40	2.6974	O40-N3	3.2855
O40-O50	2.6803	O40-N3'	3.9322
O50-N3'	3.1669	O50-N1	3.1679
O60-O30	3.2691	O60-N1'	3.3284
O60-O1'	3.110	O60-O2'	2.6824
O70-O2	2.7033	O80-O10	2.7230
O80-O50	2.9749	O80-N3'	3.1871
O80-N1	2.8585		

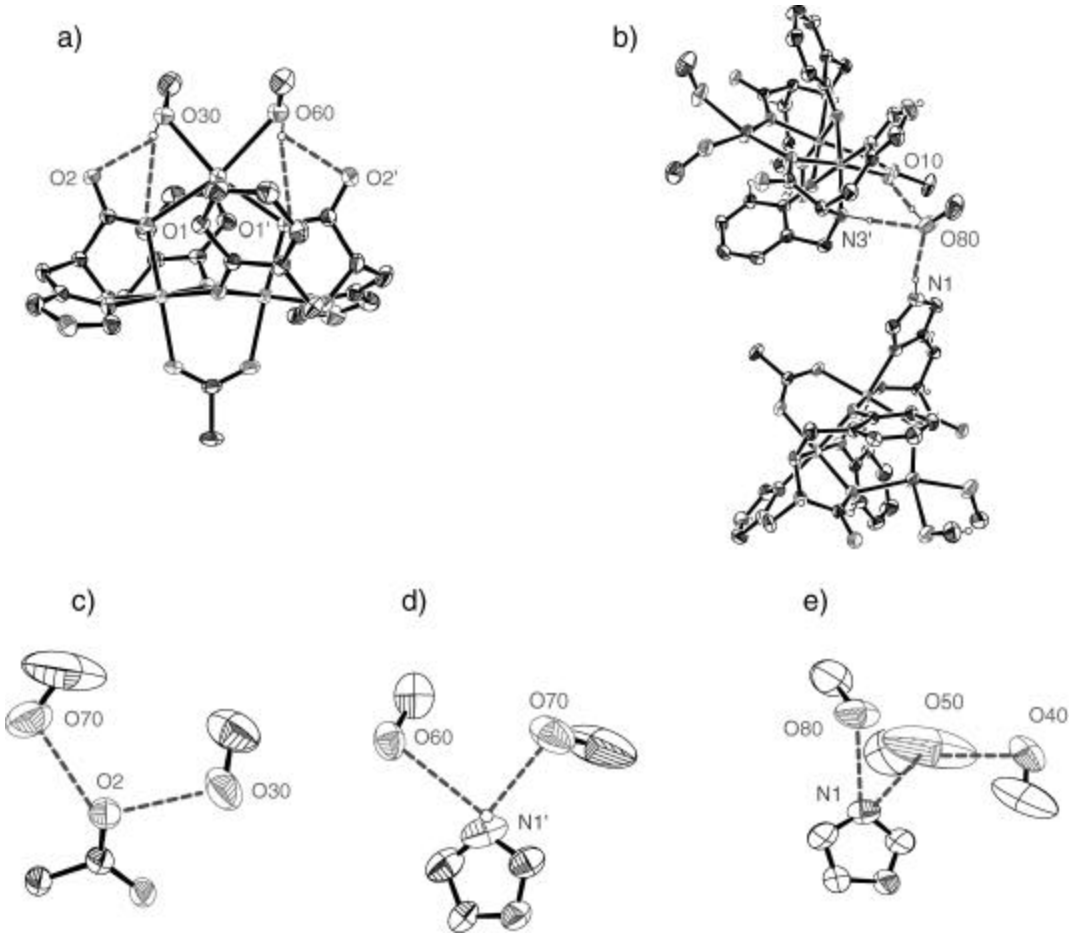

Figure 5.4 Intra and inter-molecular hydrogen bonding

5.3.3 UV-visible studies

The complex **1** exhibits two distinct absorption bands at 618 and 1025 nm and a shoulder at 355 nm. Considering octahedral coordination around the nickel (II) ions, the two bands at 1025 and 618 nm can be assigned to the spin-allowed d-d transitions $^3T_{2g}$ $^3A_{2g}$ and $^3T_{1g}$ $^3A_{2g}$ respectively. More accurately the symmetry around Ni(II) should be considered C_{2v}. In that case several closely spaced transitions are possible.[148] For example, $^3T_{2g}$ $^3A_{2g}$ transition in octahedral symmetry will become three closely spaced $^3A_1 \leftarrow {}^3B_1$, $^3A_2 \leftarrow {}^3B_1$ and $^3B_2 \leftarrow {}^3B_1$ transition. This might be the reason for the asymmetric nature of the absorptions. The absorption at 775 nm is possibly due to the

spin forbidden $^1E_g \leftarrow {}^3A_{2g}$ (considering octahedral) usually observed in Ni(II) complexes.[149] The shoulder at 355nm is LMCT band and masks the low intensity $^3T_{1g}(P) \leftarrow {}^3A_{2g}$ transition. These types of transition were observed in bridged octahedral complexes (Table 5.F). The transition at 1025 nm ($^3T_{2g} \rightarrow {}^3A_{2g}$) is ~10Dq value, i.e. the ligand field strength. Comparing this value with $[Ni(H_2O)_6]^{2+}$, $[Ni(his)_2]$ and other N_6 coordinated complexes, the ligand field of the present complex is found to be higher than $[Ni(H_2O)_6]^{2+}$ but lower than $[Ni(his)_2]$ complex [149] (Table 5.F). The characteristic UV-visible spectrum for the complex **1** in methanolic solution is shown in Figure 5.5.

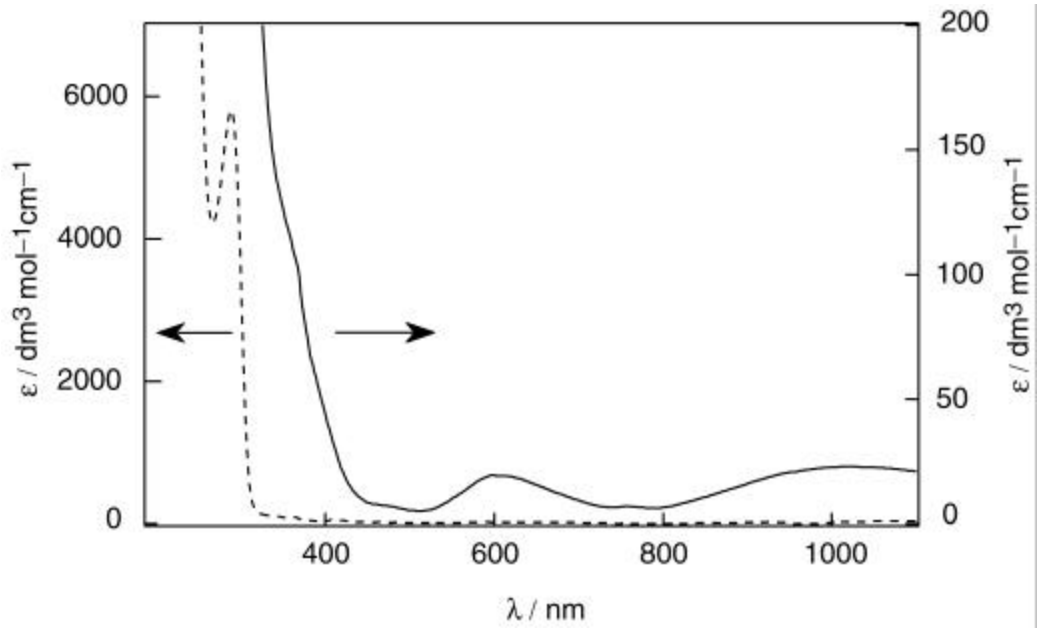

Figure 5.5 UV-visible spectrum of the complex **1** in MeOH

Table 5.F UV-visible spectroscopic data

Complexes	λ_{max} (nm)[ε_{max} /(dm^3 mol^1 cm^{-1})]	Solvent	Ref.
$[Ni_2(salhis)_2(OAc)]$	1025(21), 618(16), 355(sh), 288(5800)	MeOH	This work
$[Ni_2(L^3)(OAc)]^{2+}$	500(80), 381(12000), 295(39000)	MeCN	147
$[Ni_2(L^1)(OAc)]^{2+}$	1008(20), 649(19), 411(34)	DMF	150
$[Ni_2(L^2)(OAc)]^{2+}$	1017(23), 644(23), 407(39)	DMF	150
$[Ni_2(L^2)(Opr)]^{2+}$	1027(22), 647(20), 409(35)	DMF	150
$[Ni(H_2O)_6]^{2+}$	1176(2), 724(2), 395(5)		149
$[Ni(his)_2]$	934(7), 555(8), 357(10)		149
$[Ni(Im)_6]^{2+}$	970, 568, 355		149

HL^1 = *N,N,N',N'*,tetrakis[(1-methyl-2-benzimidazolyl)-methyl]-2-hydroxy-1,3-diaminopropane; HL^2 = *N,N,N',N'*-tetrakis[(1-ethyl-2-benzimidazolyl)-methyl]-2-hydroxy-1,3-diaminopropane; HL^3 = 2-(2-Hydroxyphenyl)-1,10-phenanthroline.

Conclusions

We have synthesized an enantiopure dinuclear Ni(II) complex, which has a C_2 symmetric polar cavity formed around four carboxylate oxygen (possible H-bond acceptor). Interestingly, one square planar Na^+ ion is bound in this cavity. However, the molar conductance value of 70 (S cm^2 mol^{-1}) in MeOH (expected for 1:1 electrolyte is 80-115 S cm^2 mol^{-1}) shows that it is ionized almost completely in polar solvent. Different types of inter and intra molecular H-bonding was observed in the crystal. This once again shows that the present ligand utilizes all the possible H-bond donor/acceptor present in the ligand (Chapter II, Figure 2.1) to form severely H-bonded lattices.

Chapter VI

Nitrate bridged Iron(III) complexes for colorimetric and conductometric detection of amines in solution and vapor phase

In this chapter we have presented the synthesis and characterization of three high-spin binuclear iron(III) complexes with the general formula, $[Fe_2(L)_2(NO_3)_2]$. IR spectroscopy, elemental analysis and ESI-mass spectra support the formulation of the complexes. Each of the complexes displays a strong phenolate to Fe(III) charge-transfer transition in the range of 520-585 nm with a moderately high extinction coefficient. The color and conductance of the solutions of binuclear Fe(III) complexes change on addition of amines. The molar conductance of the complexes in methanol shows 1:1 electrolyte characteristics, however addition of amines to the methanolic solution of the complexes increases molar conductance that behaves like 1:2 electrolyte.

Amines are essential components of food such as banana, cheese, fish and are present as pollutants in wastewater from surfactant, fertilizer, pharmaceutical and dye manufacturing industries.[151] As amines are biologically important and at the same time toxic in higher concentration level, several methods to detect amines in solution and vapor state have been reported.[151-155] Majority of the methods use the Schiff base formation of amine with chromogenic aldehyde to detect amine colorimetrically.[151-154] In this chapter we tried to understand the reason for the change in color and conductance in case of our complexes. Additionally we have checked the feasibility of using these complexes as amine detector in solution and on solid support.

6.1 Experimental Section

6.1.1 Solvents and Reagents

Triethylamine was dried by distillation over KOH. Chloroform was made acid free by washing with saturated sodium bicarbonate solution, then by washing five to six times with water followed by keeping over anhydrous $CaCl_2$ for 24 hour and distilled. Hexane was purified by distillation. Dichloromethane was purified by washing with 5 per cent sodium carbonate solution, followed by water, and dried over anhydrous $CaCl_2$. Details of solvent purification and starting materials other than stated above are already discussed in chapter 2.

6.1.2 Measurements

Solid-state magnetic susceptibility was recorded by using Sherwood Scientific balance MSB–1. Variable-temperature (80 to 300 K) solid-state magnetic susceptibility

measurements were recorded by the Faraday technique using a locally built magnetometer at IIT Kanpur, India. The setup consists of an electromagnet with constant gradient pole caps (polytronic Corporation, Mumbai, India), Sartorius M25-D/S balance (Germany), a closed cycle refrigerator and a Lake Shore temperature controller (Cryo Industries, USA). All measurements were made at fixed main field strength of 10 kG.

Solution magnetic susceptibility measurements were performed by usual NMR method[156] with a PMX-60 JEOL (60 MHz) spectrometer and made use of the paramagnetic shift of the methyl protons of benzene / methanol and the $SiMe_4$ reference as the measured NMR parameter using the Equation 3. 1

$$\text{Mass susceptibility } \chi_m = \frac{3\Delta f}{2\pi f m} + \chi_0 + \frac{X_0 (d_0 - d_S)}{m} \qquad (3.\ 1)$$

Where Δf is the frequency separation between the two TMS or solvent peaks in Hz, f is the frequency at which the proton resonances are being studied in Hz, m is the mass of the substance contained in 1 mL of solution, χ_0 is the mass susceptibility of the solvent, d_0 is the density of the solvent and d_S that of solution. Final term involved in Equation 3. 1 is negligible for the highly paramagnetic substances.

The temperature of the NMR probe was determined[157] using CH_3OH proton signals using Equation 3. 2

$$T = 435.5 - 1.193\ (\Delta f) - 29.3\ (\Delta f \times 10^{-2})^2 \qquad (3.\ 2)$$

Where Δf is the frequency difference between the positions of $-CH_3$ and $-OH$ protons in Hz. Solvent susceptibilities[158] and diamagnetic corrections[159] were taken from literature tabulations. The instrumentation details for other measurements have already been discussed in Chapter 2.

6.2 Syntheses of Fe(III) complexes

6.2.1 $[Fe_2$ (*S*-Salhis)$_2(NO_3)_2]\cdot$ 3MeOH$\cdot$ 1.5H_2O (1)

A methanolic solution of $Fe(NO_3)_3\cdot 9H_2O$ (0.404 gm , 1.00 mmol) was added drop wise to a clear solu tion of *S*-H_2SalHis (0.258 gm, 0.987 mmol) and KOH (0.112 gm, 1.99

mmol) in 25 mL dry methanol. After stirring for 30 min the color of the solution was changed from brown to violet with some undissolved white suspension. The mixture was filtered off and the filtrate was evaporated to dryness. This solid (0.350gm) was triturated with acetonitrile, filtered and dried under reduced pressure. This solid contains excess of KNO_3 that was removed by dissolution of the solid in pyridine and subsequent filtering of the undissolved KNO_3. The pyridine was removed and washed with excess acetonitrile. The solid was redissolved in methanol and diethyl ether was added. On cooling the solution in freeze for two days yielded the complex as violet colored solid. After filtration the solid was washed with dry diethyl ether and dried under reduced pressure (yield, 0.200 gm, 65%).

Anal. Calcd. for $C_{26}H_{26}N_8O_{12}Fe_2 \cdot 3CH_3OH \cdot 1.5H_2O$: C, 39.70; H, 4.70; N, 12.77. Found: C, 39.73; H, 4.30; N, 12.43. IR (KBr, cm^{-1}) $\nu(COO)_{assym}$, 1627 and 1593; $\nu(NO_3)$ 1383. UV-visible in MeOH [λ_{max} /nm (ε /dm^3 mol^{-1} cm^{-1})]: 275(12700), 310(sh) 520(2800). Λ_M (MeOH): 97 S cm^2 mol^{-1}. μ_{eff}(solid, 298 K); 6.50 B.M./2Fe; μ_{eff} (MeOH, 298 K) 5.65 B.M./2Fe.

6.2.2 $[Fe_2(S\text{-Salmet})_2(NO_3)_2] \cdot 3H_2O$ (2)

For the synthesis of **2**, we added a methanolic solution of $Fe(NO_3)_3 \cdot 9H_2O$ (0.404 gm , 1.00 mmol) to a clear solution of *S*-H_2Salmet (0.258 gm, 1.00 mmol) and KOH (0.1122 gm, 2.00 mmol) in 25 mL of dry methanol. The reaction mixture was stirred for 30 min resulting in the color change from brown to violet of the solution with some undissolved white suspension. The mixture was filtered off and the filtrate was evaporated to dryness. This solid (0.300 gm) was triturated with acetonitrile, filtered and dried under reduced pressure. The excess KNO_3 was removed by treatment with pyridine. The resulting solid material was further purified by using methanol / Et_2O. The solid product was dried under reduced pressure, (yield, 0.248 gm 60%)

Anal. Calcd. for $C_{24}H_{30}N_4O_{12}S_2Fe_2 \cdot 3H_2O$: C, 36.19; H, 4.56; N, 7.03. Found: C, 36.39; H, 4.56; N, 7.31. IR (KBr, cm^{-1}) $\nu(COO)_{assym}$ 1598, $\nu(NO_3)$ 1383. UV-visible in MeOH [λ_{max} /nm (ε /dm^3 mol^{-1} cm^{-1})]: 275(16600), 307(sh) 525 (3200). Λ_M (MeOH): 120 S cm^2 mol^{-1}. ESI-MS(+) in MeOH for $[Fe_2(SalMet)_2NO_3]^+$ *m/z* calculated 680, found 680.2, μ_{eff}(solid, 298 K) 3.99 B.M./Fe.

6.2.3 [Fe_2 *o*-Me-(*S*)-Salmet)$_2$(NO_3)$_2$]· 3H_2O (3)

In a similar procedure $Fe(NO_3)_3$· $9H_2O$ (0.300 gm , 0.745 mmol) in methanol was added to a mixture of *o*-Me-(*S*)H_2SalMet (0.200 gm, 0.745 mmol) and KOH (0.084 gm, 1.487mmol) in 25 mL dry methanol. After stirring for 30 min. the color of the solution was changed from brown to violet with some undissolved white suspension. The mixture was filtered off and the filtrate was evaporated to dryness. Excess KNO_3 was removed from the solution in a similar way as stated above. The resulting solid material was further dissolved in minimum volume of dichloromethane and diethyl ether was added as a precipitant. The reaction mixture was kept overnight in the freeze. The solid product was filtered and dried under reduced pressure (yield, 0.150 gm, 50 %).

Anal. Calcd. for $C_{26}H_{34}N_4O_{12}S_2Fe_2$· $3H_2O$: C, 37.86; H, 4.89; N, 6.79. Found: C, 38.04; H, 4.92; N, 6.61. IR (KBr, cm^{-1}) í(COO)$_{assym}$ 1605(s), 1598(s), ν(NO_3) 1383. UV-visible [λ_{max} /nm (ε /dm^3 mol^{-1} cm^{-1})] in MeOH 275(18500), 305(sh), 555(3400); in CH_2Cl_2: 330(sh), 585(1650). Ë$_M$: (CH_2Cl_2) 0.5 S cm^2 mol^{-1}, (MeOH) 125 S cm^2 mol^{-1} ESI-MS(+) in MeOH for [Fe_2(*o*-Me-SalMet)$_2NO_3$]$^+$ *m/z* calculated 708.1 found 708.2. ì$_{eff}$ (solid, 298 K) 4.95 B.M./Fe; ì$_{eff}$(MeOH, 298 K) 5.15 B.M./2Fe.

6.3 Results and Discussion

6.3.1 Syntheses and Selected Properties

Mixing of $Fe^{III}(NO_3)_3$· $9H_2O$, ligand and KOH respectively in MeOH at 1:1:2 ratio, the solution turned bluish-purple for complexes **1** and **2** but blue color for complex **3**. All the complexes were treated with pyridine to remove excess KNO_3. Complexes **1** and **2** were purified from methanol/ diethyl ether. On the other hand complex **3** was purified from CH_2Cl_2 / diethyl ether as this was the only complex soluble in less polar solvent such as CH_2Cl_2.

Comparing the IR spectrum of **1**, **2** and **3** with that of deprotonated ligand and the Fe(III) complexes characterized in the previous chapter, the peaks at 1640 and 1598 cm^{-1} were identified as asymmetric carboxylate stretch of the ligand. The symmetric carboxylate stretch is overlapped with strong NO_3 stretch at 1381 cm^{-1}. The presence of the NO_3^- was confirmed from the peaks at 1381 cm^{-1} (strong) which was absent in the [Fe_2(μ-OH)(μ-OAc)(*S*-Salhis)$_2$] complex characterized in Chapter IV. Several authors

reported coordination of NO_3^-, as monodentate or bidentate ligand, based on the IR analyses.[76] However, the deterministic peaks mentioned could not be identified in the present complexes due to the presence of ligand peaks in those region. Thus the presence of NO_3^- could be confirmed from the IR but their mode of coordination (monodentate, bidentate or bridging) could not be determined conclusively. All the complexes show broad stretches at 3410 cm^{-1} and two sharp stretches at 3185, 3111 cm^{-1} due to water and N-H stretches respectively.

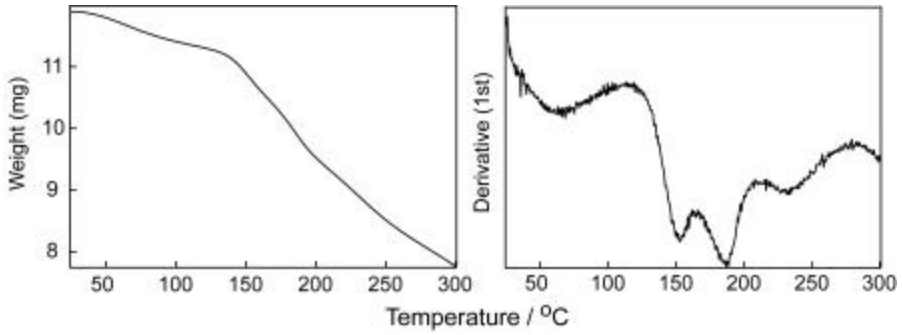

Figure 6.1 TGA and DTA plot of complex **1**

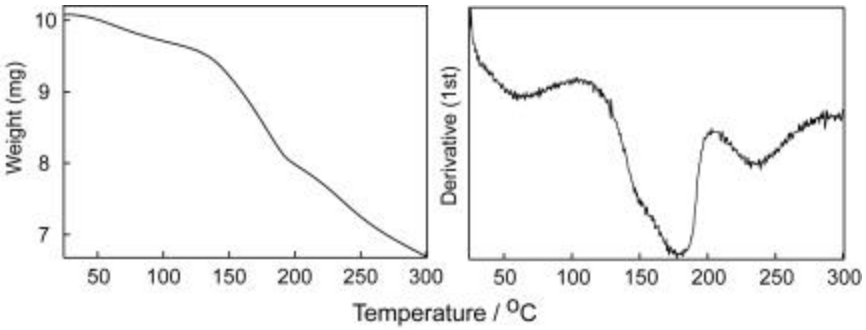

Figure 6.2 TGA and DTA plot of complex **2**

The elemental analysis (experimental section) supported the formulation of the complexes as $[Fe_2$ (*S*-Salhis)$_2(NO_3)_2]\cdot$ 3MeOH$\cdot$ 1.5H_2O **1,** $[Fe_2$ (*S*-Salmet)$_2(NO_3)_2]\cdot$ 3H_2O **2** and $[Fe_2$ *o*-Me-(*S*)-Salmet$)_2(NO_3)_2]\cdot$ 3H_2O **3** respectively. The thermogravimetric analysis (TGA) between 30 – 110º C shows weight loss of 7.7 % for **1**, 6.1 % for **2** and 5.8 % for complex **3** against the calculated values of 8.6 % for 4H_2O (7.4 % for 2MeOH), 6.8 % (3H_2O) and 6.6 % (3H_2O) respectively (Figure 6.1 and 6.2). After heating at 180º C

the complexes decomposes. The amount of solvent loss in **1** is less than as expected from CHN analysis. This might be due to the fact that some of the solvent molecules might have been lost near 120-150° C region. Loss of solvent between 120-180° C has been observed in $[Fe_2(OAc)(OH)(S)\text{-Salhis})_2]\cdot 4H_2O$ (120° C, Chapter 4) and $Na[Ni_2(OAc)(S\text{-Salhis})_2]\cdot 4H_2O$ complexes (~ 180° C, Chapter 5).

All the three complexes have molar conductance in the range of 97-120 S cm^2 mol^{-1} in methanol (Table 6.A). Which are corresponding to the 1:1 electrolyte in methanol.[77] Only the complex **3** is soluble in CH_2Cl_2 and the conductance in CH_2Cl_2 was found to be only 0.5 S cm^2 mol^{-1}, which indicates the non-electrolyte nature of the complex in CH_2Cl_2. Possibly in CH_2Cl_2 the complex **3** prefer to stay as $[Fe_2(o\text{-Me-Salmet})_2(NO_3)_2]$ and in methanol as $[Fe_2(o\text{-Me-Salmet})_2(NO_3)](NO_3)$.

6.3.2 UV-visible spectrum

The electronic spectra of all the complexes at different solvent are summarized in the Table 6.A. The electronic spectra (Figure 6.3) of all the three complexes have relatively intense charge-transfer (CT) band that gives rise to the reddish purple to bluish purple colors (at 520-585 nm) and which can be assigned to a LMCT transition from the phenolate oxygen to the ferric ion.[160] Such LMCT transitions usually are intense. Ligand field transition are not expected for high-spin Fe(III) ion. A second CT band occurs at 315 nm.

Table 6.A Electronic absorption and conductivity data of the complexes

Complexes	Solvent	λ_{max} (nm)	Λ_M (S cm^2 mol^{-1})	Ref.
1	MeOH	275(12700), 310(sh) 520(2800)	97	This work
2	MeOH	275(16600), 307(sh) 525 (3200)	120	This work
3	MeOH	275(18500), 305(sh), 555(3400)	125	This work
3	CH_2Cl_2	330(sh), 585(1650),	0.5	This work
$[Fe(\mathbf{IIIa})_2(MeOH)]NO_3$	EtOH	563(4570), 305(19000)		160
$[Fe(\mathbf{IIIa})_2(Im)_2]NO_3$	EtOH	530		160
$[Fe(\mathbf{VIII})]^+$	MeOH	540		160
$[Fe(\mathbf{VIII})(Im)]$	MeOH	480		160

[IIIa] 2-(5-methylpyrazol-3-yl)phenol; [VIII] *N,N'*-bis(2-hydroxybenzyl)ethylenediamine

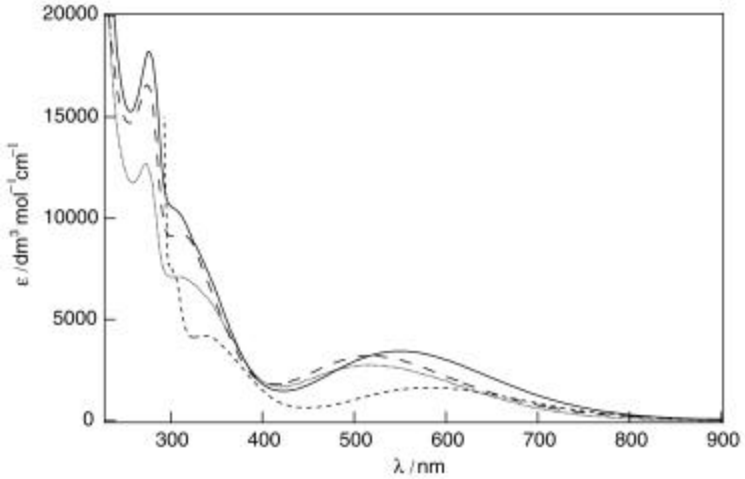

Figure 6.3 UV-visible spectrum of 1 (Ì Ì Ì Ì Ì Ì Ì) in MeOH, 2 (—) in MeOH and 3 (——) in MeOH, complex 3 (· · · · · · · · ·) in CH_2Cl_2

6.3.3 Proposed structures of the complexes

From conductance values, it can be inferred that the complex **3** in CH_2Cl_2 is non-conducting but behaves as 1:1 electrolyte in MeOH. In case of **1** and **2**, which are not soluble in CH_2Cl_2, behaves as 1:1 electrolyte in MeOH. We can explain this by considering one bridging NO_3^- in the complexes in MeOH. The similarity in UV-visible spectra of all three complexes in MeOH might be due to similar structural features present in all the complexes. In case of **3,** both the NO_3^- might be bridged or coordinated in CH_2Cl_2 as a result behaves as a neutral species. Taking all these in consideration and the fact that there are very few thioethers coordinated to Fe(III) complexes exist[161] we propose the structure of the complexes as shown in Figure 6.4. In MeOH all the complexes possibly have one nitrato bridge. However, possibility of a second aquo or

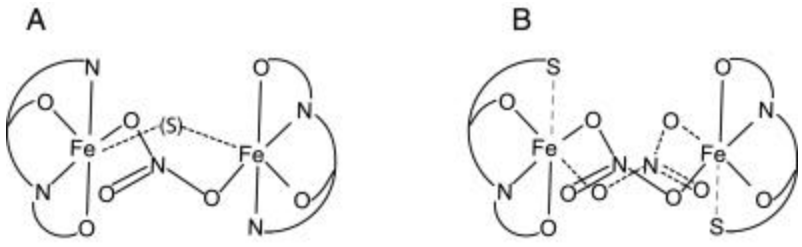

Figure 6.4 Proposed structure of the complex **1** in MeOH (A) and **3** in CH_2Cl_2 (B) where S is the solvent or water.

solvent bridge could not be ruled out. The assumption of two bridge and orientation of the nitrato bridge originated from the structure of dibridged $[Fe_2(OAc)(OH)(S)\text{-}Salhis)_2]\cdot 4H_2O$ complex. The UV-visible spectra of $[Fe_2(OAc)(OH)(S)\text{-}Salhis)_2]\cdot 4H_2O$ is similar to the present complexes. Thioether might be remaining noncoordinated. To further substantiate the bridging binuclear structure of the complexes, we have performed temperature dependent magnetic measurement to determine the magnetic coupling in the complexes in the next section.

6.3.4 Magnetism

The room temperature magnetic moment for **1, 2** and **3** are 4.60, 2.82 and 3.50 B.M. /per iron respectively which are less than expected for a uncoupled S=5/2 system but higher than low-spin S=1/2 system (expected 5.93 B.M. for S= 5/2 and 1.73 to 2.5 B.M. for S=1/2 uncoupled system)[78] indicating the possible presence of antiferromagnetically coupled iron(III) center. The solution magnetic moment[156] of **1** and **3** in MeOH are 3.99 and 3.64 B.M./Fe, shows that coupling observed is preserved in solution and can not be due to solid state interactions only. Magnetic susceptibility (Table 6.B) for complexes **1** and **2** were measured in the range of 81-300 K to determine the magnetic coupling constant J. Plots of χ_M and μ_{eff} versus T are shown in Figure 6.5 and Figure 6.6. The experimental μ_{eff} value at room temperature are 6.50 and 3.99 B.M. /2Fe respectively. Upon cooling the magnetic moment decreases gradually. These features, together with the temperature dependent behavior of χ_M are characteristic of an antiferromagnetic interaction between the two Fe(III) ions. For diiron(III) complexes ($S_1 = S_2 = 5/2$), the theoretical expression of the magnetic susceptibility based on $= -2J_{1\ 2}$ is

$$\chi = (1-\rho)\frac{N_A m_B^2}{kT} g^2 \times \left[\frac{2e^{2x}+10e^{6x}+28e^{12x}+60e^{20x}+110e^{30x}}{1+3e^{2x}+5e^{6x}+7e^{12x}+9e^{20x}+11e^{30x}}\right] + \rho \frac{N_A m_B^2}{3kT} g^2 \quad s(s+1) + N_\alpha \qquad \text{with, } x = \frac{J}{kT}$$

Where, N_A: Avogadro constant; μ: Bohr magneton; g: spectroscopic splitting factor; k: Boltzmann constant; ρ: paramagnetic fraction per monomer; N_α: temperature independent

paramagnetism per monomer. An isotropic *g* value of 2.00 was assumed. The simulation of experimental data for **1** was found to be $J = -32$ cm^{-1}, $N_\alpha = 0.0021$cm^3 mol^{-1}, $\rho = 0.20$, Final residual error = 1.85×10^{-7} and for **2**, $J = -76$ cm^{-1}, $N_\alpha = 0.16$ cm^3 mol^{-1}, $\rho = 0.0011$, Final residual error = 2.49×10^{-7}.

The negative *J* values indicate the presence of antiferromagnetic coupling. The *J* values in both cases are higher than corresponding hydroxo bridged $[Fe_2(OAc)(OH)(S\text{-Salhis})_2]\cdot 4H_2O$ complex signifying a stronger coupling. Presence of two bridging nitrate in the solid state might be the reason for higher coupling values. Literatures on NO_3^- bridged diiron(III) complexes are limited[162] thus *J* values could not be compared with other dinitrato bridged Fe(III) complexes. Another possibility was to consider bis-phenoxo and acetate tribridged structures similar to the $Na[Ni_2(S\text{-Salhis})_2(OAc)(H_2O)_4]$ structure (Chapter V). However, bis-phenoxo bridged diiron(III) usually have lower *J* values which has been observed in these cases. Crystal structure of at least one of the complexes would have solved this problem. Despite our best effort we could not get suitable crystal for any of these complexes.

Table 6.B Variable temperature magnetic susceptibility data for complexes **1** and **2**

Temperature (K)	Complex **1**		Complex **2**	
	$\chi_M \times 10^{-2}$ cm^3 mol^{-1}	μ_{eff} / 2Fe (B.M)	$\chi_M \times 10^{-3}$ cm^3 mol^{-1}	μ_{eff} / 2Fe (BM)
300	1.761	6.50	6.635	3.99
280	1.847	6.43	6.881	3.93
260	1.910	6.30	7.106	3.84
240	1.981	6.16	7.311	3.75
220	2.074	6.04	7.583	3.65
200	2.188	5.91	7.794	3.53
180	2.339	5.80	8.275	3.45
160	2.467	5.61	8.792	3.35
140	2.689	5.48	9.195	3.21
120	2.927	5.30	9.904	3.08
100	3.156	5.02	10.632	2.92
81	3.420	4.70	11.491	2.73

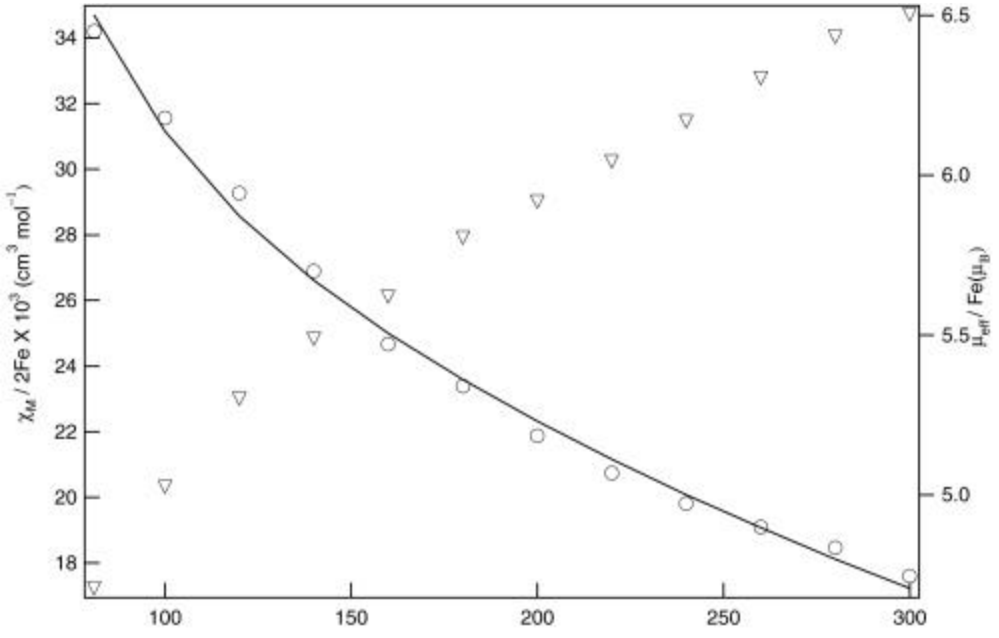

Figure 6.5 χ_M and μ_{eff} *vs* Temperature plot for the complex **1**

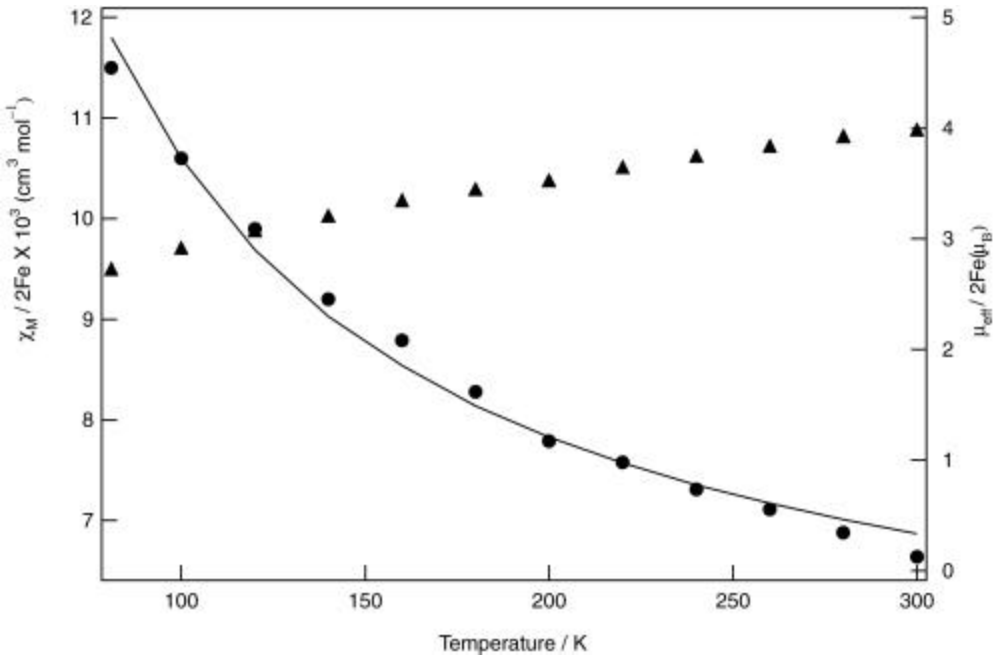

Figure 6.6 χ_M and μ_{eff} *vs* Temperature plot for the complex **2**

6.3.5 Addition of external ligand and its effect on LMCT

Our prime objective was to make coordination complex with vacant coordination site or weak binding site through H-bonding inside chiral environment to facilitate preferential binding of one enantiomer over other. In previous two chapters we have synthesized and characterized binuclear Iron(III) and Ni(II) complexes where the former have an open H-bond capable hydrophilic site and the other have a chiral hydrophilic site. We had synthesized the NO_3^- complexes (this chapter) with the following expectations:

(a) Similar chiral cavity will be formed

(b) NO_3^- being weaker ligand compared to acetate, might be easier to be replaced by an external chiral ligand

(c) Phenolate→Fe(III) CT Band will be more susceptible to change in coordination and will act as visual indicator of binding compared to a Ni(II) complex.

Lack of structural analysis prohibits checking the cavity formation. However, we have tested the effect on adding external reagents into these complexes.

Table 6.C LMCT band maxima of complex **1**, **2** and **3** on addition of excess external ligands

External ligand	pKa	**1** in MeOH	**2** in MeOH	**3** in MeOH	**3** in CH_2Cl_2
No Addition		520	525	555	585
Triethylamine	10.7	469	469	499	485
Imidazole	6.92	469	469	502	515
S-Methylbenzylamine	6.88	469	469	500	485
R-Methylbenzylamine	6.88	468	468	499	485
D-Ephedrine	6.00	510	n.d[a]	513	No shift
Pyridine	5.19	487	485	514	521
Aniline	4.58	487	486	502	540
Diphenylamine	0.79	520	525	555	585

[a]n.d = not determined.

We have added various monodentate N-donor ligands and monitor the shift of phenolate →Fe(III) charge transfer band in methanol and for **3** both in methanol and

CH_2Cl_2 . Complex **1** and **2** are not soluble in CH_2Cl_2. The results are summarized in Table 6.C. In methanol all the N donor reagents, except diphenylamine, interact with the complexes as indicated by color change (purple to orange) due to shift in charge transfer band. The halide ions (Cl^-, Br^- or I^-) on the other hand do not causes any change in color. The fact that none of the halides causes any shift but triethylamine do, indicates that the color shift may not be due to coordination of external ligand but due to some other kind of interaction/reaction. Triethylamine usually does not coordinate to Fe(III) but halide in

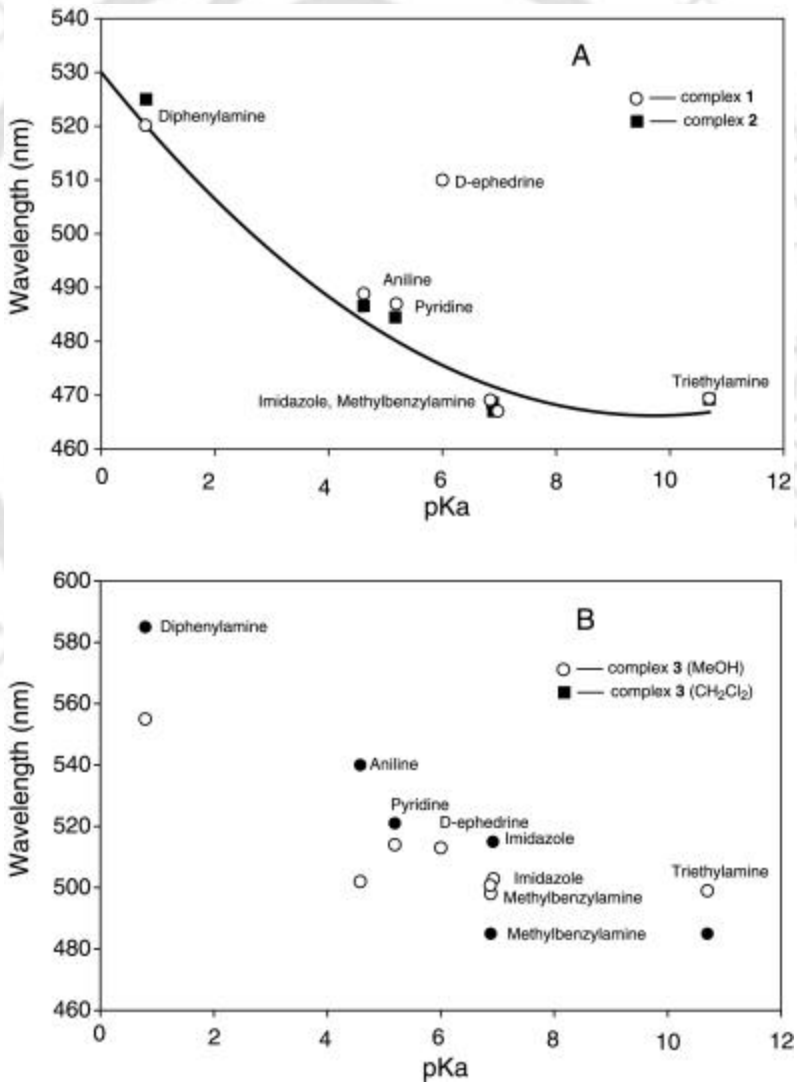

Figure 6.7 Wavelength (nm) vs pK_a plot (A) for complexes **1** and **2** in MeOH, (B) for complex **3** in MeOH and CH_2Cl_2

principle can form Fe(III) coordinated complexes. We did not try external ligands stronger than NO_3^- as that might cause replacement of the nitrates. Another possibility is that the basicity of the external ligand might be effecting in the color change. So we have plotted the λ_{max} (phenolate → Fe(III)) values against the pK_a values. The trends showed that shift in color increases with increasing pK_a value of added reagent. The trend is not linear. In MeOH, both **1** and **2** (Figure 6.7 A) show similar trend. The lower shift by D-ephedrine for **1** in MeOH might be due to the fact that its sterically crowded secondary amine N is not accessible. Triethylamine, despite having high pK_a, shifts the color by same amount as is done by methylbenzylamines (Table 6.C). The reason might be due to either steric reason or due to the fact that methylbenzylamine (pK_a 6.88) is a base strong enough to cause the complete change. Thus increase of pK_a does not cause any further shift. For **3**, shifts are more erratic both in MeOH and CH_2Cl_2 (Figure 6.7 B). The introduction of *o*-methyl group in the ligand of **3** might have increased the steric crowding around the interaction site causing the other factors to interfere. The spectroscopic studies do not show any appreciable difference in binding with different enantiomers that have been tried in this work.

6.3.6 Addition of amine and its effect on Conductance

Along with color change, all the three complexes show considerable change in conductance upon addition of triethylamine or methylbenzylamines (Table 6.D and Figure 6.8). Both conductance and UV-visible changes on addition of amines were plotted in Figure 6.9. All the three complexes showed 1:1 electrolyte in MeOH before addition of amines. On addition of amine in methanol, conductance value increases and gets saturated upon addition of 2 equivalent of the amine and at that point the solution behaves as a 1:2 electrolyte. The increase of conductance on addition of amines is surprising, as amines being neutral should not change the conductance appreciably. The complex **3** in dichloromethane does not show saturation behavior in either color or conductance change and the nature of the plots (Figure 6.8 D and D') suggesting the presence of equilibrium. Considering the lower polarity of the medium, ionization or nitrate release is expected to be disfavored. Lack of proper isobestic point in the titration spectra (Figure 6.8) hindered the calculation of binding constant.

Table 6.D Change in conductance on addition of 5 equivalent of amines

Complexes	External Ligands	Solvents	Before addition of amines (S cm^2 mol^{-1})	After addition of amines (S cm^2 mol^{-1})
1	*R*-methyl Benzyl amine	MeOH	97	135
	S-methyl Benzyl amine	MeOH	97	135
	Et_3N	MeOH	97	153
2	*R*-methyl Benzyl amine	MeOH	120	163
	S-methyl Benzyl amine	MeOH	120	163
	Et_3N	MeOH	120	180
3	*R*-methyl Benzyl amine	MeOH	125	165
	S-methyl Benzyl amine	MeOH	125	165
	Et_3N	MeOH	125	188
3	*R*-methyl Benzyl amine	CH_2Cl_2	0.5	1.40
	S-methyl Benzyl amine	CH_2Cl_2	0.5	1.40
	Et_3N	CH_2Cl_2	0.5	3

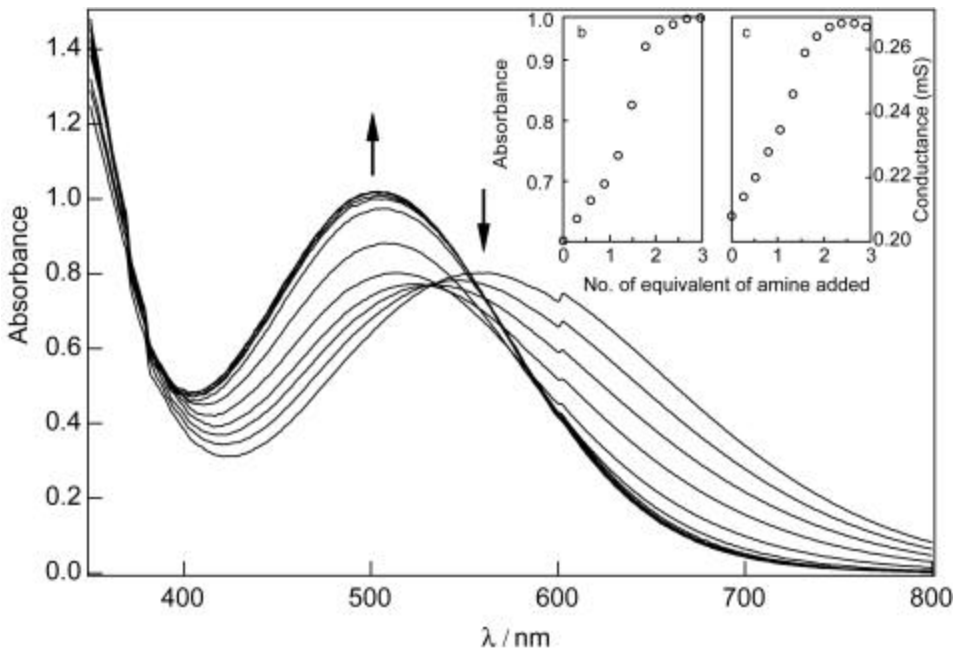

Figure 6.8 Spectrophotometric titration of complex **3** in MeOH, plot of Absorbance and Conductance *vs* number of amine (inset)

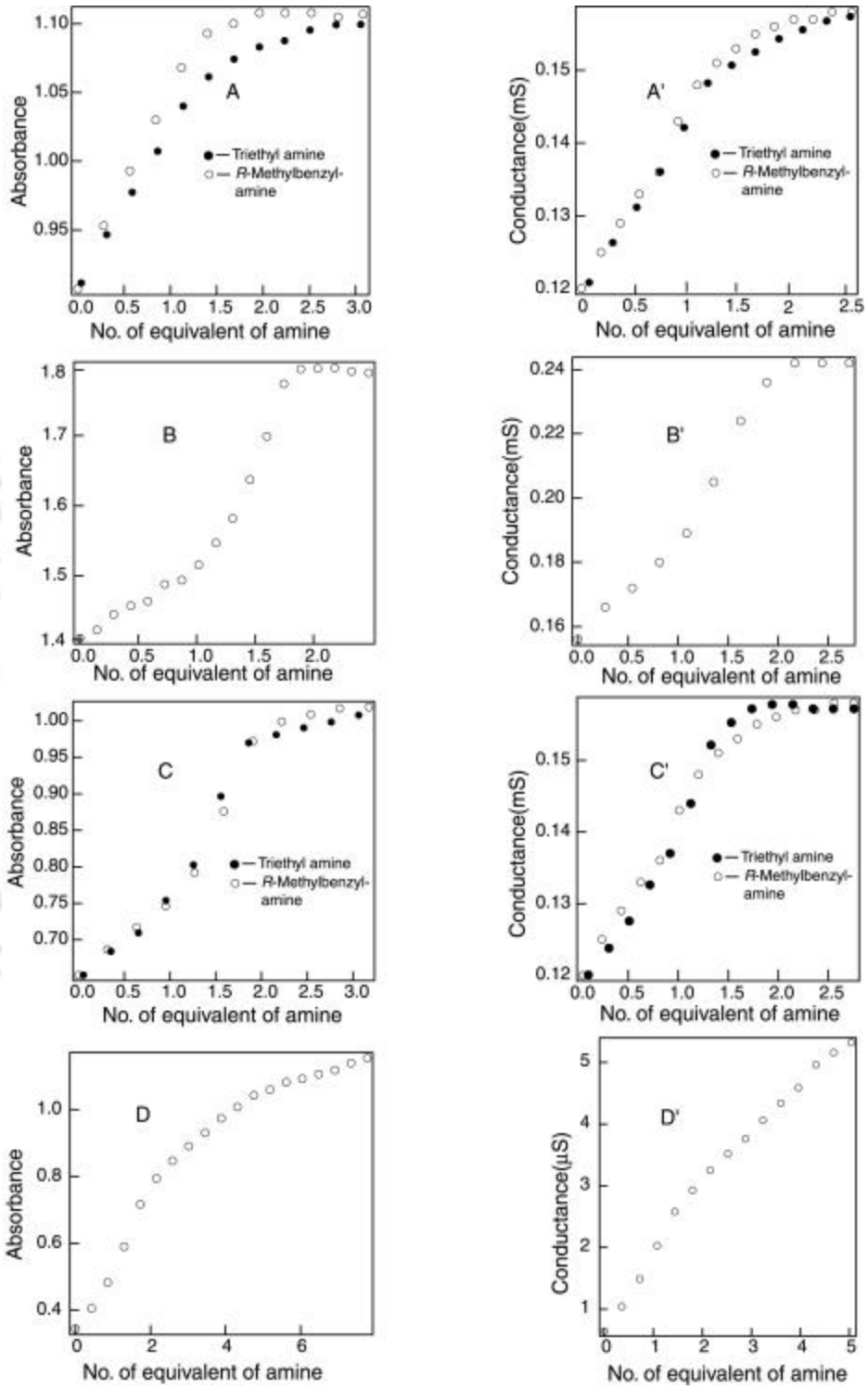

Figure 6.9 Spectrophotometric titration of the complexes **1, 2** and **3** (**A, B** and **C**) in MeOH, **3** (**D**) in CH_2Cl_2 **(**left) and corresponding conductometric titration (right)

6.3.7 The process involved for the increase of conductance

From the above experiments we can summarize the results as follows:

(a) Addition of solvent in **3** causes ionization of one nitrate possibly by replacement of the nitrate bridge by a solvent or water molecule. Ionization of **1** and **2** possibly take place in the similar way.

(b) Addition of 2 equivalent of a strong base (methylbenzylamine or triethylamine) increases the conductance to ~ 1:2.

The orange solution produced by addition of amines could not be characterized. Addition of precipitant or evaporation of the solvent always results in a orange oil which remains partially undissolved even in coordinating solvents such as DMF or DMSO. This might be due to the formation of some amount of hydrated ferric oxide. The ESI-MS of the orange solution from **3** and methylbenzylamine or triethylamine shows $\{(PhCHCH_3NH)^+Fe^{III}(o\text{-Me-Salmet})_2\}^+$ or $\{(Et_3NH)^+ Fe^{III}(o\text{-Me-Salmet})_2\}^+$ respectively. Based on the experimental results we have outlined the process in Scheme 6.I.

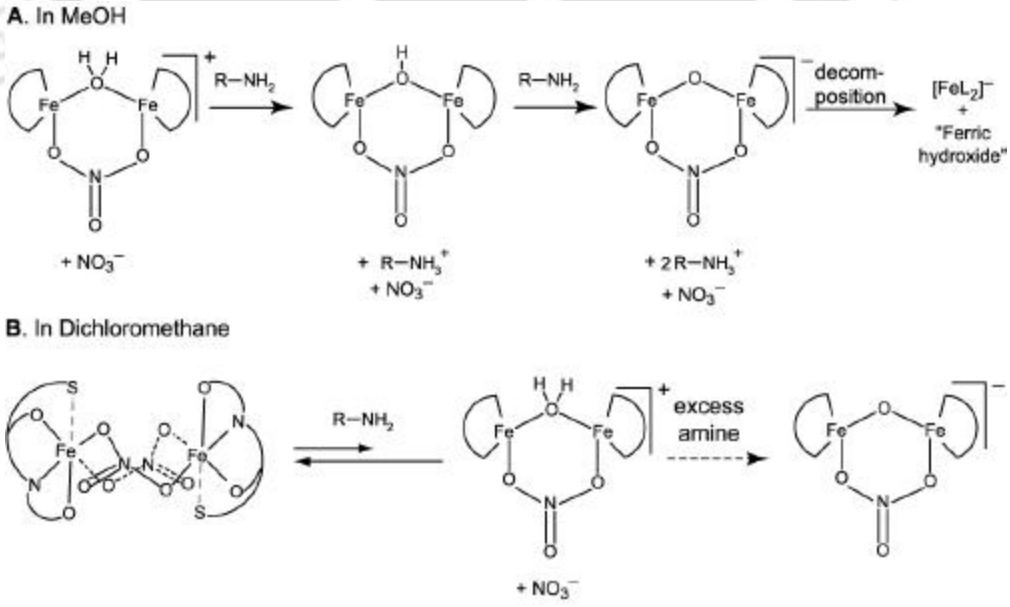

Scheme 6.I The process involved for the increase of conductance

6.3.8 Use as sensor

The fact that on addition of amines, the color and the conductance of the solution changes considerably led us to think about its possible use as colorimetric and/or conductometric sensor for amines. Colorimetric determinations of amines are done in many chemical detection processes related to pharmaceutical process.[151] In the existing process, a conjugated aldehyde is used to form a colored imine (usually yellow color) to detect the amine.[151-154] The fact that the present Fe(III) complex reacts with amines with a visual color change from blue to orange and absorbance varies linearly up to the saturation point in MeOH (Figure 6.9). The complex can be used both as a visual indicator and for quantitative estimation purpose of primary amines. Tertiary amine such as triethylamine detection is important but particularly difficult through Schiff base formation. Detection by conductance is easier to implement in the detector fabrication but amines being neutral species are not expected to change conduction appreciably. Fortunately in our complexes the conductance change is large. Thus, in order to test the suitability of our complex we soaked a Whatman® filter paper in CH_2Cl_2 solution of the complex **3** and dried it. We choose the complex **3** for the sensing of amines, as the shift in color was largest for this complex (Table 6.C). The blue colored paper was held on the mouth of the bottles of triethylamine, ammonia and methylbenzylamine separately. The color changed was observed immediately to orange in all the cases. A representative picture is shown in Figure 6.10. The conductivity also changed for the coated paper.

Figure 6.10 (A) Complex **3** coated filter paper before and after exposing to triethylamine vapor and (B) methanolic solution of **3** before and after addition of Et_3N. Circular portion of the filter paper is treated with conc. triethylamine solution to view maximum color change possible in filter paper

Thus the complex **3** in a supported medium can detect volatile amine vapor. The resistance of the filter paper coated with **3** showed an initial value of 260 MΩ which changes to 210 MΩ after exposing to NEt_3 vapor.

To check the reversibility of the change, the complex soaked paper was exposed to NEt_3 and was heated at 100°C for 15 minutes, as a result the paper turned to its original blue color. Repeating the process of amine vapor expose and heating it was observed that the color did not come back completely to the original blue color. Similar experiments were done in solution, however reversible color change was not observed. So the process is reversible at least to one cycle on the supported medium but irreversible in solution.

Conclusions

In this chapter we have synthesized three Fe(III) complexes of the general formula $[Fe(L)_2(NO_3)_2]$ (where L = tetradentate ligands). Characterization data supports the binuclear Fe(III) formulation with two bridging nitrate in the solution. All these complexes show charge transfer spectra at visible region. Upon addition of amine both color and conductance of the solution changes considerably. Using this observation, we have tested their potential use as conductometric and/or colorimetric detector for amines. These complexes can detect even the tertiary amine both in solution as well as in vapor state, an advantage over the Schiff base formation method usually used. The lack of structural characterization of the complexes prohibited us in understanding the complete mechanism of color and conductance change. However, as the complexes have potential to detect amine vapors in a supporting medium, efforts will be on to further study these complexes in future.

Chapter VII

Syntheses and characterization of mononuclear Iron(III) catecholate complexes

The complexes reported in the previous chapters, except for the Cu(II) complex with ligand H_2(*S*)-Salhis and imidazole, were all multinuclear in nature. The multinuclear complexes studied in this thesis include the molecular capsule, diiron(III) complex with helical array and bridged dinuclear Fe(III) nitrate complexes. The ligands self-assembled with the metal centers have two *cis* vacant sites in octahedral complexes, which helped in forming bridged multinuclear complexes in all cases. In this chapter we present the synthesis and characterization of two mononuclear Iron(III) complexes of general formula [Fe^{III}(L)(catecholate)] (L = histidine or methionine derived ligand) where two *cis* sites in the complexes were blocked facilitating the formation of mononuclear complexes. Although the complexes could not be structurally characterized yet, the variable temperature magnetic data and EPR studied support the monomeric formulation. Our choice of catecholate as a bidentate ligand was influenced by the fact that the resulting complex (with histidine derived ligand) might serve as a structural model for the active site of catechol dioxygenase, a catechol-cleaving enzyme.

Iron complexes with two available binding sites in the *cis* position are important as models for active sites in many mononuclear iron containing proteins. For example, protocatechuate 3,4-dioxygenase;[163-165] 2,3-dihydroxybiphenyl 1,2-dioxygenase;[166] soybean lipoxygenase-1[167] and isopenicilline synthase[168] have iron(II)/ (III) centers with either four or five coordination from the amino acid residue and one or two coordination sites occupied by water molecules present in the active site structure (Table 7.A). All these proteins have two *cis* binding sites available for substrate and / or reactant binding by the removal of two *cis* water molecules, however in the case of protocatechuate 3,4 dioxygenase removal of one water and one tyrosine residue facilitates the substrate binding. Availability of two binding sites in *cis* position is important in the functioning of these proteins. Several tripodal tetradentate ligands providing N_4, N_3O, and N_2O_2 donor atoms were used in synthesizing model complexes to elucidate the structural aspect and reaction mechanism of some of these proteins. Tris-pyridylmethyl amine and its various derivatives have been used most extensively in elucidating the machanism of catechol cleaving dioxygenase proteins. Recently, two different groups reported iron(III) complexes with tridentate N_3 type ligand which cleaves catechol.[169-171] The synthesis of Fe(III) complexes with the ligands synthesized by us in this thesis work can provide N_2O_2 donor site, where one imidazole, one carboxylate and one phenolate coordination from

the ligand mimic the histidine, aspertate, and tyrosine residues of the protein. Additionally, the use of methionine derived H_2*S*-Salmet was explored to check the effect in spectroscopic property upon substituting the histidine.

Table 7.A Feature of the active site structures of selected proteins

Protein	Coordination Number	Metal	Ligand
Protocatechuate 3,4 dioxygenase	5	Fe(III) high-spin	2His, 2Tyr, 1Water
2,3 dihydroxybiphenyl 1,2 dioxygenase	5	Fe(II) high-spin	2His, 1Glu, 2Water
Tyrosine hydroxylase	5	Fe(II)	2His, 1Glu, 2Water
Isopenicilline synthase	6	Fe(II)	2His, 1Asp, 2Water, 1Gln

7.1 Experimental Section

Details of solvent purification and starting materials are already discussed in chapter 2. The details of ligand synthesis are given in Chapter 2 (Section 2.4.1 and Section 2.4.3). The instrumental details for other spectroscopic measurements have already been stated in Chapter 2 and 3.

7.2 Syntheses of Fe(III) complexes

7.2.1 K[Fe(*S*-Salhis)($C_6H_4O_2$)]· $3H_2O$ (1)

A methanolic solution of $Fe(NO_3)_3$· $9H_2O$ (0.422 gm, 1.04 mmol) was added drop wise to a clear solution of H_2(*S*)-Salhis (0.267 gm, 1.03 mmol) and KOH (0.121 gm, 2.17 mmol) in 25 mL dry methanol. After stirring for 30 min. the color of the solution changed from brown to violet with some undissolved white suspension. UV-vis (MeOH): 273 nm, 309 (sh), 520 nm. To this solution N_2 gas was passed for 15 min. In another round bottom flask catechol (0.1150 gm, 1.04 mmol) was dissolved in dry methanol and N_2 gas was passed. Catechol solution was added to the reaction mixture slowly with no color change observed. KOH (0.125 gm, 2.18 mmol) in methanol under N_2 atmosphere was added in

the reaction mixture, whereupon the color of the solution was observed to change from bluish-violet to blue. UV-visible (MeOH): 285 nm, broad band 438 nm to 597 nm. The reaction mixture was stirred 30 min. under N_2 atmosphere. The mixture was filtered off and the filtrate was evaporated to dryness. This solid was triturated with acetonitrile, filtered and dried under reduced pressure (yield: 0.4729 gm, 75 %). Finally the complex was purified from methanol/ diethyl ether and dried under reduced pressure.

Anal. Calcd. for $C_9H_{23}N_3O_8KFe$: C, 44.19; H, 4.49; N, 8.14. Found: C, 44.02; H, 4.29; N, 8.04. IR (KBr cm^{-1}) í(COO)$_{assym,}$ 1623, 1595 í(COO)$_{sym}$ 1381.UV-vis in MeOH (λ_{max} /nm (ε /dm^3 mol^{-1} cm^{-1}): 282(9500), 328(sh), 438-597(1750) (broad band). Ë$_M$ (MeOH): 50 S cm^2 mol^{-1}. ESI-MS(–): 423.1 for [Fe(*S*-SalHis)(cat)]$^-$. ì$_{eff}$(solid, 298 K); 5.73 B.M/Fe. EPR (77 K): powder, 4.28; MeOH: 7.56, 4.30.

7.2.2 K[Fe(*S*-Salmet) ($C_6H_4O_2$)]· 1.5H_2O (2)

A methanolic solution of $Fe(NO_3)_3$· $9H_2O$ (0.350 gm, 0.866 mmol) was added drop wise to a mixture of *S*-H_2Salmet (0.221 gm, 0.867 mmol) and KOH (0.097 gm, 1.75 mmol) in 25 mL dry methanol. The reaction mixture was stirred for 30 minutes, as a result some white suspension of KNO_3 was observed. The color of the solution changed from brown to violet with characteristic UV-visible peaks at 273 nm, 309 nm and 520 nm. To this solution N_2 gas was passed for about 15 minutes. Catechol (0.095 gm, 0.866 mmol) was dissolved in dry methanol in another round bottom flask and N_2 gas was passed to remove dissolved oxygen. Upon the addition of catechol solution to the reaction mixture there was no observable change in color of the solution. However on addition of KOH (0.098 gm, 1.75 mmol) in methanol under N_2 atmosphere to the reaction mixture color of the solution changed to blue from the original blue-violet. UV-visible (MeOH): 280 nm, broad band 372 nm to 580 nm. The reaction mixture was stirred for 30 min. under N_2 atmosphere. The mixture was filtered off and the filtrate was evaporated to dryness. The resulting solid was triturated with acetonitrile, filtered and dried under reduced pressure (yield: 0.290 gm, 73 %). The complex was purified from methanol/ diethyl ether and dried under reduced pressure.

Anal. Calcd. for $C_{18}H_{22}NO_{6.5}SKFe$: C, 44.72; H, 4.58; N, 2.89. Found: C, 44.59; H, 4.69; N, 3.12. IR (KBr cm^{-1}) í(COO)$_{assym,}$ 1633, 1593 í(COO)$_{sym}$ 1381.UV-visible in MeOH (λ_{max} /nm (ε /dm^3 mol^{-1} cm^{-1}): 280(5600), 313(sh), 372-579(1150) (broad band).

$\ddot{E}_M$ (MeOH): 45 S cm^2 mol^{-1}. $\grave{I}_{eff}$(solid, 298 K); 5.24 B.M/Fe. EPR (77 K): power, 8.80, 4.28 broad; MeOH: 8.80, 4.28.

7.3 Results and Discussion

7.3.1 Syntheses and Selected Properties

By mixing $Fe^{III}(NO_3)_3 \cdot 9H_2O$, *S*-$H_2$Salhis for complex **1**, *S*-H_2Salmet for **2** and KOH in MeOH at 1:1:2, the solution turned blue-purple in both the cases. On addition of deprotonated catechol solution the color turned into blue-violet. Addition of diethyl ether into the methanolic solution of complexes **1** and **2** gives dark blue powder with ~60-65 % yield. Comparing the IR spectra of **1** and **2** with that of deprotonated ligand and the Fe(III) complexes characterized in the previous chapter, the two peaks at 1623, 1595 and one peak at 1381 cm^{-1} for **1,** similarly, two peaks at 1633, 1593 and one peak at 1381 cm^{-1} for **2** were identified as asymmetric and symmetric carboxylate stretches originated from the ligand respectively. Both the complexes also show broad stretches at 3401 cm^{-1} and two broad stretches at 3192, 3111 cm^{-1} due to OH (water or H-bonded OH) stretch and N-H stretches (from ligand) respectively. Further both the complexes show the appearance of a band at 1250 cm^{-1}, likely to be the metal-catecholate C-O stretching.[172] The IR spectra do not show any characteristic stretching for NO_3^-. The elemental analysis support the formulation of the complexes as K[Fe(*S*-Salhis)($C_6H_4O_2$)]$\cdot$ $3H_2O$ and K[Fe(*S*-Salmet) ($C_6H_4O_2$)]$\cdot$ $1.5H_2O$ for **1** and **2** respectively Table 7.B.

Table7.B Microanalytical Data[a] of Iron (III) Complexs

Complex	Empirical formula	% C	% H	% N
1	$C_{19}H_{23}N_3O_8KFe$	44.02 (44.19)	4.29 (4.49)	8.04 (8.14)
2	$C_{18}H_{22}NO_{6.5}SKFe$	44.59 (44.72)	4.69 (4.58)	3.12 (2.89)

[a] Value in parentheses are calculated ones

The thermogravimetric analysis (TGA) between 35- 125° C shows weight loss of 9.5 % for **1** and 4.8 % for **2** as against the calculated values of 10.5 % ($3H_2O$) and 5.6 % ($1.5H_2O$) respectively. Figure 7.1 shows a representative TGA plot.

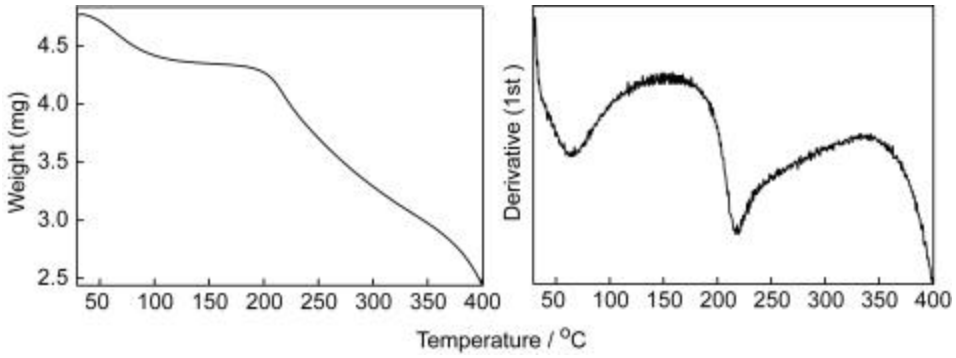

Figure 7.1 TGA and DTA plot of complex **1**

The room temperature magnetic moment for **1** and **2** were found to be 5.72 and 5.24 B.M. /per iron respectively and are slightly less than expected for a uncoupled S=5/2 system but very much higher than low-spin S=1/2 system (expected 5.93 B.M. for S= 5/2 and 1.73 to 2.5 B.M. for S=1/2 uncoupled system)[78]. The results indicate the possible presence of very weak antiferromagnetic coupling between two high-spin Fe(III) centers.

The molar conductance of complexes **1** and **2** are 50 and 45 S cm^2 mol^{-1} in methanol respectively (expected for 1:1 electrolyte in methanol is in the range of 85-115 S cm^2 mol^{-1}). Conductance of the complex is lower than 1:1 electrolyte in methanol but very much higher that the non-electrolytes.[77]

7.3.2 Temperature dependent magnetic measurements

Magnetic susceptibility for complexes **1** and **2** were measured in the range of 81-300 K to determine the magnetic coupling constant *J*. Plots of χ_M and μ_{eff} versus T are shown in Figure 7.2 and Figure 7.3, values are substantiated in Table 7.C. The experimental μ_{eff} value at room temperature are 5.72 and 5.24 B.M. respectively, below the spin-only value (5.93 B.M.) expected for an uncoupled Fe(III) high spin unit. Upon cooling, the magnetic moment declines gradually. These features, together with the temperature dependence behavior of χ_M are characteristic of an antiferromagnetic interaction between the two Fe(III) ions.

For diiron(III) complexes (S_1 = S_2 = 5/2), the theoretical expression of the magnetic susceptibility based on = -2*J* *1* *2* is

$$\chi = (1-\rho)\frac{N_A m_B^2}{kT} g^2 \times \left[\frac{2e^{2x} + 10e^{6x} + 28e^{12x} + 60e^{20x} + 110e^{30x}}{1 + 3e^{2x} + 5e^{6x} + 7e^{12x} + 9e^{20x} + 11e^{30x}}\right] + \rho \frac{N_A m_B^2}{3kT} g^2 \quad s(s+1)$$

$+ N_\alpha$ with, $x = \frac{J}{kT}$

Where, N_A: Avogadro constant; μ: Bohr magneton; g: spectroscopic splitting factor; k: Boltzmann constant; ρ: paramagnetic fraction per monomer; N_α: temperature independent paramagnetism per monomer. An isotropic g value of 2.00 was assumed. The simulation of experimental data for **1** was found to be $J = -4.8$ cm^{-1}, $N_\alpha = 4.116 \times 10^{-4}$ cm^3 mol^{-1}, $\rho = 9.77 \times 10^{-2}$ and for **2**, $J = -9.0$ cm^{-1}, $N_\alpha = 3.64 \times 10^{-4}$ cm^3 mol^{-1}, $\rho = -1.64 \times 10^{-2}$. The low J values, suggested a very weak antiferromagnetic exchange between the two iron(III) centers also observed for other catecholate complexes as mentioned in Table 7.D. As the present ligands have shown the capability of forming extended H-bonded network, the small exchange constant might be due to weak interaction between the monomeric units but unlikely to be from a bridged dinuclear Fe(III) complex. This substantiates the monomeric nature of **1** and **2**.

Table 7.C Variable Temperature Magnetic Susceptibility data for complexes **1** and **2**

Temperature (K)	Complex **1** $\chi_M \times 10^{-2}$ cm^3 mol^{-1}	μ_{eff} (BM)	Complex **2** $\chi_M \times 10^{-2}$ cm^3 mol^{-1}	μ_{eff} (BM)
300	2.735	5.73	2.285	5.24
280	2.851	5.65	2.328	5.11
260	3.027	5.61	2.448	5.05
240	3.213	5.55	2.582	4.98
220	3.557	5.59	2.775	4.94
200	3.741	5.47	2.958	4.86
180	4.026	5.38	3.255	4.84
160	4.479	5.35	3.402	4.67
140	5.022	5.30	3.713	4.56
120	5.238	5.01	3.944	4.35
100	5.811	4.82	4.111	4.05
81	6.594	4.62	4.247	3.72

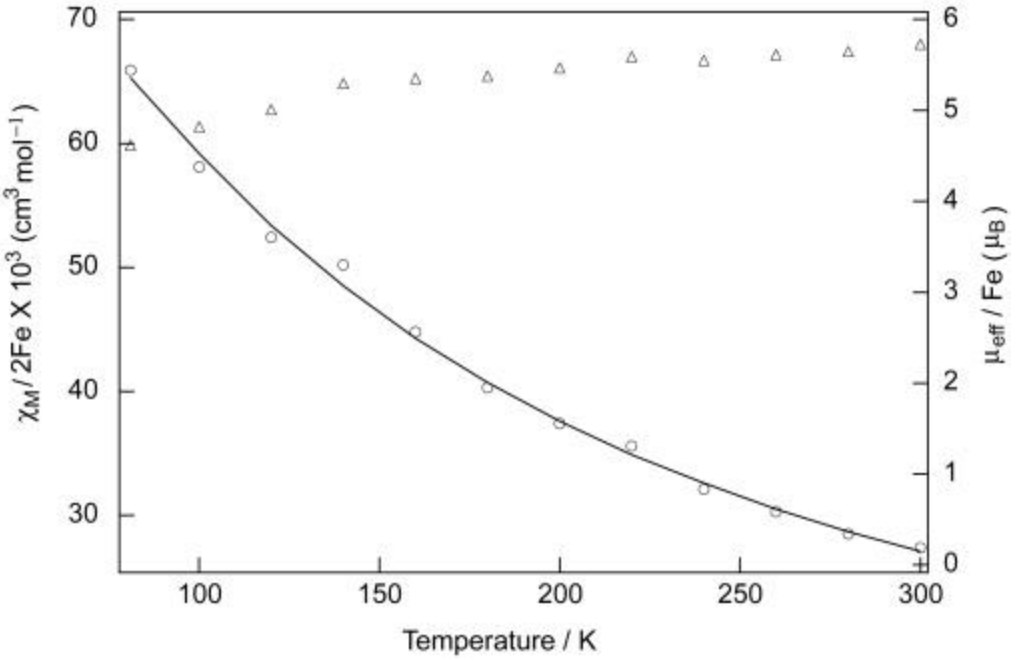

Figure 7.2 χ_M and μ_{eff} versus Temperature of complex **1**

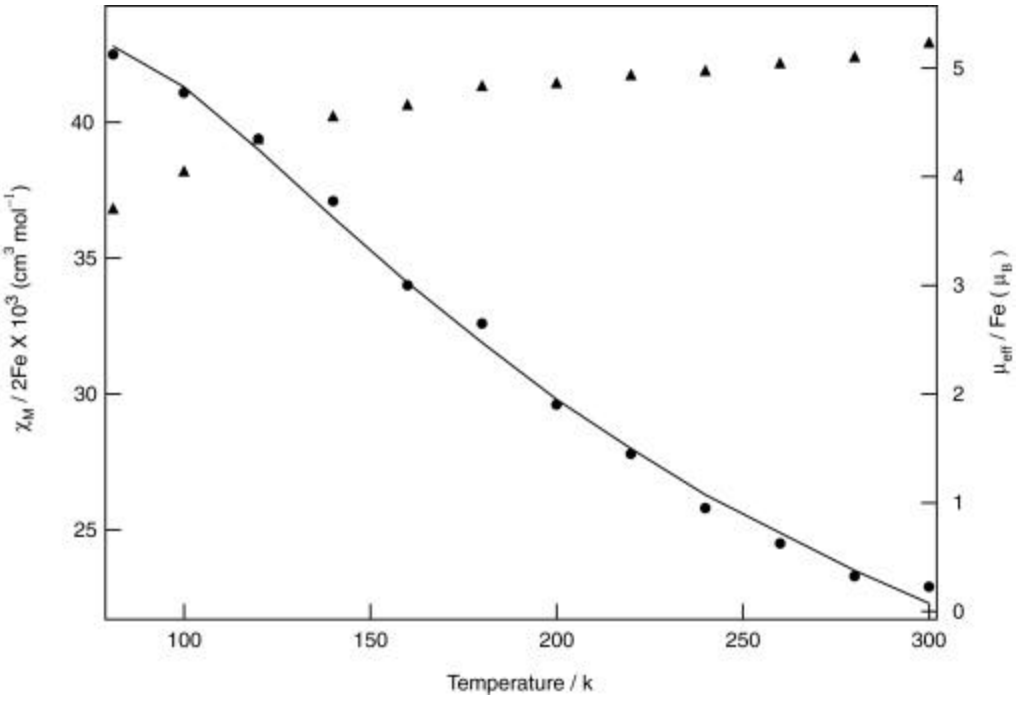

Figure 7.3 χ_M and μ_{eff} versus Temperature of complex **2**

Table 7.D Magnetic Susceptibility Data

Complexes	μ_{eff} / Fe	*T*, K	*J*, cm^{-1}	Ref.
1	5.72	300	–4.8	This work
2	5.24	300	–9.0	This work
Fe(salen)catH	5.51±0.03	293	–5.1±0.1	173
Fe(salen)(Oph-2-Br)	5.52±0.03	298	–4.1±0.1	173

7.3.3 Electron Paramagnetic Resonance (EPR)

At 77 K both **1** and **2** showed strong EPR signal at g ~ 4.3 in powder as well as in methanolic solution. The data is consistent with high-spin Fe(III) (S = 5/2) nature of the complexes. The signal at g = 4.3, due to rhombic high spin Fe(III), is usually strong and occurrence of it seldom associated with Fe(III) impurity in protein or metal complexes. However, g = 4.3 signal in pure metal complex with substituted catecholate is also known

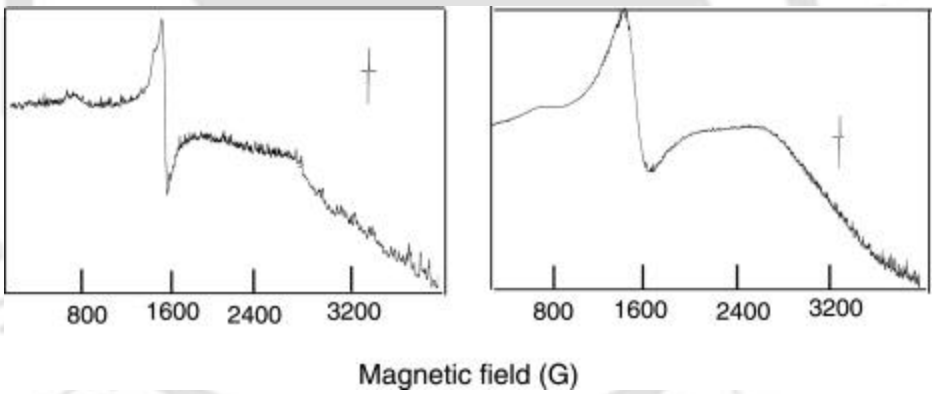

Figure 7.4 EPR spectrum of **2** [in MeOH, at 77 K (left) power at 77 K (right)]

and was observed for $[Fe(NTB)DBC]^{+}$ (Table 7.E). Both **1** and **2** also show minor peaks in solution, EPR spectra with E/D calculated as 0.07 and 0.17 respectively.[174,175] The EPR spectra values of the complexes along with few other previously structurally characterized complexes with catecholate are shown in Table 7.E. Representative spectra are shown in Figure 7.4. Incidentally, the protein protocatechuate 3, 4 dioxygenase shows EPR signal at 9.70 (weak) and 4.29 (strong).

Table 7.E EPR data of some [Fe(L)cat] complexes

Complex	Observed EPR g values	Ref.
1	EPR powder, (298K) 4.21 (77 K): 4.27; MeOH, (77K) 4.30 (strong), 7.56, 5.40 (weak)	This work
2	Powder, 8.80, 4.28 broad; MeOH: 4.28, 8.80, 2.40 (weak)	This work
$[Fe(NTB)DBC]^{+}$	DMF/DMSO/Toluene (7K) 9.6, 4.3 (major) 8.5, 5.5 (minor)	174
$[Fe(NTA)cat]^{2-}$	8.9, 5.0, 3.6, 3.3	174
[Fe(BPG)DBC]	9.4, 5.1, 3.8, 3.5	174
$[Fe(PDA)DBC]^{-}$	9.4, 5.1, 3.8, 3.5	174
$[Fe(HDA)DBC]^{2-}$	8.5, 5.3, 3.2, 2.8	174

NTA = N,N-bis(carboxymethyl)glycine; PDA = N-(2-pyridylmethyl)-N-(carboxymethyl)glycine; BPG = N,N-bis(2-pyridylmethyl)glycine; TPA = Tris(2-pyridylmethyl)amine.

7.3.4 UV-visible Spectrum

In visible region both the complexes show broad overlapping band between 400–800 nm (Figure 7.5). The data are given in Table 7.F. The molar extinction coefficient > 1500 M^{-1} cm^{-1} at 463nm for **1** indicates the origin of transitions as LMCT. The presence

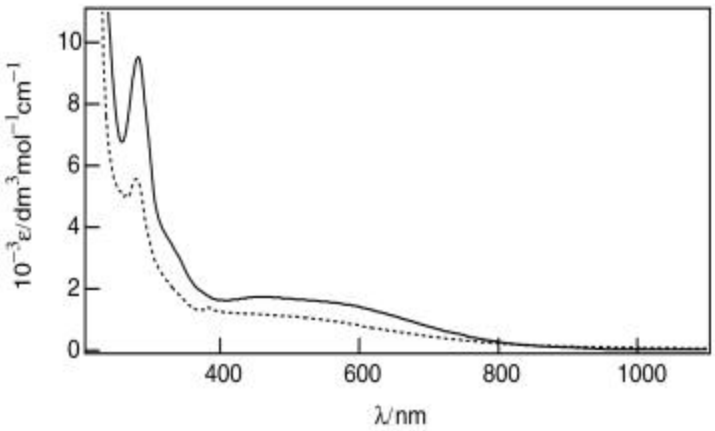

Figure 7.5 UV-visible of complexes **1** and **2** in MeOH

of Fe^{3+}, phenolate and catecholate warrants occurrence of LMCT bands as seen in other catecholate, phenolate containing Fe^{3+} complexes (Table 7.F). In the reported Fe^{3+} complexes with catecholate as one ligand, usually two LMCT transitions were observed in the similar range to the overlapping transitions present in **1** and **2** (Table 7.F). The difference in the present case is due to the overlapping nature and relative blue shift of the higher wavelength transition possibly due to the difference in the donor groups such as imidazole instead of pyridine etc. The decrease in intensity and the change in nature of the absorbance ~ 463nm in **2** compared to **1** might be due to the absence of the histidine→Fe(III) charge transfer contribution. Incidentally, protocatechuate 3, 4-dioxygenase showed a red color with a broad absorption near 450 nm, but when the substrate (protocatechuic acid) was added, the visible spectrum showed an increase in intensity at ~ 480 nm.[176]

Table 7.F Absorption maxima of LMCT bands of Iron-Catecholate complexs [a]

Ligands	λ_{max} /nm (ε /dm^3 mol^{-1} cm^{-1})	Ref.
S-Salhis	282, 328(sh), 463 (1700), 620sh	This work
S-Salmet	280, 313(sh), 413sh, 518sh	This work
Salen	339, 388, 628	173
NTA	410, 618	174
Bu_2HDA	388, 550	174
PDA	426, 656	174
BPG	460, 716	174
NTB	490, 766	174
TPA	495, 800	174

[a](Data reported in nm obtained in methanol)

NTA = N,N-bis(carboxymethyl)glycine; PDA = N-(2-pyridylmethyl)-N-(carboxymethyl)glycine; BPG = N,N-bis(2-pyridylmethyl)glycine; TPA = Tris(2-pyridylmethyl)amine.

Conclusions

In this chapter we have discussed about the preparation of two mixed ligand Fe(III) complexes of the general formula $K[Fe^{III}(L)(catecholate)]$ where L is a tetradentate ligand derived from either L-histidine or L-methionine. The low magnetic coupling constants from temperature dependent magnetic susceptibility measurements support the mononuclear formulation of the complexes. Comparison of UV-visible spectra with other mononuclear Fe(III) octahedral catecholate complexes also support the structural similarity. The slight dissimilarity between visible spectra of **1** and **2** also points

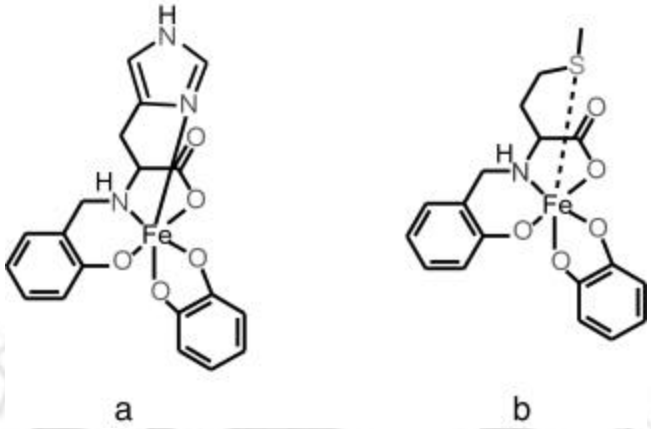

Figure7.6 Possible representative structure of the complexes **1** (a) and **2** (b)

the involvement of histidine imidazole in the coordination, thus confirming the six coordination of the Fe(III) in **1**. Taking this into consideration and the fact that catecholate can only be coordinated as *cis* bidentate ligand, confirms that *S*-H_2Salhis can work as tetradentate ligand in a mononuclear complex, which leaves *cis* site vacant for other coordination. A possible representative structure of the complexes **1** and **2** are given in Figure 7.6.

Donor atoms and spectroscopic properties of the complexes have similarity with that of some oxygenase enzyme active sites. Specially with easy manipulation of one amino acid donor (histidine *vs* methionine) possible with this set of ligands, there is a vast scope of studies in elucidating the oxygenase mechanism using these ligands for the synthesis of model systems. Unfortunately the absence of suitable crystals to confirm the methionine coordination (or non coordination) and the exact nature of weak magnetic interaction observed have inhibited fare comparison between the two complexes and with protein. Que and coworkers also showed in the past that less charge on the tetradentate ligand helps to activate the complex towards O_2, a necessity to have reactivity similarity with oxygenase proteins. At present both the complexes can be synthesized and stored indefinitely under aerobic condition suggesting that the complexes are too stable to be reactive. Efforts in the group are on to characterize thoroughly the complexes and modifying the ligand with less negative charge on it.

References

[1] J. M. Axten, R. Ivy, L. Krim, J. D. Winkler, *J. Am. Chem. Soc.* **1999**, *121*, 6511.

[2] I. Bernal, J. Cetrullo, *J. Coord. Chem.* **1989**, *20*, 247.

[3] Y. Kubo, S. Maeda, S. Tokita, M. Kubo, *Nature* **1996**, *382*, 522.

[4] J. S. Seo, D. Whang, H. Lee, S. I. Jun, J. Oh, Y. J. Jeon, K. Kim, *Nature* **2000**, *404*, 982.

[5] R. K. Castellano, R. Clark, S. L. Craig, C. Nuckolls, J. Rebek. Jr., *Proc. Natl. Acad. Sci. USA* **2000**, *79*, 12418.

[6] D. J. Cram, *Science* **1988**, *240*, 760.

[7] B. Linton, A. D. Hamilton, *Chem. Rev.* **1997**, *97*, 1669.

[8] S. L. Lee, W. Lin, *J. Am. Chem. Soc.* **2002**, *124*, 4554.

[9] J. -M. Lehn, *Comprehensive Supramolecular Chemistry*, VCH, Weinheim, **1995**.

[10] S. R. Seidel, P. J. Stang, *Acc. Chem. Res.* **2002**, *35*, 972.

[11] P. J. Stang, B. Olenyuk, *Acc. Chem. Res.* **1997**, *30*, 502.

[12] F. Hof, S. L. Craig, C. Nuckolls, J. Rebek, Jr., *Angew. Chem. Int. Ed.* **2002**, *41*, 1488.

[13] A. W. Maverick, F. E. Klavetter, *Inorg. Chem.* **1984**, *23*, 4129.

[14] A. W. Schwabacher, J. Lee, H. Lie, *J. Am. Chem. Soc.* **1992**, *114*, 7597.

[15] M. Fulita, J. Yazaki, T. Kuramochi, K. Ogura, *Bull. Chem. Soc. Jpn.* **1993**, *66*, 1837.

[16] C. A. Hunter, L. D. Sarson, *Angew. Chem. Int. Ed.* **1994**, *33*, 2313.

[17] B. Hasenknopf, J. –M. Lehn, N. Boumediene, A. D. Gervais, A. V. Dorsselaer, B. Kneisel, D. Fenske, *J. Am. Chem. Soc.* **1997**, *119*, 10956.

[18] (a) M. Fujita, *Chem. Soc. Rev.* **1998**, *27*, 417. (b) De-L. Long, A. J. Blake, N. R. Champness, M. Schroder, *Chem. Commun.* **2000**, 2273. (c) J. L. C. Rowsell, O. M. Yaghi, *Microporous and Mesoporous materials* **2004**, *73*, 3.

[19] P. J. Stang, D. H. Cao, *J. Am. Chem. Soc.* **1994**, *116*, 4981.

[20] R. M. Nielson, J. T. Hupp, E. I. Yoon, *J. Am. Chem. Soc.* **1995**, *117*, 9085.

[21] C. M. Drain, J.-M. Lehn, *J. Chem. Soc., Chem. Commun.* **1994**, 2313.

[22] H. Rauter, E. C. Hillgeris, A. Erxleben, B. Lippert, *J. Am. Chem. Soc.* **1994**, *116*, 616.

[23] B. Olenyuk, J. A. Whiteford, P. J. Stang, *J. Am. Chem. Soc.* **1996**, *118*, 8221.

[24] S. J. Lee, W. Lin, *J. Am. Chem. Soc.* **2002**, *124*, 4554.

[25] M. M. Conn, J. Rebek, Jr., *Chem. Rev.* **1997**, *97*, 1647.

[26] R. K. Castellano, S. L. Craig, C. Nuckolls, J. Rebek, Jr., *J. Am. Chem. Soc.* **2000**, *122*, 7876.

[27] D. J. Cram, M. E. Tanner, R. Thomas, *Angew. Chem. Int. Ed.* **1991**, *30*, 1024.

[28] J. Kang, J. Rebek, Jr., *Nature* **1997**, *385*, 50.

[29] A. Collet, *Tetrahedron* **1987**, *43*, 5725.

[30] C. D. Gutsche, *Acc. Chem. Res.* **1983**, *16*, 161.

[31] R. W. Saalfrank, B. Hörner, D. Stalke, J. Salbeck, *Angew. Chem. Int. Ed.* **1993**, *32*, 1179.

[32] D. J. Johnson, K. N. Raymond, *Inorg. Chem.* **2001**, *40*, 5157.

[33] D. L. Caulder, C. Brückner, R. E. Powers, S. König, T. N. Parac, J. A. Leary, K. N. Raymond, *J. Am. Chem. Soc.* **2001**, *123*, 8923.

[34] Y. –M. Jeon, J. Kim, D. Whang, K. Kim, *J. Am. Chem. Soc.* **1996**, *118*, 9790.

[35] D. Whang, J. Heo, J. H. Park, K. Kim, *Angew. Chem. Int. Ed.* **1998**, *37*, 78.

[36] J. Rebek, Jr., *Acc. Chem. Res.* **1999**, *32*, 278.

[37] J. M. Rivera, T. Martin, J. Rebek, Jr., *Science* **1998**, *279*, 1021.

[38] D. M. Rudkevich, *Bull. Chem. Soc. Jpn.* **2002**, *75*, 393.

[39] J. L. Atwood, L. J. Barbour, M. J. Hardie, C. L. Raston, *Coord. Chem. Rev.* **2001**, *222*, 3.

[40] L. R. MacGillivray, K. T. Holman, J. L. Atwood, *J. Supramol. Chem.* **2001**, *1*, 125.

[41] L. R. MacGillivray, J. L. Atwood, *Nature* **1997**, *389*, 469.

[42] Z. Zhong, A. Ikeda, M. Ayabe, S. Shinkai, S. Sakamoto, K. Yamaguchi, *J. Org. Chem.* **2001**, *66*, 1002.

[43] A. Ikeda, M. Yoshimura, H. Udzu, C. Fukuhara, S. Shinkai, *J. Am. Chem. Soc.* **1999**, *121*, 4296.

[44] O. D. Fox, N. K. Dalley, R. G. Harrison, *J. Am. Chem. Soc.* **1998**, *120*, 7111.

[45] O. D. Fox, N. K. Dalley, R. G. Harrison, *Inorg. Chem.* **1999**, *38*, 5860.

[46] O. D. Fox, N. K. Dalley, R. G. Harrison, *Inorg. Chem.* **2000**, *39*, 620.

[47] O. D. Fox, J. F. Y. Leung, J. M. Hunter, N. K. Dalley, R. G. Harrison, *Inorg. Chem.* **2000**, *39*, 783.

[48] F. Fochi, P. Jacopozzi, E. Wegelius, K. Rissanen, P. Cozzini, E. Marastoni, E. Fisicaro, P. Manini, R. Fokkens, E. Dalcanale, *J. Am. Chem. Soc.* **2001**, *123*, 7539.

[49] M. Fujita, S. Nagao, K. Ogura, *J. Am. Chem. Soc.* **1995**, *117*, 1649.

[50] T. Kusukawa, M. Fujita, *Angew. Chem. Int. Ed.* **1998**, *37*, 3142.

[51] S. –Y. Yu, T. Kusukawa, K. Biradha, M. Fujita, *J. Am. Chem. Soc.* **2000**, *122*, 2665.

[52] J. Chin, S. S. Lee, K. J. Lee, S. Park, D. H. Kim, *Nature* **1999**, *401*, 254.

[53] R. R. Fenton, F. S. Stephens, R. S. Vagg, P. A. Williams, *Inorg. Chem. Acta* **1995**, *236*, 109.

[54] P. V. Bernhardt, P. Comba, T. Gyr, K. Várnagy, *Inorg. Chem.* **1992**, *31*, 1220.

[55] P. V. Bernhardt, P. Comba, T. W. Hambley, I. Sóvágó, K. Várnagy, *J. Chem. Soc., Dalton Trans.* **1993**, 2023.

[56] Y. Kubo, S. Maeda, S. Tokita, M. Kubo, *Nature* **1996**, *382*, 522.

[57] Y. Sunatsuki, Y. Motoda, N. Matsumoto, *Coord. Chem. Rev.* **2002**, *226*, 199.

[58] (a) L. Casella, M. Gullotti, G. Pacchioni, *J. Am. Chem. Soc.* **1982**, *104*, 2386. (b) L. Casella, M. Gullotti, *Inorg. Chem.* **1986**, *25*, 1293.

[59] M. R. Wagner, F. A. Walker, *Inorg. Chem.* **1983**, *22*, 3021.

[60] L. L. Koh, J. O. Ranford, W. T. Robinson, J. O. Svensson, A. L. C. Tan, D. Wu, *Inorg. Chem.* **1996**, *35*, 6466.

[61] L. A. Meiske, R. J. Angelici, *Inorg. Chem.* **1980**, *19*, 3783.

[62] M. Kitazawa, K. Iwasaki, (Ajinomoto Co. Inc., Japan). *PCT Int. Appl.* (Patent No. WO 9414755), **1994**.

[63] K. E. Voss, R. J. Angelici, R. A. Jacobson, *Inorg. Chem.* **1978**, *17*, 1922.

[64] J. J. Vittal, X. Wang, J. D. Ranford, *Inorg. Chem.* **2003**, *42*, 3390.

[65] B.S. Furniss, A. J. Hannaford, V. Rogers, P.W. Smith, A. R. Tatchell, *Vogal's Textbook of Practical Organic Chemistry*, 4th ed., ELBS, Longman, **1984**.

[66] Program Dsympc.exe developed by G. H. Gele, R. Spiske, H. W. Hffken, T. Lenzen, U. Weber, S. Goudetsidis, Phosphorous, Sulfur and Silicon, **1999**, *77*, 262. The program was downloaded from http://www.ccl.net/cca/software/MS-DOS/NMR-simulation/index.shtml.

[67] C. J. Pouchert, J. Behnke, *The Aldrich Library of ^{13}C and ^{1}H FT NMR Spectra, Vol. II*, 1st ed. **1993**.

[68] F. Taddei, L. Pratt, *J. Chem. Soc.* **1964**, 1553.

[69] R. B. Martin, R. Mathur, *J. Am. Chem. Soc.* **1965**, *87*, 1065.

[70] M. Fujita, K. Umemoto, M. Yoshizawa, N. Fujita, T. Kusukawa, K. Biradha, *Chem. Commun.* **2001**, 509.

[71] [00] M. Yoshizawa, Y. Takeyama, T. Kusukawa, M. Fujita, *Angew. Chem. Int. Ed.* **2002**, *41*, 1347.

[72] N. Walker, D. Stuart, *Acta Crystallogr. A* **1983**, *39*, 158.

[73] G. M. Sheldrick, SHELXL-97, Program for the Solution of Crystal Structures, University of Göttingen, Göttingen, Germany, **1997**.

[74] R. Blessing, *Acta Crystallogr. A* **1995**, *51*, 33.

[75] C. K. Johnson, ORTEP, Report ORNL-3794, Oak Ridge National Laboratory, Oak Ridge, TN, **1976**.

[76] K. Nakamoto, *Infrared and Raman Spectra of Inorganic Compounds*, 5th ed., Part B **1997**.

[77] W. J. Geary, *Coord. Chem. Rev.* **1971**, *7*, 81.

[78] A. Earnshaw, *Introduction to Magnetochemistry*, Academic Press, London, **1968**, Chapter III.

[79] B. N. Figgis, J. Lewis, *Progress in Inorganic Chemistry*, ed. F. A. Cotton, Interscience Publishers, **1964**, *Volume* 6, pp 211.

[80] The (imidazole) NH…O(carboxylate) distances in **1** are between 2.69 to 2.78 Å. Reported range 2.69-2.98 Å; S. M. Couchman, J. C. Jeffery, M. D. Ward, *Polyhedron* **1999**, *18*, 2633.

[81] K. Sakai, K. Matsumoto, *J. Am. Chem. Soc.* **1989**, *111*, 3074.

[82] A. W. Addision, T. N. Rao, J. Reedijk, J. van Rijn, G. C. Verschoor, *J. Chem. Soc., Dalton Trans.* **1984**, 1349.

[83] M. B. Ferrari, G. G. Fava, M. Lanfranchi, C. Pelizzi, P. Tarasconi, *J. Chem. Soc., Dalton Trans.* **1991**, 1951.

[84] R. Anulewicz, I. Wawer, T. M. Krygowski, F. Männle, H. Limbach, *J. Am. Chem. Soc.* **1997**, *119*, 12223.

[85] O. P. Anderson, A. B. Packard, *Inorg. Chem.* **1980**, *19*, 2123.

[86] G. A. Barclay, C. H. L. Kennard, *J. Chem. Soc.* **1961**, 5244.

[87] "Tables of Interatomic Distances and Configuration in Molecules and Ions," *Chem. Soc. Special Publ.* No.11.

[88] K. N. Raymond, C. J. Carrano, *Acc. Chem. Res.* **1979**, *12*, 183.

[89] Y. Wan, O. Mitkin, L. Barnhurst, A. Kurchan, A. Kutateladze, *Org. lett.* **2000**, 3817.

[90] F. M. H. de Groot, C. Albrecht, R. Koekkoek, P. H. Beusker, H. W. Scheeren, *Angew. Chem. Int. Ed.* **2003**, *43*, 4490.

[91] C. T. Yang, B. Mubaraki, K. S. Murray, J. D. Ranford, J. J. Vittal, *Inorg. Chem.* **2001**, *40*, 5934.

[92] K. W. So, C. T. Yang, J. J. Vittal, J. D. Ranford, *Inorg. Chim. Acta* **2003**, *349*, 135.

[93] L. E. Cheruzel, M. S. Pometun, M. R. Cecil, M. S. Mashutta, R. J. Wittebort, R. M. Buchanan, *Angew. Chem. Int. Ed.* **2003**, *42*, 5452.

[94] (a) S. Pal, N. B. Sankaran, A. Samanta, *Angew. Chem. Int. Ed.* **2003**, *43*, 1741. (b) A. Mukherjee, M. K. Saha, M. Nethaji, A. R. Chakravarty, *Chem. Commun.* **2004**, 716.

[95] F. N. Keutsch, R. J. Saykally, *Proc. Natl. Acad. Sci.* **2001**, *98*, 10533.

[96] D. P. Tieleman, P. C. Biggin, G. R. Smith, M. S. P. Sansom, *Q. Rev. Biophys.* **2001**, *34*, 473.

[97] H. Adams, N. A. Bailey, C. O. R. de Barbarin, D. E. Fanton, *J. Chem. Soc., Dalton Trans.* **1995**, 2323.

[98] H. Yokoi, A. W. Addison, *Inorg. Chem.* **1977**, *16*, 1341.

[99] B. Bleaney, K. D. Bowers, *Proc. R. Soc. Lond. A* **1952**, *214*, 451.

[100] D. A. Doyle, J. M. Cabral, R. A. Pfuetzner, A. Kuo, J. M. Gulbis, S. L. Cohen, B. T. Chait, R. MacKinnon, *Science* **1998**, *280*, 69.

[101] B. L de Groot, A. Engel, H. Grubmüller, *J. Mol. Biol.* **2003**, *325*, 485.

[102] B. L de Groot, H. Grubmüller, *Science* **2001**, *294*, 2353.

[103] H. Sui, B. G. Han, J. K. Lee, P. Walian, B. K. Jap, *Nature* **2001**, *414*, 872.

[104] M. F. Perutz, J. T. Finch, J. Berriman, A. Lesk, *Proc. Natl. Acad. Sci. USA*, **2002**, *99*, 5591.

[105] G. Chang, R. H. Spencer, A. T. Lee, M. T. Barclay, D. C. Rees, *Science* **1998**, *282*, 2220.

[106] D. Fu, A. Libson, L. J. W. Miercke, C. Weitzman, P. Nollert, J. Krucinski, R. M. Stroud, *Science* **2000**, *290*, 481.

[107] M. E. Davis, *Nature* **2002**, *417*, 813.

[108] O. Ikkala, G. ten Brinke, *Science* **2002**, *295*, 2407.

[109] G. M. Whitesides, B. Grzybowski, *Science* **2002**, *295*, 2418.

[110] H. Li, A. Laine, M. O'Keeffe, O. M. Yaghi, *Science* **1999**, *283*, 1145.

[111] L. A. Cuccia, J. –M. Lehn, J. –C. Homo, M. Schmutz, *Angew. Chem. Int. Ed.* **2000**, *39*, 233.

[112] M. Ikegame, K. Tajima, T. Aida, *Angew. Chem. Int. Ed.* **2003**, *42*, 2154.

[113] R. Kitaura, S. Kitagawa, Y. Kubota, T. C. Kobayashi, K. Kindo, Y. Mita, A. Matsuo, M. Kobayashi, H. C. Chang, T. C. Ozawa, M. Suzuki, M. Sakata, M. Takata, *Science* **2002**, *298*, 2358.

[114] B. F. Abrahams, M. Moylan, S. D. Orchard, R. Robson, *Angew. Chem. Int. Ed.* **2003**, *42*, 1848.

[115] R. Herges, M. Deichmann, T. Wakita, Y. Okamoto, *Angew. Chem. Int. Ed.* **2003**, *42*, 1170.

[116] B. Zhao, P. Cheng, Y. Dai, C. Cheng, D. Z. Liao, S. –P. Yan, Z. –H. Jiang, G. L. Wang, *Angew. Chem. Int. Ed.* **2003**, *42*, 934.

[117] X. Xu, M. Nieuwenhuyzen, S. L. James, *Angew. Chem. Int. Ed.* **2002**, *41*, 764.

[118] A. W. Coleman, E. Da Silva, F. Nouar, M. Nierlich, A. Navaza, *Chem. Commun.* **2003**, 826.

[119] S. A. Dalrymple, G. K. H. Shimizu, *Chem. Commun.* **2002**, 2224.

[120] R. Kniep, H. G. Will, I. Boy, C. Röhr, *Angew. Chem. Int. Ed.* **1997**, *36*, 1013.

[121] A. D. C. -V. Noord, J. W. Kampf, V. L. Pecoraro, *Angew. Chem. Int. Ed.* **2002**, *41*, 4668.

[122] C. R. Woods, M. Benaglia, F. Cozzi, J. S. Siegel, *Angew. Chem. Int. Ed.* **1996**, *35*, 1830.

[123] R. Custelcean, M. D. Ward, *Angew. Chem. Int. Ed.* **2002**, *41*, 1724.

[124] C. –D. Wu, C. –Z. Lu, X. Lin, D. –M. Wu, S. –F. Lu, H. –H. Zhuang, J. –S. Huang, *Chem. Commun.* **2003**, 1284.

[125] R. J. Smithson, C. A. Kilner, A. R. Brough, M. A. Halcrow, *Polyhedron* **2003**, *22*, 725.

[126] B. Hasenknopf, J. -M. Lehn, B. O. Kneisel, G. Baum, D. Fenske, *Angew. Chem. Int. Ed.* **1996**, *35*, 1838.

[127] A. Petitjean, L. A. Cuccia, J. –M. lehn, H. Nierengarten, M. Schmutz, *Angew. Chem. Int. Ed.* **2002**, *41*, 1195.

[128] J. Liang, Y. Wang, J. Yu, Y. Li, R. Xu, *Chem. Commun.* **2003**, 882.

[129] M. J. Krische, J. –M. Lehn, E. Cheung, G. Vaughn, A. L. Krische, *C. R. Acad. Sci. Paris* **1999**, 549.

[130] S. M. Gorun, S. L. Lippard, *Inorg. Chem.* **1991**, *30*, 1642.

[131] W. H. Armstrong, S. J. Lippard, *J. Am. Chem. Soc.* **1984**, *106*, 4632.

[132] B. P. Murch, F. C. Bradley, P. D. Boyle, V. Papaefthymiou, L. Que, Jr., *J. Am. Chem. Soc.* **1987**, *109*, 7993.

[133] S. Yan, L. Que, Jr., *J. Am. Chem. Soc.* **1988**, *110*, 5222.

[134] P. N. Turowski, W. H. Armstrong, S. Liu, S. Liu, S. N. Brown, S. J. Lippard, *Inorg. Chem.* **1994**, *33*, 636.

[135] Y. Lindqvist, E. Johansson, H. Kaija, P. Vihko, G. Schneider, *J. Mol. Biol.* **1999**, *291*, 135.

[136] Reported range for N-H…O distances 2.69-2.98 Å; S. M. Couchman, J. C. Jeffery, M. D. Ward, *Polyhedron* **1999**, *18*, 2633.

[137] K. Sakai, K. Matsumoto, *J. Am. Chem. Soc*. **1989**, *111*, 3074.

[138] J. Y. Lu, A. M. Babb, *Inorg. Chem.* **2002**, *41*, 1339.

[139] J. Y. Lu, A. M. Babb, *Chem. Commun.* **2003**, 1346.

[140] H. A. Benesi, J. H. Hildebrand, *J. Am. Chem. Soc*. **1949**, *71*, 2703.

[141] A. B. Lever, *Inorganic Electronic Spectroscopy*, 2nd ed., Elsevier, **1984**.

[142] H. Kurosaki, H. Yoshida, M. Ito, H. Koike, E. Higuchi, M. Goto, *Bioorg. Med. Chem. Lett.* **2001**, *11*, 785.

[143] L. W. Guddat, A. S. McAlpine, D. Hume, S. Hamilton, J. de Jersey, J. L. Martin, *Structure* **1999**, *7*, 157.

[144] J, Bassett, R. C. Denney, G. H. Jeffery, J. Mendham, *Vogle's Textbook of Quantitative Inorganic Analysis Including Elementary Instrumental Analysis*, 4th ed., ELBS, **1978**.

[145] T. Koga, H. Furutachi, T. Nakamura, N. Fukita, M. Ohba, K. Takahashi, H. Okawa, *Inorg. Chem.* **1998**, *37*, 989.

[146] R. J. Butcher, C. J. O'Connor, E. Sinn, *Inorg. Chem.* **1982**, *21*, 616.

[147] B. M. Holligan, J. C. Jeffery, M. D. Ward, *J. Chem. Soc., Dalton Trans*. **1992**, 3337.

[148] A. B. Lever, *Inorganic Electronic Spectroscopy*, 2nd ed., Elsevier, **1984**, pp 516.

[149] A. B. Lever, *Inorganic Electronic Spectroscopy*, 2nd ed., Elsevier, **1984**, pp 507.

[150] Y. Hosokawa, H. yamane, Y. Nakao, K. Matsumoto, S. Takamizawa, W. Mori, S. Suzuki, H. Kimoto, *Inorg. Chim. Acta* **1998**, *283*, 118.

[151] G. J. Mohr, C. Demuth, C. E. S. Keller, *Anal. Chem.* **1998**, *70*, 3868.

[152] S. Nakatsuji, R. nakano, M. Kawano, K. Nakashima, S. Akiyama, *Chem. Pharm. Bull.* **1982**, *30*, 2467.

[153] F. Takacs, D. Hippmann, *Arzneim. Forsch.* **1983**, *33*, 5.

[154] S. C. Beale, *Anal. Chem.* **1998**, *70*, 279.

[155] D. C. Johnson, J. C. Hoekstra, *Anal. Chem.* **1998**, *70*, 83.

[156] D. F. Evans, *J. Chem. Soc.* **1959**, 2003.

[157] A. L. van Geet, *Anal. Chem.* **1968**, *40*, 2227.

[158] W. Gerger; U. Mayer; V. Gutmann, *Montash. Chem.* **1977**, *108*, 417.

[159] C. J. O'Connor, *Prog. Inorg. Chem.* **1982**, *29*, 203.

[160] E. N. Ainscough, A. M. Brodie, J. E. Plowman, K. L. Brown, A. W. Addition, A. R. Gainford. *Inorg. Chem.* **1980**, *19*, 3655.

[161] P. Chakraborty, S. K. Chandra, A. Chakravorty, *Inorg. Chem.* **1994**, *33*, 6429.

[162] (a)G. Aromi, S. Bhaduri, P. Artús, K. Folting, G. Christou, *Inorg. Chem.* **2002**, *41*, 805. (b) W. Schmitt, M. Murugesu, J. C. Goodwin, J. P. Hill, A. mandel, R. Bhalla, C. E. Anson, S. L. Heath, A. K. Powell, *Polyhedrone* **2001**, 1687.

[163] L. Que. Jr., R. Y. N. Ho, *Chem. Rev*. **1996**, *96*, 2607.

[164] D. H. Ohlendrof, J. D. Lipscomb, P. C. Weber, *Nature* **1988**, *336*, 403.

[165] D. H. Ohlendrof, A. M. Orville, J. D. Lipscomb, *J. Mol. Biol.* **1994**, *244*, 586.

[166] T. Senda, K. Sugiyama, H. Narita, T. Yamamoto, K. Kimbara, M. Fukuda, M. Sato, K. Yano, Y. Mitsui, *J. Mol. Biol.* **1996**, *255*, 735.

[167] J. C. Boyington, B. J. Gaffney, M. Arnzel, *Science* **1993**, *260*, 1482.

[168] P. L. Roach, I. J. Clifton, V. Fülöp, K. Harlos, G. J. Barton, J. Hajdu, I. Andersson, C. J. Schofield, J. E. Baldwin, *Nature* **1995**, *375*, 700.

[169] M. Pascaly, M. Duda, F. Schweppe, K. Zurlinden, F. K. Müller, B. Krebs, *J. Chem. Soc., Dalton Trans.* **2001**, 828.

[170] G. Lin, G. Reid, T. D. H. Bugg, *Chem. Commun.* **2000**, 1119.

[171] T. D. H. Bugg, G. Lin, *Chem. Commun.* **2001**, 941.

[172] M. W. Lynch, M. Valentine, D. N. Hendrickson, *J. Am. Chem. Soc.* **1982**, *104*, 6982.

[173] R. H. Heistand II, R. B. Lauffer, E. Fikrig, L. Que, Jr., *J. Am. Chem. Soc.* **1982**, *104*, 2789.

[174] D. D. Cox, S. J. Benkovic, L. M. Bloom, F. C. Bradley, M. J. Nelson, L. Que, Jr. *J. Am. Chem. Soc.* **1988**, *110*, 2026.

[175] L. Que, Jr., *Physical Methods in Bioinorganic Chemistry Spectroscopy and Magnetism*, University Science Books, Sausalita, California, **2000**.

[176] Y. Tatsuno, Y. Saeki, M. Iwaki, T. Yagi, M. Nozaki, *J. Am. Chem. Soc.* **1978**, *100*, 4614.

Conclusions

In this thesis work we set our goals, as outlined in the chapter I, to synthesize enantiopure metal complexes or their assemblies with cavity of varying size and shapes. As the resulting enantiopure complexes may find use in material science, enantiomer separation, chiral sensor or drug delivery, the synthetic procedure needed to be simple and efficient. In order to synthesize cavity for a particular purpose in future we needed to understand the coordination chemistry of the complexes and the structural factors leading to the formation of the cavity.

Utilizing an easy to synthesize enantiopure ligand we have synthesized and thoroughly characterized enantiopure binuclear and multinuclear metal complexes. While Cu(II) formed a tetranuclear large cup shaped cavity (~1nm width) in solution, Fe(III) and Ni(II) formed bridged binuclear complexes with a smaller hydrophilic pocket. The chiral environment around the hydrophilic pocket could be engineered from an open cavity in Fe(III) complex to a sterically crowded one in Ni(II) complex, albeit serendipitously.

Our choice of the amino acid as the source of chirality in the ligand was driven by the fact that natural amino acids are one of the cheaper sources of enantiomerically pure organic compound. We did expect to see H-bonding playing an important role in the solid, as outlined in the beginning of Chapter II, but the trapping of pyridine through H-bond and metal coordination (Chapter III), sealing of two cups into a capsular cavity (Chapter III), helical channel formation in Fe(III) complex (Chapter IV) and the helical water chain (Chapter III) were remarkable.

As materials, the crystals of the Fe(III) complex (Chapter IV) with helical channels have future potential due to its thermal stability and accessibility of the channels to external reagents. The binding and chiral recognition capability of the cavities of the tetranuclear Cu(II) complex and Ni(II) complexes will be explored in future. Although the Fe(III) complexes in chapter VI showed amine detectability but lack of structural information severely hampered our effort to use it effectively.

Additionally, as the donor groups in the ligands used also represents amino acid residues in metalloproteins closely, some of the complexes might be used as active site structural model complex in future.

List of Publications

1. "Synthesis of a Self-Assembled Molecular Capsule that Traps Pyridine Molecules by a Combination of Hydrogen Bonding and Copper(II) Coordination" M. A. Alam, M. Nethaji, M. Ray, *Angew. Chem. Int. Ed.* **2003**, *42*, 1940.

2. "Enantiopure One-dimentional Helical Channels Assembled from Hydroxo-bridged Binuclear Iron(III) Complex and Its Iodine Adduct" M. A. Alam, M. Nethaji, M. Ray, (manuscript submitted).

Manuscript to be submitted

3. "Assembly and Disassembly of Molecular Capsule in Presence of External Ligands" M. A. Alam, M. Nethaji, M. Ray.

4. "Simultaneous Colorimetric and Conductometric Detection of Amines in Solution and Vapor using two Iron(III) Complexes" M. A. Alam, P. Devi, V. Balamurugan, M. Ray.

Appendix

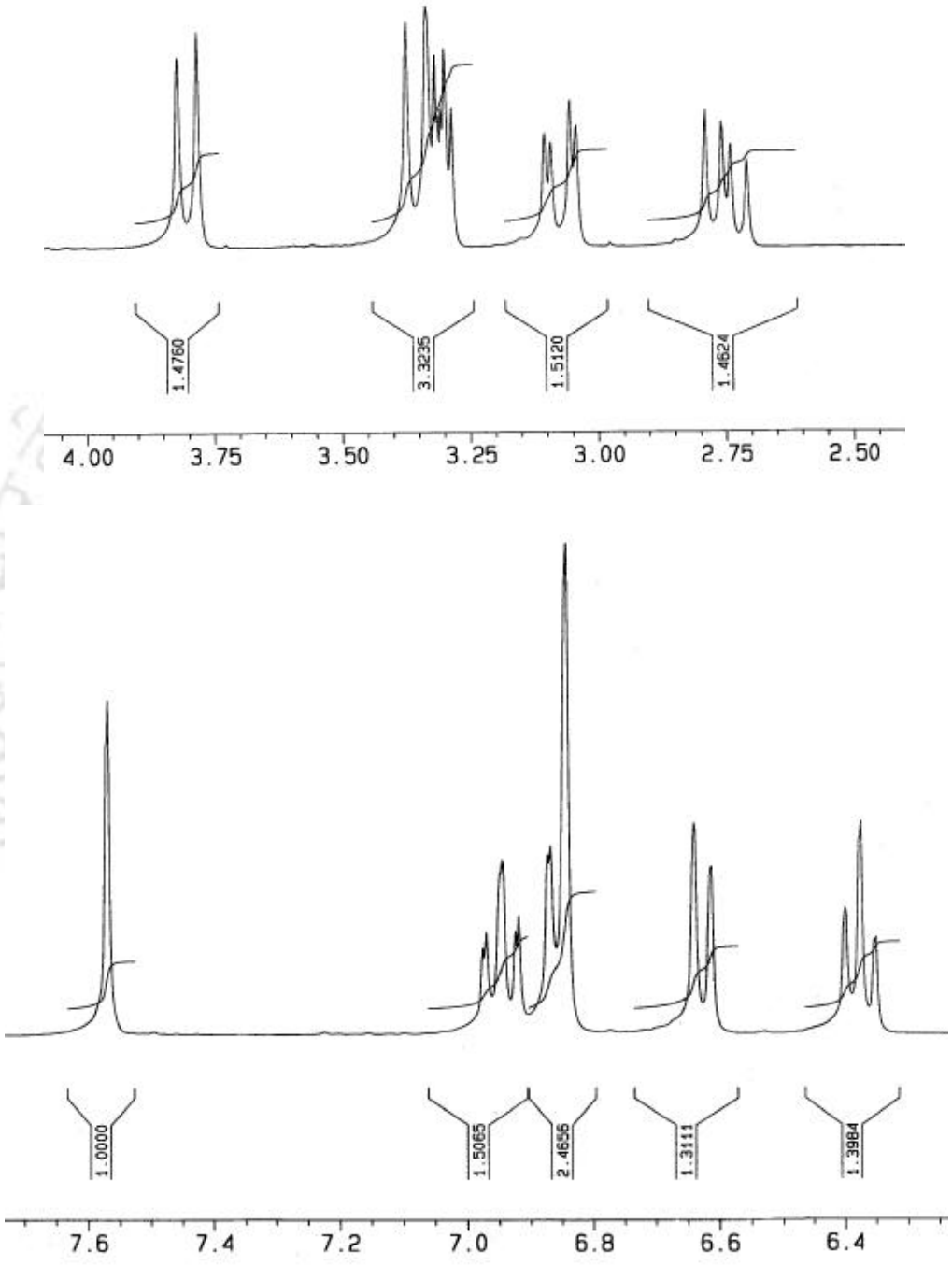

Figure A.1 ^{1}H NMR of ligand Li_2 (*R*) Salhis in CD_3OH

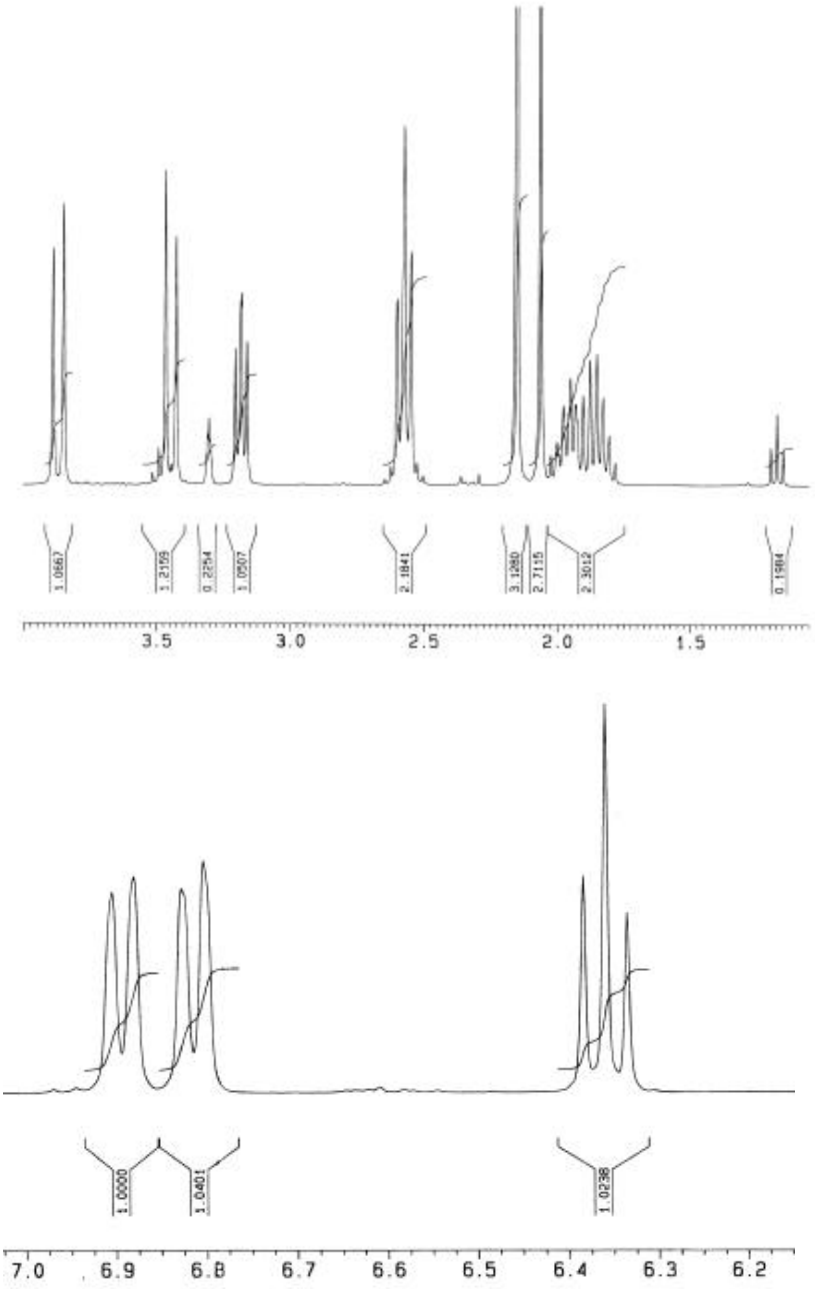

Figure A.2 ^{1}H NMR of ligand Li_2 (*S*) *o*-Me-Salmet in CD_3OD

Table I: Selected bond Distances (Å) of complex **[Cu_8(*S*-SalHis)$_8$(Py)$_{10}$]·Py·3MeOH·(C_2H_5)$_2$O] (1)**

Atoms	Distances	Atoms	Distances
Cu(1)-O(3A)	1.926(7)	N(2A)-C(4A)	1.371(10)
Cu(1)-N(3A)	2.000(8)	N(2B)-C(6B)	1.309(10)
Cu(1)-N(1D)	2.009(8)	N(2B)-C(4B)	1.365(10)
Cu(1)-O(1A)	2.029(7)	N(2C)-C(6C)	1.318(8)
Cu(1)-N(4A)	2.430(9)	N(2C)-C(4C)	1.352(10)
Cu(2)-O(3B)	1.910(7)	N(2D)-C(6D)	1.286(10)
Cu(2)-N(1A)	1.967(7)	N(2D)-C(4D)	1.324(10)
Cu(2)-O(1B)	1.985(6)	N(3A)-C(7A)	1.439(10)
Cu(2)-N(3B)	2.030(7)	N(3A)-C(2A)	1.517(11)
Cu(2)-N(4B)	2.425(11)	N(3B)-C(7B)	1.464(11)
Cu(3)-O(3C)	1.865(7)	N(3B)-C(2B)	1.505(9)
Cu(3)-N(3C)	1.980(8)	N(3C)-C(7C)	1.436(10)
Cu(3)-O(1C)	1.989(6)	N(3C)-C(2C)	1.525(10)
Cu(3)-N(1B)	2.005(8)	N(3D)-C(2D)	1.512(9)
Cu(4)-O(3D)	1.941(7)	N(3D)-C(7D)	1.515(9)
Cu(4)-O(1D)	1.946(6)	C(1A)-C(2A)	1.524(14)
Cu(4)-N(1C)	1.993(7)	C(2A)-C(3A)	1.539(13)
Cu(4)-N(3D)	1.999(7)	C(3A)-C(4A)	1.495(11)
Cu(4)-N(4D)	2.407(10)	C(4A)-C(5A)	1.384(13)
O(1A)-C(1A)	1.287(10)	C(7A)-C(8A)	1.454(15)
O(1B)-C(1B)	1.306(9)	C(8A)-C(9A)	1.408(17)
O(1C)-C(1C)	1.275(9)	C(8A)-C(13A)	1.417(16)
O(1D)-C(1D)	1.264(8)	C(9A)-C(10A)	1.377(18)
O(2A)-C(1A)	1.224(12)	C(10A)-C(11A)	1.54(2)
O(2B)-C(1B)	1.286(10)	C(11A)-C(12A)	1.33(2)
O(2C)-C(1C)	1.192(9)	C(12A)-C(13A)	1.40(2)
O(2D)-C(1D)	1.301(10)	C(1B)-C(2B)	1.477(13)
O(3A)-C(9A)	1.258(13)	C(2B)-C(3B)	1.503(12)
O(3B)-C(9B)	1.375(12)	C(3B)-C(4B)	1.502(13)
O(3C)-C(9C)	1.296(12)	C(4B)-C(5B)	1.305(13)
O(3D)-C(9D)	1.345(11)	C(7B)-C(8B)	1.438(15)
N(1A)-C(6A)	1.310(11)	C(8B)-C(13B)	1.367(17)
N(1A)-C(5A)	1.420(9)	C(8B)-C(9B)	1.451(14)
N(1B)-C(6B)	1.353(9)	C(9B)-C(10B)	1.374(15)
N(1B)-C(5B)	1.356(9)	C(10B)-C(11B)	1.361(17)
N(1C)-C(6C)	1.291(9)	C(11B)-C(12B)	1.400(18)
N(1C)-C(5C)	1.357(9)	C(12B)-C(13B)	1.336(19)
N(1D)-C(6D)	1.281(9)	C(1C)-C(2C)	1.549(12)
N(1D)-C(5D)	1.393(11)	C(2C)-C(3C)	1.510(13)
N(2A)-C(6A)	1.348(9)	C(3C)-C(4C)	1.517(11)

Atoms	Distances	Atoms	Distances
C(4C)-C(5C)	1.422(12)	N(4C)-C(14C)	1.304(19)
C(7C)-C(8C)	1.506(14)	C(14C)-C(15C)	1.38(3)
C(8C)-C(13C)	1.414(16)	C(15C)-C(16C)	1.46(3)
C(8C)-C(9C)	1.427(15)	C(16C)-C(17C)	1.22(2)
C(9C)-C(10C)	1.413(15)	C(17C)-C(18C)	1.309(19)
C(10C)-C(11C)	1.439(17)	N(5)-C(23)	1.283(16)
C(11C)-C(12C)	1.28(2)	N(5)-C(19)	1.298(15)
C(12C)-C(13C)	1.354(18)	C(19)-C(20)	1.215(15)
C(1D)-C(2D)	1.486(13)	C(20)-C(21)	1.28(2)
C(2D)-C(3D)	1.594(13)	C(21)-C(22)	1.39(2)
C(3D)-C(4D)	1.441(14)	C(22)-C(23)	1.376(17)
C(4D)-C(5D)	1.348(13)	N(6)-C(28)	1.301(15)
C(7D)-C(8D)	1.430(13)	N(6)-C(24)	1.395(16)
C(8D)-C(9D)	1.345(13)	C(24)-C(25)	1.321(14)
C(8D)-C(13D)	1.462(15)	C(25)-C(26)	1.374(18)
C(9D)-C(10D)	1.459(16)	C(26)-C(27)	1.437(19)
C(10D)-C(11D)	1.343(16)	C(27)-C(28)	1.375(16)
C(11D)-C(12D)	1.287(17)	C(14H)-C(15H)	1.07(3)
C(12D)-C(13D)	1.343(17)	C(14H)-N(4H)	1.27(3)
N(4A)-C(14A)	1.263(16)	C(14H)-C(16H)	2.00(3)
N(4A)-C(18A)	1.375(16)	C(15H)-C(16H)	1.09(3)
C(18A)-C(17A)	1.55(2)	C(15H)-C(17H)	1.99(4)
C(17A)-C(16A)	1.30(3)	C(16H)-C(17H)	1.13(6)
C(17A)-C(15A)	1.90(3)	C(17H)-C(18H)	1.45(5)
C(16A)-C(15A)	1.06(3)	C(18H)-N(4H)	1.59(3)
C(15A)-C(14A)	1.45(2)	Cu(5)-O(3E)	1.897(8)
N(4D)-C(18D)	1.288(13)	Cu(5)-N(1F)	1.928(9)
N(4D)-C(14D)	1.295(14)	Cu(5)-O(1E)	2.007(7)
C(18D)-C(17D)	1.35(2)	Cu(5)-N(3E)	2.034(8)
C(17D)-C(16D)	1.44(3)	Cu(5)-N(4E)	2.384(9)
C(16D)-C(15D)	1.365(19)	Cu(6)-O(3F)	1.867(8)
C(15D)-C(14D)	1.366(17)	Cu(6)-O(1F)	1.989(7)
N(4B)-C(18B)	1.346(15)	Cu(6)-N(1G)	2.015(7)
N(4B)-C(14B)	1.38(2)	Cu(6)-N(3F)	2.018(7)
C(18B)-C(17B)	1.27(2)	Cu(6)-N(7)	2.409(11)
C(18B)-C(16B)	2.04(4)	Cu(7)-O(3G)	1.923(6)
C(17B)-C(16B)	1.12(4)	Cu(7)-N(1H)	1.966(8)
C(16B)-C(15B)	1.48(4)	Cu(7)-O(1G)	1.987(6)
C(15B)-C(14B)	1.38(2)	Cu(7)-N(3G)	2.034(7)
N(4C)-C(18C)	1.280(17)	Cu(7)-N(4G)	2.328(9)

Atoms	Distances	Atoms	Distances
Cu(8)-O(3H)	1.918(8)	C(1E)-C(2E)	1.539(13)
Cu(8)-O(1H)	1.958(7)	C(2E)-C(3E)	1.523(13)
Cu(8)-N(1E)	1.976(7)	C(3E)-C(4E)	1.498(12)
Cu(8)-N(3H)	2.017(7)	C(4E)-C(5E)	1.287(12)
Cu(8)-N(8)	2.393(9)	C(7E)-C(8E)	1.479(15)
O(1E)-C(1E)	1.269(10)	C(8E)-C(9E)	1.334(15)
O(1F)-C(1F)	1.250(10)	C(8E)-C(13E)	1.405(16)
O(2G)-C(1G)	1.231(9)	C(9E)-C(10E)	1.461(19)
O(1H)-C(1H)	1.296(9)	C(10E)-C(11E)	1.40(2)
O(2E)-C(1E)	1.235(11)	C(11E)-C(12E)	1.319(18)
O(2F)-C(1F)	1.233(11)	C(12E)-C(13E)	1.435(17)
O(1G)-C(1G)	1.268(10)	C(1F)-C(2F)	1.586(14)
O(2H)-C(1H)	1.228(11)	C(2F)-C(3F)	1.503(13)
O(3E)-C(13E)	1.310(12)	C(3F)-C(4F)	1.561(15)
O(3F)-C(9F)	1.336(13)	C(4F)-C(5F)	1.365(15)
O(3G)-C(9G)	1.367(11)	C(7F)-C(8F)	1.563(16)
O(3H)-C(9H)	1.265(10)	C(8F)-C(13F)	1.475(16)
N(1E)-C(5E)	1.348(10)	C(8F)-C(9F)	1.515(16)
N(1E)-C(6E)	1.360(11)	C(9F)-C(10F)	1.541(19)
N(1F)-C(6F)	1.287(11)	C(10F)-C(11F)	1.246(16)
N(1F)-C(5F)	1.395(12)	C(11F)-C(12F)	1.268(17)
N(1G)-C(6G)	1.312(9)	C(12F)-C(13F)	1.341(18)
N(1G)-C(5G)	1.322(9)	C(1G)-C(2G)	1.542(13)
N(1H)-C(5H)	1.351(9)	C(2G)-C(3G)	1.592(13)
N(1H)-C(6H)	1.377(10)	C(3G)-C(4G)	1.499(12)
N(2E)-C(6E)	1.309(9)	C(4G)-C(5G)	1.326(12)
N(2E)-C(4E)	1.365(10)	C(7G)-C(8G)	1.462(13)
N(2F)-C(6F)	1.414(10)	C(8G)-C(13G)	1.315(14)
N(2F)-C(4F)	1.417(11)	C(8G)-C(9G)	1.393(15)
N(2G)-C(6G)	1.292(9)	C(9G)-C(10G)	1.378(15)
N(2G)-C(4G)	1.334(9)	C(10G)-C(11G)	1.264(16)
N(2H)-C(6H)	1.342(10)	C(11G)-C(12G)	1.43(2)
N(2H)-C(4H)	1.395(11)	C(12G)-C(13G)	1.413(19)
N(3E)-C(7E)	1.456(10)	C(1H)-C(2H)	1.571(13)
N(3E)-C(2E)	1.469(9)	C(2H)-C(3H)	1.557(12)
N(3F)-C(2F)	1.464(10)	C(3H)-C(4H)	1.550(14)
N(3F)-C(7F)	1.487(12)	C(4H)-C(5H)	1.395(14)
N(3G)-C(7G)	1.452(9)	C(7H)-C(8H)	1.540(15)
N(3G)-C(2G)	1.470(9)	C(8H)-C(9H)	1.291(13)
N(3H)-C(2H)	1.466(11)	C(8H)-C(13H)	1.318(14)
N(3H)-C(7H)	1.523(10)	C(9H)-C(10H)	1.386(16)

Atoms	**Distances**	**Atoms**	**Distances**
C(10H)-C(11H)	1.350(17)	C(15G)-C(14G)	1.295(18)
C(11H)-C(12H)	1.266(16)	N(7)-C(33)	1.287(11)
C(12H)-C(13H)	1.415(16)	N(7)-C(29)	1.367(16)
N(4E)-C(14E)	1.202(18)	C(29)-C(30)	1.43(2)
N(4E)-C(18E)	1.259(17)	C(30)-C(31)	1.26(2)
C(18E)-C(17E)	1.23(2)	C(30)-C(32)	2.04(2)
C(17E)-C(16E)	1.24(3)	C(31)-C(32)	1.23(2)
C(16E)-C(15E)	1.28(2)	C(32)-C(33)	1.582(17)
C(15E)-C(14E)	1.65(2)	O(200)-C(40)	1.2765
N(8)-C(38)	1.356(14)	O(300)-C(41)	1.2719
N(8)-C(34)	1.414(16)	O(400)-C(39)	1.2461
C(34)-C(35)	1.540(19)	C(40)-C(39)#1	1.9064
C(35)-C(36)	1.42(2)	C(39)-C(40)#2	1.9064
C(36)-C(37)	1.29(3)	C(3)-C(1)	1.2570
C(37)-C(38)	1.345(18)	C(3)-O(100)	1.2903
N(4G)-C(14G)	1.232(14)	C(3)-C(2)	1.9284
N(4G)-C(18G)	1.328(15)	C(3)-C(5)	2.0076
C(18G)-C(17G)	1.317(16)	C(5)-C(2)	1.6465
C(17G)-C(16G)	1.24(2)	C(5)-C(1)	1.9874
C(16G)-C(15G)	1.47(2)	C(2)-O(100)	1.4262

Table II: Selected bond Angles (°) of the complex **[Cu_8(*S*-SalHis)$_8$(Py)$_{10}$]·Py·3MeOH·(C_2H_5)$_2$O] (1)**

Atoms	**Angles**	**Atoms**	**Angles**
O(3A)-Cu(1)-N(3A)	94.2(3)	O(3A)-Cu(1)-N(3A)	94.2(3)
O(3A)-Cu(1)-N(1D)	90.2(3)	O(3A)-Cu(1)-N(1D)	90.2(3)
N(3A)-Cu(1)-N(1D)	165.5(3)	N(3A)-Cu(1)-N(1D)	165.5(3)
O(3A)-Cu(1)-O(1A)	175.0(3)	O(3A)-Cu(1)-O(1A)	175.0(3)
N(3A)-Cu(1)-O(1A)	82.2(3)	N(3A)-Cu(1)-O(1A)	82.2(3)
N(1D)-Cu(1)-O(1A)	92.5(3)	N(1D)-Cu(1)-O(1A)	92.5(3)
O(3A)-Cu(1)-N(4A)	95.3(3)	O(3A)-Cu(1)-N(4A)	95.3(3)
N(3A)-Cu(1)-N(4A)	100.5(3)	N(3A)-Cu(1)-N(4A)	100.5(3)
N(1D)-Cu(1)-N(4A)	92.9(3)	N(1D)-Cu(1)-N(4A)	92.9(3)
O(1A)-Cu(1)-N(4A)	88.8(3)	O(1A)-Cu(1)-N(4A)	88.8(3)
O(3B)-Cu(2)-N(1A)	92.9(3)	O(3B)-Cu(2)-N(1A)	92.9(3)
O(3B)-Cu(2)-O(1B)	175.9(3)	O(3B)-Cu(2)-O(1B)	175.9(3)
N(1A)-Cu(2)-O(1B)	89.7(3)	N(1A)-Cu(2)-O(1B)	89.7(3)
O(3B)-Cu(2)-N(3B)	93.5(3)	O(3B)-Cu(2)-N(3B)	93.5(3)
N(1A)-Cu(2)-N(3B)	161.4(3)	N(1A)-Cu(2)-N(3B)	161.4(3)
O(1B)-Cu(2)-N(3B)	83.1(3)	O(1B)-Cu(2)-N(3B)	83.1(3)
O(3B)-Cu(2)-N(4B)	90.6(3)	O(3B)-Cu(2)-N(4B)	90.6(3)
N(1A)-Cu(2)-N(4B)	100.3(2)	N(1A)-Cu(2)-N(4B)	100.3(2)
O(1B)-Cu(2)-N(4B)	92.0(3)	O(1B)-Cu(2)-N(4B)	92.0(3)
N(3B)-Cu(2)-N(4B)	97.1(2)	N(3B)-Cu(2)-N(4B)	97.1(2)
O(3C)-Cu(3)-N(3C)	93.4(3)	O(3C)-Cu(3)-N(3C)	93.4(3)
O(3C)-Cu(3)-O(1C)	175.5(3)	O(3C)-Cu(3)-O(1C)	175.5(3)
N(3C)-Cu(3)-O(1C)	83.7(3)	N(3C)-Cu(3)-O(1C)	83.7(3)
O(3C)-Cu(3)-N(1B)	89.6(3)	O(3C)-Cu(3)-N(1B)	89.6(3)
N(3C)-Cu(3)-N(1B)	172.8(3)	N(3C)-Cu(3)-N(1B)	172.8(3)
O(1C)-Cu(3)-N(1B)	92.8(3)	O(1C)-Cu(3)-N(1B)	92.8(3)
O(3D)-Cu(4)-O(1D)	172.1(3)	O(3D)-Cu(4)-O(1D)	172.1(3)
O(3D)-Cu(4)-N(1C)	90.9(3)	O(3D)-Cu(4)-N(1C)	90.9(3)
O(1D)-Cu(4)-N(1C)	91.2(3)	O(1D)-Cu(4)-N(1C)	91.2(3)
O(3D)-Cu(4)-N(3D)	92.9(3)	O(3D)-Cu(4)-N(3D)	92.9(3)
O(1D)-Cu(4)-N(3D)	83.3(3)	O(1D)-Cu(4)-N(3D)	83.3(3)
N(1C)-Cu(4)-N(3D)	165.7(3)	N(1C)-Cu(4)-N(3D)	165.7(3)
O(3D)-Cu(4)-N(4D)	92.5(2)	O(3D)-Cu(4)-N(4D)	92.5(2)
O(1D)-Cu(4)-N(4D)	94.9(2)	O(1D)-Cu(4)-N(4D)	94.9(2)
N(1C)-Cu(4)-N(4D)	94.3(2)	N(1C)-Cu(4)-N(4D)	94.3(2)
N(3D)-Cu(4)-N(4D)	99.3(2)	N(3D)-Cu(4)-N(4D)	99.3(2)
C(1A)-O(1A)-Cu(1)	113.0(6)	C(1A)-O(1A)-Cu(1)	113.0(6)
C(1B)-O(1B)-Cu(2)	110.1(5)	C(1B)-O(1B)-Cu(2)	110.1(5)
C(1C)-O(1C)-Cu(3)	114.8(4)	C(1C)-O(1C)-Cu(3)	114.8(4)
C(1D)-O(1D)-Cu(4)	112.6(5)	C(1D)-O(1D)-Cu(4)	112.6(5)
C(9A)-O(3A)-Cu(1)	115.0(6)	C(9A)-O(3A)-Cu(1)	115.0(6)

Atoms	Angles	Atoms	Angles
C(16A)-C(15A)-C(14A)	138(3)	C(23)-N(5)-C(19)	113.1(11)
C(14A)-C(15A)-C(17A)	96.7(13)	C(20)-C(19)-N(5)	129.3(14)
N(4A)-C(14A)-C(15A)	118.2(17)	C(19)-C(20)-C(21)	118.3(16)
C(18D)-N(4D)-C(14D)	115.9(12)	C(20)-C(21)-C(22)	121.9(13)
C(18D)-N(4D)-Cu(4)	114.8(9)	C(23)-C(22)-C(21)	111.4(13)
C(14D)-N(4D)-Cu(4)	129.2(9)	N(5)-C(23)-C(22)	125.8(15)
N(4D)-C(18D)-C(17D)	123.5(16)	C(28)-N(6)-C(24)	119.9(11)
C(18D)-C(17D)-C(16D)	118.4(16)	C(25)-C(24)-N(6)	121.8(13)
C(15D)-C(16D)-C(17D)	117.8(16)	C(24)-C(25)-C(26)	120.6(14)
C(16D)-C(15D)-C(14D)	114.1(14)	C(25)-C(26)-C(27)	117.2(12)
N(4D)-C(14D)-C(15D)	129.0(12)	C(28)-C(27)-C(26)	119.4(13)
C(18B)-N(4B)-C(14B)	115.3(14)	N(6)-C(28)-C(27)	121.0(14)
C(18B)-N(4B)-Cu(2)	121.9(11)	C(15H)-C(14H)-N(4H)	118(2)
C(14B)-N(4B)-Cu(2)	122.7(11)	N(4H)-C(14H)-C(16H)	96.5(16)
C(17B)-C(18B)-N(4B)	127.4(19)	C(14H)-C(15H)-C(16H)	137(4)
N(4B)-C(18B)-C(16B)	98.8(13)	C(14H)-C(15H)-C(17H)	112(3)
C(16B)-C(17B)-C(18B)	117(3)	C(15H)-C(16H)-C(17H)	128(4)
C(17B)-C(16B)-C(15B)	126(3)	C(17H)-C(16H)-C(14H)	108(3)
C(15B)-C(16B)-C(18B)	94.7(15)	C(16H)-C(17H)-C(18H)	109(4)
C(14B)-C(15B)-C(16B)	112(2)	C(18H)-C(17H)-C(15H)	86(2)
N(4B)-C(14B)-C(15B)	118.2(19)	C(17H)-C(18H)-N(4H)	112(2)
C(18C)-N(4C)-C(14C)	117.5(14)	C(14H)-N(4H)-C(18H)	110(2)
N(4C)-C(14C)-C(15C)	107(2)	O(3E)-Cu(5)-N(1F)	91.1(3)
C(14C)-C(15C)-C(16C)	123.9(19)	O(3E)-Cu(5)-O(1E)	173.3(3)
C(17C)-C(16C)-C(15C)	113.0(18)	N(1F)-Cu(5)-O(1E)	93.9(3)
C(16C)-C(17C)-C(18C)	115(2)	O(3E)-Cu(5)-N(3E)	93.3(3)
N(4C)-C(18C)-C(17C)	133.0(19)	N(1F)-Cu(5)-N(3E)	159.8(3)
O(3F)-Cu(6)-N(7)	102.3(3)	O(1E)-Cu(5)-N(3E)	80.5(3)
O(1F)-Cu(6)-N(7)	88.1(3)	O(3E)-Cu(5)-N(4E)	95.4(3)
N(1G)-Cu(6)-N(7)	99.3(2)	N(1F)-Cu(5)-N(4E)	100.2(3)
N(3F)-Cu(6)-N(7)	92.3(2)	O(1E)-Cu(5)-N(4E)	88.1(3)
O(3G)-Cu(7)-N(1H)	91.0(3)	N(3E)-Cu(5)-N(4E)	99.0(3)
O(3G)-Cu(7)-O(1G)	172.7(3)	O(3F)-Cu(6)-O(1F)	169.4(4)
O(3G)-Cu(7)-N(3G)	92.3(3)	O(3F)-Cu(6)-N(1G)	89.3(3)
N(1H)-Cu(7)-N(3G)	161.4(3)	O(1F)-Cu(6)-N(1G)	91.4(3)
O(1G)-Cu(7)-N(3G)	82.3(3)	O(3F)-Cu(6)-N(3F)	93.2(3)
N(1G)-Cu(6)-N(7)	99.3(2)	O(1F)-Cu(6)-N(3F)	83.9(3)
N(1H)-Cu(7)-O(1G)	92.7(3)	N(1G)-Cu(6)-N(3F)	167.4(3)
O(3G)-Cu(7)-N(4G)	94.2(3)	N(3G)-Cu(7)-N(4G)	100.4(3)
N(1H)-Cu(7)-N(4G)	97.6(3)	O(3H)-Cu(8)-O(1H)	168.7(4)
O(1G)-Cu(7)-N(4G)	91.5(3)	O(3H)-Cu(8)-N(3H)	92.8(3)
O(3H)-Cu(8)-N(1E)	89.1(3)	O(1H)-Cu(8)-N(3H)	83.5(3)
O(1H)-Cu(8)-N(1E)	92.4(3)	N(1E)-Cu(8)-N(3H)	168.6(3)
O(1H)-Cu(8)-N(8)	88.6(3)	O(3H)-Cu(8)-N(8)	102.0(3)

Atoms	Angles	Atoms	Angles
N(1E)-Cu(8)-N(8)	101.6(2)	C(5G)-N(1G)-Cu(6)	126.9(5)
N(3H)-Cu(8)-N(8)	89.0(2)	C(5H)-N(1H)-C(6H)	106.1(6)
C(1E)-O(1E)-Cu(5)	113.9(5)	C(5H)-N(1H)-Cu(7)	126.4(5)
C(1F)-O(1F)-Cu(6)	114.5(5)	C(6H)-N(1H)-Cu(7)	127.1(5)
C(1H)-O(1H)-Cu(8)	118.7(4)	C(6E)-N(2E)-C(4E)	105.7(6)
C(1G)-O(1G)-Cu(7)	114.6(4)	C(6F)-N(2F)-C(4F)	103.7(7)
C(13E)-O(3E)-Cu(5)	121.8(5)	C(6G)-N(2G)-C(4G)	109.9(6)
C(9F)-O(3F)-Cu(6)	128.0(6)	C(6H)-N(2H)-C(4H)	103.1(6)
C(9G)-O(3G)-Cu(7)	123.5(5)	C(7E)-N(3E)-C(2E)	115.6(6)
C(9H)-O(3H)-Cu(8)	124.6(5)	C(7E)-N(3E)-Cu(5)	112.4(4)
C(5E)-N(1E)-C(6E)	101.9(6)	C(2E)-N(3E)-Cu(5)	106.4(4)
C(5E)-N(1E)-Cu(8)	128.5(5)	C(2F)-N(3F)-C(7F)	106.3(6)
C(6E)-N(1E)-Cu(8)	128.9(5)	C(2F)-N(3F)-Cu(6)	111.2(4)
C(6F)-N(1F)-C(5F)	105.6(7)	C(7F)-N(3F)-Cu(6)	114.2(4)
C(6F)-N(1F)-Cu(5)	125.9(6)	C(7G)-N(3G)-C(2G)	116.0(5)
C(5F)-N(1F)-Cu(5)	128.5(5)	C(7G)-N(3G)-Cu(7)	112.8(4)
C(6G)-N(1G)-C(5G)	104.5(6)	C(2G)-N(3G)-Cu(7)	105.0(4)
C(6G)-N(1G)-Cu(6)	127.9(5)	C(2H)-N(3H)-C(7H)	113.6(6)
O(3E)-C(13E)-C(8E)	125.0(10)	C(2H)-N(3H)-Cu(8)	109.4(4)
O(3E)-C(13E)-C(12E)	118.3(11)	C(7H)-N(3H)-Cu(8)	111.9(4)
C(8E)-C(13E)-C(12E)	116.7(11)	O(2E)-C(1E)-O(1E)	124.7(9)
O(2F)-C(1F)-O(1F)	123.8(10)	O(2E)-C(1E)-C(2E)	118.5(8)
O(2F)-C(1F)-C(2F)	116.6(8)	O(1E)-C(1E)-C(2E)	116.7(8)
O(1F)-C(1F)-C(2F)	119.6(9)	N(3E)-C(2E)-C(3E)	112.1(7)
N(3F)-C(2F)-C(3F)	111.3(8)	N(3E)-C(2E)-C(1E)	108.1(7)
N(3F)-C(2F)-C(1F)	107.7(7)	C(3E)-C(2E)-C(1E)	107.9(8)
C(3F)-C(2F)-C(1F)	109.5(8)	C(4E)-C(3E)-C(2E)	118.3(8)
C(2F)-C(3F)-C(4F)	114.7(7)	C(5E)-C(4E)-N(2E)	107.3(8)
C(9E)-C(8E)-C(13E)	123.8(12)	C(5E)-C(4E)-C(3E)	134.3(10)
C(9E)-C(8E)-C(7E)	120.1(12)	N(2E)-C(4E)-C(3E)	118.3(8)
C(13E)-C(8E)-C(7E)	116.1(10)	C(4E)-C(5E)-N(1E)	112.8(9)
C(8E)-C(9E)-C(10E)	118.5(12)	N(2E)-C(6E)-N(1E)	112.2(7)
C(11E)-C(10E)-C(9E)	116.8(13)	N(3E)-C(7E)-C(8E)	112.9(8)
C(12E)-C(11E)-C(10E)	123.8(15)	N(1F)-C(6F)-N(2F)	113.4(8)
C(11E)-C(12E)-C(13E)	119.9(14)	N(3F)-C(7F)-C(8F)	109.5(9)
C(5F)-C(4F)-N(2F)	106.3(10)	C(13F)-C(8F)-C(9F)	112.5(12)
C(5F)-C(4F)-C(3F)	132.3(10)	C(13F)-C(8F)-C(7F)	129.1(10)
N(2F)-C(4F)-C(3F)	121.3(9)	C(9F)-C(8F)-C(7F)	118.3(10)
C(4F)-C(5F)-N(1F)	110.8(10)	O(3F)-C(9F)-C(8F)	119.9(12)
C(10F)-C(11F)-C(12F)	127.5(16)	O(3F)-C(9F)-C(10F)	124.6(11)
C(11F)-C(12F)-C(13F)	121.5(13)	C(8F)-C(9F)-C(10F)	115.1(11)
C(12F)-C(13F)-C(8F)	123.3(11)	C(11F)-C(10F)-C(9F)	119.8(13)
O(2G)-C(1G)-O(1G)	125.2(8)	O(2G)-C(1G)-C(2G)	118.8(8)
N(3G)-C(2G)-C(1G)	109.7(7)	O(1G)-C(1G)-C(2G)	115.8(8)

Atoms	Angles	Atoms	Angles
N(3G)-C(2G)-C(3G)	111.1(7)	C(13G)-C(8G)-C(7G)	121.3(12)
C(1G)-C(2G)-C(3G)	111.0(8)	C(9G)-C(8G)-C(7G)	122.2(9)
C(4G)-C(3G)-C(2G)	114.9(7)	O(3G)-C(9G)-C(10G)	117.7(11)
C(5G)-C(4G)-N(2G)	103.4(7)	O(3G)-C(9G)-C(8G)	119.1(10)
C(5G)-C(4G)-C(3G)	132.1(9)	C(10G)-C(9G)-C(8G)	123.1(10)
N(2G)-C(4G)-C(3G)	124.5(8)	C(11G)-C(10G)-C(9G)	119.9(14)
N(1G)-C(5G)-C(4G)	112.1(8)	C(10G)-C(11G)-C(12G)	120.9(14)
N(2G)-C(6G)-N(1G)	110.1(7)	C(13G)-C(12G)-C(11G)	116.9(14)
N(3G)-C(7G)-C(8G)	110.3(7)	C(8G)-C(13G)-C(12G)	122.2(15)
C(13G)-C(8G)-C(9G)	116.4(12)	O(2H)-C(1H)-O(1H)	132.0(8)
C(38)-N(8)-C(34)	116.9(11)	O(2H)-C(1H)-C(2H)	115.1(7)
C(38)-N(8)-Cu(8)	119.5(9)	O(1H)-C(1H)-C(2H)	112.9(8)
C(34)-N(8)-Cu(8)	122.8(9)	N(3H)-C(2H)-C(3H)	110.2(8)
N(8)-C(34)-C(35)	115.4(13)	N(3H)-C(2H)-C(1H)	112.3(7)
C(36)-C(35)-C(34)	122.3(16)	C(3H)-C(2H)-C(1H)	112.5(8)
C(37)-C(36)-C(35)	113(2)	C(4H)-C(3H)-C(2H)	112.2(7)
C(36)-C(37)-C(38)	28.7(19)	C(5H)-C(4H)-N(2H)	110.2(8)
C(37)-C(38)-N(8)	123.7(14)	C(5H)-C(4H)-C(3H)	128.5(10)
C(14G)-N(4G)-C(18G)	113.5(11)	N(2H)-C(4H)-C(3H)	121.0(9)
C(14G)-N(4G)-Cu(7)	127.5(9)	N(1H)-C(5H)-C(4H)	107.1(8)
C(18G)-N(4G)-Cu(7)	118.8(8)	N(2H)-C(6H)-N(1H)	113.5(7)
C(17G)-C(18G)-N(4G)	129.4(14)	N(3H)-C(7H)-C(8H)	110.9(8)
C(16G)-C(17G)-C(18G)	113.0(16)	C(9H)-C(8H)-C(13H)	126.4(12)
C(17G)-C(16G)-C(15G)	122.5(15)	C(9H)-C(8H)-C(7H)	117.4(9)
C(14G)-C(15G)-C(16G)	113.4(16)	C(13H)-C(8H)-C(7H)	115.9(10)
N(4G)-C(14G)-C(15G)	127.2(15)	O(3H)-C(9H)-C(8H)	129.3(11)
C(33)-N(7)-C(29)	126.6(12)	O(3H)-C(9H)-C(10H)	119.6(10)
C(33)-N(7)-Cu(6)	114.3(8)	C(8H)-C(9H)-C(10H)	111.1(11)
C(29)-N(7)-Cu(6)	118.6(10)	C(11H)-C(10H)-C(9H)	128.2(13)
N(7)-C(29)-C(30)	109.7(16)	C(12H)-C(11H)-C(10H)	114.7(15)
C(31)-C(30)-C(29)	134.5(18)	C(11H)-C(12H)-C(13H)	122.1(13)
O(100)-C(2)-C(5)	107.8	C(8H)-C(13H)-C(12H)	117.2(11)
C(5)-C(2)-C(3)	67.8	C(14E)-N(4E)-C(18E)	121.0(14)
C(3)-O(100)-C(2)	90.3	C(14E)-N(4E)-Cu(5)	113.8(11)
C(29)-C(30)-C(32)	100.1(12)	C(18E)-N(4E)-Cu(5)	125.2(10)
C(32)-C(31)-C(30)	109.7(17)	C(17E)-C(18E)-N(4E)	123.3(19)
C(31)-C(32)-C(33)	128.2(16)	C(18E)-C(17E)-C(16E)	129(3)
C(33)-C(32)-C(30)	92.6(8)	C(17E)-C(16E)-C(15E)	109(2)
N(7)-C(33)-C(32)	110.9(10)	C(16E)-C(15E)-C(14E)	119.8(16)
O(200)-C(40)-C(39)#1	75.8	N(4E)-C(14E)-C(15E)	112.1(16)
O(400)-C(39)-C(40)#2	101.2	C(2)-C(5)-C(1)	99.3
C(1)-C(3)-O(100)	164.1	C(2)-C(5)-C(3)	62.8
C(1)-C(3)-C(2)	119.9	C(3)-C(1)-C(5)	72.5
C(1)-C(3)-C(5)	70.8	O(100)-C(3)-C(5)	95.3

Table III: Selected bond Distances (Å) of complex **8[Cu(*S*-SalHis)(Imodazole)]·15H_2O (2)**

Atoms	Distances	Atoms	Distances
Cu1 -O3A	1.930(9)	N4B -C16B	1.408(18)
Cu1 -N4A	1.989(13)	N5B -C15B	1.30(3)
Cu1 -N2A	2.042(12)	N5B -C14B	1.42(2)
Cu1 -N3A	2.051(11)	C1B -C2B	1.50(3)
Cu1 -O1A	2.262(13)	C2B -C3B	1.54(2)
O1A -C1A	1.250(18)	C3B -C4B	1.45(2)
O2A -C1A	1.259(19)	C4B -C5B	1.34(2)
O3A -C9A	1.370(17)	C7B -C8B	1.49(2)
N1A -C6A	1.327(18)	C8B -C13B	1.40(2)
N1A -C5A	1.36(2)	C8B -C9B	1.45(2)
N2A -C4A	1.353(18)	C9B -C10B	1.45(3)
N2A -C6A	1.357(18)	C10B -C11B	1.36(3)
N3A -C7A	1.482(18)	C11B -C12B	1.38(3)
N3A -C2A	1.521(19)	C12B -C13B	1.31(3)
N4A -C16A	1.287(19)	C15B -C16B	1.32(2)
N4A -C14A	1.41(2)	Cu3 -O3C	1.936(11)
N5A -C16A	1.29(2)	Cu3 -N4C	1.985(14)
N5A -C15A	1.32(2)	Cu3 -N2C	1.999(13)
C1A -C2A	1.51(2)	Cu3 -N3C	2.049(11)
C2A -C3A	1.52(2)	Cu3 -O1C	2.305(12)
C3A -C4A	1.51(2)	O1C -C1C	1.283(18)
C4A -C5A	1.42(2)	O2C -C1C	1.224(18)
C7A -C8A	1.54(2)	O3C -C9C	1.38(2)
C8A -C13A	1.34(2)	N1C -C6C	1.314(19)
C8A -C9A	1.38(2)	N1C -C5C	1.40(2)
C9A -C10A	1.41(2)	N2C -C6C	1.321(19)
C10A -C11A	1.34(2)	N2C -C4C	1.45(2)
C11A -C12A	1.36(3)	N3C -C7C	1.490(18)
C12A -C13A	1.41(3)	N3C -C2C	1.525(19)
C14A -C15A	1.38(2)	N4C -C14C	1.21(2)
Cu2 -N4B	1.891(13)	N4C -C16C	1.37(2)
Cu2 -O3B	1.978(11)	C15C -C16C	1.27(3)
Cu2 -N2B	2.008(12)	C15C -N5C	1.39(3)
Cu2 -N3B	2.014(11)	C1C -C2C	1.53(2)
Cu2 -O1B	2.219(10)	C2C -C3C	1.60(2)
O1B -C1B	1.28(2)	C3C -C4C	1.44(2)
O2B -C1B	1.30(2)	C4C -C5C	1.31(2)
O3B -C9B	1.29(2)	C7C -C8C	1.46(2)
N1B -C5B	1.38(2)	C8C -C9C	1.36(2)
N1B -C6B	1.400(19)	C8C -C13C	1.43(2)
N2B -C6B	1.343(19)	C9C -C10C	1.45(2)
N2B -C4B	1.405(17)	C10C -C11C	1.35(2)

Atoms	**Distances**	**Atoms**	**Distances**
N2D -C6D	1.321(18)	C14C -N5C	1.34(2)
N2D -C4D	1.404(19)	Cu4 -O3D	1.938(11)
N3D -C2D	1.448(19)	Cu4 -N4D	1.986(12)
N3D -C7D	1.482(19)	Cu4 -N3D	1.998(12)
N4D -C14D	1.314(18)	Cu4 -N2D	2.014(11)
N4D -C16D	1.338(19)	Cu4 -O1D	2.344(13)
N5D -C14D	1.289(18)	N1D -C6D	1.278(18)
N5D -C15D	1.339(19)	N1D -C5D	1.33(2)
O1D -C1D	1.30(2)	C7E -C8E	1.54(3)
O2D -C1D	1.200(19)	C8E -C9E	1.42(3)
O3D -C9D	1.32(2)	C8E -C13E	1.46(2)
C1D -C2D	1.59(2)	C9E -C10E	1.44(3)
C2D -C3D	1.60(2)	C10E -C11E	1.37(3)
C3D -C4D	1.52(2)	C11E -C12E	1.41(3)
C4D -C5D	1.29(2)	C12E -C13E	1.37(3)
C7D -C8D	1.55(3)	C15E -C16E	1.38(2)
C8D -C9D	1.36(3)	Cu6 -O3F	1.891(12)
C8D -C13D	1.41(2)	Cu6 -N4F	2.000(17)
C9D -C10D	1.41(2)	Cu6 -N3F	2.002(12)
C10D -C11D	1.35(2)	Cu6 -N2F	2.008(15)
C11D -C12D	1.39(3)	Cu6 -O1F	2.299(11)
C12D -C13D	1.33(3)	O1F -C1F	1.253(19)
C15D -C16D	1.35(2)	O2F -C1F	1.26(2)
Cu5 -O3E	1.888(12)	O3F -C9F	1.38(2)
Cu5 -N3E	1.960(14)	N1F -C5F	1.28(3)
Cu5 -N4E	1.989(14)	N1F -C6F	1.41(3)
Cu5 -N2E	2.039(12)	N2F -C6F	1.35(2)
Cu5 -O1E	2.332(12)	N2F -C4F	1.37(2)
O1E -C1E	1.17(3)	N3F -C7F	1.47(2)
O2E -C1E	1.37(3)	N3F -C2F	1.478(18)
O3E -C9E	1.29(3)	N4F -C16F	1.33(3)
N1E -C6E	1.357(19)	N4F -C14F	1.42(3)
N1E -C5E	1.37(2)	C15F -N5F	1.27(4)
N2E -C6E	1.276(19)	C15F -C16F	1.32(3)
N2E -C4E	1.392(19)	C1F -C2F	1.51(2)
N3E -C7E	1.42(2)	C2F -C3F	1.52(2)
N3E -C2E	1.56(2)	C3F -C4F	1.45(3)
N4E -C14E	1.30(2)	C4F -C5F	1.37(3)
N4E -C16E	1.39(2)	C7F -C8F	1.47(2)
N5E -C14E	1.34(2)	C8F -C13F	1.37(2)
N5E -C15E	1.38(2)	C8F -C9F	1.40(2)
C1E -C2E	1.51(2)	C9F -C10F	1.43(2)
C2E -C3E	1.45(2)	C10F -C11F	1.38(3)
C3E -C4E	1.50(2)	C11F -C12F	1.35(3)
C4E -C5E	1.33(2)	C12F -C13F	1.39(3)

Atoms	**Distances**	**Atoms**	**Distances**
N4G -C16G	1.356(19)	C14F -N5F	1.493(6)
N5G -C15G	1.26(2)	N5F -C16F	1.96(4)
N5G -C14G	1.35(2)	Cu7 -O3G	1.934(10)
C1G -C2G	1.53(2)	Cu7 -N4G	1.976(15)
C2G -C3G	1.56(3)	Cu7 -N3G	2.002(13)
C3G -C4G	1.43(3)	Cu7 -N2G	2.026(15)
C4G -C5G	1.45(3)	Cu7 -O1G	2.277(12)
C7G -C8G	1.48(2)	O1G -C1G	1.27(2)
C8G -C9G	1.39(2)	O2G -C1G	1.225(18)
C8G -C13G	1.40(2)	O3G -C9G	1.39(2)
C9G -C10G	1.40(3)	N1G -C6G	1.32(2)
C10G -C11G	1.36(3)	N1G -C5G	1.34(3)
C11G -C12G	1.32(3)	N2G -C6G	1.32(3)
C12G -C13G	1.35(3)	N2G -C4G	1.43(2)
C15G -C16G	1.37(2)	N3G -C7G	1.43(2)
Cu8 -O3H	1.922(12)	N3G -C2G	1.47(2)
Cu8 -N4H	1.960(13)	N4G -C14G	1.30(2)
Cu8 -N2H	2.004(12)	O3H -C9H	1.353(18)
Cu8 -N3H	2.036(11)	C1H -C2H	1.62(3)
Cu8 -O1H	2.349(13)	C2H -C3H	1.52(2)
N1H -C6H	1.29(2)	C3H -C4H	1.49(2)
N1H -C5H	1.35(2)	C4H -C5H	1.32(2)
N2H -C6H	1.31(2)	C7H -C8H	1.50(2)
N2H -C4H	1.42(2)	C8H -C13H	1.38(2)
N3H -C7H	1.459(19)	C8H -C9H	1.40(2)
N3H -C2H	1.49(2)	C9H -C10H	1.43(3)
N4H -C16H	1.29(2)	C10H -C11H	1.36(3)
N4H -C14H	1.31(2)	C12H -C13H	1.39(3)
N5H -C14H	1.26(2)	C12H -C11H	1.40(3)
N5H -C15H	1.37(2)	C15H -C16H	1.44(3)
O1H -C1H	1.22(2)	O2H -C1H	1.26(2)

Table IV: Selected bond Angles (º) of the complex **8[Cu(*S*-SalHis)(Imidazole)]·15H_2O (2)**

Atoms	Angles	Atoms	Angles
O3A -Cu1 -N4A	83.8(5)	C4H -C3H -C2H	119.2(14)
O3A -Cu1 -N2A	164.7(5)	C5H -C4H -N2H	107.8(15)
N4A -Cu1 -N2A	93.7(5)	C5H -C4H -C3H	130.2(17)
O3A -Cu1 -N3A	92.0(4)	N2H -C4H -C3H	121.9(15)
N4A -Cu1 -N3A	175.4(5)	C4H -C5H -N1H	107.4(17)
N2A -Cu1 -N3A	90.8(5)	N1H -C6H -N2H	111.8(15)
O3A -Cu1 -O1A	108.1(5)	N3H -C7H -C8H	113.9(13)
N4A -Cu1 -O1A	102.0(5)	C13H -C8H -C9H	116.1(17)
N2A -Cu1 -O1A	87.2(5)	C13H -C8H -C7H	124.0(17)
N3A -Cu1 -O1A	77.6(4)	C9H -C8H -C7H	119.9(16)
C1A -O1A -Cu1	110.1(11)	O3H -C9H -C8H	121.4(17)
C9A -O3A -Cu1	123.4(9)	O3H -C9H -C10H	118.7(16)
C6A -N1A -C5A	108.3(13)	C8H -C9H -C10H	119.9(15)
C4A -N2A -C6A	105.3(13)	C11H -C10H -C9H	120.9(19)
C4A -N2A -Cu1	124.8(11)	C13H -C12H -C11H	117(2)
C6A -N2A -Cu1	128.1(10)	C10H -C11H -C12H	121(2)
C7A -N3A -C2A	111.5(13)	C8H -C13H -C12H	125(2)
C7A -N3A -Cu1	111.9(9)	N5H -C14H -N4H	113.3(19)
C2A -N3A -Cu1	105.6(9)	N5H -C15H -C16H	98.4(18)
C16A -N4A -C14A	104.3(14)	N4H -C16H -C15H	112.7(18)
C16A -N4A -Cu1	135.8(13)	C3G -C4G -C5G	133(2)
C14A -N4A -Cu1	119.7(10)	N2G -C4G -C5G	101(2)
C16A -N5A -C15A	108.3(14)	N1G -C5G -C4G	114(2)
O1A -C1A -O2A	127.5(17)	N2G -C6G -N1G	120(2)
O1A -C1A -C2A	118.6(16)	N3G -C7G -C8G	117.9(16)
O2A -C1A -C2A	113.9(14)	C9G -C8G -C13G	114.7(19)
C1A -C2A -C3A	113.6(13)	C9G -C8G -C7G	119.8(15)
C1A -C2A -N3A	108.7(13)	C13G -C8G -C7G	124.5(19)
C3A -C2A -N3A	112.0(14)	C8G -C9G -O3G	115.6(17)
C2A -C3A -C4A	113.0(12)	C8G -C9G -C10G	121.0(18)
N2A -C4A -C5A	109.0(15)	O3G -C9G -C10G	123.4(18)
N2A -C4A -C3A	124.9(13)	C11G -C10G -C9G	117(2)
C5A -C4A -C3A	126.1(14)	C12G -C11G -C10G	124(3)
N1A -C5A -C4A	105.3(14)	C11G -C12G -C13G	116(2)
N1A -C6A -N2A	111.9(14)	C12G -C13G -C8G	125(2)
N3A -C7A -C8A	108.9(13)	N4G -C14G -N5G	111.0(18)
C13A -C8A -C9A	119.6(17)	N5G -C15G -C16G	108.1(18)
C13A -C8A -C7A	122.0(15)	N4G -C16G -C15G	108.1(17)
C9A -C8A -C7A	118.3(15)	O3H -Cu8 -N4H	89.6(5)
O3A -C9A -C8A	119.7(15)	O3H -Cu8 -N2H	158.6(6)
O3H -Cu8 -N3H	95.7(5)	N4H -Cu8 -N2H	91.0(5)

Atoms	Angles	Atoms	Angles
C11A -C12A -C13A	115.3(18)	O3H -Cu8 -O1H	106.4(6)
C8A -C13A -C12A	122.5(18)	N4H -Cu8 -O1H	90.7(6)
C15A -C14A -N4A	106.3(16)	N2H -Cu8 -O1H	95.0(5)
N5A -C15A -C14A	106.6(16)	N3H -Cu8 -O1H	78.3(5)
N4A -C16A -N5A	114.2(16)	C6H -N1H -C5H	108.6(16)
N4B -Cu2 -O3B	86.9(5)	C6H -N2H -C4H	104.3(13)
N4B -Cu2 -N2B	92.1(5)	C6H -N2H -Cu8	128.8(11)
O3B -Cu2 -N2B	168.9(5)	C4H -N2H -Cu8	126.6(11)
N4B -Cu2 -N3B	175.3(6)	C7H -N3H -C2H	109.3(13)
O3B -Cu2 -N3B	93.5(5)	C7H -N3H -Cu8	110.7(9)
N2B -Cu2 -N3B	86.5(5)	C2H -N3H -Cu8	107.9(9)
N4B -Cu2 -O1B	105.5(5)	C16H -N4H -C14H	104.4(15)
O3B -Cu2 -O1B	95.5(5)	C16H -N4H -Cu8	127.9(13)
N2B -Cu2 -O1B	95.4(5)	C14H -N4H -Cu8	127.3(12)
N3B -Cu2 -O1B	79.2(5)	C14H -N5H -C15H	111.1(18)
C1B -O1B -Cu2	106.7(12)	C1H -O1H -Cu8	103.9(12)
C9B -O3B -Cu2	116.7(11)	C9H -O3H -Cu8	122.7(10)
C5B -N1B -C6B	105.1(14)	O1H -C1H -O2H	125.0(18)
C6B -N2B -C4B	106.1(13)	O1H -C1H -C2H	120.1(17)
C6B -N2B -Cu2	128.1(10)	O2H -C1H -C2H	114.9(16)
C4B -N2B -Cu2	125.1(11)	N3H -C2H -C3H	108.9(16)
C2B -N3B -C7B	112.6(12)	N3H -C2H -C1H	110.9(13)
C2B -N3B -Cu2	106.1(10)	C3H -C2H -C1H	103.5(14)
C7B -N3B -Cu2	112.4(10)	C13F -C8F -C7F	122.7(16)
C14B -N4B -C16B	100.5(13)	C9F -C8F -C7F	118.3(14)
C14B -N4B -Cu2	129.2(11)	O3F -C9F -C8F	124.3(13)
C16B -N4B -Cu2	129.9(11)	O3F -C9F -C10F	116.0(16)
C15B -N5B -C14B	107.9(15)	C8F -C9F -C10F	119.6(16)
O1B -C1B -O2B	124.5(18)	C11F -C10F -C9F	117.8(18)
O1B -C1B -C2B	117.2(18)	C12F -C11F -C10F	122.7(18)
O2B -C1B -C2B	118.3(17)	C11F -C12F -C13F	118.9(18)
N3B -C2B -C1B	114.9(15)	C8F -C13F -C12F	122(2)
N3B -C2B -C3B	111.6(14)	N4F -C14F -N5F	90.5(15)
C1B -C2B -C3B	107.5(14)	C15F -N5F -C14F	123.5(17)
C4B -C3B -C2B	114.7(14)	C15F -N5F -C16F	41.8(13)
C5B -C4B -N2B	108.7(15)	C14F -N5F -C16F	81.7(14)
C5B -C4B -C3B	127.4(14)	C15F -C16F -N4F	115(3)
N2B -C4B -C3B	123.8(15)	C15F -C16F -N5F	39.6(19)
C4B -C5B -N1B	109.7(14)	N4F -C16F -N5F	75(2)
N2B -C6B -N1B	110.5(14)	O3G -Cu7 -N4G	84.7(5)
C8B -C7B -N3B	110.9(13)	O3G -Cu7 -N3G	92.3(5)
C13B -C8B -C9B	119.7(17)	N4G -Cu7 -N3G	177.0(6)
C13B -C8B -C7B	123.4(16)	O3G -Cu7 -N2G	160.4(6)
C9B -C8B -C7B	116.9(15)	N4G -Cu7 -N2G	93.2(6)
O3B -C9B -C10B	125.0(19)	N3G -Cu7 -N2G	89.7(6)

Atoms	Angles	Atoms	Angles
C11B -C10B -C9B	119.0(18)	N3G -Cu7 -O1G	77.0(5)
C10B -C11B -C12B	125.3(19)	N2G -Cu7 -O1G	88.5(5)
C13B -C12B -C11B	116.9(19)	C1G -O1G -Cu7	110.8(10)
C12B -C13B -C8B	123.9(19)	C9G -O3G -Cu7	124.8(10)
N4B -C14B -N5B	111.2(16)	C6G -N1G -C5G	100(2)
N5B -C15B -C16B	105(2)	C6G -N2G -C4G	103.8(19)
C15B -C16B -N4B	115.0(19)	C6G -N2G -Cu7	129.8(15)
O3C -Cu3 -N4C	88.5(5)	C4G -N2G -Cu7	122.2(15)
O3C -Cu3 -N2C	149.2(5)	C7G -N3G -C2G	110.3(15)
N4C -Cu3 -N2C	95.3(6)	C7G -N3G -Cu7	110.6(10)
O3C -Cu3 -N3C	92.9(4)	C2G -N3G -Cu7	109.2(10)
N4C -Cu3 -N3C	162.6(6)	C14G -N4G -C16G	104.8(16)
N2C -Cu3 -N3C	92.4(5)	C14G -N4G -Cu7	131.9(13)
O3C -Cu3 -O1C	120.8(5)	C16G -N4G -Cu7	123.2(12)
N4C -Cu3 -O1C	87.1(6)	C15G -N5G -C14G	107.9(17)
N2C -Cu3 -O1C	90.0(5)	O2G -C1G -O1G	125.2(16)
N3C -Cu3 -O1C	77.2(4)	O2G -C1G -C2G	118.7(17)
C1C -O1C -Cu3	108.8(10)	O1G -C1G -C2G	115.9(14)
C9C -O3C -Cu3	123.6(10)	N3G -C2G -C1G	109.7(14)
C6C -N1C -C5C	109.4(15)	N3G -C2G -C3G	111.8(15)
C6C -N2C -C4C	105.6(13)	C1G -C2G -C3G	111.5(17)
C6C -N2C -Cu3	127.5(11)	C4G -C3G -C2G	112.8(16)
C4C -N2C -Cu3	125.6(10)	C3G -C4G -N2G	126(2)
C7C -N3C -C2C	108.4(12)	O3E -C9E -C8E	122.7(19)
C7C -N3C -Cu3	106.9(9)	O3E -C9E -C10E	126(2)
C2C -N3C -Cu3	107.1(8)	C8E -C9E -C10E	111(2)
C14C -N4C -C16C	104.2(17)	C11E -C10E -C9E	129(3)
C14C -N4C -Cu3	125.8(15)	C10E -C11E -C12E	117(2)
C16C -N4C -Cu3	130.0(14)	C13E -C12E -C11E	119(2)
C16C -C15C -N5C	109(2)	C12E -C13E -C8E	121(2)
O2C -C1C -O1C	125.0(16)	N4E -C14E -N5E	111.5(17)
O2C -C1C -C2C	116.1(15)	N5E -C15E -C16E	106.7(15)
O1C -C1C -C2C	118.7(15)	C15E -C16E -N4E	106.7(15)
N3C -C2C -C1C	109.4(13)	O3F -Cu6 -N4F	86.4(6)
N3C -C2C -C3C	108.0(12)	O3F -Cu6 -N3F	94.7(5)
C1C -C2C -C3C	111.1(12)	N4F -Cu6 -N3F	170.3(6)
C4C -C3C -C2C	118.7(12)	O3F -Cu6 -N2F	152.7(6)
C5C -C4C -C3C	130.0(18)	N4F -Cu6 -N2F	92.1(7)
C5C -C4C -N2C	108.4(16)	N3F -Cu6 -N2F	91.4(6)
C3C -C4C -N2C	121.6(14)	O3F -Cu6 -O1F	119.5(5)
C4C -C5C -N1C	106.1(18)	N4F -Cu6 -O1F	94.9(6)
N1C -C6C -N2C	110.1(15)	N3F -Cu6 -O1F	76.1(4)
C8C -C7C -N3C	110.2(13)	N2F -Cu6 -O1F	87.7(5)
C9C -C8C -C13C	117.1(16)	C1F -O1F -Cu6	108.1(10)
C9C -C8C -C7C	122.9(15)	C9F -O3F -Cu6	123.0(10)

Atoms	Angles	Atoms	Angles
C8C -C9C -C10C	120.5(18)	C6F -N2F -Cu6	122.8(16)
O3C -C9C -C10C	117.4(19)	C4F -N2F -Cu6	126.5(14)
C11C -C10C -C9C	121(2)	C7F -N3F -C2F	110.8(12)
C10C -C11C -C12C	119.2(18)	C7F -N3F -Cu6	109.4(9)
C13C -C12C -C11C	119.9(17)	C2F -N3F -Cu6	107.8(9)
C12C -C13C -C8C	121.8(17)	C16F -N4F -C14F	113(2)
N4C -C14C -N5C	117(2)	C16F -N4F -Cu6	123.9(18)
C14C -N5C -C15C	101(2)	C14F -N4F -Cu6	123.4(18)
C15C -C16C -N4C	109(2)	N5F -C15F -C16F	99(3)
O3D -Cu4 -N4D	90.5(5)	O1F -C1F -O2F	124.4(17)
O3D -Cu4 -N3D	93.7(5)	O1F -C1F -C2F	118.4(15)
N4D -Cu4 -N3D	165.1(5)	O2F -C1F -C2F	117.0(15)
O3D -Cu4 -N2D	143.2(5)	N3F -C2F -C1F	109.4(12)
N4D -Cu4 -N2D	96.3(5)	N3F -C2F -C3F	112.6(14)
N3D -Cu4 -N2D	89.0(5)	C1F -C2F -C3F	110.0(13)
O3D -Cu4 -O1D	118.7(5)	C4F -C3F -C2F	117.4(17)
N4D -Cu4 -O1D	88.7(5)	N2F -C4F -C5F	108(2)
N3D -Cu4 -O1D	76.8(5)	N2F -C4F -C3F	123.3(18)
N2D -Cu4 -O1D	97.6(5)	C5F -C4F -C3F	129(2)
C6D -N1D -C5D	109.5(14)	N1F -C5F -C4F	105(2)
C6D -N2D -C4D	103.8(13)	N2F -C6F -N1F	100.9(19)
C6D -N2D -Cu4	127.5(10)	N3F -C7F -C8F	113.5(13)
C4D -N2D -Cu4	128.6(11)	C13F -C8F -C9F	119.0(15)
C2D -N3D -C7D	112.7(13)	C8D -C9D -C10D	114.5(18)
C2D -N3D -Cu4	106.7(10)	C11D -C10D -C9D	123.2(19)
C7D -N3D -Cu4	110.8(10)	C10D -C11D -C12D	121(2)
C14D -N4D -C16D	104.1(12)	C13D -C12D -C11D	118(2)
C14D -N4D -Cu4	127.4(11)	C12D -C13D -C8D	122(2)
C16D -N4D -Cu4	128.2(10)	N5D -C14D -N4D	112.5(13)
C14D -N5D -C15D	108.0(12)	N5D -C15D -C16D	105.1(14)
C1D -O1D -Cu4	103.7(10)	N4D -C16D -C15D	110.2(14)
C9D -O3D -Cu4	126.9(11)	O3E -Cu5 -N3E	93.3(6)
O2D -C1D -O1D	130.1(16)	O3E -Cu5 -N4E	88.8(5)
O2D -C1D -C2D	115.2(16)	N3E -Cu5 -N4E	164.9(5)
O1D -C1D -C2D	114.4(14)	O3E -Cu5 -N2E	144.8(6)
N3D -C2D -C1D	113.7(1)	N3E -Cu5 -N2E	90.7(5)
N3D -C2D -C3D	110.1(13)	N4E -Cu5 -N2E	96.1(5)
C1D -C2D -C3D	110.7(13)	O3E -Cu5 -O1E	117.8(6)
C4D -C3D -C2D	114.6(14)	N3E -Cu5 -O1E	77.2(5)
C5D -C4D -N2D	108.6(15)	N4E -Cu5 -O1E	88.6(5)
C5D -C4D -C3D	130.4(16)	N2E -Cu5 -O1E	97.2(5)
N2D -C4D -C3D	121.0(15)	C1E -O1E -Cu5	99.7(12)
C4D -C5D -N1D	107.3(14)	C9E -O3E -Cu5	127.1(13)
N1D -C6D -N2D	110.7(15)	C6E -N1E -C5E	102.7(13)
N3D -C7D -C8D	112.8(13)	C6E -N2E -C4E	109.0(13)

Atoms	**Angles**	**Atoms**	**Angles**
C13D -C8D -C7D	118(2)	C7E -N3E -C2E	111.6(14)
O3D -C9D -C8D	124.8(18)	C7E -N3E -Cu5	116.5(13)
O3D -C9D -C10D	120.6(17)	C2E -N3E -Cu5	104.5(10)
C3E -C2E -C1E	115.1(15)	C14E -N4E -C16E	107.8(15)
C3E -C2E -N3E	112.1(15)	C14E -N4E -Cu5	125.0(13)
C1E -C2E -N3E	105.4(15)	C16E -N4E -Cu5	126.7(11)
C2E -C3E -C4E	118.2(15)	C14E -N5E -C15E	107.2(14)
C5E -C4E -N2E	103.7(15)	O1E -C1E -O2E	124.9(16)
C5E -C4E -C3E	135.4(17)	O1E -C1E -C2E	126.9(19)
N2E -C4E -C3E	120.9(14)	O2E -C1E -C2E	108(2)
C4E -C5E -N1E	112.4(15)	C9E -C8E -C13E	121.5(18)
N2E -C6E -N1E	112.1(15)	C9E -C8E -C7E	121.6(16)
N3E -C7E -C8E	109.1(14)	C13E -C8E -C7E	116.8(18)

Atomic coordinates for the complex **[Cu_8(*S*-SalHis)$_8$($Py)_{10}$]·Py·3MeOH·($C_2H_5)_2$O] (1)**

Atoms	**X/a**	**Y/b**	**Z/c**
Cu1	0.04252(8)	0.31502(7)	0.24635(7)
Cu2	-0.44838(8)	0.26022(7)	0.12856(7)
Cu3	-0.47168(9)	-0.05189(8)	-0.10756(7)
Cu4	-0.00253(8)	-0.00032(8)	0.00001(7)
O1A	0.01786(41)	0.28508(35)	0.33406(35)
O1B	-0.48603(38)	0.16872(35)	0.17201(35)
O1C	-0.46316(39)	-0.14921(35)	-0.06919(30)
O1D	0.03327(37)	-0.04040(36)	0.09104(33)
O2A	-0.01720(47)	0.32994(40)	0.41853(38)
O2B	-0.61224(39)	0.07155(37)	0.15254(36)
O2C	-0.44453(43)	-0.25872(35)	-0.09506(36)
O2D	0.15394(38)	-0.02347(38)	0.19694(36)
O3A	0.05470(45)	0.34180(43)	0.15859(37)
O3B	-0.41422(44)	0.34337(34)	0.08066(39)
O3C	-0.46987(46)	0.04182(38)	-0.14114(37)
O3D	-0.04126(40)	0.05049(41)	-0.08369(38)
N1A	-0.33442(45)	0.29828(41)	0.21538(41)
N1B	-0.53327(48)	-0.02685(44)	-0.04580(41)
N1C	-0.11873(44)	-0.08581(45)	-0.04212(36)
N1D	0.10075(45)	0.23259(41)	0.24553(39)
N2A	-0.23184(50)	0.31299(41)	0.32393(42)
N2B	-0.60314(42)	-0.03562(41)	0.02475(37)
N2C	-0.22764(43)	-0.18756(43)	-0.05368(34)
N2D	0.15622(43)	0.14079(41)	0.26935(41)
N3A	-0.04347(49)	0.37419(38)	0.23990(41)
N3B	-0.54779(43)	0.19420(41)	0.03542(40)
N3C	-0.39793(47)	-0.07599(41)	-0.15691(36)
N3D	0.10057(45)	0.09310(47)	0.05847(41)
C1A	-0.00828(59)	0.33432(57)	0.36121(62)
C2A	-0.02528(60)	0.39929(51)	0.31835(59)
C3A	-0.10036(57)	0.42496(52)	0.32854(61)
C4A	-0.19243(60)	0.36775(54)	0.29196(57)
C5A	-0.25692(58)	0.35869(51)	0.22217(57)
C6A	-0.31578(67)	0.27167(59)	0.27692(52)
C7A	-0.03492(72)	0.43734(54)	0.20025(58)
C8A	-0.05896(72)	0.40862(61)	0.12461(70)
C9A	-0.00950(82)	0.36112(72)	0.11495(60)
C10A	-0.03545(82)	0.33124(71)	0.04342(95)
C11A	-0.10416(103)	0.35307(95)	-0.02137(94)
C12A	-0.14662(91)	0.39757(99)	-0.00427(85)
C13A	-0.12449(81)	0.42983(89)	0.06735(80)
C1B	-0.56854(58)	0.12711(54)	0.13054(62)
C2B	-0.61688(51)	0.14259(49)	0.05716(49)
C3B	-0.67374(58)	0.07133(54)	0.00152(55)
C4B	-0.62005(60)	0.02330(54)	-0.01197(49)
C5B	-0.57574(59)	0.02757(50)	-0.05330(56)
C6B	-0.55446(58)	-0.06752(53)	0.00291(48)
C7B	-0.58413(63)	0.23973(58)	-0.01971(64)
C8B	-0.52134(77)	0.28644(67)	-0.04504(74)
C9B	-0.43660(74)	0.33891(60)	0.00728(63)
C10B	-0.37523(79)	0.38664(64)	-0.01378(66)
C11B	-0.39516(87)	0.38089(71)	-0.08618(88)

Atoms	X/a	Y/b	Z/c
C12B	-0.47293(113)	0.32540(102)	-0.13639(79)
C13B	-0.53608(90)	0.28330(67)	-0.11675(69)
C1C	-0.44398(53)	-0.19499(50)	-0.10595(43)
C2C	-0.42074(59)	-0.16349(57)	-0.16865(48)
C3C	-0.34876(58)	-0.19259(61)	-0.17715(48)
C4C	-0.25596(59)	-0.15860(58)	-0.11601(50)
C5C	-0.18516(55)	-0.09085(57)	-0.10814(48)
C6C	-0.14611(52)	-0.14219(51)	-0.01163(47)
C6D	0.11365(58)	0.18175(51)	0.28672(50)
C7C	-0.41794(71)	-0.04832(64)	-0.22508(54)
C8C	-0.38391(64)	0.03842(69)	-0.21141(60)
C9C	-0.41284(70)	0.07780(63)	-0.16659(58)
C10C	-0.38154(77)	0.15904(73)	-0.15762(59)
C11C	-0.32682(83)	0.19893(83)	-0.19301(78)
C12C	-0.30026(86)	0.16432(87)	-0.23351(102)
C13C	-0.32800(74)	0.08654(92)	-0.23995(68)
C1D	0.11219(57)	-0.00275(55)	0.13564(51)
C2D	0.16726(56)	0.06422(54)	0.11642(51)
C3D	0.22672(60)	0.13036(63)	0.18525(55)
C4D	0.17853(57)	0.16523(53)	0.21608(51)
C5D	0.14106(61)	0.22204(66)	0.19845(59)
C7D	0.13863(59)	0.13658(60)	0.00937(54)
C8D	0.07588(62)	0.17079(64)	-0.03716(56)
C9D	-0.00764(72)	0.12658(64)	-0.08190(67)
C10D	-0.06676(79)	0.16354(82)	-0.13194(66)
C11D	-0.03588(98)	0.23873(79)	-0.13465(74)
C12D	0.04518(95)	0.27951(80)	-0.09279(69)
C13D	0.10539(89)	0.25176(75)	-0.04464(71)
N4A	0.18379(61)	0.40886(54)	0.32793(62)
C18A	0.22775(91)	0.45927(77)	0.29513(98)
C17A	0.32252(101)	0.50807(88)	0.35047(126)
C16A	0.36422(152)	0.50270(168)	0.41809(163)
C15A	0.31606(135)	0.46301(151)	0.43195(108)
C14A	0.22294(120)	0.41417(124)	0.39593(85)
N4D	0.07411(57)	-0.06444(52)	-0.05075(50)
C18D	0.05110(95)	-0.06612(98)	-0.11953(66)
C17D	0.07997(143)	-0.10554(185)	-0.15883(90)
C16D	0.13189(115)	-0.15447(99)	-0.12386(93)
C15D	0.16342(89)	-0.14731(81)	-0.05007(81)
C14D	0.13201(80)	-0.09979(71)	-0.01937(65)
N4B	-0.54009(64)	0.32348(64)	0.16247(67)
C18B	-0.56329(88)	0.38253(72)	0.13128(90)
C17B	-0.60257(103)	0.42503(117)	0.14965(130)
C16B	-0.63405(174)	0.40491(124)	0.18816(212)
C15B	-0.61007(132)	0.35079(128)	0.23895(132)
C14B	-0.56731(102)	0.30511(98)	0.21796(107)
N4C	-0.62440(72)	-0.12781(72)	-0.20665(62)
C14C	-0.66337(114)	-0.19779(111)	-0.20061(105)
C15C	-0.74863(162)	-0.22249(134)	-0.25583(191)
C16C	-0.80525(106)	-0.17267(127)	-0.28171(98)
C17C	-0.76209(109)	-0.10675(120)	-0.27936(91)
C18C	-0.67531(105)	-0.08874(108)	-0.24033(75)
N5	-0.19200(58)	0.22683(55)	0.16592(62)
C19	-0.21478(78)	0.17531(65)	0.20322(72)
C20	-0.28147(99)	0.11937(81)	0.18441(71)

Atoms	X/a	Y/b	Z/c
C21	-0.33811(93)	0.10488(75)	0.11796(108)
C22	-0.32795(78)	0.15377(83)	0.06858(76)
C23	-0.24901(93)	0.21401(83)	0.09963(85)
N6	-0.25463(65)	0.01179(62)	-0.01145(60)
C24	-0.23830(88)	-0.02551(80)	0.04900(68)
C25	-0.16490(78)	0.00304(79)	0.10947(61)
C26	-0.10140(90)	0.07108(90)	0.11464(86)
C27	-0.11978(82)	0.10992(71)	0.05264(89)
C28	-0.19792(89)	0.07762(80)	-0.00844(74)
C14H	-0.90648(99)	-0.23715(99)	-0.85973(145)
C15H	-0.90414(195)	-0.27850(112)	-0.82384(131)
C16H	-0.94681(259)	-0.33481(199)	-0.82345(199)
C17H	-1.02184(295)	-0.36107(165)	-0.85503(281)
C18H	-1.04914(115)	-0.32924(146)	-0.92183(162)
N4H	-0.97837(113)	-0.24951(98)	-0.91703(122)
Cu5	-0.89629(9)	0.02568(8)	-0.49375(7)
Cu6	-1.29495(9)	0.04959(8)	-0.54333(8)
Cu7	-1.58394(8)	-0.28552(7)	-0.83159(7)
Cu8	-1.18508(9)	-0.29532(8)	-0.79209(8)
O1E	-0.87227(38)	0.05692(37)	-0.58022(35)
O1F	-1.26253(42)	0.14940(39)	-0.57753(36)
O2G	-1.67139(40)	-0.10609(34)	-0.88306(34)
O2E	-0.79528(43)	0.03583(40)	-0.64330(39)
O2F	-1.17942(49)	0.27023(39)	-0.53895(37)
O1G	-1.60557(38)	-0.19656(34)	-0.88093(33)
O3E	-0.92386(52)	-0.01588(40)	-0.41765(39)
O3F	-1.33436(55)	-0.03468(47)	-0.50202(41)
O3G	-1.55306(42)	-0.36206(33)	-0.77294(36)
N1E	-1.06767(49)	-0.21314(41)	-0.75136(42)
N1F	-0.94551(51)	0.10781(47)	-0.48569(42)
N1G	-1.41179(49)	0.01032(43)	-0.63217(42)
N2E	-0.94693(45)	-0.12076(45)	-0.74424(45)
N2F	-0.99963(53)	0.20826(47)	-0.51242(45)
N2G	-1.52349(45)	0.00725(41)	-0.72984(40)
N3E	-0.88676(46)	-0.07470(44)	-0.53285(40)
N3F	-1.19099(50)	0.10505(45)	-0.44893(40)
N3G	-1.59546(44)	-0.22438(40)	-0.75081(38)
C1E	-0.83055(58)	0.01825(59)	-0.60014(51)
C2E	-0.81977(58)	-0.05323(54)	-0.56438(49)
C3E	-0.83353(60)	-0.11702(59)	-0.62263(54)
C4E	-0.92583(66)	-0.15167(56)	-0.68178(51)
C5E	-0.99777(60)	-0.20370(55)	-0.68699(56)
C6E	-1.03110(63)	-0.15947(55)	-0.78503(55)
C7E	-0.86963(64)	-0.12502(63)	-0.47857(52)
C8E	-0.94293(70)	-0.14920(70)	-0.45313(62)
C9E	-0.98710(79)	-0.22379(69)	-0.46125(66)
C10E	-1.05754(104)	-0.24555(81)	-0.43376(74)
C11E	-1.07439(90)	-0.18564(107)	-0.40131(76)
C12E	-1.02926(90)	-0.11217(74)	-0.39290(66)

Atoms	X/a	Y/b	Z/c
C13E	-0.96339(71)	-0.08959(72)	-0.42313(59)
C1F	-1.20506(64)	0.20351(60)	-0.52867(63)
C2F	-1.16444(67)	0.18848(58)	-0.44755(55)
C3F	-1.06361(62)	0.22312(60)	-0.41565(51)
C4F	-1.01425(65)	0.18399(67)	-0.45108(52)
C5F	-0.97948(64)	0.12435(67)	-0.43555(56)
C6F	-0.95483(59)	0.15878(58)	-0.52771(55)
C7F	-1.21006(79)	0.09221(68)	-0.38342(60)
C8F	-1.22440(67)	0.00570(79)	-0.37434(57)
C9F	-1.28830(82)	-0.05541(85)	-0.43975(72)
C10F	-1.30352(89)	-0.13907(83)	-0.42510(74)
C11F	-1.26559(104)	-0.15195(86)	-0.36253(72)
C12F	-1.20781(93)	-0.10351(83)	-0.30709(75)
C13F	-1.18597(75)	-0.02756(91)	-0.30871(55)
C1G	-1.64265(56)	-0.15759(51)	-0.85558(50)
C2G	-1.65798(53)	-0.18210(53)	-0.78807(50)
C3G	-1.64657(61)	-0.10937(58)	-0.73487(53)
C4G	-1.55332(61)	-0.05311(48)	-0.70119(51)
C5G	-1.48249(58)	-0.04874(52)	-0.64066(48)
C6G	-1.44000(60)	0.04363(56)	-0.68914(50)
C7G	-1.61969(62)	-0.27209(53)	-0.70143(53)
C8G	-1.54772(68)	-0.30434(57)	-0.66264(53)
C9G	-1.51591(70)	-0.34832(61)	-0.69875(57)
C10G	-1.45034(80)	-0.38145(63)	-0.66324(60)
C11G	-1.41252(97)	-0.36882(82)	-0.59468(86)
C12G	-1.44234(99)	-0.32608(84)	-0.55270(80)
C13G	-1.50804(94)	-0.29156(77)	-0.59131(71)
C1H	-1.27097(57)	-0.32205(50)	-0.94494(57)
C2H	-1.31466(60)	-0.39835(52)	-0.92171(58)
C3H	-1.41856(64)	-0.43062(55)	-0.96591(58)
C4H	-1.46861(59)	-0.37761(52)	-0.94865(58)
C5H	-1.50135(55)	-0.37837(48)	-0.89459(53)
C6H	-1.51906(60)	-0.28137(55)	-0.95161(54)
C7H	-1.28011(67)	-0.46076(51)	-0.81063(62)
C8H	-1.26613(68)	-0.44989(59)	-0.73039(61)
C9H	-1.20242(71)	-0.39027(60)	-0.68774(60)
C10H	-1.19338(85)	-0.39087(77)	-0.61655(81)
C11H	-1.23605(83)	-0.44695(76)	-0.58922(80)
C12H	-1.29827(88)	-0.50172(75)	-0.63636(78)
C13H	-1.31552(70)	-0.50662(65)	-0.71099(67)
N4E	-0.74057(68)	0.08861(61)	-0.42038(50)
C18E	-0.68656(103)	0.13410(98)	-0.44054(95)
C17E	-0.60495(165)	0.15880(122)	-0.40413(104)
C16E	-0.56285(141)	0.16739(119)	-0.33715(134)
C15E	-0.60750(113)	0.11672(101)	-0.31176(90)
C14E	-0.71592(116)	0.07323(105)	-0.35997(96)
N8	-1.28390(56)	-0.22793(50)	-0.78023(53)
C34	-1.31111(79)	-0.23069(74)	-0.72183(82)
C35	-1.35918(68)	-0.17185(87)	-0.71492(86)
C36	-1.37109(115)	-0.11606(97)	-0.76159(124)

Atoms	X/a	Y/b	Z/c
C37	-1.34596(91)	-0.12560(90)	-0.81348(94)
C38	-1.30437(77)	-0.17554(64)	-0.82409(72)
N4G	-1.73352(59)	-0.36020(54)	-0.89630(56)
C18G	-1.76253(87)	-0.42854(81)	-0.87869(71)
C17G	-1.84065(90)	-0.48288(86)	-0.91120(88)
C16G	-1.89588(91)	-0.46276(126)	-0.96180(102)
C15G	-1.87037(117)	-0.39172(99)	-0.99023(112)
C14G	-1.79035(83)	-0.34636(74)	-0.94983(74)
N7	-1.19775(64)	0.00938(54)	-0.58906(56)
C29	-1.17567(90)	0.04699(100)	-0.63981(76)
C30	-1.13382(83)	0.00492(103)	-0.67061(77)
C31	-1.10621(90)	-0.05274(113)	-0.65642(90)
C32	-1.12912(80)	-0.08150(83)	-0.60987(88)
C33	-1.18089(47)	-0.05249(44)	-0.56840(36)
O200	-0.62338(47)	-0.10399(44)	-0.41853(36)
O300	-0.94118(47)	-0.36829(44)	-0.59673(36)
O400	-1.54527(47)	-0.07339(44)	-0.46993(36)
C41	-0.91470(47)	-0.36553(44)	-0.64813(36)
C40	-0.65390(47)	-0.17593(44)	-0.44373(36)
C39	-1.60870(47)	-0.13003(44)	-0.51063(36)
C3	-0.91428(47)	0.11961(44)	-0.22573(36)
C5	-0.79058(47)	0.10921(44)	-0.19773(36)
C1	-0.92030(47)	0.04935(44)	-0.23245(36)
C2	-0.79930(47)	0.19675(44)	-0.20065(36)
O100	-0.88670(47)	0.19315(44)	-0.20475(36)

Atomic coordinates for the complex **8[Cu(*S*-SalHis)(Imodazole)]·15H_2O (2)**

Atoms	X/a	Y/b	Z/c
Cu1	1.89533(9)	1.62645(22)	0.39791(4)
O1A	1.88993(69)	1.85276(135)	0.41245(26)
O2A	1.82380(57)	2.03687(114)	0.39925(26)
O3A	1.97339(47)	1.60275(132)	0.37163(23)
N1A	1.74601(64)	1.55822(160)	0.46545(30)
N2A	1.80927(59)	1.59639(131)	0.42310(29)
N3A	1.83890(57)	1.71260(126)	0.36038(27)
N4A	1.95667(64)	1.54757(159)	0.43250(29)
N5A	2.01105(70)	1.48633(145)	0.47649(31)
C1A	1.84052(74)	1.91059(198)	0.39805(36)
C2A	1.79554(93)	1.82470(182)	0.37533(38)
C3A	1.73359(71)	1.76439(161)	0.39095(34)
C4A	1.75185(73)	1.67364(160)	0.41965(38)
C5A	1.71208(84)	1.65477(208)	0.44723(40)
C6A	1.80277(75)	1.52482(167)	0.45094(35)
C7A	1.88271(81)	1.77100(181)	0.33546(34)
C8A	1.92205(84)	1.65172(165)	0.32000(39)
C9A	1.96844(71)	1.57754(173)	0.33917(37)
C10A	2.00542(81)	1.46896(203)	0.32544(45)
C11A	1.99553(120)	1.44420(206)	0.29392(43)
C12A	1.95313(102)	1.51820(272)	0.27370(49)
C13A	1.91479(99)	1.62211(231)	0.28845(36)

Atoms	X/a	Y/b	Z/c
C14A	1.99595(91)	1.42906(191)	0.42620(42)
C15A	2.03237(89)	1.39867(213)	0.45452(41)
C16A	1.96885(89)	1.57204(187)	0.46264(38)
Cu2	1.73485(9)	1.85627(23)	0.17922(4)
O1B	1.71162(70)	2.08078(108)	0.18442(26)
O2B	1.67205(67)	2.24868(121)	0.14942(29)
O3B	1.82750(58)	1.86709(136)	0.19959(27)
N1B	1.53961(68)	1.72936(178)	0.14519(34)
N2B	1.64621(57)	1.80814(134)	0.15612(27)
N3B	1.76485(67)	1.92978(132)	0.13666(28)
N4B	1.70750(62)	1.77230(151)	0.21779(28)
N5B	1.70398(91)	1.65721(170)	0.26503(37)
C1B	1.69986(88)	2.12850(230)	0.15588(49)
C2B	1.71991(82)	2.03873(164)	0.12827(42)
C3B	1.65371(96)	1.98419(215)	0.11142(41)
H3B2	1.66493(0)	1.94361(0)	0.09093(0)
C4B	1.61717(87)	1.88123(179)	0.12972(36)
C5B	1.55382(85)	1.83343(216)	0.12364(44)
C6B	1.59856(78)	1.71734(182)	0.16511(36)
C7B	1.83987(83)	1.97614(194)	0.13810(48)
C12B	1.98201(98)	1.71475(259)	0.14396(57)
C13B	1.93573(99)	1.80135(224)	0.13210(44)
C14B	1.74183(91)	1.68922(180)	0.23743(38)
C15B	1.64702(141)	1.72664(293)	0.26286(49)
C16B	1.64832(80)	1.79345(167)	0.23523(39)
Cu3	1.67963(10)	2.12753(24)	0.32214(5)
O1C	1.68719(58)	2.35866(129)	0.30798(24)
O2C	1.76201(66)	2.52898(120)	0.31745(27)
O3C	1.61011(53)	2.06436(128)	0.35052(26)
N1C	1.82406(79)	2.02152(162)	0.25765(33)
N2C	1.76126(69)	2.08517(139)	0.29656(31)
N3C	1.73824(57)	2.21018(130)	0.35929(25)
N4C	1.61256(66)	2.10638(176)	0.28546(34)
C15C	1.52169(116)	2.05798(328)	0.25675(82)
C1C	1.74217(91)	2.40942(174)	0.32092(38)
C2C	1.78425(81)	2.31955(163)	0.34485(36)
C3C	1.84421(69)	2.24041(194)	0.32734(37)
C4C	1.82694(86)	2.15388(180)	0.30004(41)
C5C	1.86382(114)	2.11707(205)	0.27576(40)
C6C	1.76309(73)	2.01355(180)	0.26949(40)
C7C	1.69088(80)	2.28142(162)	0.38108(34)
C8C	1.65192(79)	2.17916(182)	0.39857(40)
C9C	1.61563(86)	2.07565(211)	0.38369(44)
C10C	1.57738(83)	1.97775(219)	0.40229(53)
C11C	1.57503(94)	1.98981(221)	0.43465(40)
C12C	1.60743(91)	2.10193(240)	0.45000(45)
C13C	1.64829(91)	2.18913(201)	0.43283(36)
C14C	1.61493(111)	2.16442(276)	0.25966(44)
N5C	1.55970(105)	2.15343(253)	0.24000(44)
C16C	1.55384(75)	2.02873(219)	0.28297(50)
Cu4	2.26560(9)	1.71476(21)	0.45592(4)
N1D	2.10237(71)	1.70482(167)	0.39141(30)
N2D	2.19316(58)	1.73692(131)	0.42058(28)
N3D	2.33439(63)	1.78625(131)	0.42581(32)
N4D	2.20199(63)	1.69049(135)	0.49150(26)

Atoms	X/a	Y/b	Z/c
N5D	2.16462(67)	1.63748(139)	0.53826(26)
O1D	2.27589(62)	1.94997(130)	0.47006(28)
O2D	2.25834(64)	2.12488(131)	0.43423(28)
O3D	2.32817(56)	1.58199(129)	0.47601(26)
C1D	2.27937(77)	2.01290(160)	0.44258(46)
C2D	2.31066(86)	1.92159(154)	0.41498(41)
C3D	2.25719(101)	1.90480(191)	0.38532(36)
C4D	2.19563(87)	1.81515(185)	0.39213(41)
C5D	2.13989(84)	1.79441(183)	0.37519(36)
C6D	2.13314(75)	1.67489(184)	0.41819(35)
C7D	2.40316(73)	1.79133(171)	0.44184(46)
C8D	2.43081(95)	1.64533(235)	0.45123(46)
C9D	2.39152(104)	1.55673(204)	0.46809(39)
C10D	2.42286(90)	1.42848(193)	0.47592(38)
C11D	2.48768(105)	1.39748(236)	0.46875(55)
C12D	2.52600(114)	1.48937(281)	0.45096(61)
C13D	2.49688(94)	1.60820(256)	0.44194(48)
C14D	2.21339(70)	1.62279(167)	0.51865(40)
C15D	2.11636(87)	1.71669(181)	0.52383(38)
C16D	2.14096(85)	1.74963(155)	0.49485(36)
Cu5	1.74242(10)	2.33418(22)	0.05550(5)
O1E	1.73257(72)	2.57010(116)	0.04322(35)
O2E	1.75153(62)	2.74650(127)	0.07822(33)
O3E	1.67899(59)	2.21102(143)	0.03546(28)
N1E	1.91814(62)	2.31404(179)	0.11465(36)
N2E	1.82039(62)	2.35141(139)	0.08918(28)
N3E	1.67723(67)	2.40033(134)	0.08658(32)
N4E	1.80107(68)	2.31233(130)	0.01788(30)
N5E	1.83143(74)	2.25861(152)	-0.03048(30)
C1E	1.73031(92)	2.61570(216)	0.06928(61)
C2E	1.70738(92)	2.54111(189)	0.09892(40)
C3E	1.75970(94)	2.52189(176)	0.12407(41)
C4E	1.81992(80)	2.43196(158)	0.11699(42)
C5E	1.87950(93)	2.40276(258)	0.13196(43)
C6E	1.87780(77)	2.28967(173)	0.08799(36)
C7E	1.60859(85)	2.41503(199)	0.07510(61)
C8E	1.58077(75)	2.27141(168)	0.06450(47)
C9E	1.61869(132)	2.18079(220)	0.04484(44)
C10E	1.58109(120)	2.05645(222)	0.03696(49)
C11E	1.51703(98)	2.01953(256)	0.04572(55)
C12E	1.48427(129)	2.10810(266)	0.06715(65)
C13E	1.51360(99)	2.23304(235)	0.07545(57)
C14E	1.78321(89)	2.24849(186)	-0.00869(43)
C15E	1.88256(93)	2.34191(189)	-0.01729(43)
C16E	1.86316(86)	2.37769(182)	0.01328(37)
Cu6	1.33467(10)	1.74508(23)	0.16646(5)
O1F	1.33401(51)	1.97652(114)	0.18030(25)
O2F	1.26452(75)	2.15565(130)	0.17125(29)
O3F	1.40355(60)	1.67663(134)	0.14010(26)
N1F	1.18312(100)	1.67181(214)	0.22893(42)
N2F	1.25045(84)	1.72255(173)	0.19185(36)
N3F	1.28111(57)	1.83547(123)	0.13019(29)
N4F	1.39521(82)	1.68672(188)	0.20388(42)
C15F	1.43720(165)	1.68932(315)	0.25464(65)

Atoms	X/a	Y/b	Z/c
C1F	1.28169(87)	2.03103(193)	0.16746(43)
C2F	1.23865(76)	1.94563(170)	0.14400(35)
C3F	1.17711(94)	1.88778(225)	0.16057(49)
C4F	1.18976(102)	1.79082(203)	0.18671(49)
C5F	1.14909(115)	1.75993(257)	0.21185(53)
C6F	1.24739(115)	1.63620(238)	0.21723(45)
C7F	1.32829(85)	1.89437(158)	0.10715(42)
C8F	1.36556(67)	1.78865(158)	0.08938(34)
C9F	1.39915(72)	1.68311(166)	0.10694(44)
C10F	1.43661(76)	1.57952(202)	0.09033(50)
C11F	1.43643(88)	1.58665(254)	0.05708(46)
C12F	1.40637(101)	1.69137(235)	0.04021(47)
C13F	1.36826(91)	1.78874(226)	0.05641(42)
C14F	1.44853(87)	1.58716(224)	0.20153(76)
N5F	1.46744(87)	1.60576(224)	0.23642(76)
C16F	1.39330(131)	1.74290(343)	0.23300(65)
Cu7	1.11784(9)	2.24948(23)	0.09964(5)
O1G	1.12181(60)	2.47471(124)	0.08288(30)
O2G	1.18919(62)	2.65737(131)	0.09050(26)
O3G	1.04573(53)	2.22263(158)	0.12944(24)
N1G	1.25348(100)	2.17184(175)	0.02612(44)
N2G	1.20020(71)	2.21023(157)	0.07317(40)
N3G	1.17861(67)	2.33962(161)	0.13338(30)
N4G	1.05408(71)	2.15985(136)	0.06803(34)
N5G	0.99095(92)	2.09757(179)	0.02595(39)
C1G	1.17246(97)	2.53735(158)	0.09611(40)
C2G	1.21885(94)	2.44909(173)	0.11841(53)
C3G	1.28009(101)	2.38765(211)	0.10020(50)
C4G	1.25881(99)	2.29936(223)	0.07393(71)
C5G	1.29071(103)	2.26001(297)	0.04442(65)
C6G	1.20440(125)	2.14194(252)	0.04580(66)
C7G	1.13919(93)	2.39709(191)	0.15846(48)
C8G	1.09875(109)	2.30023(178)	0.17777(37)
C9G	1.05568(84)	2.20473(210)	0.16240(46)
C10G	1.02319(107)	2.10097(282)	0.17983(59)
C11G	1.02924(138)	2.10856(344)	0.21239(62)
C12G	1.07571(133)	2.18399(277)	0.22830(59)
C13G	1.10919(122)	2.27851(268)	0.21085(51)
C14G	1.03801(113)	2.18813(211)	0.03810(46)
C15G	0.97773(95)	2.01194(215)	0.04789(51)
C16G	1.01426(74)	2.04985(186)	0.07528(44)
Cu8	2.27540(10)	1.25919(25)	0.32922(5)
N1H	2.47552(75)	1.15959(201)	0.35117(37)
N2H	2.36953(61)	1.21953(142)	0.34738(29)
N3H	2.24783(63)	1.30057(138)	0.37496(28)
N4H	2.30818(68)	1.25713(176)	0.28528(31)
N5H	2.30839(96)	1.22365(211)	0.23410(46)
O1H	2.28711(70)	1.50217(135)	0.33148(32)
O2H	2.34299(72)	1.62977(142)	0.36776(30)
O3H	2.18452(61)	1.22313(158)	0.31236(25)
C1H	2.30863(97)	1.52427(193)	0.35891(43)
C2H	2.29095(91)	1.41811(237)	0.38753(38)
C3H	2.36053(83)	1.36149(192)	0.39863(38)
C4H	2.39989(94)	1.27524(188)	0.37603(36)
C5H	2.46486(93)	1.23908(254)	0.37722(51)
C6H	2.41875(92)	1.14852(216)	0.33450(41)

Atoms	X/a	Y/b	Z/c
C7H	2.17610(79)	1.34035(177)	0.37536(36)
C8H	2.12807(85)	1.23050(175)	0.36266(43)
C9H	2.13361(72)	1.18078(215)	0.33109(42)
C10H	2.08482(109)	1.08370(251)	0.31815(43)
C12H	2.02661(104)	1.08177(239)	0.36777(64)
C11H	2.03299(131)	1.03787(253)	0.33597(46)
C13H	2.07484(101)	1.17707(240)	0.37973(47)
C14H	2.27990(108)	1.19512(243)	0.26005(37)
C15H	2.36156(86)	1.31490(253)	0.23945(57)
C16H	2.35775(116)	1.32790(244)	0.27395(45)
O1	1.99280(70)	1.96229(216)	0.45558(30)
O2	2.24410(102)	1.35325(194)	0.47428(51)
O3	1.01419(89)	2.58738(194)	0.04411(32)
O4	1.88395(82)	2.71438(186)	0.04433(51)
O5	2.12309(68)	2.09127(146)	0.46403(35)
O6	1.86322(66)	1.80920(140)	0.48791(32)
O7	1.86342(75)	2.92872(154)	-0.00648(32)
O8	1.17612(95)	1.50880(207)	0.28763(40)
O9	1.76513(104)	2.97252(198)	0.03711(55)
O10	1.55276(163)	2.46155(373)	0.30627(77)
O11	1.54768(151)	2.31903(335)	0.17732(71)
O12	1.46404(154)	2.07993(340)	0.17755(73)
O13	2.21504(141)	0.91792(300)	0.29533(66)
O14	1.75409(191)	2.34002(437)	0.21966(89)
O15	1.09457(163)	1.74299(388)	0.29015(78)

Table I: Selected bond distances (Å) of complex **[Fe_2(*S*-Salhis)$_2$(OH)(OAc) ·4H_2O] (1)**

Atoms	**Distances**	**Atoms**	**Distances**
Fe1-O3	1.9465(19)	N6 -C14	1.492(4)
Fe1-O1	1.9723(19)	C1 -C6	1.375(4)
Fe1 -O4	1.987(2)	C1 -C2	1.393(5)
Fe1 -O8	1.999(2)	C2 -C3	1.404(6)
Fe1 -N4	2.131(2	C3 -C4	1.350(6)
Fe1 -N6	2.203(2)	C4 -C5	1.372(6)
Fe2 -O2	1.9315(19)	C5 -C6	1.370(5)
Fe2 -O1	1.9696(19)	C6 -C7	1.507(4)
Fe2 -O6	2.018(2)	C8 -C9	1.387(5)
Fe2 -O5	2.031(2)	C8 -C13	1.395(5)
Fe2 -N2	2.140(2)	C9 -C10	1.360(6)
Fe2 -N1	2.201(2)	C10 -C11	1.371(6)
O2 -C1	1.365(4)	C11 -C12	1.395(6)
O3 -C8	1.352(4)	C12 -C13	1.369(6)
O4 -C23	1.254(4)	C13 -C14	1.479(5)
O5 -C23	1.223(4)	C15 -C17	1.340(4)
N1 -C27	1.473(4)	C17 -C18	1.480(4)
N1 -C7	1.492(4)	C18 -C25	1.512(4)
N2 -C19	1.314(4)	C20 -C21	1.352(4)
N2 -C21	1.376(4)	C21 -C22	1.489(4)
N3 -C20	1.331(4)	C22 -C27	1.524(4)
N3 -C19	1.337(4)	C23 -C24	1.513(5)
N4 -C16	1.304(4)	C25 -C26	1.509(5)
N4 -C17	1.393(4)	C27 -C28	1.528(5)
N5 -C16	1.325(4)	O11 -O13A	1.00(3) 1_545
N5 -C15	1.364(4)	O13A -O11	1.00(3) 1_565
N6 -C25	1.487(4)		

Table II: Selected bond Angles (º) of the complex **[Fe_2(*S*-Salhis)$_2$(OH)(OAc)·4H_2O] (1)**

Atoms	**Angles**	**Atoms**	**Angles**
O3 -Fe1 -O1	94.14(8)	O3 -Fe1 -N6	87.26(9)
O3 -Fe1 -O4	91.27(9)	O1 -Fe1 -N6	172.22(10)
O1 -Fe1 -O4	93.61(8)	O4 -Fe1 -N6	94.00(9)
O3 -Fe1 -O8	93.91(8)	O8 -Fe1 -N6	77.90(9)
O1 -Fe1 -O8	94.36(8)	N4 -Fe1 -N6	82.82(9)
O4 -Fe1 -O8	170.15(8)	Fe2 -O1 -Fe1	126.35(11)
O3 -Fe1 -N4	169.25(9)	C1 -O2 -Fe2	121.24(17)
O1 -Fe1 -N4	96.24(9)	C8 -O3 -Fe1	119.76(18)
O4 -Fe1 -N4	85.31(10)	C23 -O4 -Fe1	131.11(19)

Atoms	**Angles**	**Atoms**	**Angles**
O8 -Fe1 -N4	88.08(10)	O2 -Fe2 -N2	168.62(9)
C28 -O6 -Fe2	117.51(19)	O1 -Fe2 -N2	95.62(9)
C26 -O8 -Fe1	118.2(2)	O6 -Fe2 -N2	87.51(9)
C27 -N1 -C7	110.2(2)	O5 -Fe2 -N2	85.68(9)
C27 -N1 -Fe2	104.77(16)	O2 -Fe2 -N1	87.01(8)
C7 -N1 -Fe2	112.87(17)	O1 -Fe2 -N1	167.01(8)
C19 -N2 -C21	106.5(2)	O6 -Fe2 -N1	76.49(8)
C19 -N2 -Fe2	122.88(19)	O5 -Fe2 -N1	97.14(8)
C21 -N2 -Fe2	130.49(18)	N2 -Fe2 -N1	82.95(9)
C20 -N3 -C19	108.2(3)	C10 -C9 -C8	120.8(4)
C16 -N4 -C17	106.5(2)	C9 -C10 -C11	120.6(4)
C16 -N4 -Fe1	124.1(2)	C10 -C11 -C12	118.8(4)
C17 -N4 -Fe1	129.39(18)	C13 -C12 -C11	121.5(4)
C16 -N5 -C15	108.0(3)	C12 -C13 -C8	118.8(4)
C25 -N6 -C14	110.6(2)	C12 -C13 -C14	122.9(3)
C25 -N6 -Fe1	103.66(17)	C8 -C13 -C14	118.3(3)
C14 -N6 -Fe1	112.98(19)	C13 -C14 -N6	112.1(3)
O2 -C1 -C6	119.9(3)	C17 -C15 -N5	106.9(3)
O2 -C1 -C2	121.0(3)	N4 -C16 -N5	110.8(3)
C6 -C1 -C2	119.1(3)	C15 -C17 -N4	107.9(3)
C1 -C2 -C3	118.8(3)	C15 -C17 -C18	129.0(3)
C4 -C3 -C2	121.2(4)	N4 -C17 -C18	122.7(3)
C3 -C4 -C5	119.3(4)	C17 -C18 -C25	116.0(2)
C6 -C5 -C4	120.9(4)	N2 -C19 -N3	110.1(3)
C5 -C6 -C1	120.6(3)	N3 -C20 -C21	107.5(3)
C5 -C6 -C7	122.0(3)	C20 -C21 -N2	107.7(2)
C1 -C6 -C7	117.4(3)	C20 -C21 -C22	129.4(3)
N1 -C7 -C6	111.2(2)	N2 -C21 -C22	122.9(3)
O3 -C8 -C9	121.3(3)	C21 -C22 -C27	114.3(2)
O3 -C8 -C13	119.2(3)	O5 -C23 -O4	125.3(3)
C9 -C8 -C13	119.5(3)	O4 -C23 -C24	116.3(3)
O2 -Fe2 -O1	95.36(8)	N6 -C25 -C26	109.7(2)
O2 -Fe2 -O6	95.36(8)	N6 -C25 -C18	111.8(3)
O1 -Fe2 -O6	90.56(8)	C26 -C25 -C18	111.4(3)
O2 -Fe2 -O5	90.28(9)	O9 -C26 -O8	122.6(3)
O1 -Fe2 -O5	95.62(8)	O9 -C26 -C25	121.4(3)
O6 -Fe2 -O5	171.22(8)	O7 -C28 -O6	124.6(3)
O8 -C26 -C25	116.0(3)	O7 -C28 -C27	118.5(3)
N1 -C27 -C22	111.6(2)	O6 -C28 -C27	116.9(3)
N1 -C27 -C28	108.4(2)	C22 -C27 -C28	112.3(3)
C23 -O5 -Fe2	128.3(2)		

Table III: Selected bond distances (Å) of complex **[Fe_2(*S*-Salhis)$_2$(OH)(OAc)·H_2O] (2)**

Atoms	Distances	Atoms	Distances
Fe1-O3	1.957(3)	N5-C16	1.312(6)
Fe1-O1	1.969(3)	N5-C15	1.381(6)
Fe1-O4	1.995(3)	N6-C14	1.469(6)
Fe1-O8	2.000(3)	N6-C25	1.476(6)
Fe1-N4	2.142(4)	C1-C2	1.395(7)
Fe1-N6	2.211(4)	C1-C6	1.401(6)
Fe2-O2	1.946(3)	C2-C3	1.385(9)
Fe2-O1	1.72(3)	C3-C4	1.375(10)
Fe2-O6	2.016(3)	C4-C5	1.412(9)
Fe2-O5	2.031(3)	C5-C6	1.376(7)
Fe2-N2	2.51(4)	C6-C7	1.492(7)
Fe2-N1	2.206(3)	C8-C9	1.386(8)
O2-C1	1.360(5)	C8-C13	1.400(7)
O3-C8	1.349(6)	C9-C10	1.346(10)
O4-C23	1.261(5)	C10-C11	1.380(11)
O5-C23	1.253(5)	C11-C12	1.408(10)
O6-C28	1.287(6)	C12-C13	1.357(9)
O7-C28	1.207(6)	C13-C14	1.493(8)
O8-C26	1.297(5)	C15-C17	1.338(7)
O9-C26	1.224(6)	C17-C18	1.495(7)
N1-C27	1.481(5)	C18-C25	1.532(7)
N1-C7	1.503(5)	C20-C21	1.365(6)
N2-C19	1.309(6)	C21-C22	1.489(7
N2-C21	1.386(5)	C22-C27	1.525(6)
N3-C19	1.347(6)	C23-C24	1.495(7)
N3-C20	1.359(7)	C25-C26	1.533(7)
N4-C16	1.305(6)	C27-C28	1.536(7)
N4-C17	1.406(5)		

Table IV: Selected bond Angles (º) of the complex **[Fe_2(*S*-Salhis)$_2$(OH)(OAc)·H_2O] (2)**

Atoms	Angles	Atoms	Angles
O8 -Fe1 -N6	77.51(14)	O1 -Fe2 -N1	167.23(12)
N4 -Fe1 -N6	83.13(16)	O6 -Fe2 -N1	76.45(12)
O2 -Fe2 -O1	95.19(13)	O5 -Fe2 -N1	97.08(12)
O2 -Fe2 -O6	94.95(13)	N2 -Fe2 -N1	82.76(13)
O1 -Fe2 -O6	90.84(13)	Fe1-O1 -Fe2	126.69(16)
O2 -Fe2 -O5	90.59(13)	C1 -O2 -Fe2	121.0(3)
O1 -Fe2 -O5	95.43(12)	C8 -O3 -Fe1	120.0(3)
O6 -Fe2 -O5	171.23(11)	C23 -O4 -Fe1	130.0(3)

Atoms	**Angles**	**Atoms**	**Angles**
O2 -Fe2 -N2	168.76(13)	C23 -O5 -Fe2	128.3(3)
O1 -Fe2 -N2	95.68(13)	C28 -O6 -Fe2	118.0(3)
O6 -Fe2 -N2	87.75(13)	C26 -O8 -Fe1	118.7(3)
O5 -Fe2 -N2	85.54(13)	C27 -N1 -C7	110.6(3)
O2 -Fe2 -N1	87.27(13)	C27 -N1 -Fe2	104.9(2)
C7 -N1 -Fe2	112.0(2)	C12 -C13 -C14	122.8(5)
C19 -N2 -Fe2	123.0(3)	C8 -C13 -C14	118.7(5)
C19 -N2 -C21	106.6(3)	N6 -C14 -C13	113.0(4)
C21 -N2 -Fe2	130.2(3)	C17 -C15 -N5	105.9(4)
C19 -N3 -C20	107.7(4)	N4 -C16 -N5	111.6(4)
C16 -N4 -C17	105.6(4)	C15 -C17 -N4	108.6(4)
C16 -N4 -Fe1	124.8(3)	C15 -C17 -C18	128.6(4)
C17 -N4 -Fe1	129.6(3)	N4 -C17 -C18	122.7(4)
C16 -N5 -C15	108.3(4)	C17 -C18 -C25	115.6(4)
C14 -N6 -C25	111.1(4)	N2 -C19 -N3	110.8(4)
C14 -N6 -Fe1	113.5(3)	N3 -C20 -C21	106.7(4)
C25 -N6 -Fe1	104.3(3)	C20 -C21 -N2	108.1(4)
O2 -C1 -C2	122.3(4)	C20 -C21 -C22	128.3(4)
O2 -C1 -C6	118.6(4)	N2 -C21 -C22	123.6(4)
C2 -C1 -C6	119.2(4)	C21 -C22 -C27	113.9(3)
C3 -C2 -C1	119.6(5)	O5 -C23 -O4	125.6(4)
C4 -C3 -C2	122.1(6)	O5 -C23 -C24	118.4(4)
C3 -C4 -C5	118.2(6)	O4 -C23 -C24	115.9(4)
C6 -C5 -C4	120.6(6)	N6 -C25 -C18	112.8(4)
C5 -C6 -C1	120.4(4)	N6 -C25 -C26	108.8(4)
C5 -C6 -C7	121.8(4)	C18 -C25 -C26	111.6(4)
C1 -C6 -C7	117.7(4)	O9 -C26 -O8	123.4(5)
C6 -C7 -N1	111.5(4)	O9 -C26 -C25	120.9(4)
O3 -C8 -C9	122.7(5)	O8 -C26 -C25	115.6(4)
O3 -C8 -C13	118.9(4)	N1 -C27 -C22	112.1(4)
C9 -C8 -C13	118.5(5)	N1 -C27 -C28	108.2(3)
C10 -C9 -C8	123.5(7)	C22 -C27 -C28	112.9(4)
C9 -C10 -C11	118.3(6)	O7 -C28 -O6	124.7(5)
C10 -C11 -C12	119.3(7)	O7 -C28 -C27	119.1(4)
C13 -C12 -C11	121.7(7)	O6 -C28 -C27	116.1(4)
C12 -C13 -C8	118.6(5)		

Table V: Selected bond distances (Å) of complex **[Fe_2(S-Salhis)$_2$(OH)(OAc) ·H_2O·I_2] (3)**

Atoms	Distances	Atoms	Distances
Fe1 -O3	1.961(5)	I1 -I2	2.658(5)
Fe1 -O1	1.983(6)	I1 -I2'	2.784(6)
Fe1 -O4	1.992(6)	I2 -I'	1.149(6)
Fe1 -O8	2.016(5)	I2 -I1'	2.852(7)
Fe1 -N4	2.119(6)	I1' -I2'	2.584(8)
Fe1 -N6	2.213(7)	O2 -C8	1.381(10)
Fe2 -O2	1.931(6)	O3 -C1	1.349(12)
Fe2 -O1	1.966(5)	O4 -C23	1.285(10)
Fe2 -O6	2.024(6)	O5 -C23	1.236(10)
Fe2 -O5	2.034(6)	O6 -C26	1.271(11)
Fe2 -N2	2.144(6)	O7 -C26	1.212(10)
Fe2 -N1	2.216(6)	O8 -C28	1.303(10)
I1 -I1'	1.142(7)	O9 -C28	1.228(10)
N1 -C14	1.465(10)	C6 -C7	1.500(15)
N1 -C25	1.481(9)	C8 -C13	1.390(12)
N2 -C16	1.304(11)	C8 -C9	1.392(14)
N2 -C17	1.385(10)	C9 -C10	1.458(17)
N3 -C15	1.311(14)	C10 -C11	1.271(19)
N3 -C16	1.326(12)	C11 -C12	1.294(18)
N4 -C19	1.295(12)	C12 -C13	1.419(12)
N4 -C21	1.415(10)	C13 -C14	1.491(13)
N5 -C19	1.372(11)	C15 -C17	1.391(13)
N5 -C20	1.398(12)	C17 -C18	1.477(13)
N6 -C7	1.468(13)	C18 -C25	1.525(11)
N6 -C27	1.500(11)	C20 -C21	1.359(13)
C1 -C2	1.372(15)	C21 -C22	1.483(13)
C1 -C6	1.393(15)	C22 -C27	1.539(13)
C2 -C3	1.413(19)	C23 -C24	1.483(12)
C3 -C4	1.38(3)	C25 -C26	1.538(11)
C4 -C5	1.43(2)	C27 -C28	1.514(12)
C5 -C6	1.383(16)		

Table VI: Selected bond Angles (º) of the complex **[Fe_2(*S*-Salhis)$_2$(OH)(OAc)·H_2O·I_2] (3)**

Atoms	Angles	Atoms	Angles
O3 -Fe1 -O1	94.5(2)	C14 -N1 C25	110.2(6)
O3 -Fe1 -O4	90.9(3)	C14 -N1 -Fe2	113.0(5)
O1 -Fe1 -O4	93.3(2)	C25 -N1 -Fe2	104.0(4)

Atoms	**Angles**	**Atoms**	**Angles**
O3 -Fe1 -O8	94.2(2)	C16 -N2 -C17	106.4(7)
O1 -Fe1 -O8	94.3(2)	C16 -N2 -Fe2	124.0(6)
O4 -Fe1 -O8	170.5(2)	C17 -N2 -Fe2	129.3(5)
O3 -Fe1 -N4	169.0(3)	C15 -N3 -C16	108.9(8)
O1 -Fe1 -N4	96.2(3)	C19 -N4 -C21	104.8(7)
O4 -Fe1 -N4	85.9(3)	C19 -N4 -Fe1	124.4(5)
O8 -Fe1 -N4	87.6(3)	C21 -N4 -Fe1	130.7(6)
O3 -Fe1 -N6	86.6(3)	C19 -N5 -C20	104.7(8)
O1 -Fe1 -N6	172.7(3)	C7 -N6 -C27	110.8(6)
O4 -Fe1 -N6	93.9(3)	C7 -N6 -Fe1	113.3(6)
O8 -Fe1 -N6	78.4(2)	C27 -N6 -Fe1	103.7(5)
N4 -Fe1 -N6	83.1(3)	O3 -C1 -C2	120.0(10)
O2 -Fe2 -O1	94.6(2)	O3 -C1 -C6	119.2(8)
O2 -Fe2 -O6	93.6(3)	C2 -C1 -C6	120.8(10)
O1 -Fe2 -O6	90.9(2)	C1 -C2 -C3	120.6(13)
O2 -Fe2 -O5	91.3(3)	C4 -C3 -C2	117.6(13)
O1 -Fe2 -O5	95.8(2)	C3 -C4 -C5	122.0(14)
O6 -Fe2 -O5	171.3(2)	C6 -C5 -C4	118.1(14)
O2 -Fe2 -N2	169.8(3)	C5 -C6 -C1	120.3(11)
O1 -Fe2 -N2	95.5(2)	C5 -C6 -C7	122.0(11)
O6 -Fe2 -N2	87.7(3)	C1 -C6 -C7	117.7(9)
O5 -Fe2 -N2	86.2(3)	N6 -C7 -C6	112.6(8)
O2 -Fe2 -N1	87.0(2)	O2 -C8 -C13	117.2(8)
O1 -Fe2 -N1	167.5(2)	O2 -C8 -C9	122.5(8)
O6 -Fe2 -N1	76.6(2)	C13 -C8 -C9	120.3(8)
O5 -Fe2 -N1	96.5(2)	C8 -C9 -C10	115.2(10)
N2 -Fe2 -N1	83.4(2)	C11 -C10 -C9	122.7(11)
I1' -I1 -I2	87.8(4)	C10 -C11 -C12	120.3(12)
I1' -I1 -I2'	68.0(4)	C11 -C12 -C13	122.7(12)
I2 -I1 -I2'	24.24(13)	C8 -C13 -C12	116.7(9)
I2' -I2 -I1	84.1(3)	C8 -C13 -C14	119.7(7)
I2' -I2 -I1'	64.9(3)	C12 -C13 -C14	123.3(9)
I1 -I2 -I1'	23.58(15)	N1 -C14 -C13	112.6(7)
I1 -I1' -I2'	87.8(4)	N3 -C15 -C17	107.2(8)
I1 -I1' -I2	68.6(4)	N2 -C16 -N3	111.2(8)
I2' -I1' -I2	23.75(14)	N2 -C17 -C15	106.3(8)
I2 -I2' -I1'	91.4(3)	N2 -C17 -C18	124.1(7)
I2 -I2' -I1	71.7(3)	C15 -C17 -C18	129.5(8)
I1' -I2' -I1	24.19(17)	C17 -C18 -C25	114.0(6)
Fe2 -O1 -Fe1	126.6(3)	N4 -C19 -N5	114.0(8)
C8 -O2 -Fe2	121.0(5)	C21 -C20 -N5	107.1(8)
C1 -O3 -Fe1	121.1(5)	C20 -C21 -N4	109.2(7)
C23 -O4 -Fe1	131.3(5)	C20 -C21 -C22	128.8(8)
C23 -O5 -Fe2	129.7(5)	N4 -C21 -C22	121.7(8)

Atoms	Angles	Atoms	Angles
C26 -O6 -Fe2	117.9(5)	O5 -C23 -C24	120.5(7)
C28 -O8 -Fe1	116.6(5)	C21 -C22 -C27	115.6(7)
O6 -C26 -C25	116.5(6)	O5 -C23 -O4	123.8(7)
N6 -C27 -C28	108.3(7)	O4 -C23 -C24	115.6(7)
N6 -C27 -C22	110.8(7)	N1 -C25 -C18	113.0(7)
C28 -C27 -C22	113.7(7)	N1 -C25 -C26	108.5(6)
O9 -C28 -O8	121.1(8)	C18 -C25 -C26	111.5(6)
O9 -C28 -C27	121.0(8)	O7 -C26 -O6	123.7(8)
O8 -C28 -C27	117.9(7)	O7 -C26 -C25	119.9(8)

Table VII: Selected bond distances (Å) of complex **[Fe_2(*R*-Salhis)$_2$(OH)(OAc) ·2H_2O] (4)**

Atoms	Distances	Atoms	Distances
Fe1 -O3	1.961(2)	N5 -C15	1.397(5)
Fe1 -O1	1.971(2)	N6 -C25	1.473(5)
Fe1 -O4	1.997(2)	N6 -C14	1.486(5)
Fe1 -O8	2.001(2)	C1 -C2	1.389(5)
Fe1 -N4	2.136(3)	C1 -C6	1.395(5)
Fe1 -N6	2.220(3)	C2 -C3	1.407(9)
Fe2 -O2	1.943(2)	C3 -C4	1.372(9)
Fe2 -O1	1.968(2)	C4 -C5	1.374(7)
Fe2 -O6	2.024(2)	C5 -C6	1.380(6)
Fe2 -N2	2.141(3)	C6 -C7	1.487(5)
Fe2 -N1	2.211(3)	C8 -C13	1.395(6)
O2 -C1	1.364(4)	C8 -C9	1.409(6)
O3 -C8	1.346(5)	C9 -C10	1.341(7)
O4 -C23	1.273(4)	C10 -C11	1.385(9)
O5 -C23	1.260(4)	C11 -C12	1.436(9)
O6 -C28	1.274(5)	C12 -C13	1.372(7)
O7 -C28	1.214(5)	C13 -C14	1.507(6)
O8 -C26	1.295(4)	C15 -C17	1.344(5)
O9 -C26	1.228(5)	C17 -C18	1.485(5)
N1 -C27	1.475(4)	C18 -C25	1.546(5)
N1 -C7	1.502(4)	C20 -C21	1.325(6)
N2 -C19	1.327(5)	C21 -C22	1.503(5)
N2 -C21	1.385(4)	C22 -C27	1.535(5)
N3 -C19	1.346(5)	C23 -C24	1.483(5)
N3 -C20	1.350(6)	C25 -C26	1.537(5)
N4 -C16	1.330(5)	C27 -C28	1.533(5)
N4 -C17	1.391(4)	N5 -C16	1.325(5)

Table VIII: Selected bond Angles (°) of the complex **[Fe_2(*R*-Salhis)$_2$(OH)(OAc)·2H_2O] (4)**

Atoms	Angles	Atoms	Angles
O3 -Fe1 -O1	94.20(10)	C10 -C9 -C8	121.5(5)
O3 -Fe1 -O4	91.56(11)	C9 -C10 -C11	120.8(5)
O1 -Fe1 -O4	93.59(10)	C10 -C11 -C12	118.9(5)
O3 -Fe1 -O8	94.11(10)	C13 -C12 -C11	119.4(5)
O1 -Fe1 -O8	94.10(10)	C12 -C13 -C8	120.7(4)
O4 -Fe1 -O8	170.08(10)	C12 -C13 -C14	122.0(4)
O3 -Fe1 -N4	168.88(11)	C8 -C13 -C14	117.3(4)
O1 -Fe1 -N4	96.64(11)	N6 -C14 -C13	111.8(3)
O4 -Fe1 -N4	85.32(12)	C17 -C15 -N5	105.9(3)
O8 -Fe1 -N4	87.57(11)	N5 -C16 -N4	111.0(3)
O3 -Fe1 -N6	87.21(11)	C15 -C17 -N4	109.4(3)
O1 -Fe1 -N6	172.07(11)	C15 -C17 -C18	127.6(3)
O4 -Fe1 -N6	94.17(11)	N4 -C17 -C18	122.8(3)
O8 -Fe1 -N6	78.01(11)	C17 -C18 -C25	115.6(3)
N4 -Fe1 -N6	82.39(11)	N2 -C19 -N3	110.9(3)
O2 -Fe2 -O1	95.21(10)	C21 -C20 -N3	109.0(4)
O2 -Fe2 -O6	95.39(10)	C20 -C21 -N2	108.4(3)
O1 -Fe2 -O6	90.53(10)	C20 -C21 -C22	129.3(4)
O2 -Fe2 -O5	90.21(11)	N2 -C21 -C22	122.3(3)
O1 -Fe2 -O5	95.66(9)	C21 -C22 -C27	113.7(3)
O6 -Fe2 -O5	171.25(9)	O5 -C23 -O4	124.6(3)
O2 -Fe2 -N2	168.36(11)	O5 -C23 -C24	119.0(3)
O1 -Fe2 -N2	96.04(11)	O4 -C23 -C24	116.4(3)
O6 -Fe2 --N2	87.51(10)	N6 -C25 -C26	109.3(3)
O5 -Fe2 -N2	85.70(10)	N6 -C25 -C18	112.0(3)
O2 -Fe2 -N1	87.14(10)	C26 -C25 -C18	110.6(3)
O1 -Fe2 -N1	166.56(9)	O9 -C26 -O8	123.8(4)
O6 -Fe2 -N1	76.07(10)	O9 -C26 -C25	120.1(3)
O5 -Fe2 -N1	97.56(9)	O8 -C26 -C25	116.1(3)
N2 -Fe2 -N1	82.61(10)	N1 -C27 -C28	108.4(3)
Fe2 -O1 -Fe1	126.83(12)	N1 -C27 -C22	111.8(3)
C1 -O2 -Fe2	121.2(2)	C28 -C27 -C22	112.4(3)
C8 -O3 -Fe1	119.5(2)	O7 -C28 -O6	125.4(4)
C23 -O4 -Fe1	130.7(2)	O7 -C28 -C27	118.1(4)
C23 -O5 -Fe2	128.6(2)	O6 -C28 -C27	116.5(3)
C28 -O6 -Fe2	117.8(2)	O2 -C1 -C6	118.8(3)
C26 -O8 -Fe1	118.4(2)	C2 -C1 -C6	119.4(4)
C27 -N1 -C7	111.2(2)	C1 -C2 -C3	119.5(5)
C27 -N1 -Fe2	104.9(2)	C4 -C3 -C2	120.4(4)
C7 -N1 -Fe2	112.30(19)	C3 -C4 -C5	119.6(5)

Atoms	**Angles**	**Atoms**	**Angles**
C19 -N2 -C21	105.5(3)	C4 -C5 -C6	121.2(5)
C19 -N2 -Fe2	122.9(2)	C5 -C6 -C1	119.8(4)
C21 -N2 -Fe2	131.4(2)	C5 -C6 -C7	122.1(4)
C19 -N3 -C20	106.2(3)	C1 -C6 -C7	118.1(3)
C16 -N4 -C17	105.9(3)	C6 -C7 -N1	112.2(3)
C16 -N4 -Fe1	123.7(2)	O3 -C8 -C13	119.8(3)
C17 -N4 -Fe1	130.4(2)	O3 -C8 -C9	121.6(4)
C16 -N5 -C15	107.9(3)	C13 -C8 -C9	118.6(4)
C25 -N6 -C14	110.4(3)	C14 -N6 -Fe1	112.4(2)
C25 -N6 -Fe1	104.2(2)	O2 -C1 -C2	121.8(3)

Atomic coordinates for the complex **[Fe_2(*S*-Salhis)$_2$(OH)(OAc)·4H_2O (1)**

Atoms	**X/a**	**Y/b**	**Z/c**
Fe1	0.95762(3)	0.38367(3)	-0.00044(1)
Fe2	0.71091(3)	0.18204(3)	-0.05123(1)
O1	0.86317(16)	0.23464(17)	-0.02706(5)
O2	0.62041(16)	0.13613(17)	-0.00626(5)
O3	1.02277(16)	0.47545(17)	-0.04510(5)
O4	0.82909(16)	0.42138(17)	0.00031(5)
O5	0.71998(16)	0.34057(16)	-0.04946(5)
O6	0.69382(17)	0.02335(16)	-0.06106(5)
O7	0.63274(28)	-0.11875(23)	-0.10194(8)
O8	1.09371(16)	0.35846(18)	0.00739(5)
O9	1.24715(19)	0.39903(23)	0.04220(7)
N1	0.54296(19)	0.08727(17)	-0.08085(6)
N2	0.78066(19)	0.23086(19)	-0.10572(6)
N3	0.91009(23)	0.32354(25)	-0.14844(7)
N4	0.89812(20)	0.31431(23)	0.05333(6)
N5	0.78211(24)	0.20163(26)	0.09613(7)
N6	1.08025(19)	0.54191(21)	0.03061(7)
C1	0.52262(24)	0.14614(23)	-0.00249(8)
C2	0.51472(32)	0.21467(32)	0.02534(10)
C3	0.41207(38)	0.22180(34)	0.02815(13)
C4	0.32186(35)	0.16348(36)	0.00452(12)
C5	0.33103(30)	0.09661(33)	-0.02284(10)
C6	0.43019(24)	0.08826(25)	-0.02645(8)
C7	0.44200(25)	0.01439(25)	-0.05600(9)
C8	1.03455(26)	0.58323(27)	-0.04784(9)
C9	0.97940(30)	0.61001(32)	-0.07563(11)
C10	0.99106(38)	0.71850(38)	-0.07788(12)
C11	1.05645(43)	0.80331(37)	-0.05245(15)
C12	1.11316(41)	0.77730(35)	-0.02470(13)
C13	1.10428(31)	0.66934(29)	-0.02232(10)
C14	1.16459(29)	0.63938(29)	0.00642(10)
C15	0.88544(29)	0.27699(29)	0.11302(9)
C16	0.79348(29)	0.22719(32)	0.06053(9)
C17	0.95849(26)	0.34637(25)	0.08669(8)
C18	1.07782(27)	0.44911(28)	0.09041(9)
C19	0.88675(28)	0.31826(28)	-0.11243(9)
C20	0.81682(29)	0.23738(29)	-0.16520(8)
C21	0.73414(26)	0.17938(25)	-0.13918(8)
C22	0.61381(26)	0.07656(25)	-0.14321(8)
C23	0.75981(23)	0.41535(24)	-0.02444(9)
C24	0.72088(30)	0.50564(31)	-0.02281(11)
C25	1.14333(25)	0.50062(26)	0.05484(8)
C26	1.16513(25)	0.41373(29)	0.03427(8)
C27	0.55959(25)	0.01198(24)	-0.10732(8)
C28	0.63366(30)	-0.03325(25)	-0.08888(9)
O10	0.96128(43)	0.63658(62)	0.07830(15)
O11	0.95376(142)	0.09525(147)	-0.01219(52)
O11A	0.90905(168)	0.99727(175)	-0.14188(60)
O12	0.88053(181)	0.93443(195)	-0.08100(67)
O12A	0.84658(198)	1.01100(173)	-0.20297(62)
O13	1.05299(227)	1.08410(188)	-0.11439(70)
O13A	0.95706(290)	1.08940(308)	-0.03968(90)

Atomic coordinates for the complex **[Fe_2(*S*-Salhis)$_2$(OH)(OAc)·H_2O (2)**

Atoms	X/a	Y/b	Z/c
Fe1	0.04192(0)	0.42553(0)	0.14682(0)
Fe2	0.28868(0)	0.47036(0)	0.19744(0)
O1	0.13615(0)	0.37122(0)	0.17337(0)
H1	0.10557(0)	0.29052(0)	0.17469(0)
O2	0.37957(0)	0.51453(0)	0.15239(0)
O3	-0.02324(0)	0.45257(0)	0.19147(0)
O4	0.17103(0)	0.59238(0)	0.14579(0)
O5	0.27969(0)	0.61994(0)	0.19579(0)
O6	0.30607(0)	0.32893(0)	0.20701(0)
O7	0.36591(0)	0.24670(0)	0.24796(0)
O8	-0.09456(0)	0.26425(0)	0.13895(0)
O9	-0.24766(0)	0.15098(0)	0.10380(0)
N1	0.45681(0)	0.54355(0)	0.22705(0)
N2	0.21871(0)	0.44952(0)	0.25183(0)
N3	0.08890(0)	0.41360(0)	0.29462(0)
N4	0.10184(0)	0.41591(0)	0.09315(0)
N5	0.21808(0)	0.42003(0)	0.05055(0)
N6	-0.08213(0)	0.46064(0)	0.11618(0)
C1	0.47611(0)	0.62251(0)	0.14846(0)
C2	0.48505(0)	0.70006(0)	0.12095(0)
C3	0.58550(0)	0.80906(0)	0.11843(0)
C4	0.67854(0)	0.84347(0)	0.14198(0)
C5	0.66910(0)	0.76475(0)	0.16977(0)
C6	0.56968(0)	0.65633(0)	0.17286(0)
C7	0.55744(0)	0.57099(0)	0.20179(0)
C8	-0.03490(0)	0.54840(0)	0.19435(0)
C9	0.01924(0)	0.63147(0)	0.22166(0)
C10	0.00913(0)	0.72795(0)	0.22483(0)
C11	-0.05529(0)	0.74729(0)	0.19881(0)
C12	-0.11459(0)	0.66235(0)	0.17153(0)
C13	-0.10538(0)	0.56437(0)	0.16899(0)
C14	-0.16482(0)	0.47452(0)	0.13973(0)
C15	0.11409(0)	0.39238(0)	0.03327(0)
C16	0.20558(0)	0.43134(0)	0.08567(0)
C17	0.04197(0)	0.38958(0)	0.05957(0)
C18	-0.07884(0)	0.37218(0)	0.05580(0)
C19	0.11272(0)	0.42990(0)	0.25856(0)
C20	0.18459(0)	0.42208(0)	0.31169(0)
C21	0.26662(0)	0.44580(0)	0.28522(0)
C22	0.38614(0)	0.46142(0)	0.28936(0)
C23	0.23943(0)	0.65510(0)	0.17087(0)
C24	0.28001(0)	0.78328(0)	0.16881(0)
C25	-0.14441(0)	0.35829(0)	0.09176(0)
C26	-0.16700(0)	0.24775(0)	0.11252(0)
C27	0.43997(0)	0.45133(0)	0.25356(0)
C28	0.36676(0)	0.33147(0)	0.23497(0)
O10	0.35926(0)	0.03523(0)	0.23420(0)

Atomic coordinates for the complex **[Fe_2(*S*-Salhis)$_2$(OH)(OAc)·H_2O·I_2 (3)**

Atoms	**X/a**	**Y/b**	**Z/c**
Fe1	0.57071(9)	0.95617(8)	0.16319(3)
Fe2	0.52628(9)	0.71080(8)	0.11206(3)
I1	0.90714(29)	-0.11596(30)	0.04097(11)
I2	1.00576(28)	0.10962(28)	0.02526(10)
I1'	0.89368(51)	-0.09375(54)	0.07033(21)
I2'	1.03855(43)	0.12204(41)	0.05517(15)
O1	0.62486(49)	0.86175(46)	0.13627(15)
H1	0.70498(0)	0.89191(0)	0.13496(0)
O2	0.48684(54)	0.62206(51)	0.15728(15)
O3	0.54212(49)	1.02105(50)	0.11839(14)
O4	0.40544(49)	0.82759(53)	0.16395(17)
O5	0.37676(45)	0.71820(47)	0.11421(16)
O6	0.66680(45)	0.69276(52)	0.10219(15)
O7	0.74690(59)	0.62816(81)	0.06295(22)
O8	0.73252(46)	1.09237(43)	0.17085(15)
O9	0.84228(65)	1.24472(60)	0.20574(20)
O10	0.96788(144)	0.65364(240)	0.07574(53)
N1	0.45175(51)	0.54214(52)	0.08252(17)
N2	0.54735(60)	0.78073(58)	0.05745(17)
N3	0.58963(75)	0.91049(71)	0.01470(20)
N4	0.58289(67)	0.89877(57)	0.21671(15)
N5	0.57837(81)	0.77851(73)	0.26082(20)
N6	0.53408(65)	1.07804(57)	0.19427(19)
C1	0.44739(83)	1.03336(72)	0.11530(26)
C2	0.37056(98)	0.98075(112)	0.08678(31)
C3	0.26450(116)	0.98182(148)	0.08548(48)
C4	0.24952(141)	1.05174(158)	0.11045(47)
C5	0.33080(100)	1.11096(123)	0.13940(41)
C6	0.42892(98)	1.09969(94)	0.14136(33)
C7	0.52015(84)	1.16001(85)	0.17052(32)
C8	0.37821(75)	0.52507(70)	0.16220(24)
C9	0.30459(103)	0.51588(89)	0.19099(31)
C10	0.19005(103)	0.41107(119)	0.19055(35)
C11	0.16553(119)	0.32468(112)	0.16972(37)
C12	0.23173(82)	0.33602(92)	0.14195(33)
C13	0.34574(73)	0.43294(68)	0.13781(24)
C14	0.42531(77)	0.44403(67)	0.10704(24)
C15	0.58163(98)	0.81952(94)	-0.00234(26)
C16	0.56666(84)	0.88535(74)	0.05021(25)
C17	0.55590(71)	0.73417(71)	0.02417(21)
C18	0.53708(81)	0.61514(83)	0.01983(21)
C19	0.56950(98)	0.79716(77)	0.22402(22)
C20	0.60855(91)	0.88466(84)	0.27777(26)
C21	0.60864(82)	0.95683(76)	0.25111(22)
C22	0.62097(96)	1.07385(84)	0.25511(25)
C23	0.34064(62)	0.75737(66)	0.13856(23)
C24	0.21479(79)	0.71883(92)	0.14124(35)
C25	0.54374(64)	0.55938(61)	0.05586(20)
C26	0.66307(62)	0.63184(73)	0.07460(24)
C27	0.63821(73)	1.14146(65)	0.21894(23)
C28	0.74556(73)	1.16386(66)	0.19750(22)

Atomic coordinates for the complex **[Fe_2(*R*-Salhis)$_2$(OH)(OAc)·2H_2O (4)**

Atoms	X/a	Y/b	Z/c
Fe1	0.57365(0)	0.61519(0)	0.06056(0)
Fe2	0.52889(0)	0.81711(0)	0.00979(0)
O1	0.62777(0)	0.76390(0)	0.03397(0)
H1	0.70852(0)	0.81420(0)	0.03271(0)
O2	0.48402(0)	0.86353(0)	0.05470(0)
O3	0.54662(0)	0.52198(0)	0.01602(0)
O4	0.40650(0)	0.57741(0)	0.06160(0)
O5	0.37849(0)	0.65860(0)	0.01149(0)
O6	0.67166(0)	0.97607(0)	0.00011(0)
O7	0.75497(0)	1.11638(0)	-0.04141(0)
O8	0.73586(0)	0.64189(0)	0.06833(0)
O9	0.84981(0)	0.60208(0)	0.10345(0)
O10	0.97474(0)	1.32087(0)	-0.02703(0)
O11	0.86869(0)	0.89033(0)	0.04719(0)
N1	0.45767(0)	0.91432(0)	-0.01990(0)
N2	0.54935(0)	0.76840(0)	-0.04444(0)
N3	0.58648(0)	0.67371(0)	-0.08727(0)
N4	0.58437(0)	0.68441(0)	0.11418(0)
N5	0.57857(0)	0.79800(0)	0.15686(0)
N6	0.53881(0)	0.45619(0)	0.09183(0)
C1	0.37626(0)	0.85365(0)	0.05842(0)
C2	0.29877(0)	0.78564(0)	0.08579(0)
C3	0.18850(0)	0.77811(0)	0.08839(0)
C4	0.15787(0)	0.83837(0)	0.06437(0)
C5	0.23569(0)	0.90646(0)	0.03762(0)
C6	0.34406(0)	0.91471(0)	0.03425(0)
C7	0.42906(0)	0.98687(0)	0.00527(0)
C8	0.45043(0)	0.41477(0)	0.01356(0)
C9	0.36720(0)	0.38655(0)	-0.01455(0)
C10	0.27045(0)	0.28030(0)	-0.01663(0)
C11	0.24848(0)	0.19457(0)	0.00918(0)
C12	0.33385(0)	0.21918(0)	0.03735(0)
C13	0.43204(0)	0.32851(0)	0.03913(0)
C14	0.52565(0)	0.35941(0)	0.06769(0)
C15	0.60870(0)	0.72185(0)	0.17406(0)
C16	0.56618(0)	0.77315(0)	0.12145(0)
C17	0.61149(0)	0.65263(0)	0.14751(0)
C18	0.62998(0)	0.55070(0)	0.15162(0)
C19	0.56809(0)	0.68000(0)	-0.05132(0)
C20	0.57866(0)	0.76194(0)	-0.10337(0)
C21	0.55601(0)	0.81997(0)	-0.07805(0)
C22	0.53891(0)	0.92414(0)	-0.08223(0)
C23	0.34213(0)	0.58265(0)	0.03653(0)
C24	0.21512(0)	0.49504(0)	0.03847(0)
C25	0.64256(0)	0.49662(0)	0.11555(0)
C26	0.75270(0)	0.58580(0)	0.09456(0)
C27	0.55024(0)	0.98893(0)	-0.04620(0)
C28	0.66988(0)	1.03285(0)	-0.02788(0)

Table I: Selected bond distances (Å) of complex **[Ni_2(*S*-Salhis)$_2$(OAc) ·4H_2O] (1)**

Atoms	**Distances**	**Atoms**	**Distances**
Ni1 -O3'	2.037(3)	N1' -C4'	1.351(6)
Ni1 -O3	2.060(3)	N3' -C7'	1.460(6)
Ni1 -O1	2.063(3)	N3' -C2'	1.466(6)
Ni1 -N2	2.069(3)	C1 -C2	1.528(5)
Ni1 -O20	2.077(3)	C2 -C3	1.540(6)
Ni1 -N3	2.089(4)	C3 -C4	1.501(6)
Ni2 -O3	2.029(3)	C4 -C5	1.334(6)
Ni2 -N2'	2.031(4)	C7 -C8	1.512(6)
Ni2 -O3'	2.058(3)	C8 -C13	1.390(7)
Ni2 -N3'	2.071(4)	C8 -C9	1.409(6)
Ni2 -O1'	2.080(3)	C9 -C10	1.397(6)
Ni2 -O10	2.088(3)	C10 -C11	1.386(7)
Na1 -O1'	2.333(3)	C11 -C12	1.360(9)
Na1 -O30	2.3463(18)	C12 -C13	1.356(8)
Na1 -O1	2.386(3)	C1' -C2'	1.523(6)
Na1 -O60	2.4102(19)	C2' -C3'	1.538(6)
Na1 -C10'	2.980(5)	C3' -C4'	1.488(7)
O1 -C1	1.270(5)	C5' -C6'	1.306(7)
O2 -C1	1.236(5)	C7' -C8'	1.506(6)
O3 -C9	1.326(5)	C8' -C13'	1.379(6)
O1' -C1'	1.265(5)	C8' -C9'	1.406(6)
O2' -C1'	1.238(5)	C9' -C10'	1.404(5)
O3' -C9'	1.330(5)	C10' -C11'	1.378(6)
O10 -C20	1.236(6)	C11' -C12'	1.378(8)
O20 -C20	1.253(5)	C12' -C13'	1.380(7)
N2 -C6	1.307(6)	C20 -C21	1.522(6)
N2 -C4	1.389(5)	O30 -C30	1.3879
N1 -C6	1.339(6)	O40 -C40	1.3991
N1 -C5	1.375(6)	O50 -C50	1.4156
N3 -C2	1.454(6)	O60 -C60	1.4098
N3 -C7	1.469(6)	O60 -Na1	2.410(2)
N2' -C6'	1.293(6)	O70 -C70	1.3417
N2' -C4'	1.388(6)	O80 -C80	1.4413
N1' -C5'	1.343(9)		

Table II: Selected bond Angles (º) of the complex **[Fe_2(*S*-Salhis)$_2$(OAc)·4H_2O] (1)**

Atoms	Angles	Atoms	Angles
O3' -Ni1 -O3	84.02(10)	C2 -N3 -Ni1	104.4(2)
O3' -Ni1 -O1	96.07(11)	C7 -N3 -Ni1	113.2(3)
O3 -Ni1 -O1	88.52(11)	C6' -N2' -C4'	106.1(4)
O3' -Ni1 -N2	98.62(12)	C6' -N2' -Ni2	126.8(3)
O3 -Ni1 -N2	177.01(12)	C4' -N2' -Ni2	127.1(3)
O1 -Ni1 -N2	89.81(13)	C5' -N1' -C4'	106.7(5)
O3' -Ni1 -O20	87.64(12)	C7' -N3' -C2'	115.3(4)
O3 -Ni1 -O20	88.55(12)	C7' -N3' -Ni2	112.8(3)
O1 -Ni1 -O20	175.00(12)	C2' -N3' -Ni2	104.5(2)
N2 -Ni1 -O20	92.94(13)	O2 -C1 -O1	123.7(4)
O3' -Ni1 -N3	174.36(12)	O2 -C1 -C2	118.7(4)
O3 -Ni1 -N3	90.83(12)	O1 -C1 -C2	117.6(3)
O1 -Ni1 -N3	81.46(12)	N3 -C2 -C1	111.0(3)
N2 -Ni1 -N3	86.47(14)	N3 -C2 -C3	110.8(3)
O20 -Ni1 -N3	94.54(13)	C1 -C2 -C3	109.6(3)
O3 -Ni2 -N2'	96.83(13)	C4 -C3 -C2	116.1(3)
O3 -Ni2 -O3'	84.27(11)	C5 -C4 -N2	108.6(4)
N2' -Ni2 -O3'	178.27(13)	C5 -C4 -C3	127.4(4)
O3 -Ni2 -N3'	176.05(13)	N2 -C4 -C3	124.0(4)
N2' -Ni2 -N3'	86.58(15)	C4 -C5 -N1	107.1(4)
O3' -Ni2 -N3'	92.36(12)	N2 -C6 -N1	111.0(4)
O3 -Ni2 -O1'	97.30(11)	N3 -C7 -C8	113.4(4)
N2' -Ni2 -O1'	91.13(13)	C13 -C8 -C9	119.8(5)
O3' -Ni2 -O1'	90.05(11)	C13 -C8 -C7	121.4(4)
N3' -Ni2 -O1'	80.62(13)	C9 -C8 -C7	118.7(4)
O3 -Ni2 -O10	88.97(12)	O3 -C9 -C10	122.5(4)
N2' -Ni2 -O10	90.88(13)	O3 -C9 -C8	119.8(4)
O3' -Ni2 -O10	87.80(11)	C10 -C9 -C8	117.7(4)
N3' -Ni2 -O10	92.96(14)	C11 -C10 -C9	119.8(5)
O1' -Ni2 -O10	173.15(12)	C12 -C11 -C10	122.1(5)
O1' -Na1 -O30	158.95(12)	C13 -C12 -C11	118.8(5)
O1' -Na1 -O1	112.15(11)	C12 -C13 -C8	121.7(5)
O30 -Na1 -O1	80.92(9)	O2' -C1' -O1'	125.0(4)
O1' -Na1 -O60	81.92(9)	O2' -C1' -C2'	118.2(4)
O30 -Na1 -O60	86.82(6)	O1' -C1' -C2'	116.9(4)
O1 -Na1 -O60	165.41(11)	N3' -C2' -C1'	110.9(3)
O1' -Na1 -C10'	87.96(12)	N3' -C2' -C3'	111.0(4)
O30 -Na1 -C10'	112.29(10)	C1' -C2' -C3'	110.0(4)
O1 -Na1 -C10'	72.08(12)	C4' -C3' -C2'	116.0(4)
O60 -Na1 -C10'	105.81(11)	N1' -C4' -N2'	107.3(5)
C1 -O1 -Ni1	112.7(2)	N1' -C4' -C3'	129.4(5)

Atoms	**Angles**	**Atoms**	**Angles**
C1 -O1 -Na1	133.0(2)	N2' -C4' -C3'	123.3(4)
Ni1 -O1 -Na1	110.78(11)	C6' -C5' -N1'	108.3(4)
C9 -O3 -Ni2	134.2(3)	N2' -C6' -C5'	111.6(5)
C9 -O3 -Ni1	117.7(2)	N3' -C7' -C8'	114.8(4)
Ni2 -O3 -Ni1	94.55(11)	C13' -C8' -C9'	120.2(4)
C1' -O1' -Ni2	112.9(3)	C13' -C8' -C7'	120.2(4)
C1' -O1' -Na1	131.5(3)	C9' -C8' -C7'	119.5(4)
Ni2 -O1' -Na1	110.39(12)	O3' -C9' -C10'	122.3(4)
C9' -O3' -Ni1	134.6(2)	O3' -C9' -C8'	119.8(3)
C9' -O3' -Ni2	116.7(2)	C10' -C9' -C8'	117.9(4)
Ni1 -O3' -Ni2	94.40(11)	C11' -C10' -C9'	120.0(4)
C20 -O10 -Ni2	127.3(3)	C11' -C10' -Na1	108.4(3)
C20 -O20 -Ni1	127.9(3)	C9' -C10' -Na1	83.9(2)
C6 -N2 -C4	106.3(4)	C10' -C11' -C12'	122.0(4)
C6 -N2 -Ni1	128.0(3)	C11' -C12' -C13'	118.1(4)
C4 -N2 -Ni1	125.7(3)	C8' -C13' -C12'	121.7(4)
C6 -N1 -C5	106.9(4)	O10 -C20 -O20	126.3(4)
C2 -N3 -C7	115.1(3)	O10 -C20 -C21	116.1(4)
C60 -O60 -Na1	121.79(5)	O20 -C20 -C21	117.6(4)
C30 -O30 -Na1	124.80(5)		

Atomic coordinates for the complex **[Ni_2(*S*-Salhis)$_2$(OAc)·4CH_3OH**

Atoms	X/a	Y/b	Z/c
Ni1	0.07585(4)	0.03712(3)	0.09678(2)
Ni2	0.30850(4)	0.10178(3)	0.14236(2)
Na1	0.30116(17)	-0.15566(13)	0.11253(8)
O1	0.09707(22)	-0.11228(19)	0.09616(10)
O2	-0.01064(27)	-0.24736(20)	0.10084(11)
O3	0.15277(24)	0.03924(20)	0.16515(10)
O1'	0.41297(23)	-0.02404(19)	0.14173(11)
O2'	0.60498(28)	-0.06905(25)	0.14258(14)
O3'	0.24561(25)	0.06911(19)	0.07368(10)
O10	0.21813(30)	0.23479(20)	0.13690(11)
O20	0.04659(29)	0.18609(20)	0.10314(12)
N2	-0.00802(29)	0.02993(27)	0.02949(13)
N1	-0.05281(37)	0.05146(32)	-0.04725(14)
N3	-0.09050(30)	-0.00162(25)	0.12660(13)
N2'	0.37153(35)	0.13824(27)	0.20949(13)
N1'	0.49172(66)	0.17439(40)	0.27095(19)
N3'	0.46731(35)	0.15907(25)	0.11506(13)
C1	-0.00196(34)	-0.15753(28)	0.10089(14)
C2	-0.11656(34)	-0.09662(30)	0.10555(15)
C3	-0.17631(36)	-0.08588(32)	0.05514(17)
C4	-0.10965(35)	-0.02485(30)	0.01857(15)
C5	-0.13628(44)	-0.01231(37)	-0.02848(17)
C6	0.02329(42)	0.07347(34)	-0.01098(17)
C7	-0.09238(41)	0.00209(34)	0.18015(17)
C8	0.00529(41)	-0.05854(30)	0.20369(16)
C9	0.12648(39)	-0.03327(31)	0.19531(14)
C10	0.21498(48)	-0.08626(35)	0.21995(16)
C11	0.18196(60)	-0.16223(39)	0.25046(19)
C12	0.06501(64)	-0.18862(44)	0.25691(21)
C13	-0.02225(57)	-0.13581(40)	0.23455(20)
C1'	0.52478(37)	-0.00646(31)	0.14083(17)
C2'	0.56219(34)	0.10017(33)	0.13771(15)
C3'	0.59364(46)	0.13885(37)	0.18880(18)
C4'	0.49097(45)	0.14962(33)	0.22324(16)
C5'	0.37632(54)	0.17610(42)	0.28559(17)
C6'	0.30819(50)	0.15593(34)	0.24808(16)
C7'	0.46957(48)	0.16227(35)	0.06184(16)
C8'	0.43872(39)	0.06742(30)	0.03713(14)
C9'	0.32318(35)	0.02727(28)	0.04321(12)
C10'	0.29372(40)	-0.05604(29)	0.01596(14)
C11'	0.37869(47)	-0.09844(37)	-0.01390(16)
C12'	0.49350(49)	-0.06137(38)	-0.01833(17)
C13'	0.52152(42)	0.02226(35)	0.00724(15)
C20	0.11722(44)	0.24948(30)	0.11941(16)
C21	0.07720(66)	0.35543(37)	0.11676(27)
O30	0.21664(0)	-0.31227(0)	0.10967(0)
O40	0.80883(0)	0.20890(0)	0.08662(0)
O50	0.64254(0)	0.34105(0)	0.11203(0)
O60	0.49454(0)	0.76504(0)	0.11656(0)
O70	0.81734(0)	0.65154(0)	0.14887(0)
O80	0.39073(0)	0.37482(0)	0.14494(0)
C30	0.22815(0)	-0.38202(0)	0.14604(0)
C40	0.80244(0)	0.24412(0)	0.03878(0)